GENETIC AND REGULATORY DISRUPTIONS IMPACTING DOPAMINE TRANSPORTER FUNCTION CONTRIBUTE TO NEUROPSYCHIATRIC DISEASE PHENOTYPES

By

Aparna Shekar

Dissertation

Submitted to the Faculty of the

Graduate School of Vanderbilt University

in partial fulfillment of the requirements

for the degree of

DOCTOR OF PHILOSOPHY

in

Pharmacology

February 28, 2019

Nashville, Tennessee

Approved:

Christine Konradi, Ph.D.
James W. Bodfish, Ph.D.
Eugenia Gurevich, Ph.D.
Hassane Mchaourab, Ph.D.
C. David Weaver, Ph.D.
Aurelio Galli, Ph.D.

Dedicated to the taxpayer,

the greatest proponent of scientific research.

ACKNOWLEDGEMENTS

My achievements in graduate school would not have been possible without the endless personal and professional support I received during my tenure at Vanderbilt University. I wish to thank all those whom I've had the fortune to share this journey with, and I'm grateful to each and every individual I've learnt from and leaned on along the way.

First of all, I would like to thank my advisor, Dr. Aurelio Galli. He has made me the scientist I am today and has recognized capabilities in me that I wasn't aware I possessed. I am deeply grateful to him for his teachings and for believing in my potential. I would also like to thank my Ph.D. thesis committee members Drs. Christine Konradi, James W. Bodfish, Eugenia Gurevich, Hassane Mchaourab and C. David Weaver for their patience and invaluable input during my committee meetings. My thesis is truly a compilation of their insights from diverse expert knowledge and many years of experience. I appreciate them for every meeting, email, doodle poll and review, all of which have been extremely constructive and motivating. I would like to especially thank Dr. Konradi for being a wonderful personal mentor and being available during rough patches, in spite of her busy schedule. For the incredible support I've received from the Pharmacology department, I would like to share my deep gratitude for both Dr. Joey Barnett and Karen Gieg. I'm appreciative not only for the academic support I received from Dr. Barnett, but also for his encouragement in gaining professional development experiences that helped tremendously in achieving my long-term career goals beyond graduate school.

I've had the fortune of gaining wisdom from several other mentors during my time at Vanderbilt, and I'm especially thankful for the advice and support from Drs. Roger Colbran, Karoly Mirnics and Kathleen Gould. My induction into the Vanderbilt International Scholar Program was the beginning of my academic journey and I thank all three of them for offering me a position in the 2013 incoming year and providing funding for my research. Dr. Colbran's contribution to my professional development did not end there, as with his help, I was able to obtain an American

Heart Association Predoctoral Fellowship in 2015, which helped fund my research as well. I would also like to thank Drs. Galli, Barnett and Weaver for their support in obtaining this fellowship.

The funding and achievements in my research would not have been possible without the strong backing of a lab that runs smoothly. My everyday experiences in the Galli Laboratory have been exceptionally productive and heart-warming and for that, I would like to thank all members of the lab, past and present. I would like to especially thank Peter Hamilton, Andrea Belovich and Jenny Aguilar for being wonderful colleagues and friends. Two individuals from my lab have become family to me owing to their friendship and wisdom over all these years – Nicole Christianson and Heiner Matthies. They have both been academic and personal pillars of support and I count myself lucky to have met them along the way.

I now truly appreciate my incredible (and incredibly long list of) friends I've had the fortune to make at and before graduate school, who have contributed time and again towards my well-being and happiness by always being just a phone call away. Finally, I would like to thank my extended family who have always offered their support to me. Most of all, I would like to acknowledge my mother, Kala, my brother, Arjun, and my partner, Raaj, who have been my biggest advocates. My mother and brother helped me create the foundation of my success with their unconditional love. Raaj inspires me every day towards building my largely ambitious future with his unwavering belief in me. They are, and will always be, an integral part of my every achievement, big or small.

TABLE OF CONTENTS

LIST OF FIGURES

LIST OF ABBREVIATIONS

5-HT Serotonin

AC Adenylyl Cyclase

ACh Acetylcholine

ADE Anomalous Dopamine Efflux

ADIR Autism Diagnostic Interview Revised

ADOS Autism Diagnostic Observational Session

ADHD Attention-deficit hyperactivity disorder

AMPH Amphetamine

ANOVA Analysis of Variance

ASD Autism Spectrum Disorder

BoNT/C Botulinum Toxin Serotype C

CaMKII Calcium/calmodulin-dependent Kinase II

cAMP Cyclic Adenosine Monophosphate

CHO Chinese Hamster Ovary

CK2 Casein Kinase 2

CK2i Casein Kinase 2 Inhibitor

CNS Central Nervous System

CNV Copy Number Variation

COC Cocaine

COMT Catechol-o-methyltransferase

CSF Cerebrospinal Fluid

CTR Control

DA Dopamine

DAG Diacylglycerol

DAT Dopamine Transporter

dDAT *Drosophila melanogaster* Dopamine Transporter

DEER Double Electron Electron Resonance

DR Dopamine Receptor

ECL Extracellular Loop

EPI Electrostatic Potential Isosurfaces

EPR Electron Paramagnetic Resonance

ERK Extracellular signal-regulated kinase

GAT γ-aminobutyric Acid Transporter

GFP Green Fluorescent Protein

GIRK G protein-coupled inwardly-rectifying potassium channels

GST Glutathione S-transferase

hDAT Human Dopamine Transporter

HEK Human Embryonic Kidney

HFA High Functioning Autism

hM1R Human Muscarinic Acetylcholine Receptor M1

IP3 Inositol Trisphosphate

LeuT Leucine Transporter

MD Molecular Dynamics

MDPV 3,4-Methylenedioxypyrovalerone

MPH Methylphenidate

NET Norepinephrine Transporter

NMDA N-methyl D-Aspartate

NSS Neurotransmitter:Sodium Symporters

PET Positron Emission Tomography

PH Pleckstrin Homology

PI3K Phosphatidylinositol 3-Kinase

PIP2 Phosphatidylinositol (4,5)-bisphosphate

PIP3 Phosphatidylinositol (3,4,5)-trisphosphate

PKA Protein Kinase A

PKC Protein Kinase C

PKCβ Protein Kinase C β

PLCδ Phospholipase Cδ

POPC Phosphatidylcholine

POPE Phosphatidylethanolamine

RFP Red Fluorescent Protein

SCG Superior Cervical Ganglion

SCMFM Self-consistent mean-field model

SERT Serotonin Transporter

SLC6 Solute Carrier 6

SN Substantia Nigra

SNARE Soluble NSF Attachment Receptor

SNP Single Nucleotide Polymorphism

SNV Single Nucleotide Variation

SRS Social Responsiveness Scale

Stx1 Syntaxin 1

TBB 4,5,6,7-tetrabromobenzotriazole

TH Tyrosine Hydroxylase

TMD Transmembrane Domain

VMAT Vesicular Monoamine Transporter

VTA Ventral Tegmental Area

WES Whole Exome Sequencing

WT Wildtype

Chapter I

INTRODUCTION

The catecholamine neurotransmitter dopamine (3,4-Dihydroxyphenethylamine or DA) is a phylogenetically conserved molecule that is found in central and peripheral nervous systems across vertebrate and invertebrate organisms (Björklund & Dunnett, 2007b). It is an excitatory neurotransmitter that plays a major role in the regulation of several biological functions such as pituitary function (Smythe, 1977), heart rate (Goldberg, 1972), kidney function (M. R. Lee, 1982) and vasoconstriction (Goldberg, 1984), as well as behaviors such as cognition (Joseph, Frith, & Waddington, 1979), reward (Arias-Carrión & Pŏppel, 2007), motivation (Bromberg-Martin, Matsumoto, & Hikosaka, 2010) and motor activity (Fahn, 2018). DA was first recognized as an intermediate metabolite in the synthesis of norepinephrine (NE, another catecholamine and a hormone): Blaschko in 1957 attributed the formation of DA from L-3,4-dihydroxyphenylalanine (L-DOPA, a precursor to DA and NE) as one of the intermediate steps in the biosynthesis of NE (Blaschko, 1957b). But, the small and varying amounts of DA in various tissues led to several hypothesis that DA might have some regulatory functions that were not yet discovered. Shortly thereafter, the catechol compound (initially named “hydroxytramine”) was discovered in the brain of several mammalian and invertebrate species (Blaschko, 1957a, 1958). Later to be called DA, this study spearheaded multiple reports on the localization and relevance of DA in the central nervous system (CNS). One of the early significant findings was from Carlsson and his group, who, using a novel spectroflourimetry technique, showed that reserpine (through the blockade of the vesicular monoamine transporter (VMAT2)) depleted the rabbit brain of DA and NE (Carlsson, Lindqvist, & Magnusson, 1957). Moreover, they also demonstrated that L-DOPA restored 3-hydroxytyramine levels in the brain. That this compound’s levels were made to disappear almost completely by intravenous administration of reserpine, whereas injection of L-DOPA caused a marked increase, led to further speculation that it wasn’t merely a precursor to NE, but had specific

functions of its own. Carlsson established in the following year that DA was indeed present in the brain by developing a robust and reliable method for its chemical assay (Carlsson, Lindqvist, Magnusson, & Waldeck, 1958). Subsequently, the regional distribution of DA was mapped both in the brains of both animals and humans (Bertler & Rosengren, 1959a, 1959b, 1959c; Sano et al., 1959). These and other studies led to substantiation that DA plays a pivotal role in the control of movement, especially with the findings related to lack of extra-pyramidal control over movement in Parkinson's disease (PD) patients, PD-like symptoms in subjects treated with reserpine, central stimulation of movement by L-DOPA, and finally the treatment of movement deficits in PD patients by L-DOPA (Fahn, 2018). These early studies on the role of DA as an agonist and neurotransmitter in its own right, although met with initial skepticism, eventually formed the basis for several studies on DA localization, synthesis, storage, release and inactivation.

The discovery of DA's role in several disease states provided the impetus to further understand the localization of DA in the brain. Falck *et al*. in 1961 developed techniques that enabled the sensitive visualization of catecholamines, including DA, in specific cell bodies in the midbrain and their nerve terminals (Carlsson, Falck, Hillarp, Thieme, & Torp, 1961). These studies led to the discovery of the nigrostriatal DA pathway through lesions of the substantia nigra (SN), showing the loss of DA in both the SN and the striatum (Carlsson et al., 1961). Furthermore, studies showed that removal of the striatum resulted in the accumulation of fluorescence associated with DA in the cell bodies in the SN (Anden et al., 1964). Subsequent systematic efforts were carried out to determine the localization of DA and other monoamines using this technique. Following the advent of immunohistochemical techniques utilizing probes targeted against genes specific to DA neurons in the 1970s, mapping of DA neurons was carried out in further detail, elegantly reviewed in Bjorklund and Dunnett 2007 (Björklund & Dunnett, 2007a). Decades of study resulted in the establishment of nine distinct cell groups of DAergic neurons in the midbrain, hypothalamus, olfactory tubercle and retina. Below is a detailed description of

DAergic pathways, synthesis, degradation and associated functions and behaviors in the mammalian brain.

Dopaminergic Neurotransmission

To understand the impact of DA signaling in the brain, it was important to delineate the regions that DAergic neurons projected to. Mapping of DAergic neurons and pathways was spearheaded by the introduction of immunohistofluorescence for the catecholamine-synthesizing enzymes, tyrosine hydroxylase (TH), amino acid decarboxylase (AADC) and dopamine beta-hydroxylase (DBH) in the 1970s (Jonsson & Sachs, 1970), enabling researchers to distinguish more accurately between the catecholamines. Today, it is well known that the major DAergic pathways in the brain include (1) the mesolimbic pathway that projects from the Ventral Tegmental Area (VTA) to the Ventral Striatum or Nucleus Accumbens (NAcc), (2) the mesocortical pathway that projects from the VTA to the prefrontal cortex, (3) the nigrostriatal pathway that projects from the Substantia Nigra pars compacta to the Dorsal Striatum and the (4) tubero-infundibular pathway that projects from the hypothalamus to the pituitary gland (Figure 1) (Björklund & Dunnett, 2007a). These projection neurons express the components of the DA synthesis and metabolism pathway. DA neurotransmission is tightly controlled by the synaptic components that determine the amount of DA released by the presynaptic neuron, the amount of DA that reaches the presynaptic and postsynaptic receptors, the downstream signaling mechanisms of the dopamine G protein-coupled receptors (GPCRs) and the duration of DA signal in the synaptic space.

DA synthesis in the presynaptic neuron is dependent upon the availability of the polar amino acid, tyrosine, in the cytosol. Tyrosine can rapidly penetrate the blood brain barrier via active transport through large, neutral amino acid transporters, specifically the L-type amino acid transporter 1 (LAT-1) (Hawkins, O'Kane, Simpson, & Viña, 2006; Tamai & Tsuji, 2000). Several groups have now shown that peripheral administration of tyrosine stimulates catecholamine

production in the brain (Fernstrom & Fernstrom, 2007; Garabal, Arévalo, Díaz-Palarea, Castro, & Rodríguez, 1988; Wiesel et al., 1991). Tyrosine is a precursor for DA; it is first converted to L-DOPA by Tyrosine hydroxylase (TH), which is the rate-limiting step in DA synthesis (Figure 2) (Musso, Brenci, Setti, Indiveri, & Lotti, 1996; Nguyen-Legros, Krieger, & Simon, 1994). TH is a mixed-function oxygenase whose short-term activity is modulated via feedback inhibition by catecholamines, including DA, among other mechanisms. L-DOPA is converted to DA by DOPA decarboxylase and packaged into vesicles by VMAT2 (Howell et al., 1994; Nirenberg, Chan, Liu, Edwards, & Pickel, 1996; Takahashi et al., 1997). The packaging of a high density of neurotransmitter molecules at a high concentration into the small space available in vesicles requires a substantial energy source. The transport of DA into vesicles by VMAT2 relies on the pH and electrochemical gradient generated by a vesicular H^+-ATPase (a proton pump) as the source of energy. Following its packaging into vesicles by VMAT2, DA is released from the presynaptic neuron by vesicular fusion mechanisms upon neuronal excitation. DA release, similar to DA packaging into vesicles occurs in an activity-dependent manner, and signals via DA receptors found on the presynaptic and post-synaptic neurons.

Termination of the DAergic signal at the synapse occurs through several mechanisms; of which DA clearance via the dopamine transporter (DAT) expressed at the presynaptic neuron is of special interest to our group (Wu & Gu, 1999), and discussed in great detail in this document. Other clearance mechanisms include the breakdown or catabolism of DA by enzymes present in the presynaptic or postsynaptic neuron, or in the extrasynaptic space (Figure 2) (Blaschko, 1957c; Goldstein, Friedhoff, & Simmons, 1959; Kopin, 1994). DA is methylated to 3-Methoxytyramine by the enzyme catechol-o-methyltransferase (COMT), followed by breakdown to Homovanillic Acid (HVA) by the aldehyde dehydrogenase enzyme, Monoamine Oxidase (MAO), localized in the mitochondrial outer membrane (Naoi, Riederer, & Maruyama, 2016). Another enzymatic route of DA clearance is a conversion of DA to 3,4-Dihydroxyphenyl Acetic Acid (DOPAC) first by MAO,

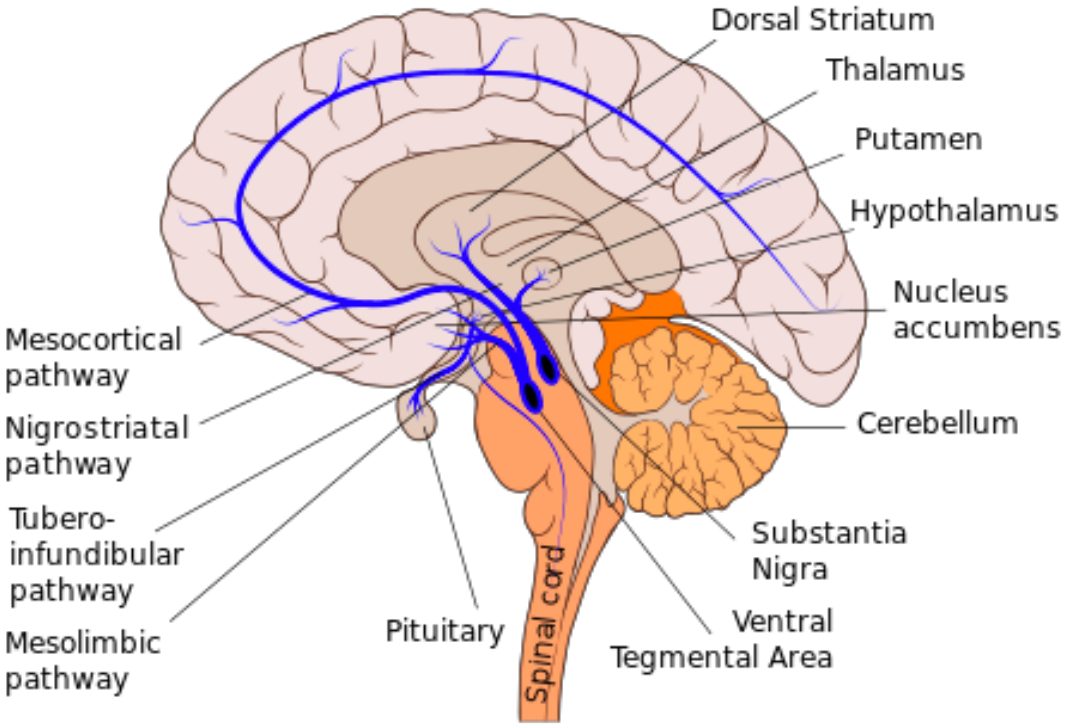

Figure 1: The dopaminergic pathway in the human CNS.

Representation of a sagittal section of the human brain highlighting the regions associated with DAergic signaling and the DAergic pathways (Mesocortical, Nigrostriatal, Tuberoinfundibular and Mesolimbic pathways) in purple.

Reference: Wikimedia Commons

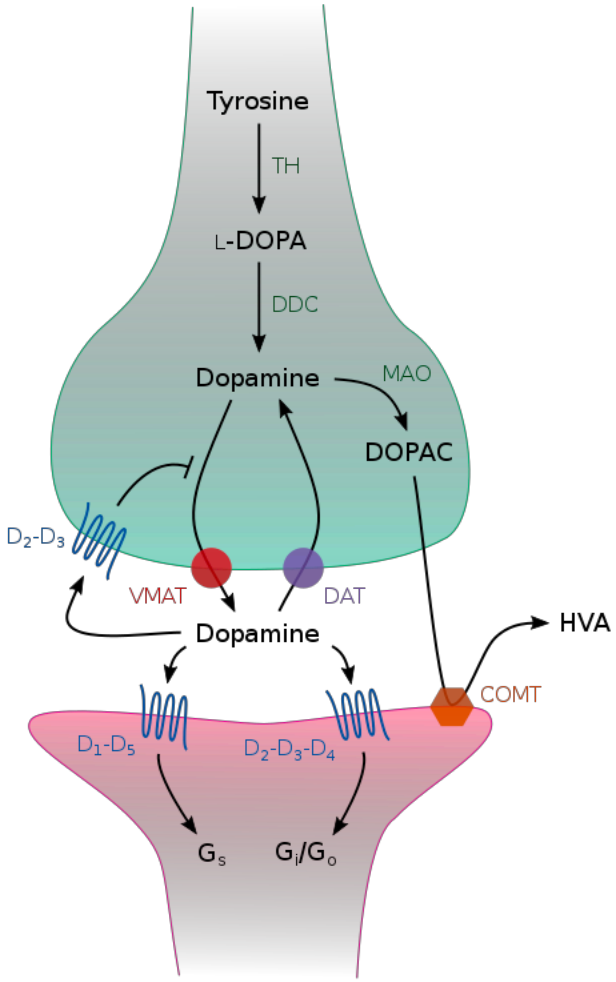

Figure 2: Cartoon schematic of a dopaminergic synapse

The presynaptic component is represented in green, and the post-synaptic component is represented in red.

Reference: By Smedlib, based on original work by Pancrat - Own work, CC BY-SA 4.0, https://commons.wikimedia.org/w/index.php?curid=60353296

followed by the conversion of DOPAC to HVA by COMT. Through either of these routes of breakdown, the major metabolite of DA enzymatic clearance is HVA, and the accumulation of this metabolite in brain or CSF is used as an index of function of DAergic neurons in an organism (R. Sharma et al., 1989; Stefani et al., 2017).

Dopamine Signaling

The DAergic system expresses five types of DA receptors: Dopamine 1 Receptor (D1R), and similarly, D2R, D3R, D4R and D5R (Bunzow et al., 1988; Bull & Sheehan, 1991; Richtand, Kelsoe, Segal, & Kuczenski, 1995). DA receptors are GPCRs and are classified into D1-like (D1 and D5) and D2-like (D2, D3, and D4) (Andersen et al., 1990), based on their G protein signaling partner, elegantly summarized in Savica and Benarroch, 2014, and represented in Figure 3 (Savica & Benarroch, 2014). D1-like receptors are coupled to $G\alpha_{olf}$ or $G\alpha_{s}$, which activate the membrane-anchored enzyme adenylyl cyclase (AC). AC activation leads to the production of cyclic adenosine monophosphate (cAMP) and cAMP-mediated activation of protein kinase A (PKA), which phosphorylates several downstream substrates. Additionally, when D1-like receptors are activated by DA, it leads to the inhibition of voltage-gated potassium (K^+) channels such as Kv4 as well as inward rectifying K^+ channels (Kir), and activation of Cav1 (L-type) calcium (Ca^{2+}) channel currents. D1-like receptor activation also inhibits Cav2 channels, that leads to the reduction of Ca^{2+} influx and secondary activation of Ca^{2+}-dependent, small conductance K^+ (SK) channels. Activation of D1-like receptors further potentiates the effects of glutamate acting via glutamatergic ion channels. Through their multiple signaling pathways, D1-like receptors have the capabilities to increase excitability and firing in pyramidal neurons of the prefrontal cortex and in striatal medium spiny neurons (MSNs). The D2-like receptors are coupled to $G\alpha_{i/o}$, which arrest the production of cAMP via inhibition of AC. Similar to the D1-like receptors with multiple affects, the D2-like receptors, via membrane interactions of their Gβγ subunit, also activate inward rectifier K^+ channels and inhibit Cav1 and Cav2.2 channels. Activation of D2-like receptors leads to a

decrease in overall excitability of neurons in the cortex and striatal MSNs. D1-like and D2-like receptors may form heteromeric complexes with each other and with other receptors. D1/D2 heteromer complexes are linked to Ca^{2+} signaling via coupling with G_q and phospholipase C (PLC) transduction pathways. This leads to production of inositol triphosphate (IP_3), which acting via its receptor (IP_3R) triggers Ca^{2+} release from the endoplasmic reticulum (ER); and diacylglycerol (DAG), which activates protein kinase C (PKC). DA neurotransmission also affects the amount of presynaptic γ-amino butyric acid (GABA) release from GABAergic MSNs in the striatum and the subsequent downstream signaling pathways (Harsing & Zigmond, 1998; Yasumoto, Tanaka, Hattori, Maeda, & Higashi, 2002).

D2Rs, when expressed on the presynaptic neuron, are referred to and function as D2 autoreceptors or D2ARs (Filloux, Wamsley, & Dawson, 1987; Bull & Sheehan, 1991; Feuerstein, 2008). Their functions as autoreceptors/feedback inhibitory signaling proteins upon DA binding include but are not limited to: mediating an intracellular signaling cascade that elevates surface expression levels of the DAT (Witkovsky, Patel, Lee, & Rice, 2009), inhibiting TH function as a negative feedback mechanism (Gowrishankar et al., 2018), and inducing rapid hyperpolarization via activation of presynaptic G protein-coupled inwardly-rectifying potassium channels (GIRK) channels in the soma (Sharpe, Varela, Bettinger, & Beckstead, 2014). Somatodendritic D2ARs in the VTA mediate a negative modulatory feedback on DAergic neurons projecting to the striatum (Mayfield & Zahniser, 2001; Ford, 2014); presynaptic D2 receptors in the NAcc decrease neurotransmitter release that affects the DA signal that reaches the striatal MSNs (de Jong et al., 2015; H. Zhang & Sulzer, 2012). The subsequent chapters delve into more detail on the importance of the D2R-DAT interaction and relevance to DA neurotransmission.

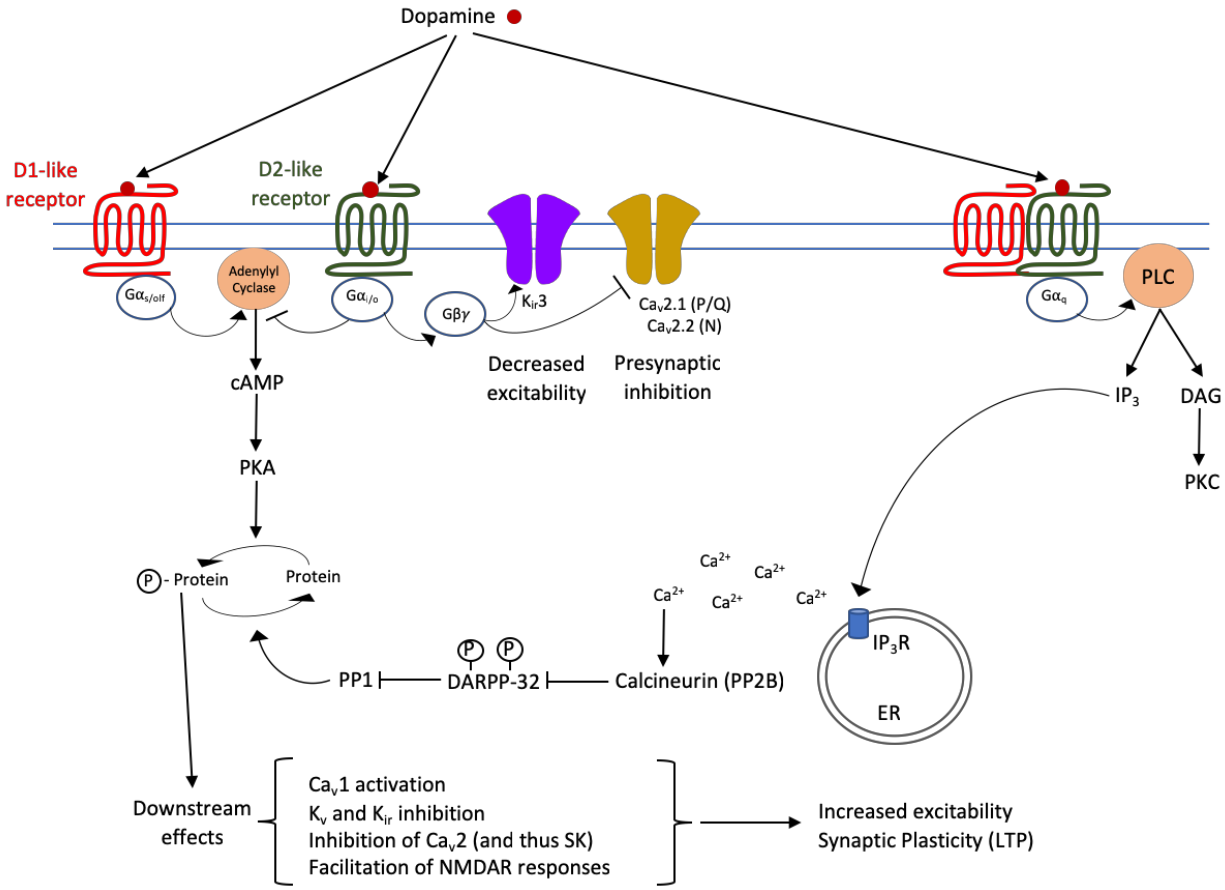

Figure 3: Downstream signaling mechanisms and effectors of dopamine receptors

DA receptors are G-protein coupled receptors (GPCRs) and can be classified into two groups based on the G-protein type that they are coupled to: D1-like receptors (D1R and D5R) are coupled to Gαs G-proteins and D2-like receptors (D2R, D3R and D4R) are coupled to Gαi/o G-proteins. The D1-like receptors, being coupled to Gαs, stimulate the production of cAMP by Adenylyl Cyclase in the cell when activated. This leads to an activation of PKA and resulting in an increase in cell excitability. On the other hand, D2-like receptors are coupled to $G\alpha_{i/o}$ and inhibit Adenylyl Cyclase's production of cAMP upon activation, resulting in a dampening effect on cell activity.

Dopamine Transporter

Upon activity-dependent vesicular release, DA is cleared from the synapse by the DAT. The transporter's role was first suggested to be an integral part of neurotransmitter inactivation as early as in the 1960s, when Julius Axelrod described the reuptake of catecholamine molecules into adrenergic nerves (Weil-Malherbe, Whitby, & Axelrod, 1961). It has been a subject of intense investigation over the past 50 years; researchers have been intrigued by the transporter's structural modalities as well as it's functional role in maintaining DA homeostasis in the CNS. It has been shown by multiple groups now that alterations in DAT function can result in phenotypes associated with several neuropsychiatric and neurodevelopmental disorders, such as attention deficit hyperactivity disorder (ADHD) (Cook et al., 1995; Gill, Daly, Heron, Hawi, & Fitzgerald, 1997), autism spectrum disorder (ASD) , schizophrenia (Blum et al., 1997), bipolar disorder (BPD) (De bruyn, Souery, Mendelbaum, Mendlewicz, & Van Broeckhoven, 1996), substance abuse disorders (Ashok, Mizuno, Volkow, & Howes, 2017; N. D. Volkow, Ding, Fowler, & Wang, 1996; N. D. Volkow, Fowler, & Wang, 1999) and infantile parkinsonism and dystonia (Kurian et al., 2009; Ng et al., 2014), which has made it an important protein and pharmacological target warranting comprehensive investigation.

Another factor that makes the DAT an interesting protein of study is its pharmacology. DAT is the target of a variety of psychostimulant drugs of abuse, of which the most widely studied are cocaine and amphetamine (AMPH) (dela Peña, Gevorkiana, & Shi, 2015; Ritz & Kuhar, 1989). Both drugs possess the ability to cross the blood brain barrier (Caldwell & Sever, 1974) and have addictive properties in vertebrates (Van Rossumj & Hurkmans, 1964) and invertebrates (Huber, Panksepp, Nathaniel, Alcaro, & Panksepp, 2011; Kaun, Devineni, & Heberlein, 2012). They alter the function of the transporter to elevate extracellular DA levels, but with different mechanisms of action (Figure 4). Cocaine and methylphenidate (Ritalin™) are conventional DAT antagonists that block DA reuptake (Gether, Andersen, Larsson, & Schousboe, 2006), thereby elevating DA levels during ongoing vesicular DA release. In contrast, AMPH, in addition to blocking DAT-mediated

DA uptake as a competitive inhibitor, also acts as a substrate that is transported into the cell through DAT. Once inside the cell, AMPH acts as a weak base substrate for VMAT2, sequestering protons and blocking neurotransmitter packaging (David Sulzer, Sonders, Poulsen, & Galli, 2005). Besides being a substrate for DAT, AMPH alters transporter conformation, placing DAT in an "efflux-prone state", a process that consists of a cascade of signaling mechanisms involving changes in DAT phosphorylation (Fog et al., 2006; Khoshbouei et al., 2004), localization and protein associations (Cremona et al., 2011). These changes ultimately lead to the extrusion of cytoplasmic DA from the cell via DAT, a process known as non-vesicular DA release, DA efflux or DAT-mediated DA release. Hence, an important distinction in the actions of AMPH vs. conventional DAT antagonists like cocaine, is that AMPH-induced, transporter-mediated non-vesicular DA efflux is not contingent upon activity-dependent vesicular DA release. Indeed, the action of AMPH can be seen as moving synaptic DA release away from, rather than amplifying, activity-dependent vesicular DA release. Other interesting aspects of this pharmacological agent are that (1) prolonged AMPH application has also been shown, in heterologous cells, to promote DAT internalization (Saunders et al., 2000). But further efforts are needed to explore the various cellular factors that underlie AMPH-induced DAT trafficking. Additionally, (2) Adderall, an AMPH salt, is now widely used as a treatment measure for behaviors associated with ADHD and ASD (A. Sharma & Couture, 2014), in spite of a lack of clear understanding of the mode of action of AMPH in patients diagnosed with these disorders. Hence, several labs over the years have carefully considered the importance of DA clearance and DAT's ability to maintain DA homeostasis in DA neurotransmission, both in the context of neurological diseases as well as drug addiction.

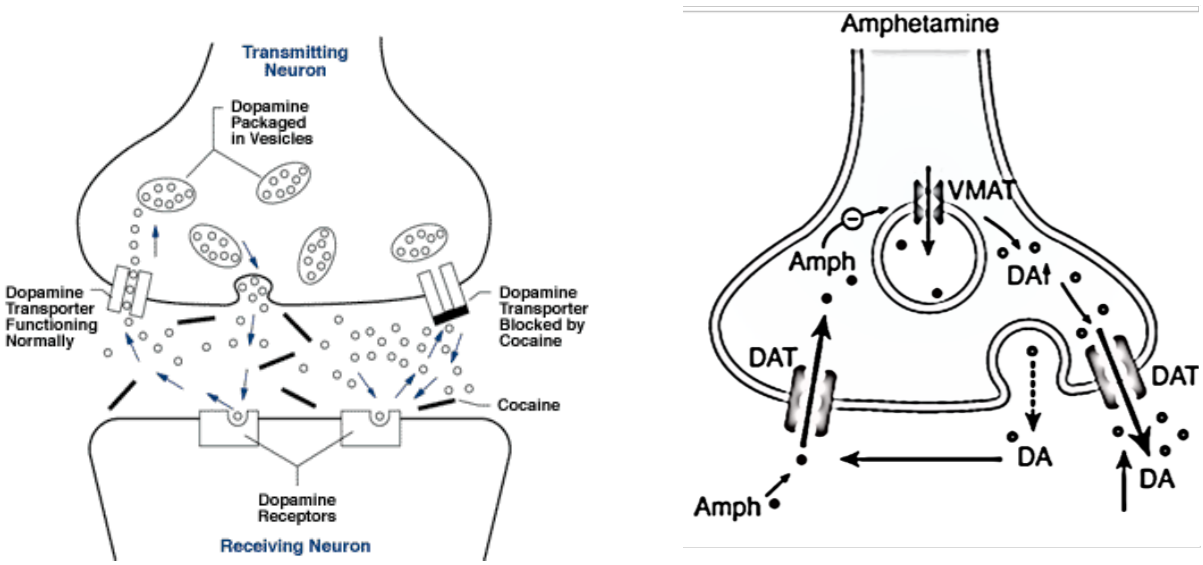

Figure 4: Actions of psychostimulants on the dopamine transporter.

Left: Cocaine acts as a high-affinity antagonist of the DAT that competitively binds to the transporter to prevent substrate reuptake into the presynaptic neuron. Cocaine-mediated elevation of DA in the synaptic cleft is activity-dependent. Right: AMPH acts as a substrate of the DAT, and undergoes competitive reuptake into the presynaptic neuron, following which it carries out multiple actions on the VMAT, DAT and DA metabolizing enzymes to results in DAT-mediated DA efflux. AMPH-mediated elevation of DA at the synaptic cleft is activity-independent. Actions of cocaine and AMPH result in increased DAergic signaling at DA receptors on the post-synaptic neuron.

References: www.drugabuse.gov, www.nimh.nih.gov

Dopamine Transporter: Structure and Topology

The DAT belongs to the *SLC6* class of neurotransmitter transporters and is an integral membrane protein. Its topology features 12 transmembrane helices, with intracellular amino- and carboxy-termini, 4 extracellular loops and 5 intracellular loops (Figure 5). This was confirmed in 2005 by Yamashita *et al*. in their study on the Leucine Transporter, a bacterial homolog of DAT with significant sequence identity (Yamashita, Singh, Kawate, Jin, & Gouaux, 2005), and later in 2013 by Penmatsa *et al*. who elucidated the high-resolution crystal structure of the *Drosophila melanogaster* DAT (dDAT) (Penmatsa, Wang, & Gouaux, 2015; K. H. Wang, Penmatsa, & Gouaux, 2015a) (Figure 6).

The *SLC6* transporter family also includes the serotonin and norepinephrine transporters, and secondary active transporters or symporters among many others. These proteins use the electrochemical gradient generated by Na^+/K^+ ATPase pumps in the cell to symport the substrate (in the DAT's case, DA) into the cell against its concentration gradient (Torres et al., 2003). To carry out its function, the DAT requires two Na^+ ions and one Cl^- ion co-transported into the cell with every DA molecule that it transports (Giros & Caron, 1993; Sonders & Amara, 1996).

Many groups have shown through *in silico* and *in vitro* studies that DAT carries out its function as a DA transporter via an "alternating access" model of function (Figure 7) (Forrest et al., 2008). The model speculates that when DAT exists in an "outward facing" conformation, where the substrate binding site is exposed to the extracellular milieu, DA, Na^+ and Cl^- ions are able to bind to the transporter in a fixed ratio. Following substrate binding, the transporter undergoes a conformational change as it pushes the substrate molecules along the translocation pore to acquire an "inward facing" conformation. In this state, the substrate binding site is now exposed to the intracellular milieu, resulting in the dissociation of cargo, thereby completing its function of transporting molecules from the synaptic space to the cytosol (Diallinas, 2014). The equilibrium created between the "outward facing" and "inward facing" conformations of the DAT is determined by the availability of substrate and associated ions in the extracellular and intracellular spaces,

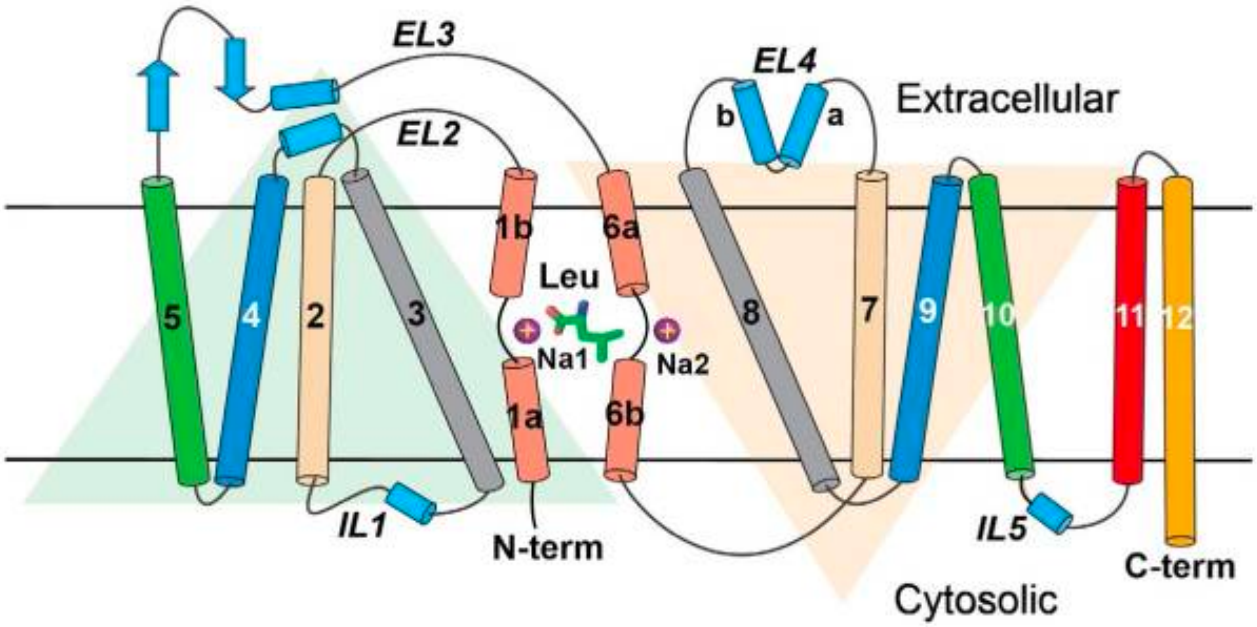

Figure 5: Leucine transporter topology

Leucine and two sodium ions (purple circles) are drawn halfway across the bilayer. Membrane boundaries are demarcated by two thick black horizontal lines. TM helices are depicted as cylinders, with TMs 1 and 6 unwound close to Leu and the two sodiums ions. Faint triangles illustrate the component helices of the 5+5 inverted repeats, each pair of which is shown in the same color.

Reference: Singh SK, Pal A. Biophysical Approaches to the Study of LeuT, a Prokaryotic Homolog of Neurotransmitter Sodium Symporters. Meth Enzymol. 2015;557:167-98.

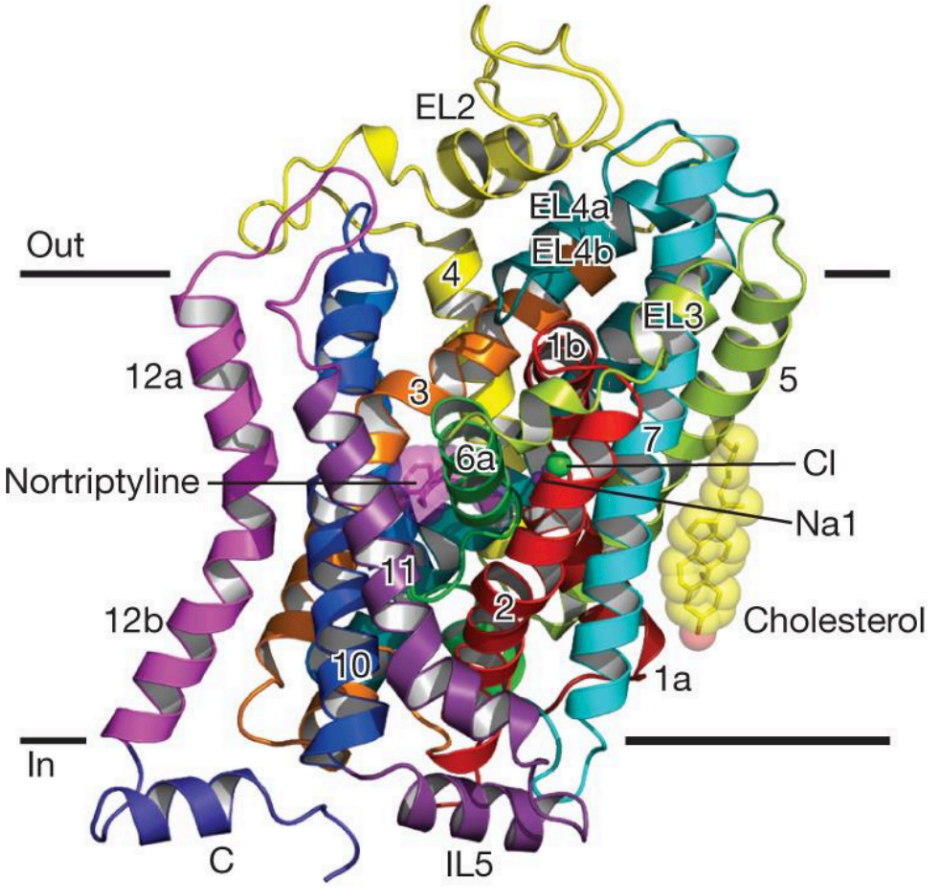

Figure 6: Structure of the *Drosophila* DAT (dDATcryst) viewed parallel to membrane.

Nortriptyline, sodium ions, a chloride ion, and a cholesterol molecule are shown in sphere representation in magenta, purple, green, and yellow, respectively.

Reference: Penmatsa A, Wang KH, Gouaux E. X-ray structure of dopamine transporter elucidates antidepressant mechanism. Nature. 2013;503(7474):85-90.

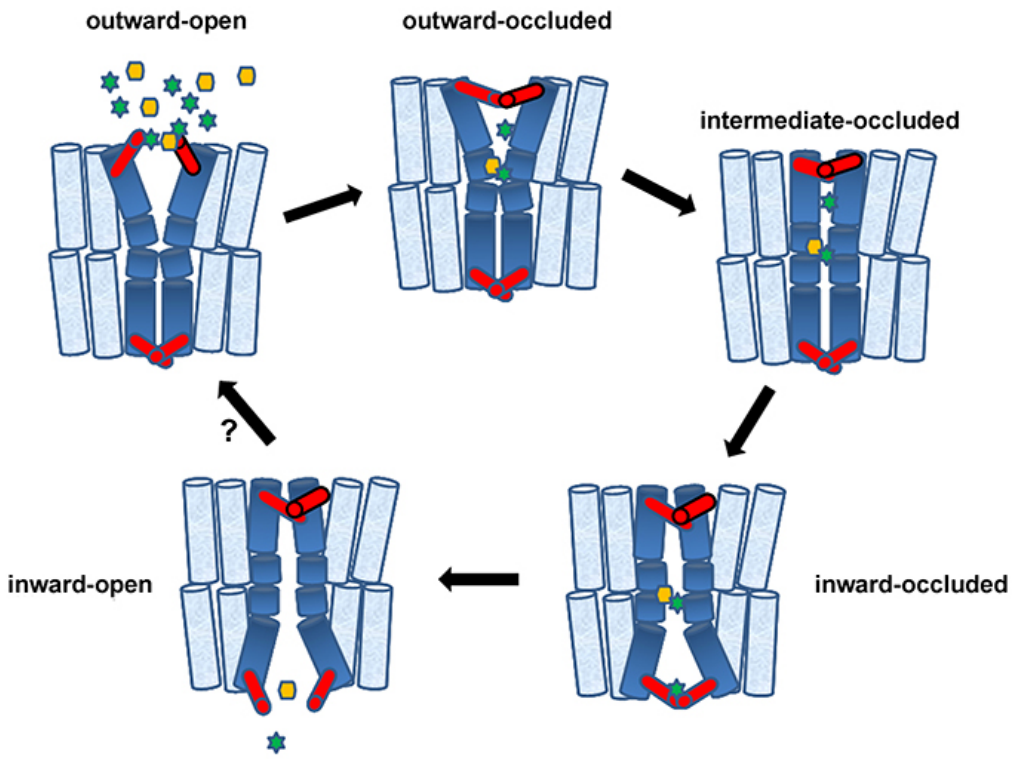

Figure 7: Accumulating evidence supports a theoretical trailer of alternating transporter conformations involving five structurally distinct basic conformations.

(1) outward-facing with extracellular gate open (cytoplasmic gate occluded), (2) outward-facing with extracellular gate occluded (cytoplasmic gate remains occluded), (3) intermediate with both gates occluded, (4) inward-facing with gates occluded, (5) inward-facing with only cytoplasmic gate open. Gates, shown in red, can be made by a few flexible amino acids or bigger domains made of parts of α-helices. Starting from (1), binding of Na+ or H+ (green stars) at the extracellular gate or deeper into the major substrate-binding pocket, stabilizes the outward-facing open state, creating a high-affinity substrate-binding site deep in the transporter body. Substrates (yellow hexagon) might also bind selectively to the extracellular gate. Following substrate and potentially additional ion binding, the extracellular gate closes and this closure promotes an induced-fit transition to the intermediate or inward-facing occluded state. This transition involves major conformational movements of flexible α-helices or parts of helices (shown in deep blue). In the inward-facing state, release of Na+ or H+ stabilizes the opening of the intracellular gate and triggers substrate release. The empty inward-facing open transporter can then transit back outward-facing state and, thereby, complete the transport cycle.

Reference: Diallinas G. Understanding transporter specificity and the discrete appearance of channel-like gating domains in transporters. Front Pharmacol. 2014;5:207.

as well as by the conformational changes that are determined by the transporter's structural domains (Drew & Boudker, 2016).

Dopamine Transporter: Functional Importance

Upon vesicular release, DA clearance at the synapse is primarily carried out via reuptake of DA through DAT, in addition to diffusion, to terminate signaling at DA receptors on the post-synaptic neuron (Giros & Caron, 1993). DAT is expressed on both somatodendritic (Nirenberg, Vaughan, Uhl, Kuhar, & Pickel, 1996) and presynaptic (Gainetdinov, Jones, Fumagalli, Wightman, & Caron, 1998) compartments of DA neurons to carry out its function of DA clearance. The importance of DAT in maintaining DA homeostasis and modulate DA neurotransmission in the CNS has been a subject of intrigue for several groups over the past 50 years. Pivotal studies with a DAT knockout mouse in 1996 brought to light key roles of this protein in maintaining regular neurotransmitter function: disruption of the transporter gene results in spontaneous hyperlocomotion in mice, accompanied by synaptic DA that persists at least 100 times longer in the extracellular space (Giros, Jaber, Jones, Wightman, & Caron, 1996). Additionally, this study elucidated that DAT was the target of cocaine and AMPH, as these psychostimulants had no effect on the DA release or uptake, or on the locomotor activity of these mice.

DAergic neurons exhibit a range of activity states, from a low-frequency tonic firing state to bursts of high-frequency phasic firing states also more commonly recorded as action potentials (Venton et al., 2003). As an effect of its role in DA clearance, DAT function contributes to tonic and phasic DA signaling differentially, studied by the Gonon group using *in vivo* amperometry techniques in mice lacking the DAT. They demonstrated that in wildtype mice, burst firing of DAergic neurons evoked significant increases in extracellular DA above basal levels that was sustained by tonic DA firing. But in the knockout mice, differences between low-frequency and high frequency firing were indiscernible, indicating the importance of DAT in mediating the two different forms of DA neurotransmission (Benoit-Marand, Jaber, & Gonon, 2000). More recently,

Lohani and colleagues demonstrated that following burst activity of DA neurons, elevation of DA in the synaptic cleft may be sustained by an intracellular mechanism that promotes DAT internalization (Lohani et al., 2018).

In addition to outlining how DAT function affects DA signaling upon DA neuron excitation, it is also important to consider the studies that demonstrate that DAT contributes directly to DA signaling, owing to its electrogenic nature and to its ability to support non-vesicular DA release. Several groups in the 90s demonstrated that DAT, being able to support the transport of Na^+ and Cl^- ions (and thus having electrogenic properties) possesses the capabilities of acting as an ion channel (Huang et al., 1999; Reith, Xu, & Chen, 1997; Sonders & Amara, 1996; Sonders, Zhu, Zahniser, Kavanaugh, & Amara, 1997). For instance, Susan Amara and colleagues demonstrated that this catecholamine transporter can acquire channel-like states, supporting DA- or AMPH-gates non-stoichiometric flow of ions (Sonders et al., 1997). Over the next decade, the Amara lab also demonstrated that DAT-mediated currents produced by DA uptake can induce membrane depolarization of cultured mesencephalic DA neurons (Ingram, Prasad, & Amara, 2002). Simultaneously Defelice and colleagues have provided evidence that in cultured DA neurons derived from *C. elegans*, the DAT mediates substrate-induced depolarizing currents and that alterations in the interaction between DAT, specifically the N-terminus and the SNARE protein syntaxin 1 (Stx1) enhance the frequency of channel-like activity in DAT.

Relevant to DAT function is the fact that it is a major target for psychostimulants like cocaine and AMPH in the CNS, and the effects mediated by them. Although, being a pharmacological target may not be a physiologically relevant mechanism of the transporter, the ability of AMPH to mediated non-vesicular, DAT-mediated reverse transport begs the question of whether DAT-mediated DA efflux can occur in physiological contexts. The occurrence of non-vesicular release was first described in 1995, when Olivier and colleagues described the release of DA in the rat striatum by two separate mechanisms, that were directly and simultaneously observed (Olivier, Guibert, & Leviel, 1995). In 2001, the Mintz group published a report in *Science*

providing evidence for DAT-mediated dendritic release of DA and the resulting self-inhibition, carried out in the absence of psychostimulants using amperometric and patch-clamp recordings (Falkenburger, Barstow, & Mintz, 2001). More recently, as a continuation to this study, Opazo *et al*. demonstrated that activation of Gq-coupled GPCRs was sufficient to induce DAT-mediated DA release in the Substantia Nigra pars reticulata, mediated by PKC (Opazo, Schulz, & Falkenburger, 2010). The factors that affect DA release were further investigated, bringing to light that membrane potential and intracellular Na^+ levels were key factors that could promote DAT-mediated efflux (Khoshbouei, Wang, Lechleiter, Javitch, & Galli, 2003). Notably, several groups, starting in as early as 1977, demonstrated that somatodendritic DA release causes inhibition of DA neuron excitability via activation of D2ARs (Aghajanian & Bunney, 1977; Ford, 2014).

An important factor that controls the rate of DA clearance, and in turn DA homeostasis is DAT surface expression levels (Horschitz, Hummerich, Lau, Rietschel, & Schloss, 2005). DAT trafficking is dynamically controlled, with neuronal depolarization reducing DAT surface levels and neuronal hyperpolarization enhancing DAT surface levels rapidly (Richardson et al., 2016). Other factors that influence DAT surface expression and function are membrane localization (Sakrikar et al., 2012), pharmacological agents (Kahlig & Galli, 2003), regulatory proteins (Loder & Melikian, 2003), and interacting partners, which are discussed in greater detail in the latter half of this chapter. Also mentioned in detail is the functional importance with relevance to systemic and behavioral consequences of DAT disruption.

Although this chapter does not contain an exhaustive list of DAT functions, an important one warranting mention is the role that the transporter plays in DA recycling. The highlight of its functions includes maintaining DA homeostasis in the synapse and modulating neurotransmitter signaling, but the DAT also plays a pivotal role in the repackaging and recycling of DA, contributing significantly to maintain the tone of vesicular release and minimize energy expenditure of the neuron (Caudle, Colebrooke, Emson, & Miller, 2008; Sossi et al., 2007).

Dopamine Reverse Transport

Over the past few decades, it has been demonstrated that DA release from presynaptic terminals occurs under multiple conditions (Besson, Cheramy, Feltz, & Glowinski, 1969), during disease conditions (P. J. Hamilton, Campbell, Sharma, Erreger, Herborg Hansen, et al., 2013; Hansen et al., 2014; Mazei-Robison et al., 2008) as well as *via* pharmacological manipulation (Breese, Kopin, & Weise, 1970). A substantial fraction of the studies on DA release and the mechanisms that control DA release have focused on the striatum and the cortex - target regions where DA projections lie (Fallon & Moore, 1978). Stimulation of DA terminals by optogenetic (Bass et al., 2010) or electrical methods (Melchior, Ferris, Stuber, Riddle, & Jones, 2015) in the striatum results in DA release, however, a more complex picture arises when trying to determine the signaling mechanisms underlying this DA release. The striatum receives glutamatergic input from the cortex, thalamus, amygdala and the hippocampus and studies have shown that stimulation of these inputs can evoke DA release through the activation of AMPA and NMDA receptors on DA terminals (Imperato, Honoré, & Jensen, 1990; Imperato, Scrocco, Bacchi, & Angelucci, 1990). Metabotropic glutamate receptors are also found on DA projections and their direct actions have also been demonstrated to regulate DA release (Yavas & Young, 2017). Interestingly, stimulation of cholinergic interneurons in the striatum and subsequent release of acetylcholine can also enhance DA in the striatum *via* the activation of either nicotinic ionotropic or muscarinic metabotropic receptors found on DA axons (Yorgason, Zeppenfeld, & Williams, 2017). Further complexity arises owing to the fact that a subset of DA neurons also co-release glutamate in addition to DA (Stuber, Hnasko, Britt, Edwards, & Bonci, 2010), resulting in the stimulation of DA release through the activation of glutamate receptors or the activation of the cholinergic interneurons (H. Zhang & Sulzer, 2012).

DAT-mediated DA release does not only occur in the DAergic projections discussed above, but also occurs in the somatodendritic compartments in the midbrain (Witkovsky et al., 2009). Somatodendritic DA release is an important component in maintaining DA homeostasis

because unlike release at the DA projections, it signals via D2AR on neighboring DA soma and dendrites to dampen DA neuron activity (Adell & Artigas, 2004). This occurs via Gβγ-mediated activation of GIRK channels that hyperpolarize the cell. This signal is typically detected as an outward current or a D2-mediated inhibitory post-synaptic current (IPSC) in DA cell bodies when measured by whole-cell patch clamp electrophysiology techniques (Beckstead, Grandy, Wickman, & Williams, 2004).

Amphetamines (AMPH and methamphetamine) stimulate the release of DA from the mesocorticolimbic system and the nigrostriatal dopamine systems (David Sulzer et al., 2005). It is a dirty drug and has off-target effects on the serotonergic and noradrenergic systems as well (Buchmayer et al., 2013; Steinkellner et al., 2015). The drug is taken up by DAT into the presynaptic neuron and mediates the reversal or efflux-mode of DAT (Fraser et al., 2014). The drug also interacts with VMAT proteins to enhance release of DA and 5-HT from vesicles (Freyberg et al., 2016). AMPH may also act as a direct agonist on central 5-HT receptors and inhibit MAOs, prolonging DA signaling (Ramsay & Hunter, 2003). In the periphery, amphetamines are believed to cause the release of noradrenaline by acting on the adrenergic nerve terminals and α- and β-adrenergic receptors (R. Yamamoto & Takasaki, 1983). The work described in this thesis is focused primarily on understanding the mechanisms underlying DAT reverse transport, under the influence of AMPH or during physiologically relevant conditions. More detailed insights on presynaptic, intracellular signaling mechanisms underlying AMPH actions are discussed in the subsequent chapters.

Rare Variants in the Dopamine Transporter

DAT tunes DA neurotransmission by active reuptake of DA from the synapse. Rare variants in the human DAT (hDAT) have been demonstrated to disrupt DA neurotransmission, contributing to the etiology of a number of neuropsychiatric disorders, including schizophrenia,

BPD, ADHD and more recently, in ASD. Over the past decade, multiple rare variants in the hDAT have been identified in patients that suffer from these disorders (Figure 8). Our group, as well as several other groups have isolated and characterized these variants – from the description of single-transporter function to the behavioral effects of the mutation in an intact organism. These studies established that disease-associated DAT mutations can lead to alterations in its structure and function and dysregulation of transporter activity, resulting in imbalances in DA homeostasis in the brain, and culminating in behavioral anomalies. Importantly, DA efflux mechanisms are affected in these DAT variants. A brief synopsis of well-analyzed variants is given below (also refer (Herborg, Andreassen, Berlin, Loland, & Gether, 2018)).

hDAT A559V: The hDAT A559V, a variant in which the Ala 559 residue on the 12th transmembrane of hDAT was mutated to a Val residue, was identified in in two brothers diagnosed with ADHD (Mazei-Robison et al., 2008). It was identified as an interesting variant to study due to its location on the 12th transmembrane (TM12) region of DAT and the alterations it induced to DAT function. Although first identified in patients diagnosed with ADHD, it was subsequently found in relation to multiple neuropsychiatric and neurodevelopmental disorders including ASD and BPD. Prior to the discovery of the hDAT A559V, there was very little information on the importance of TM12 with regards DAT structure and function. *In silico* analyses since have suggested that TM12 is important in oligomerization of DAT (Sitte, Farhan, & Javitch, 2004); while simultaneously, independent studies suggested that transporter oligomerization may play a role in AMPH-induced, DAT-mediated DA efflux (Seidel et al., 2005). Upon analysis by transient transfection in heterologous cell lines, the hDAT A559V variant showed normal total and surface expression, and comparable reuptake and affinity for DA relative to cells expressing its wildtype counterpart. Interestingly, cells expressing the hDAT A559V variant exhibited basal anomalous DA efflux (ADE), a release of DA at physiological conditions sometimes referred to as a DA “leak”. This ADE was shown by multiple studies to be transporter-dependent as it could be blocked upon

the application of methylphenidate and cocaine, conventional DAT antagonists. ADE exhibited by hDAT A559V has been measured by loading DA into hDAT A559V cells using a patch pipette and analyzing for DA efflux using carbon fiber amperometry, compared to hDAT wildtype-expressing cells (Mazei-Robison et al., 2008). The ADE exhibited by cells expressing the hDAT A559V was also found to be voltage-sensitive and amplified when transfected cells expressing the variant were held at depolarizing potentials that potentiated neuronal firing (compared to those expressing hDAT wildtype). Notably, it was found that whereas AMPH caused DAT-mediated DA efflux in cells transfected with the wildtype transporter, hDAT A559V-mediated ADE was actually blocked by AMPH, failing to further increase DAT-mediated DA efflux. Subsequently, Bowton and colleagues showed that ADE through hDAT A559V in transfected cells is sustained by the D2R expressed in small amounts in these cells, demonstrated by ADE blockade upon D2R antagonism with raclopride (Erica Bowton et al., 2010). This study also found that D2R signals through a non-canonical pathway involving Ca^{2+}/calmodulin-dependent protein kinase II (CamKII), previously shown to directly phosphorylate DAT at five distal serine residues in the N-terminus, a post-translational modification necessary for AMPH-induced, DAT-dependent DA efflux, by placing the transporter in an “efflux-prone” confirmation (Fog et al., 2006). Mergy and colleagues corroborated these findings by demonstrating *in vitro* and *in vivo* changes brought about by the A559V mutation to the transporter that were reversible by D2R antagonism (Mergy, Gowrishankar, Davis, et al., 2014; Mergy, Gowrishankar, Gresch, et al., 2014). Previous studies by Khoshbouei and colleagues had demonstrated that hDAT phosphorylation at the distal N-terminus (At Ser2, Ser4, Ser7, Ser12 and Ser13) is essential for AMPH-induced, DAT-mediated DA efflux (Khoshbouei et al., 2004). Consistent with this idea, when assayed for serine phosphorylation at the distal N-terminus, hDAT A559V was found to be hyperphosphorylated, and ADE was abolished when serines were mutated to alanines in the hDAT A559V (E. Bowton et al., 2014).

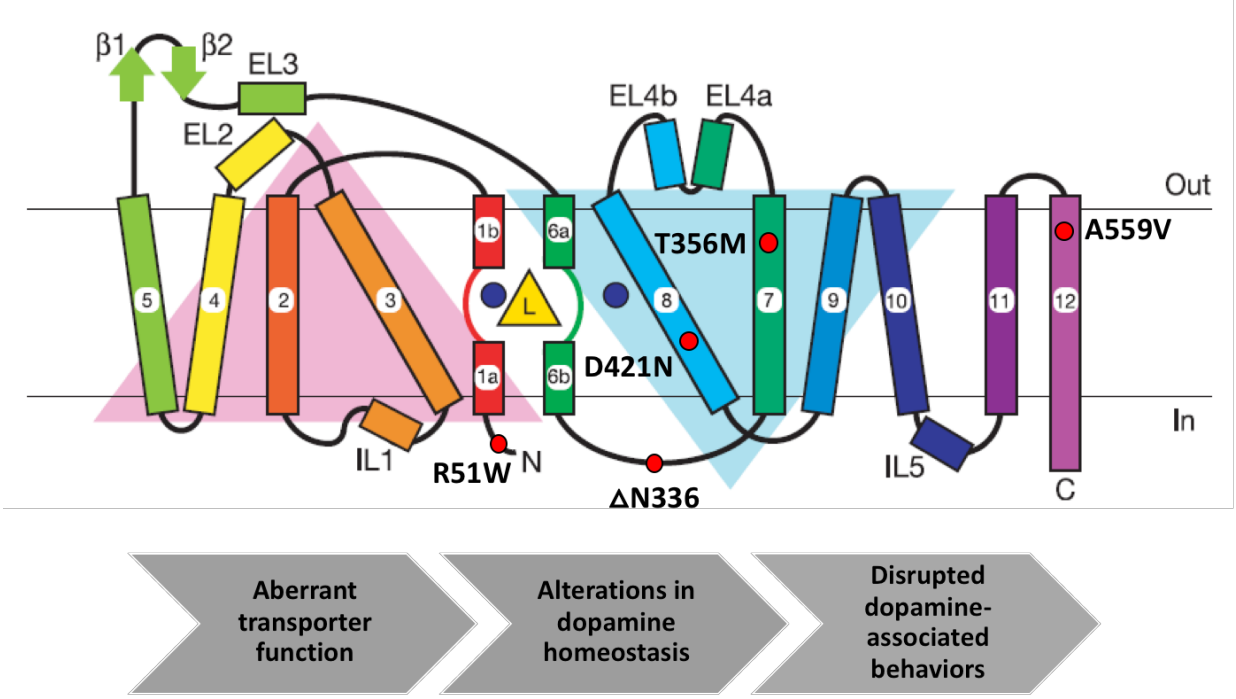

Figure 8: Rare variants in the DAT identified in patients diagnosed with neuropsychiatric disorders.

Point mutations are represented as red dots and annotated with the mutation name. A common flowchart hypothesis for the consequences of the variants is represented below.

Figure adapted from: Yamashita A, Singh SK, Kawate T, Jin Y, Gouaux E. Crystal structure of a bacterial homologue of Na+/Cl--dependent neurotransmitter transporters. Nature. 2005;437(7056):215-23.

hDAT T356M: Hamilton and Campbell *et al*. in 2013 discovered the first *de novo* hDAT variant identified in a patient diagnosed with ASD. Subjects from this family included the proband, both parents and an unaffected sibling, who were recruited from the Boston Autism Consortium (P. J. Hamilton, Campbell, Sharma, Erreger, Herborg Hansen, et al., 2013). This variant was a mutation at the conserved Thr356 residue to a Met (hDAT T356M). Transient transfection of the hDAT T356M DNA in heterologous cell lines showed that DA uptake in the hDAT T356M cells is significantly reduced (as compared to wildtype DAT uptake). The loss in transport capacity of the variant hDAT was not associated with a reduction in hDAT surface expression. hDAT T356M exhibits partially impaired efflux in response to AMPH compared to wildtype hDAT. These findings signify that the residue T356M is key in the coordination of DA uptake. Interestingly, similarly to the hDAT A559V, the hDAT T356M cells exhibited constitutive DA efflux or ADE, in the absence of AMPH, similar to the molecular phenotype shown by the hDAT A559V. Studies using Double Elctron Electron resonance (DEER), a pulse Electron Paramagnetic Resolution (EPR) technique, (in collaboration with the Mchaourab Lab) elucidated that the T356M variant is restricted to an inward-open (or inward-facing), efflux-willing conformation, explaining the constitutive efflux and resultant deficits in uptake properties of the transporter. Importantly, the discoveries made *in vitro* correlated to the findings from structural analyses and *in vivo/ex situ* studies. In this study, the use of *Drosophila melanogaster* as a significant animal model in the study of DA-associated behaviors was demonstrated. DA-associated behaviors like locomotion and circadian rhythm were elevated in the T356M transgenic flies, to signify the increase in extracellular DA in the brains of these animals. Taken together, our findings demonstrate that the hDAT T356M has aberrant transporter function which may lead to alterations in DA homeostasis and DA–associated behaviors and confer risk for ASD in the individual harboring the mutation. The next step in this project is to create transgenic mice harboring this mutation in their DAT and conduct biochemical and behavioral analyses on these animals.

hDAT D421N: In 2014, Ulrik Gether's group at the University of Copenhagen identified an adult individual with both early-onset Parkinson's Disease and ADHD out of a cohort of patients with Parkinson's-like movement disorders (Hansen et al., 2014). This individual is the first documented case of being compound heterozygous for a mutation in the hDAT, possessing a heritable variant, hDAT I312F and a *de novo* variant, hDAT D421N. The hDAT I312F, showed an impairment in DA uptake *in vitro*, but was also present in an unaffected sibling. However, the *de novo* hDAT D421N demonstrated a functional phenotype similar to the ASD *de novo* variant, hDAT T356M (Hamilton and Campbell *et al*. *2013*), namely impaired DA uptake, impaired DA efflux response to AMPH, and ADE (Hansen et al, 2014). The hDAT D421N mutation also perturbs affinity for Na^+ by interfering with the second Na^+ binding site. As is the case for hDAT T356M, there have not yet been any published investigations into the intracellular mechanisms surrounding the observed ADE, nor whether the AMPH-susceptible phosphorylation pathways are dysregulated in these variants, as is the case with the hDAT A559V. However, our groups and others are working on identifying common structural motifs in the DAT that are disrupted due to these variations, to identify key component changes in the transporter that could lead to ADE.

hDAT R51W: In 2015, Cartier and Hamilton *et al*. characterized two ASD-associated variants – one in the hDAT (hDAT R51W) and the other in Stx 1 (Stx1 R26Q) through exome sequencing in patients diagnosed with ASD (Cartier et al., 2015). They found that the hDAT R51W variant displays significantly reduced DA efflux compared to its wildtype counterpart, without impairments in uptake function. Thus, the group made efforts to determine whether this ASD-associated variant disrupted the molecular mechanisms that converge in regulating reverse transport of DA, resulting in DA dysfunction and associated behavioral abnormalities. They showed that hDAT R51W has reduced association with Stx1 (an important modulator of reverse transport), resulting in altered DA-related behaviors. Indeed, *Drosophila* expressing hDAT R51W selectively in DA neurons demonstrate reduced sensitivity to the psychomotor effects of AMPH, as observed in a

significantly lower AMPH-induced locomotion when compared to hDAT expressing flies. Interestingly, basal locomotion remained unaltered in hDAT R51W flies, indicating normal DAT-mediated uptake function as supported by the uptake data. This body of work was pivotal in our understanding of the phosphorylation state of Stx1 at Ser14 and Stx1/DAT interaction in regulating reverse transport of DA, without affecting DAT-mediated uptake functions.

hDAT ΔN336: We investigated the structural and behavioral bases of an ASD-associated in-frame deletion in hDAT at N336 (ΔN336). Computational simulations and *in silico* studies, as well as spectroscopic analyses suggest a compromise in the structural integrity of this variant transporter, that resulted in disruptions in the alternating access model of transport function. We uncovered a previously unobserved conformation of the intracellular gate of the transporter promoted by ΔN336, likely representing the rate limiting step of the transport process. It is defined by a "half-open and inward facing" state (HOIF) of the intracellular gate that leads to DA dysfunction. The HOIF state is regulated by a network of interactions conserved phylogenetically, as we observed it both in hDAT and in its bacterial homolog leucine transporter. We pioneered these dysfunctions in brains of *Drosophila melanogaster* expressing hDAT ΔN336. These flies are hyperactive and display increased fear and impaired social interactions, traits associated with ASD. Here, we describe how a genetic variation causes DA dysfunction in ASD. The hDAT ΔN336 variant is discussed in greater detail in Chapter IV.

Regulation of Dopamine Transporter Efflux Properties

DAT properties and function are controlled by several regulatory elements that are present in the intracellular milieu (Figure 9) (Vaughan & Foster, 2013). DAT is extensively glycosylated, and its sequence contains numerous consensus phosphorylation sites for PKA, PKC, and Ca^{2+}-calmodulin kinase. The large intracellular N-terminus and the 4th intracellular loop possess multiple negatively charged amino acid sequences that enhance its proclivity to interact with

positively charged lipid molecules. Additionally, DAT has been shown to directly interact with integral membrane proteins like Flotillin-1 (Flot1) that determine or can help determine its membrane localization. The direction of DA transport that is carried out by DAT is determined and tightly controlled by, more often than not, more than one of these regulatory elements. Below is an overview of the key regulatory elements that influence DAT-mediated DA efflux.

Phosphorylation and Interacting Kinases: Several putative phosphorylation sites have been identified within the intracellular domains of DAT, suggesting that the DAT is amenable to regulation by kinases (Foster & Vaughan, 2017). Indeed, the distal N-terminal region of the DAT contains crucial serine residues that, when phosphorylated, promote reverse transport of DA without affecting DAT uptake function (Khoshbouei et al., 2004). When truncated or replaced with alanine residues to prevent phosphorylation, AMPH-induced DA efflux is reduced by 80% (Khoshbouei et al., 2004). Alternatively, when these serine residues are substituted with glutamates or aspartates to mimic phosphorylation (also referred to as pseudo-phosphorylation), the ability of the DAT to efflux DA remains intact, suggesting that phosphorylation of one or more of these serines are critical for AMPH-induced DA release. Importantly, these N-terminal residues can be phosphorylated by protein kinase C (PKC) (Giambalvo, 1992; Johnson, Guptaroy, Lund, Shamban, & Gnegy, 2005) and CaMKII (Erica Bowton et al., 2010; Fog et al., 2006). Aside from the distal N-terminus, phosphorylation of the transporter at the Thr53 has been noted as significant in regulating reuptake and AMPH-induced efflux (Challasivakanaka et al., 2017; Foster et al., 2012). Finally, although the key target residues have not been clearly identified, the transporter is dephosphorylated by PP1 in *in vitro* heterologous cells and in striatal homogenates (Foster, Pananusorn, Cervinski, Holden, & Vaughan, 2003).

Both PKC and CaMKII have been revealed to be major regulators of DAT-mediated reverse transport. Researchers have discovered that administration of AMPH can induce an increase in PKC activity *in vivo* (Giambalvo, 1992). Inhibition of PKC prevents AMPH-induced DA

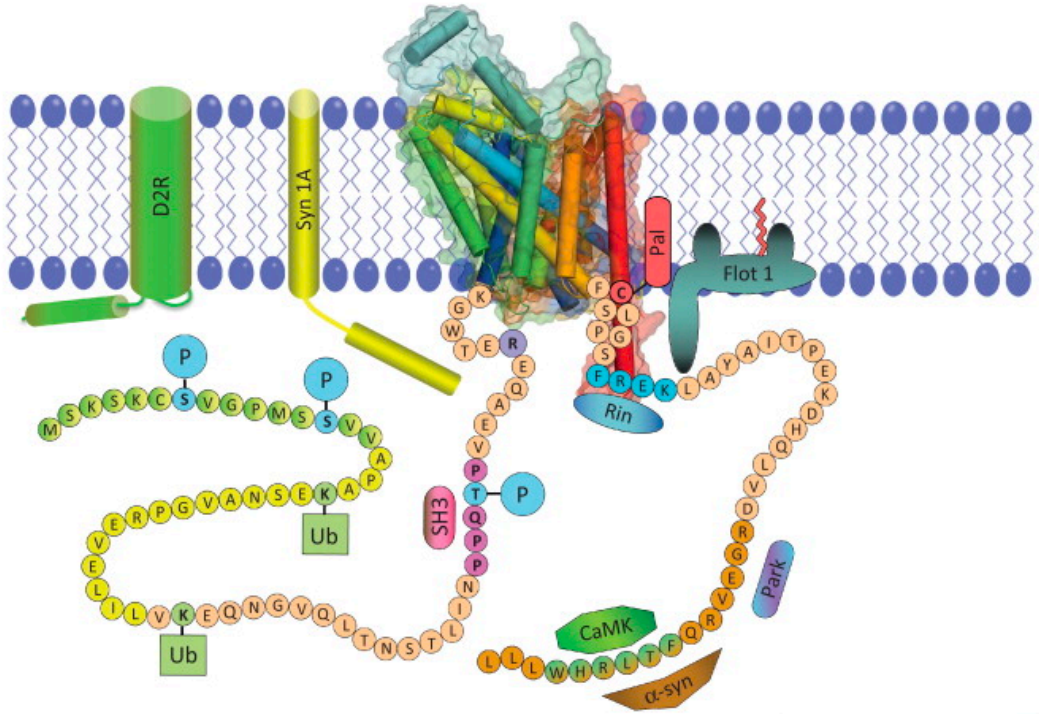

Figure 9: Regulatory elements of rat dopamine transporter N- and C-terminal domains.

A 3D model of rat DAT based on the A. aeolicus LeuT transporter was generated using PyMol (Schrödinger, LLC), with TM helices shown as barrels and light shading indicating semitransparent Connolly surfaces. The structure was positioned in a membrane bilayer with schematic depictions of N- and C-terminal tails extending into the cytoplasm. Posttranslational modifications shown are Ser7, Ser13, and Thr53 phosphorylation (blue, P), Lys19 and Lys35 ubiquitylation (light green, Ub), and Cys580 palmitoylation (red, Pal). Motifs and sequences indicated are intracellular gate residue Arg60 (R, purple), putative Src homology domain epitope (mauve, SH3), PKC endocytosis motif (blue, FREK), and domains for interactions with Syntaxin 1A (Syn1A, yellow), D2 DA receptor (D2R, green) Ras-like GTPase Rin 1 (Rin, blue), Calcium-Calmodulin-Dependent Protein Kinase (CaMK, green), and α-synuclein (α-Syn, orange) and Parkin (Park, dark blue-lavender). Flotillin 1 (Flot 1, olive green) is shown with palmitic acid modification (red line) but without a known DAT interaction site.

Reference: Vaughan RA, Foster JD. Mechanisms of dopamine transporter regulation in normal and disease states. Trends Pharmacol Sci. 2013;34(9):489-96.

efflux in rat striatal slices (Johnson et al., 2005; Kantor & Gnegy, 1998), and exposure to phorbol esters, compounds that promote PKC activity, induces DA efflux in the absence of AMPH (Cowell, Kantor, Hewlett, Frey, & Gnegy, 2000). In the rat striatum, a physical interaction was observed between the DAT and one of the PKC family isozymes, PKCβII (Johnson et al., 2005), highlighting tight regulation of the DAT by PKC. A physical interaction between CaMKII and the DAT C-terminus has been observed, as well (Fog et al., 2006). Disruption of this interaction or inhibition of CaMKII reduces reverse transport of DA in both *in vitro* and *in vivo* preparations (Fog et al., 2006). Interestingly, AMPH treatment increases CaMKII activity in striatal synaptosomes, an effect that can be blocked in the absence of extracellular Ca^{2+} or in the presence of nomifensine, a DAT inhibitor (Iwata, Hewlett, & Gnegy, 1997). This suggests that both Ca^{2+} and DAT activity are required for AMPH to potentiate CaMKII activity. Importantly, AMPH has been shown to increase intracellular Ca^{2+} in DAT expressing cells, a process mediated by DAT activity (Gnegy et al., 2004) and dependent on voltage-gated N- and L-type Ca^{2+} channel activity (Kantor, Zhang, Guptaroy, Park, & Gnegy, 2004). Therefore, AMPH may activate CaMKII and other second messenger signaling pathways by increasing intracellular Ca^{2+} concentration, whereby mediating cellular depolarization.

Syntaxin 1 (Stx 1): Stx1 is a member of the soluble N-ethylmaleimide-sensitive factor attachment protein receptor (SNARE) complex, which is required for the docking and release of synaptic vesicles (Sudhof and Rothman, 2009). Aside from its role in the SNARE complex, there is a growing body of evidence to suggest that Stx1 associates with and regulates the function of ion channels and *SLC6* transporters, including the DAT. Stx1 was first revealed to directly interact with the distal region of the DAT N-terminus in a yeast-two hybrid system by Lee and colleagues (K.H. Lee, Kim, Kim, & Lee, 2004) followed by a glutathione S-transferase (GST) pull-down assay in 2008 which helped show that both proteins interact at their N-terminal regions (Binda et al., 2008). Co-expression of Stx1 in hDAT cells has been observed to mediate a decrease in the

maximum velocity or V_{max} of DA transport in both rat striatal tissues and in heterologous expression systems (Cervinski, Foster, & Vaughan, 2010). In another study, Dipace *et al*. demonstrated that Stx1 is a potential mediator of CaMKII's influence on AMPH-induced reverse transport, albeit on the norepinephrine transporter (Dipace, Sung, Binda, Blakely, & Galli, 2007). The Stx1-DAT interactions are demonstrated to increase in response to AMPH applications, as well as play an important role in the regulation of AMPH-induced DA efflux (Binda et al., 2008). Interactions with Stx1 promotes AMPH-induced efflux via the hDAT. Moreover, the activity of the CaMKII mediates the Stx1-DAT association and AMPH-induced efflux, both of which can be negatively modulated through the use of CaMKII inhibitors. These data reveal the complexity of the events surrounding DAT-Stx1 interactions, DAT N-terminal phosphorylation, and subsequent alterations in N-terminal interactions. These molecular underpinnings of Stx1's role in DA efflux are further elucidated in Chapter V.

Membrane Lipids: Studies by Adkins *et al*., and Foster *et al*., have shown that DAT is localized to membrane microdomains that are rich in cholesterol, referred to as "membrane rafts" or "lipid rafts" (Adkins et al., 2007; Foster, Adkins, Lever, & Vaughan, 2008). Membrane rafts can be cholesterol- or sphingolipid-rich microdomains that are specialized for particular cellular functions such as receptor signaling via segregation of specific protein complexes or sequestration. The DAT population in a cell is distributed relatively equally between membrane raft and non-raft domains with raft localization reducing transporter lateral membrane mobility. DAT targeting to rafts is positively correlated with membrane cholesterol content, and requires the palmitoylated membrane raft organizing protein Flot1. Evidence suggests that DAT is localized to cholesterol-rich membrane microdomains, or the above described lipid rafts, upon AMPH actions, with studies by Cremona *et al.* and others indicating that DAT interactions with flotillin-1 is necessary for AMPH-induced DA efflux (Cremona et al., 2011; Jones, Zhen, & Reith, 2012; Pizzo et al., 2013). However, the importance of this interaction in driving efflux-prone conformations remains to be

established. It is not yet known if palmitoylation of DAT plays a role in its raft distribution or interactions with Flot1. Raft partitioning has significant consequences for regulation of DAT, as rafts represent the primary sites of its PKC-stimulated phosphorylation, interactions with Stx1, Rin1, and Flot1, and may represent sites for PKC-stimulated endocytosis. Mistargeting of DAT could thus affect processes such as efflux, down-regulation or internalization that are dependent on these mechanisms (Sakrikar et al., 2012).

Palmitoylation: Palmitoylation is a dynamic and reversible lipid modification that regulates proteins in a manner analogous to the post-translational modification involving reversible phosphorylation of a protein at key amino acid residues (Blaskovic, Blanc, & van der Goot, 2013). The DAT undergoes S-palmitoylation, a posttranslational modification in which C16-saturated palmitic acid is added via a thioester linkage to Cys508 (Foster & Vaughan, 2011). Acute pharmacological inhibition of DAT palmitoylation strongly reduces transport V_{max} and enhances PKC-induced down-regulation without affecting total or surface transporter levels, whereas longer-term inhibition or mutation of Cys508 to an Ala residue leads to enhanced DAT degradation. These findings indicate that palmitoylation functions to promote transporter capacity and oppose both short- and long-term transporter down-regulation (Rastedt, Vaughan, & Foster, 2017). These actions act conversely to those induced by PKC activation. DAT phosphorylation and palmitoylation mutants display reciprocal levels of these modifications (Moritz et al., 2015), indicating that phosphorylation and palmitoylation may define transporter populations possessing opposing levels of uptake activity or metabolic stability. Because overall DAT surface and activity levels would help establish DA tone, it is possible that loss of appropriate DAT palmitoylation and degradation could lead to hypo- or hyper-dopaminergic conditions. The close proximity of Cys580 to the PKC endocytosis motif also suggests the potential for connections between these mechanisms, although this has not yet been investigated.

Dopamine 2 Autoreceptor (D2AR): D2ARs can be isolated in a physical complex with DAT (Lee et al., 2007) as shown by coimmunoprecipitation between the two intact proteins and GST-pulldown assays between the DAT N-terminus and D2AR 3rd intracellular loop. But we still do not entirely know if these complexes are static/constitutive or transient, nor have we ruled out the possibility of populations of uncomplexed D2AR and DAT. The importance of this interaction has been shown to play a role in DAT function as well as surface expression levels. D2AR stimulation has been shown to elevate membrane transporter levels in transfected system, striatal synaptosomes and, as will be demonstrated later, in striatal slices resulting in a subsequent elevation in DAT activity. Conversely, D2AR antagonism in the striatum can inhibit DA clearance suggesting that D2AR establishes a dynamic, ongoing control of DAT activity at DAergic synapses. D2AR has been shown to carry out its actions on the transporter via the kinases, PKCβ and ERK1/2. However, the details of this signaling cascade with regards to what (if any) post-translational modifications to DAT, or changes in interacting partners brought about by the actions of these kinases are yet to be determined. In the soma and dendrites, proximity of D2AR and DAT or potential D2AR-DAT interactions and signaling mechanisms are not completely understood yet; inhibition of DAT can elevate the amplitude and prolong the decay of D2-IPSCs, and inhibit burst firing of DA neurons, presumably through the elevation of extracellular DA levels and concurrent D2AR activation. In the context of DAT-mediated DA efflux, coupling to D2AR via DA agonism at the presynaptic neuron upon DA release *via* the transporter has been shown to negatively regulate TH activity, neuronal excitability and conversely, amplify DAT activity. D2AR carries out these actions via it's downstream signaling through its associated G proteins, G$\alpha_{i/o}$ and G$\beta\gamma$, that inhibit AC activity among various other functions (Figure 3). Of these, most relevant to DA efflux are studies by Garcia-Olivares and colleagues that provided evidence for a G$\beta\gamma$ subunit-dependent mode of DAT-dependent, DA release in transfected cells (J. Garcia-Olivares et al., 2017). The Torres group had shown prior that G$\beta\gamma$ binding to DAT can inhibit DA reuptake

through DAT, and notably observed that stimulation of M5 muscarinic receptors, a $G\alpha_q$-coupled GPCR, induced DA efflux through the transporter (Jennie Garcia-Olivares et al., 2013).

Drosophila as an Animal Model to Study Dopamine Efflux

In addition to mammalian experimental animals such as mice and rats, the fruit fly, *Drosophila melanogaster*, has been shown to be an excellent model organism to study neurological processes *in vivo* through the use of sophisticated genetic techniques (Martín & Alcorta, 2017; Stephenson & Metcalfe, 2013). Furthermore, rapid advancements in genetic techniques for neuronal labeling and activity manipulation are allowing researchers to identify and characterize neuronal circuits that regulate specific behaviors (Figure 10). Since many genes involved in DA dynamics (synthesis, transport, secretion, and metabolism) and signal transduction (receptors and downstream signaling cascades) are conserved between flies and humans, *Drosophila* studies can shed light on the molecular mechanisms underlying DA biology in higher organisms (Ugur, Chen, & Bellen, 2016). In addition, many drugs that target the mammalian DAergic pathway have also been shown to be effective in flies. Pharmacological agents like cocaine that increase extracellular DA levels by blocking reuptake of DA via DAT, and methamphetamine, which increases extracellular DA levels primarily through presynaptic release mechanisms, increase activity and stereotypic behaviors (Berglund et al., 2013; Pizzo et al., 2013; Vickrey, Xiao, & Venton, 2013). Significantly, DA is a key regulator of movement and arousal in the fly (Andretic, van Swinderen, & Greenspan, 2005; Kume, Kume, Park, Hirsh, & Jackson, 2005), behaviors that have been reliably connected with brain DA levels.

DA- and DAT-associated behaviors in *Drosophila*

DA neurons make up a very small percentage of all neurons in the adult *Drosophila* brain – about 200 neurons out of a total 100,000 (Budnik & White, 1988). In spite of their modest numbers, DA neurons project widely and influence several key behaviors. DA has been shown to

play key roles in regulating basal locomotion (Riemensperger et al., 2013) as well as learning and memory (Berry, Cervantes-Sandoval, Nicholas, & Davis, 2012), courtship (S. X. Zhang, Rogulja, & Crickmore, 2016), and addiction (Bainton et al., 2000) in flies. More recently, the involvement of DA in more complex behaviors such as attention (Ye, Xi, Peng, Wang, & Guo, 2004), decision making (K. Zhang, Guo, Peng, Xi, & Guo, 2007), and appetite (Inagaki et al., 2012) have also been discussed. Intensive studies on some of these behaviors in *Drosophila* have led to identification of the responsible DAergic neurons and neuronal circuits.

Pharmacologically induced increases in extracellular DA levels also reduce sleep behaviors in the fly, both total time spent in sleep and in sleep-onset latency (Andretic et al., 2005). As may be expected, loss of DAT function resulting from genetic mutations that lead to increases in extracellular DA also increase activity levels and length of wake time (Kume et al., 2005). Conversely, reduction in DA levels achieved by feeding an inhibitor of DA biosynthesis increased sleep behaviors (Andretic et al., 2005). Interestingly, flies have a response to novel wake-promoting agents like modafinil in a similar manner to humans (Hendricks, Kirk, Panckeri, Miller, & Pack, 2003). High DA levels are associated with increased arousal with respect to mating behaviors in male flies, which demonstrate a reduced latency to courtship. Even though flies with increased DA levels are more aroused, however, they often take longer than controls to actually complete courtship and copulate, which may indicate deficits in attention. In humans, psychostimulants produce similar effects on arousal states and inability to complete mating that may relate to attention problems. DA is also involved in visual processing in the fly. Inactivating DA synaptic release by genetic means alters measured brain activity in the protocerebrum and interferes with the fly's visual tracking ability in a flight simulator (Andretic et al., 2005).

Creating transgenic *Drosophila melanogaster*

In flies, the Gal4-UAS system allows separation and identification of the role of a single gene or protein that is associated with a particular phenotype or behavior. It allows for the knock-

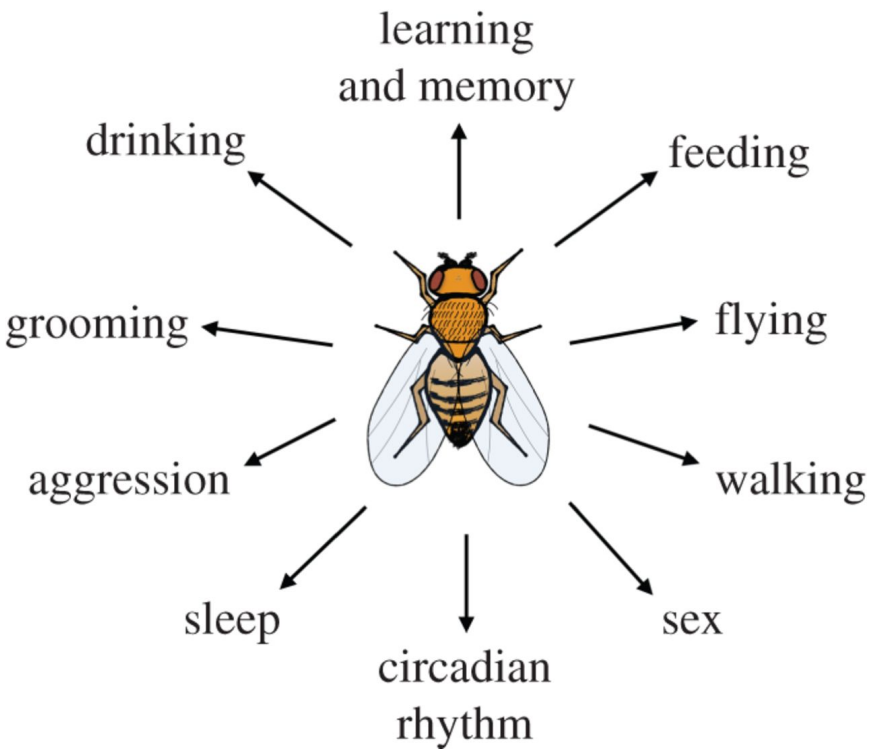

Figure 10: Schematic illustrating some of the many behaviors that have been investigated using fruit fly genetics.

Flies must decide which of the homeostatic behaviors, sleep, feed, drink, mate, fight and groom, to preferentially engage in and which mode of locomotion, walk, jump or fly, to employ to accomplish getting where they need to go. They can also adjust their strategy through learning.

Reference: Owald D, Lin S, Waddell S. Light, heat, action: neural control of fruit fly behaviour. Philos Trans R Soc Lond, B, Biol Sci. 2015;370(1677):20140211.

out or knock-in, overexpression or silencing of candidate genes (Muqit & Feany, 2002) (Figure 11). Gal4 is a modular protein consisting broadly of a DNA-binding domain and an activation domain. The Upstream Activation Sequence (UAS) to which GAL4 binds is CGG-N11-CCG, where N can be any base. Although GAL4 is a yeast protein not normally present in other organisms it has been shown to work as a transcription activator in a variety of organisms such as *Drosophila* and even in human cells, highlighting that the same mechanisms for gene expression have been conserved over the course of evolution. For study in *Drosophila*, the Gal4 gene is placed under the control of a native gene promoter (or driver gene) while the UAS controls expression of a target or reporter gene. Gal4 is then only expressed in cells where the driver gene is usually active. In turn, Gal4 only activates gene transcription where a UAS has been introduced. For example, by fusing a gene encoding a visible marker like GFP (Green Fluorescent Protein) the expression pattern of the driver genes can be determined. The Gal4 and UAS components are very useful for studying gene expression in *Drosophila* as they are not normally present, and their expression does not interfere with other processes in the cell. In the absence of GAL4, the target or reporter gene is inactive. Many cell-type- and developmentally-regulated GAL4 ('driver') lines exist at present and readily available from public stock centers. For example, GAL4/UAS-regulated transgenes in *Drosophila* have been used to alter glial expression to produce arrhythmic behavior in a known rhythmic circadian output called pigment dispersing factor (PDF), and in visualizing cholinergic neurons and neuropiles in the *Drosophila* brain (Salvaterra & Kitamoto, 2001). However, some research has indicated that over-expression of GAL4 in *Drosophila* can have side-effects, probably relating to immune and stress responses to what is essentially an alien protein (Kramer & Staveley, 2003).

Drosophila models now exist for a range of human neuropsychiatric (van Alphen & van Swinderen, 2013) and neurodevelopmental diseases (P. J. Hamilton, Campbell, Sharma, Erreger, Herborg Hansen, et al., 2013; O'Connor et al., 2017; Lowe, Hodge, & Usowicz, 2018), and the stage is set for a comprehensive genetic analysis of pathways that mediate neuronal

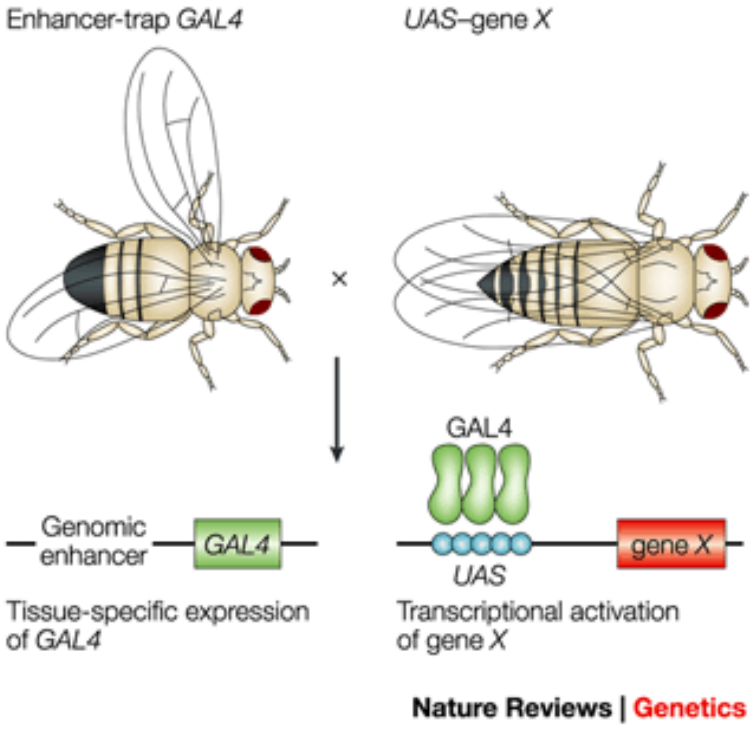

Figure 11: The Gal4-UAS system of engineering transgenic *Drosophila melanogaster*.

Nearly all of the current fly models of neurodegenerative diseases have been made using the GAL4/UAS (upstream activating sequence) system6. This system allows the ectopic expression of a human transgene in a specific tissue or cell type. Two transgenic fly lines are created. In the first (UAS–human-transgene fly), the human disease-related transgene is placed downstream of a UAS activation domain that consists of GAL4-binding sites. GAL4 is a yeast transcriptional activator; in the absence of ectopically expressed GAL4, the transgene is inactive in these transgenic flies. The transgene is activated by crossing these flies to transgenic flies that express GAL4 (enhancer-trap GAL4 fly), also known as the 'drivers'. A wide array of 'driver' flies have been made and characterized. The GAL4 gene is placed downstream of a cell- or tissue-specific promoter. Examples include the pan-neural promoter elav (embryonic lethal, abnormal vision) or the eye-specific promoter GMR (Glass Multimer Reporter). So, the transgene will be activated in the progeny of this cross in a specific cell or tissue type, depending on the 'driver'. This is especially important in studying neurodegenerative diseases, as questions regarding cell-type-specific death can be investigated.

Reference: Muqit MM, Feany MB. Modelling neurodegenerative diseases in *Drosophila*: a fruitful approach?. Nat Rev Neurosci. 2002;3(3):237-43.

degeneration (Feany & Bender, 2000; Prüßing, Voigt, & Schulz, 2013). Modifier screens continue in the polyglutamine models and are also under way in other *Drosophila* models. Identification of new genes that are involved in the pathogenesis of the human diseases will be a key goal of these studies. Mammalian homologues of *Drosophila* modifiers must be studied to verify their roles in human disease. In the long term, the products of these genes might provide valuable drug targets. In addition, homologous loci represent attractive candidates for sequencing in families with inherited forms of neurodegenerative diseases in which the underlying mutation remains unknown. Identifying mutations in familial disease in a gene that was originally isolated as a modifier in a *Drosophila* model would provide a rigorous demonstration of the relevance of the *Drosophila* system to human disease.

Application of *Drosophila* transgenic techniques in the DA system

In our studies, we implement the Gal4-UAS system modified to express hDAT or a variant of hDAT specifically in DAergic neurons, by placing Gal4 expression under the control of a Tyrosine Hydroxylase promoter (P. J. Hamilton, Campbell, Sharma, Erreger, Hansen, et al., 2013a). Doing so enables the expression of the reporter gene (in this case, hDAT) specifically in the DAergic neurons only, without affecting expression patterns in other cell types. Additionally, to eliminate background dDAT function across all our transgenic fly lines, we use dDAT KO or fumin flies, which have no functional DAT expression (Kume et al., 2005). We consistently use this system to study DAT function *ex vivo* (in intact, dissected fly brains) or *in vivo* (by imaging or by behavioral analyses) (P. J. Hamilton, Campbell, Sharma, Erreger, Herborg Hansen, et al., 2013; Peter J. Hamilton et al., 2014; Cartier et al., 2015). We explore a gamut of behaviors in the fly, including basal locomotion, anxiety and fear response, flocking, sexual impetus and courtship.

In the future, we plan not to only create more hDAT variant transgenic fly lines, but also implement the Gal4-UAS system for alterations in regulatory proteins in the DAergic system,

including D2 receptors, Stx1 and kinases associated with DAT. Fly genetics offer us a powerful toolkit to generate new lines in an inexpensive and time-effective fashion.

Chapter II

ZN^{2+} REVERSES FUNCTIONAL DEFICITS IN A *DE NOVO* DOPAMINE TRANSPORTER VARIANT ASSOCIATED WITH AUTISM SPECTRUM DISORDER

The work described in this chapter is part of, and adapted from the published manuscript "Hamilton PJ, Shekar A, Belovich AN, *et al*. Zn^{2+} reverses functional deficits in a *de novo* dopamine transporter variant associated with autism spectrum disorder. *Mol Autism*. 2015;6:8."

Preface

In 2013, Hamilton and colleagues identified and characterized the first *de novo* DAT mutation in a patient diagnosed with ASD, the hDAT T356M. This variant of DAT when expressed in cells showed deficits in transporter DA uptake properties and also, constitutive or anomalous DA efflux, in the absence of AMPH. This variant was especially interesting to us as it showed similar molecular phenotypes as previously characterized disease-associated variants, the hDAT A559V and the hDAT D421N. Anomalous efflux was a common thread that connected mutations in hDAT that were found in patients. The group studying the hDAT T356M variant was interested in understanding the changes in structural motifs in the protein induced by the mutation, in an effort to diagnose the origin of changes in the functional phenotypes of the transporter. Through EPR studies, they demonstrated in the bacterial homolog of hDAT, the leucine transporter, substitution of A289 (the homologous site to T356) with a Met promotes an outward-facing conformation upon substrate binding. This outward-facing conformation of the transporter promotes basal, constitutive efflux of the substrate and enhancement of extrasynaptic DA and associated behaviors. The full-text and details of these findings can be found in the manuscript published in the journal *Molecular Psychiatry* titled "*De novo* mutation in the dopamine transporter

gene associates dopamine dysfunction with autism spectrum disorder" by Hamilton *et al*. in 2013 (P. J. Hamilton, Campbell, Sharma, Erreger, Herborg Hansen, et al., 2013).

A follow-up to this study was to identify methods to reverse the anomalous DA efflux in hDAT T356M, and possibly reverse the hyperactive phenotype in the transgenic organisms expressing this variant. We hypothesized, based on perusing the literature, that the ion Zn^{2+} may have this reversal effect on the hDAT T356M. Studies by Loland et al. in 2002 showed that in the wildtype transporter, Zn^{2+} had the ability to potently inhibit DA uptake by binding to an "inhibitory Zn^{2+} switch" – part of a conserved motif formed by extracellular loops 1 and 3. Moreover, certain mutations that altered the substrate binding regions in the hDAT transformed the inhibitory Zn^{2+} switch to an activating Zn^{2+} switch. As the hDAT T356M variant was known to acquire the outward-facing conformation upon substrate binding, we carried out experiments to understand whether Zn^{2+} binding could switch the conformational state of this variant. Indeed, we were able to partially rescue both the deficits in uptake and reverse transport in the hDAT T356M by testing the effects of Zn^{2+} application in a dose-dependent manner. These studies led to the conclusion that mutations in hDAT that resulted in anomalous efflux can be treated with Zn^{2+} to restore regular function. Following these studies, we hope to apply this finding to other disease-associated variants identified in hDAT that exhibit anomalous DA efflux.

Abstract

Background: Alterations in dopamine (DA) homeostasis may represent a complication associated with autism spectrum disorder (ASD) and related neuropsychiatric conditions. Rare variants of the human dopamine transporter (hDAT) gene (*SLC6A3*) have been associated with a range of neuropsychiatric disorders, including ASD. Our laboratory recently characterized a novel ASD-associated *de novo* missense mutation in *SLC6A3* (hDAT T356M). This hDAT variant exhibits significantly decreased DA uptake, as well as reduced reverse transport of DA. These dysfunctional transport properties may contribute to DA dysfunction in ASD. Previous biophysical

studies have shown that binding of Zn^{2+} to an endogenous hDAT binding site can regulate hDAT functions and conformations.

Findings: hDAT T356M exhibits a profound decrease in DA uptake and reverse transport of DA, despite having comparable levels of surface expression to wild-type hDAT. Here we report that in the hDAT T356M variant, Zn^{2+} enhances both DA uptake (forward transport) and DA efflux (reverse transport). The presence of Zn^{2+} also decreases baseline DA efflux (anomalous dopamine efflux; ADE) characteristic of the hDAT T356M, putatively contributing to Zn^{2+} induced partial recovery of functional deficits in DA uptake and efflux for hDAT T356M.

Conclusions: Engaging a Zn^{2+} activated switch in the conformation of hDAT transporter reverses, at least in part, the functional deficits of ASD-associated hDAT variant T356M. Engaging a Zn2+ activated switch in the conformation of the hDAT transporter reverses, at least in part, the functional deficits of ASD-associated hDAT variant T356M. Our work suggests that the molecular mechanism targeted by Zn2+ to restore partial function in hDAT T356M as a novel therapeutic target to rescue functional deficits in hDAT variants associated with ASD.

Introduction

The dopamine (DA) transporter (DAT) tunes DA neurotransmission by active re-uptake of DA from the synapse (Kristensen et al., 2011). Rare variants (including the first identified *de novo* mutation) in the human DAT (hDAT) have been demonstrated to disrupt DA neurotransmission, contributing to the etiology of a number of neuropsychiatric disorders, including schizophrenia (Seeman & Niznik, 1990), bipolar disorder (Cousins, Butts, & Young, 2009), ADHD (Nora D. Volkow et al., 2007), and autism spectrum disorder (ASD) (Anderson et al., 2008; E. Bowton et al., 2014; Gadow, Roohi, DeVincent, & Hatchwell, 2008; P. J. Hamilton, Campbell, Sharma, Erreger, Herborg Hansen, et al., 2013; Nakamura et al., 2010). Extracellular zinc (Zn^{2+}) inhibits DA uptake (Norregaard, Frederiksen, Nielsen, & Gether, 1998). Three amino acid side chains have been identified in DAT which co-ordinate zinc: H193 in extracellular loop 2 (EL2), H375 in

the first helical part of extracellular loop 4 (EL4A) and E396 in the second helix of extracellular loop 4 (EL4B) (C. J. Loland, Norregaard, & Gether, 1999; Norregaard et al., 1998). Structural data from the DAT-homolog LeuT in the inward- and outward-facing conformation suggests that the relative orientation of H375 and E396 shifts during the transport cycle (Krishnamurthy & Gouaux, 2012).

Our laboratory has recently characterized the first *de novo* mutation in the hDAT reported in a patient diagnosed with ASD, which results in a Thr to Met substitution at site 356 (hDAT T356M) (P. J. Hamilton, Campbell, Sharma, Erreger, Herborg Hansen, et al., 2013). hDAT T356M displays decreased forward and reverse-transport function compared with wild-type hDAT. The reduced transport capacity of the mutant was not associated with a reduction in hDAT surface expression. Amphetamine (AMPH) is a psychostimulant that targets the hDAT causing reverse transport of DA (DA efflux) (David Sulzer et al., 2005). hDAT T356M exhibits impaired AMPH-induced DA efflux. Here we show that the presence of Zn^{2+} partially rescues both the DA uptake and the AMPH-induced DA efflux impairments of hDAT T356M. Zn^{2+} diminishes the anomalous DA efflux property of the hDAT T356M, which might account for its ability to partially rescue transporter functions. Rescue of hDAT function by Zn^{2+} might reveal new molecular mechanism for pharmacological interventions in patients with ASD.

Results

Zn^{2+} enhances [^{3}H]DA uptake in hDAT T356M

CHO cells were transiently transfected with either wild-type hDAT or hDAT T356M. Cells were incubated with 50 nM [^{3}H]DA at 37 ºC for 5 min in the presence of varying concentrations of Zn^{2+}. Consistent with previous reports (Krishnamurthy & Gouaux, 2012; C. J. Loland et al., 1999), Zn^{2+} decreases the DA uptake rate for wild-type hDAT (Figure 12A, filled squares). In contrast, for hDAT T356M cells, Zn^{2+} increases DA uptake, partially reversing the functional deficit of this variant (Figure 12A, open circles).

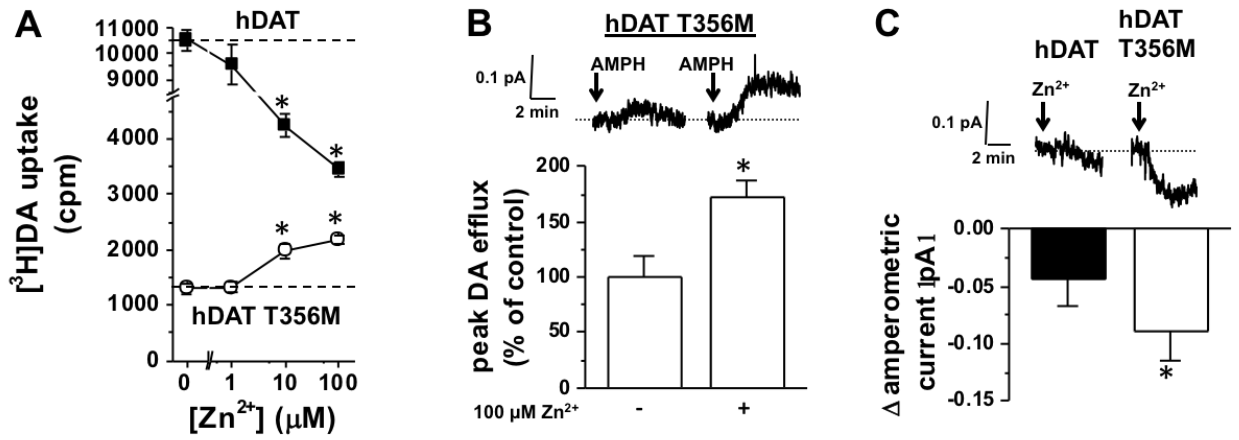

Figure 12: Zn^{2+} partially reverses the hDAT T356M deficits in [^{3}H]DA uptake and amphetamine (AMPH)-mediated efflux.

Methods were as previously described in Hamilton *et al.* [8]. A) [^{3}H]DA uptake counts (cpm) are plotted for hDAT and hDAT T356M over a range of Zn^{2+} concentrations. While Zn^{2+} inhibits hDAT [^{3}H]DA uptake, Zn^{2+} instead increases hDAT T356M [^{3}H]DA uptake (* = $p<0.05$ by one-way ANOVA followed by Dunnett's test compared to 0 Zn^{2+} control; n=4) B) *top* Representative AMPH-induced amperometric currents (reflecting DA efflux) are displayed in the presence or absence of 100 μM Zn^{2+}. Arrows indicate application of 10 μM AMPH. *bottom* Maximal DA efflux amperometric current recorded in the presence of Zn^{2+} normalized to maximal current recorded in the presence of vehicle. (* = $p<0.05$ by paired Student's t-test; n=5). C) *top* Representative Zn^{2+}-induced change in amperometric currents are displayed in response to 100 μM Zn^{2+} or vehicle control. Arrows indicate application of 100 μM Zn^{2+}. *bottom* Change in amperometric current recorded in response to 100 μM Zn^{2+} or vehicle control (* = $p<0.05$ by paired Student's t-test; n=5).

Zn^{2+} enhances AMPH-induced DA efflux in hDAT T356M

To specifically measure reverse transport, DA was loaded into the cytoplasm of hDAT T356M cells by a whole-cell patch clamp pipette held in current-clamp mode. This configuration supplies intracellular DA directly to the cell independent of forward transport by hDAT and allows the cell to control its membrane voltage. The whole-cell patch pipette was filled with an internal solution containing 2 mM DA as described previously (P. J. Hamilton, Campbell, Sharma, Erreger, Herborg Hansen, et al., 2013). DA efflux in response to 10 μM AMPH was measured by amperometry in the presence of 100 μM Zn^{2+} or vehicle control. Representative amperometric traces are shown in Figure 12B (top). The peak of DA efflux normalized to vehicle control is shown in Figure 12B (bottom). Zn^{2+} increases AMPH-induced DA efflux in hDAT T356M compared to vehicle control (Figure 12B), indicating an enhancement of reverse transport DA in the presence of Zn^{2+}. For comparison, Zn^{2+} partially rescues AMPH-induced DA efflux for hDAT T356M to a level of 48 ± 12 % of wild-type hDAT AMPH-induced DA efflux [8].

Zn^{2+} decreases baseline efflux or anomalous DA efflux in hDAT T356M

Using the whole-cell patch clamp technique coupled to amperometry, the effect of 100 μM Zn^{2+} on the baseline (anomalous) DA efflux of hDAT T356M was studied. The whole-cell patch pipette delivered intracellular DA into the cell in current-clamp mode. To determine the effect of Zn^{2+} on baseline DA efflux, the change in amperometric current was compared for application of 100 μM Zn^{2+} or vehicle control. Baseline DA efflux decreased significantly in the presence of Zn^{2+} in comparison with that of vehicle. Representative amperometric traces are shown in Figure 12C (top). The raw values representing peak of DA efflux is shown in Figure 12C (bottom).

Discussion

Here, we explore the potential for Zn^{2+} in rescuing the biophysical abnormalities in the hDAT variant T356M that we recently reported in Hamilton *et al.* 2013 (P. J. Hamilton, Campbell,

Sharma, Erreger, Herborg Hansen, et al., 2013). These functional deficits in hDAT T356M may contribute to the dysfunction in DA neurotransmission associated with ASD. Zn^{2+} was previously shown to partially restore DA uptake function in DAT mutant Y335A, which exhibits low uptake under basal conditions (Kahlig et al., 2006). Here, we demonstrate that Zn^{2+} reverses deficits in both forward and reverse transport in the T356M variant. Additionally, Zn^{2+} decreases baseline anomalous DA efflux of the hDAT T356M *de novo* mutation, possibly providing an explanation for the positive effects of Zn^{2+} on the uptake and efflux properties of this mutant transporter. This is a novel and intriguing finding in terms of ameliorating irregularities in DAT function in a *de novo* ASD-associated mutation.

T356 is located in transmembrane domain 7 and the hDAT Zn^{2+} binding site spans the spatial micro-environment between the transmembrane helices 7, 8 and extracellular loop 2 (EL2) (Claus Juul Loland, Norregaard, Litman, & Gether, 2002; Stockner et al., 2013). Binding of Zn^{2+} to DAT alters the conformational equilibrium between the inward- and outward-facing state of the DAT. However, mutation of an intracellular tyrosine to alanine (Y335A) converts the inhibitory Zn^{2+} switch into an activating Zn^{2+} switch, whereby Zn^{2+} rescues functions of the Y335A mutant transporter (Kahlig et al., 2006; Claus Juul Loland et al., 2002). Therefore the functional impact of Zn^{2+} binding to mutant transporters can be quite different than for wild-type hDAT as we observe here for T356M (Figure 12). Whereas Zn^{2+} has been suggested to promote the outward facing conformation of wild-type hDAT, the structural effect of Zn^{2+} binding to hDAT T356M is unknown and remains an interesting topic for future investigation.

Clinical data have previously established that mean serum Zn^{2+} levels are significantly lower in children diagnosed with ASD compared to unaffected children, and that there exist disturbances in Zn^{2+} metabolism in patients diagnosed with ASD (Faber, Zinn, Kern, & Kingston, 2009; Jackson & Garrod, 1978; Li, Wang, Bjørklund, Zhao, & Yin, 2014). hDAT T356M is the first *de novo* DAT mutation found in a patient with ASD and hDAT T356M functional deficits can partially be rescued by Zn^{2+}. Whether or not Zn^{2+} regulation of hDAT may be directly relevant for

the etiology of ASD is presently unknown. However, our work suggests that the molecular mechanism engaged by Zn^{2+} to partially restore function in hDAT T356M may be a novel therapeutic target to rescue, at least in part, functional deficits in hDAT variants associated with ASD.

Chapter III

ATYPICAL DOPAMINE EFFLUX CAUSED BY 3,4-METHYLENEDIOXYPYROVALERONE (MDPV) VIA THE HUMAN DOPAMINE TRANSPORTER

The work described in this chapter is part of, and adapted from the published manuscript "Shekar A, Aguilar JI, Galli G, *et al*. Atypical dopamine efflux caused by 3,4-methylenedioxypyrovalerone (MDPV) via the human dopamine transporter. *J Chem Neuroanat*. 2017"

Preface

The use and abuse of synthetic cathinone drugs or "bath salts" has become a world-wide health concern. Increasing data has shown that the common bath salts constituent, MDPV, causes many of the deleterious effects arising from consumption of bath salts. Similar to other psychostimulants, including cocaine and amphetamine, MPDV exerts its effects via action on the catecholamine dopamine transporter (DAT). Specifically, recent studies have shown that MDPV acts as a high affinity blocker at the DAT at micromolar-range concentrations and elicits amphetamine-like actions in animal behavioral tasks. Here, we used single cell amperometry to elucidate the mechanism of action of MDPV with high temporal resolution in single cells. Furthermore, we determined the behavioral effects of this drug in a well-characterized animal model of psychostimulant action, *Drosophila melanogaster*. We found that at low concentrations (1 nm), MDPV can cause release or "efflux" of dopamine via the DAT. Additionally, we show that MDPV can cause hyperactivity in *Drosophila*. These experimental paradigms lay the foundation for future studies that can elucidate further the mechanisms of action of bath salts and identify new therapeutics to treat the individuals that abuse them.

Abstract

Synthetic cathinones are similar in chemical structure to amphetamines, and their behavioral effects are associated with enhanced dopaminergic signaling. The past ten years of research on the common constituent of bath salts, MDPV (the synthetic cathinone 3,4-methylenedioxypyrovalerone), has aided the understanding of how synthetic cathinones act at the dopamine (DA) transporter (DAT). Several groups have described the ability of MDPV to block the DAT with high-affinity. In this study, we demonstrate for the first time, a new mode of action of MDPV, namely its ability to promote DAT-mediated DA efflux. Using single cell amperometric assays, we determined that low concentrations of MDPV (1 nM) can cause reverse transport of DA via DAT. Notably, administration of MDPV leads to hyperlocomotion in *Drosophila* melanogaster. These data describe further how MDPV acts at the DAT, possibly paving the way for novel treatment strategies for individuals who abuse bath salts.

Introduction

The neurotransmitter dopamine (DA) mediates behaviors relating to reward, motivation, attention, and cognition (Björklund & Dunnett, 2007b; Iversen & Iversen, 2007). Important to dopamine neurotransmission is the dopamine transporter (DAT). DAT is a presynaptic membrane protein responsible for the reuptake and recycling of DA following vesicular release (Giros & Caron, 1993). Dysfunctions in DAT can lead to dopamine-associated neuropsychiatric disorders including ADHD, autism spectrum disorders, schizophrenia, and bipolar disorder (Gowrishankar, Hahn, & Blakely, 2014). DAT is also the target of commonly abused psychostimulants and controlled substances, namely cocaine and amphetamine (AMPH). Cocaine acts as a high-affinity antagonist of the transporter and blocks DA uptake, whereas AMPH acts as a substrate of the transporter and, through a series of intracellular mechanisms, causes DAT to reverse transport or “efflux” DA into the extracellular space (Schmitt & Reith, 2010). The actions of cocaine and AMPH on the DAT are well-known to play a role in their rewarding properties and abuse potential.

Thus, determining the effects of psychostimulants on DAT function is important for understanding the neural and molecular mechanisms underlying psychostimulant drug action.

In recent years, the abuse of synthetic cathinones or “bath salts” has become a major world-wide health concern (German, Fleckenstein, & Hanson, 2014). These substances are synthetic derivatives of the naturally-occurring stimulant, cathinone, found in the flowering plant *Catha edulis* (Brenneisen, Fisch, Koelbing, Geisshüsler, & Kalix, 1990). The psychoactive effects of synthetic cathinones vary from the cocaine-like stimulant effects seen with 3,4-methylenedioxypyrovalerone (MDPV) (Baumann et al., 2013) to the MDMA-like empathogenic effects of methylone (3,4-methylenedioxymethcathinone). Among a number of identified biological sites, cathinones are known to target proteins that modulate dopamine neurotransmission, increasing dopaminergic signaling and associated behaviors (Bonano, Glennon, De Felice, Banks, & Negus, 2014; Glennon, Yousif, Naiman, & Kalix, 1987; Kehr et al., 2011; King, Wetzell, Rice, & Riley, 2015; Nguyen et al., 2016), including drug-seeking (Lisek et al., 2012; Watterson, Watterson, & Olive, 2013). When consumed in small doses, cathinones can lead to euphoria, alertness, increased libido, and elevated blood pressure. When consumed at higher doses, tremors, seizures, paranoia, violent behavior, psychoses, tachycardia (Borek & Holstege, 2012), delusions/hallucinations (Penders & Gestring, 2011), and death (Wyman et al., 2013) can occur. A recent report released by the Substance Abuse and Mental Health Services Administration (SAMHSA) showed that nearly 23,000 emergency room visits in 2011 were a result of cathinone abuse (SAMHSA 2013 Bath Salts Report). Due to the high risk associated with the use and the abuse potential of these compounds, the Drug Enforcement Administration (DEA) designated mephedrone (4-methylmethcathinone), methylone and MDPV as Schedule 1 substances under the Controlled Substances Act (DEA Drug Fact Sheet on Synthetic Cathinones). Nonetheless, illegal manufacturers continue to circumvent this ban by synthesizing “designer” substances with novel chemical structures, but which produce similar psychostimulant effects[38]. These compounds are readily available and sold with fraudulent

labels such as “plant food”, “research chemicals”, or “bath salts” at gas stations, tobacco stores, and over the Internet with a warning that the contents are not intended for human consumption. Their continued production and availability make it nearly impossible to control the exponentially rising sales and consumption of synthetic cathinones.

Despite increased data regarding the use and abuse of cathinones (Zawilska & Wojcieszak, 2013), little is known about their mechanism of action. To address this issue, several research groups have begun to study the chemistry, pharmacology, and behavioral effects of various synthetic cathinones. Of these, MDPV is most commonly implicated in high-risk use (Borek & Holstege, 2012; Coppola & Mondola, 2012b; Kriikku, Wilhelm, Schwarz, & Rintatalo, 2011; Marusich et al., 2014; Murray, Murphy, & Beuhler, 2012; Ross, Reisfield, Watson, Chronister, & Goldberger, 2012; Wright et al., 2013; Wyman et al., 2013). First synthesized in 1969, MDPV gained popularity much later in 2010 (2014 World Health Organization Critical Review Report on MDPV). As a highly lipophilic analogue of the synthetic cathinone pyrovalerone (Coppola & Mondola, 2012a), MDPV readily crosses the blood-brain barrier. Importantly, MDPV, when administered to animals exhibits striatal distribution, a brain region enriched in DA projections (Novellas et al., 2015). MDPV also shows high abuse potential in animal behavioral tasks (Kehr et al., 2011; King et al., 2015; Novellas et al., 2015; Watterson et al., 2014).

Early research on MDPV demonstrated that this drug acts similarly to cocaine (a known DAT blocker), but with a 10- to 50-fold higher potency (Baumann et al., 2013; Cameron, Kolanos, Solis, Glennon, & De Felice, 2013). However, increasing data suggests that there may be more to the action of MDPV. Work from Baumann et al. showed that after intravenous administration of MDPV, DA levels remain elevated for far longer than after cocaine administration (Baumann et al., 2013). In addition, MDPV administration results in long lasting cross-sensitization in mice, similar to the effects of methamphetamine (Watterson et al., 2013). These results suggest that MDPV, in addition to acting as a DAT blocker, may also display other modes of action. To examine further the molecular actions of MDPV on the DAT, we performed amperometric studies.

Specifically, to obtain greater temporal resolution, we studied MDPV action on human DAT (hDAT) by employing single cell amperometry. This assay has been previously used to discriminate AMPH versus cocaine actions in a single cell and these results have been reproduced in different model systems (Cartier et al., 2015). Further, we assessed MDPV-induced behaviors in *Drosophila melanogaster*, specifically focusing on known DAT-associated behaviors. *Drosophila* is a powerful genetic model for studying behaviors that are associated with DA as well as promoted by psychostimulants (Cartier et al., 2015; P. J. Hamilton, Campbell, Sharma, Erreger, Herborg Hansen, et al., 2013; Peter J. Hamilton et al., 2014), as several genes that regulate DA transport, synthesis, and signaling are conserved between flies and humans (S. Yamamoto & Seto, 2014).

Materials And Methods

Drugs

(±)-3,4-Methylenedioxypyrovalerone HCl (MDPV), was synthesized in racemic form in our laboratories. Chemical and structural analysis included nuclear magnetic resonance spectroscopy, gas- and liquid- chromatography/mass spectrometry, thin layer chromatography, and melting point determination. All data were consistent with the expected structures. All other drugs used in this study including their salt and enantiomeric forms were as follows and purchased from Sigma-Aldrich (St. Louis, MO): Dopamine, d-amphetamine hemisulphate salt and cocaine hydrochloride.

Amperometry

Chinese hamster ovary (CHO) cells stably expressing hDAT (here defined as hDAT cells) were plated at a density of ~20,000 per 35-mm culture dish. To preload cells with DA, dishes were washed with KRH assay buffer (130 mM NaCl, 4.8 mM KCl, 1.2 mM KH2PO4, 25 mM

HEPES, 1.1 mM MgSO42.2 mM CaCl2, pH 7.4) supplemented with 10 mM dextrose, 100 μM pargyline, 1 mM tropolone, and 100 μM ascorbic acid, and incubated with 1 μM DA in KRH assay buffer for 20 minutes at 37 °C. To record DA efflux, a carbon fiber electrode (ProCFE; fiber diameter of 5 μm; obtained from Dagan Corporation) juxtaposed to the plasma membrane and held at +700 mV (a potential greater than the oxidation potential of DA) was used to measure DA flux through oxidation reactions. Amperometric currents in response to the addition of 1 nM MDPV were recorded using an Axopatch 200B amplifier (Molecular Devices, Union City, CA) with a low-pass Bessel filter set at 1 kHz; traces were digitally filtered offline at 1 Hz using Clampex9 software (Molecular Devices, Union City, CA). DA efflux was quantified as the peak value of the amperometric current.

Drosophila melanogaster behavior

To measure the locomotor response to MDPV we used the TriKinetics *Drosophila* Activity Monitoring (DAM) system. Wild-type Oregon-R male flies were entrained for seven days in 12:12 h light:dark (LD) cycles at 25 °C on standard cornmeal-molasses medium. On day two, flies were transferred individually to activity tubes and acclimated for a period of five days. On day seven, flies were transferred into identical activity tubes containing 20 μM MDPV or vehicle (water) in standard medium. Flies were continuously monitored for movement using activity monitors (DAM5, Trikinetics). Activity was measured as the number of times a fly crossed the infrared beam (beam crosses) per 30 min. Activity data was recorded for six hours after drug administration. Change in activity in response to drug treatment was reported as beam crosses normalized to average beam crosses 30 min prior to drug administration.

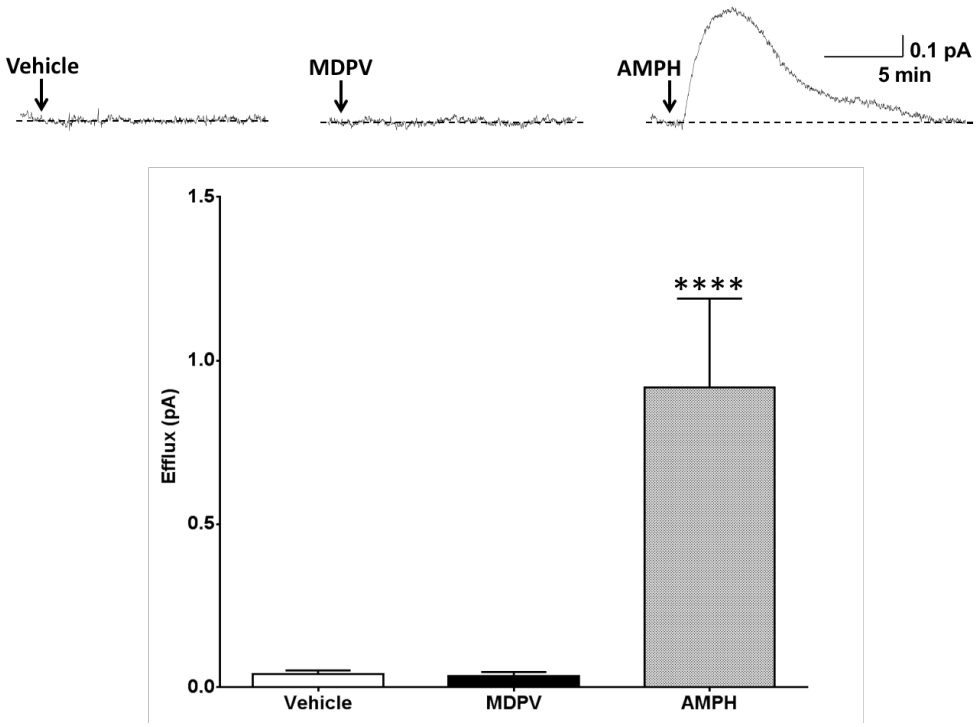

Figure 13: MDPV (1 nM) does not elicit an amperometric current in the absence of hDAT cells.

Top: Representative amperometric traces recorded from hDAT cells in response to application of vehicle to (Vehicle), application of 1 nM MDPV to bath in the absence of hDAT cells (MDPV), or application of 10 μM AMPH to hDAT cells (AMPH). Bottom: Quantitation of the peak amperometric current amplitude measured after vehicle or drug treatment (**** = $p < 0.0001$ by One-way ANOVA with Dunnett's multiple comparisons post-hoc analysis; n = 5–6).

Results

1 nM MDPV alone does not produce an amperometric signal

As a first control experiment, we demonstrated that hDAT cells pre-loaded with DA (see Methods Section) did not release DA upon application of vehicle (Fig. 13, Vehicle). Next, we tested whether MDPV alone reacts at the carbon fiber electrode. At concentrations as low as 1 nM, MDPV did not elicit any amperometric current when applied to a bath chamber in the absence of hDAT cells (Fig. 13, MDPV). Finally, to demonstrate that we can record DA efflux with our amperometric electrode, we show that bath application of 10 μM AMPH causes a robust DA efflux in the presence of hDAT cells (Fig. 13, AMPH). We have previously shown that this AMPH-induced DA efflux is mediated by the hDAT and is cocaine-sensitive (Mazei-Robison et al., 2008). These control experiments were conducted to ensure that amperometry is a suitable technique to elucidate the actions of MDPV in terms of DA efflux and that MDPV at a concentration of 1 nM does not produce a non-specific amperometric signal.

New mode of action of MDPV

24 h after plating, hDAT cells were preloaded with DA (see methods). Amperometric measurements were taken from individual hDAT cells after application of a low concentration of MDPV (1 nM) or cocaine (10 μM). As expected, 10 μM cocaine did not cause DA efflux as reflected by a lack of an upward deflection of the amperometric trace (Figure 14, cocaine). These data are in agreement with previously published studies (P. J. Hamilton, Campbell, Sharma, Erreger, Herborg Hansen, et al., 2013; Mazei-Robison et al., 2008) and also establishes that there is no anomalous dopamine efflux or “leak” associated with the transporter in this *in vitro* system, as previously shown. Surprisingly, and in contrast to the effects of cocaine, amperometric traces recorded in response to 1 nM MDPV show a clear upward deflection of the amperometric current. This upward deflection reflects DAT-mediated DA efflux (Figure 14, MDPV). In hDAT cells, the

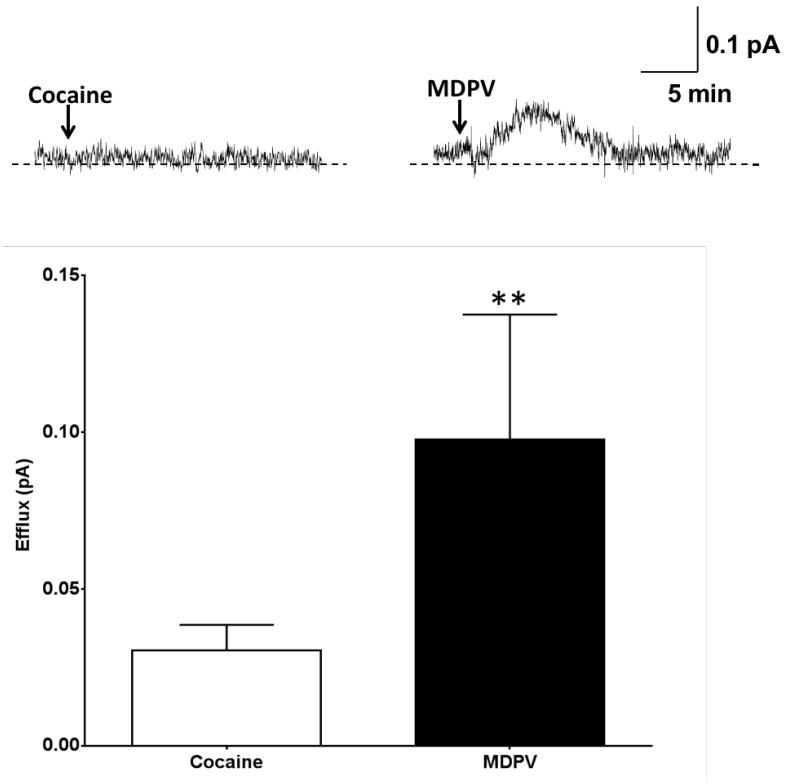

Figure 14: MDPV, but not cocaine, induces reverse transport of DA via hDAT.

Top: Representative amperometric traces recorded in response to 10 μM cocaine or 1 nM MDPV in hDAT cells. Bottom: Quantitation of DA efflux measured as peak amplitude of the amperometric current after drug or vehicle treatment (** = $p < 0.01$ by Student's t-test; n = 5–8).

peak amperometric responses for MDPV were smaller than those recorded for AMPH (positive controls; compare Figure 13 (AMPH) to Figure 14 (MDPV)).

MDPV causes hyperlocomotion in flies

Building on our *in vitro* findings, we examined MDPV's role in modifying DA-associated behaviors in *Drosophila melanogaster*. Wildtype flies were placed in locomotion chambers and acclimated for a period of five days. 20 μM MDPV or vehicle was administered orally via voluntary consumption. Locomotion was quantified as average beam crosses per 30 min normalized to pre-treatment conditions. Flies administered MDPV (n = 16) show an elevated rate of locomotion compared to those administered vehicle (n = 15) (Figure 15, left). Cumulative beam breaks over a period of 6 hours show a greater than two-fold increase in locomotion in flies administered MDPV compared to vehicle (Figure 15, right).

Discussion

DA homeostasis in the CNS is essential to regulating important brain functions, including reward. Synthetic cathinones disrupt normal dopaminergic neurotransmission and thus affect DA-associated behaviors. These drugs elicit behaviors indicative of enhanced dopaminergic signaling. The past ten years of research on MDPV and other synthetic cathinones demonstrate that the rewarding properties of synthetic cathinones are derived, in part, from their actions on monoamine transporters (Eshleman et al., 2013; Kolanos, Solis, Sakloth, De Felice, & Glennon, 2013). Understanding how MDPV disrupts normal DA neurotransmission via its actions on the DAT is essential to the development of novel treatment options that can restore normal DA homeostasis in individuals who abuse MDPV and other synthetic cathinones. In this study, we aimed at revealing new modes of action by which MDPV causes an elevation in extracellular DA levels, and the behavioral consequences of its actions on DAT.

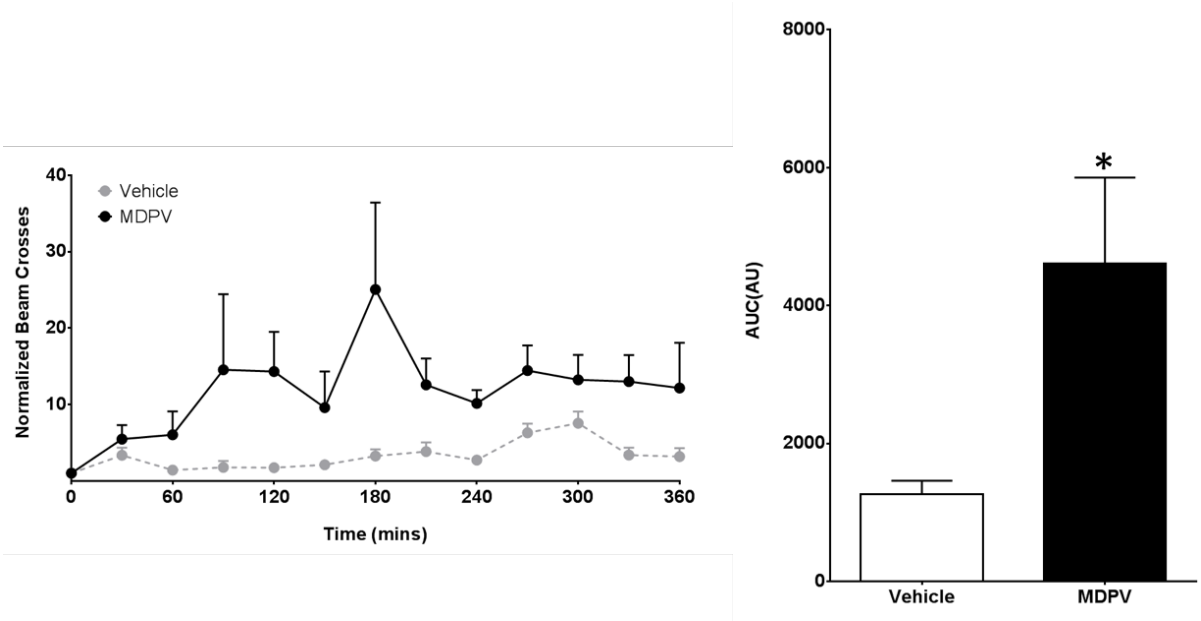

Figure 15: MDPV induces hyperlocomotion in flies.

Left: Locomotion was measured by average beam crosses following 20 μM MDPV (n = 16) or vehicle (n = 15) administration. Beam crosses were normalized to pre-treatment conditions for each fly. Right: Cumulative beam breaks were quantified for up to six hours post drug or vehicle administration. Flies exposed to MDPV displayed an increase in cumulative bream breaks compared to vehicle-controls (* = $p < 0.05$ by Student's t-test; n = 15–16).

Using single cell amperometry we reveal that low concentrations of MDPV (1 nM) cause reverse transport of DA via DAT. Amperometry is a well-established paradigm that has been used by our group and others in several studies to determine different aspects of monoamine release mediated by catecholamine transporters (Cartier et al., 2015; P. J. Hamilton, Campbell, Sharma, Erreger, Herborg Hansen, et al., 2013; Peter J. Hamilton et al., 2014, p. 2; Claus Juul Loland et al., 2002). We first established that this assay is suitable for studying reverse transport of DA mediated by MDPV. We conducted an initial characterization of MDPV to demonstrate that at low concentrations, MDPV does not interact with the carbon fiber electrode to produce an artificial signal. Next, we demonstrated that in hDAT cells, MDPV (1 nM) causes reverse transport of DA mediated by hDAT. To note is that higher concentrations of MDPV, such as 100 nM, produced a non-specific amperometric signal (i.e. an amperometric current is recorded with MDPV in the absence of hDAT cells). These data describe for the first time a novel mode of action of MDPV at the DAT. Interestingly and importantly, previous work with hDAT has shown that higher concentrations of MDPV can block DAT function (20–30 nM). Taken together, these data suggest that MDPV might have multiple modes of action that are concentration-dependent, where at low concentrations MDPV works to cause DAT reverse transport, and at high concentrations MDPV primarily causes DAT blockade.

Drosophila melanogaster has been used as a model organism to study the behavioral consequences of newly discovered molecular mechanisms of AMPH and cocaine[55]. In *Drosophila*, locomotion requires functional DA neurotransmission. Therefore, to understand the significance of the actions of MDPV in vivo, in terms of changes in extracellular DA levels, we used flies as a behavioral model. Here, we show that MDPV administration leads to hyperlocomotion in *Drosophila melanogaster*. These data point to *Drosophila melanogaster* as a suitable animal model to further characterize in vivo the multiple actions of MDPV at the hDAT. This increase in locomotor activity has been previously documented to be associated with an

increase in extracellular DA promoted by DAT blockers (e.g. cocaine) as well as DA effluxers (e.g. AMPH).

In this study, we did not determine whether the increase in *Drosophila* locomotor activity is driven by the ability of MDPV to block the hDAT, to cause DA efflux, or both. In the near future, we aim to explore these different possibilities by generating flies that are insensitive to the ability of MDPV to cause DA efflux as we have already done for AMPH (Cartier et al., 2015; Peter J. Hamilton et al., 2014).

Further studying the different mode of actions of MDPV and other synthetic cathinone drugs as well as their specific behavioral consequences will not only pave the way toward better treatment strategies for those who abuse them, but also lead to better recognition and prediction of the dangers posed by novel designer cathinones that are emerging in the market today.

Chapter IV

STRUCTURAL, FUNCTIONAL, AND BEHAVIORAL INSIGHTS OF DOPAMINE DYSFUNCTION REVEALED BY A DELETION IN *SLC6A3*

The work described in this chapter is part of and adapted from the manuscript under review at the Proceedings of the National Academy of Sciences (PNAS) "Campbell N.G. and Shekar A. *et al*. Structural, Function and Behavioral Insights of Dopamine Dysfunction Revealed by a Deletion in *SLC6A3*."

Preface

For over a decade, our group has conducted in-depth studies on rare variants in the human DAT (hDAT) that contribute to the etiology of a number of neuropsychiatric disorders, including schizophrenia, bipolar disorder, ADHD and more recently, in ASD. These variants have been demonstrated to exhibit changes in transporter properties, disrupt DA neurotransmission, resulting in altered DAergic behaviors as a major consequence. As hDAT plays an important role in tuning DA neurotransmission by active re-uptake of DA from the synapse, we hope to understand the etiology of dysfunction in naturally-occurring transporter variants, in an effort to identify therapeutic opportunities to reverse the dysfunction. In this chapter, we explore the changes in transporter biophysics and the behavioral consequences of a novel hDAT variant, comprising an in-frame deletion of asparagine at position 336 in the 3rd intracellular loop region (ΔN336). Transient transfection of wildtype and ΔN336 hDAT DNA in heterologous cell lines showed that DA uptake in the hDAT ΔN336 is completely ablated (as compared to wildtype DAT uptake). The loss in transport capacity of the variant hDAT was not associated with a reduction in hDAT surface expression. hDAT ΔN336 exhibits partially impaired efflux in response to amphetamine (AMPH, a psychostimulant that targets the hDAT causing reverse transport of DA)

compared to wildtype hDAT. These findings signify that the residue N336 is key in the coordination of DA uptake, but does not play a pivotal role in the coordination of reverse transport.

Importantly, the discoveries made *in vitro* correlated to the findings from structural analyses and *in vivo* and *ex situ* studies. Excised brains from transgenic *Drosophila melanogaster* expressing wildtype or ΔN336 hDAT specifically in dopaminergic neurons showed a complete loss in DA uptake, with only a partial loss in AMPH-induced efflux. DA-associated behaviors like locomotion and circadian rhythm were elevated in the ΔN336 variant, to signify the increase in extracellular DA in the brains of these transgenic flies. Finally, Electron Paramagnetic Resolution (EPR), crystallography and *in silico* modeling studies (in collaboration with the Mchaourab, Gouaux and Meiler Laboratories respectively) elucidated that the ΔN336 variant is restricted to a half-open inward facing (HOIF), explaining the deficits transporter properties. Taken together, our findings demonstrate that the hDAT ΔN336 has aberrant transporter function which may lead to alterations in DA homeostasis and DA–associated behaviors, and confer risk for ASD in the individuals harboring the mutation. The next step in this project is to create transgenic mice harboring this mutation in their DAT, and conduct biochemical and behavioral analyses on these animals. These studies will be conducted by future graduate students in the Galli Laboratory.

Summary

The human dopamine (DA) transporter (hDAT) mediates clearance of DA. Genetic variants in hDAT have been associated to DA dysfunction, a complication associated to several brain disorders including autism spectrum disorder (ASD). We investigated the structural and behavioral bases of an ASD-associated in-frame deletion in hDAT at N336. We uncovered a previously unobserved conformation of the intracellular gate of the transporter promoted by a deletion variant, representing likely the rate limiting step of the transport process. It is defined by a “half-open and inward facing” state (HOIF) of the intracellular gate that is stabilized by a network of interactions conserved phylogenetically, as we demonstrated it both in hDAT and in its bacterial

homolog leucine transporter. The HOIF state is associated with both DA dysfunctions demonstrated in isolated brains of *Drosophila melanogaster* expressing hDAT ΔN336 and with abnormal behaviors observed at high-time resolution. These flies display increased fear, impaired social interactions, and locomotion traits we associate with DA dysfunction and the HOIF state. Here, we describe how a genetic variation causes DA dysfunction and abnormal behaviors by promoting a HOIF state of the transporter.

Introduction

Dopamine (DA), a monoamine neurotransmitter, plays an important role in the CNS by regulating a variety of functions including cognition, emotion, motor activity, and motivation. Altered dopaminergic signaling is linked to multiple neuropsychiatric disorders such as attention deficit hyperactive disorder (ADHD), mood disorders, schizophrenia, and more recently autism spectrum disorder (ASD) (Cartier et al., 2015; Peter J. Hamilton et al., 2014; E. Bowton et al., 2014). The DA transporter (DAT), a presynaptic transmembrane Na^+/Cl^- symporter, acts by regulating duration of the dopaminergic response by reuptake of released DA. DAT is the primary target site for several psychostimulant drugs, including amphetamine (AMPH) (Koob & Bloom, 1988). AMPH promotes DAT-mediated DA efflux by inducing human DAT (hDAT) N-terminus post-translational modifications (i.e. phosphorylation), a process regulated by the interactions of the N-terminus DAT with the plasma membrane phosphatidylinositol 4,5- bisphosphate (Peter J. Hamilton et al., 2014).

Research into the structural dynamics of DAT suggests that it follows an alternating access model (Forrest et al., 2008; Krishnamurthy & Gouaux, 2012; Kazmier et al., 2014), wherein the transporter can alternate between an “outward-facing” and an “inward- facing” state. This mechanism is defined by an extracellular as well as an intracellular gate, the latter known to regulate transport cycle and conformational stability through rearrangements of several structural

elements, including the third intracellular loop (IL3), the amino N-terminus, and multiple transmembrane helices (Khelashvili, Stanley, et al., 2015).

ASD is a single condition that comprises a heterogeneous group of developmental disorders manifested by impairments across two core domains: deficits in social communication and interaction, and patterns of restricted behaviors, interests and activities (American Psychiatric Association DSM-5 Task Force., 2013). While the causes of ASD are unknown, genetic variants are established as important factors in risk. Analysis of rare variants have provided insight into multiple pathways and systems affected in ASD, and have implicated copy-number variations (CNVs), loss-of-function mutations, and *de novo* missense mutations as contributing factors (De Rubeis et al., 2014; Sanders et al., 2011).

Here, we undertook a closer examination of the structural and functional significance of a rare in-frame deletion of residue N336 in hDAT identified in an ASD patient. The functional perturbations that stem from ΔN336 provided an opportunity to obtain X-ray crystallographic insights as well as molecular dynamics details into the role of DAT structural domains controlling DA transport. They suggest that the two gates of neurotransmitter transporters can act independently during the transport process and be uncoupled by rare variants. Moreover, these finding have implications of how the DAT and other biogenic amine transporters can operate in an efflux mode (i.e. under the influence of AMPH). They also define how disruption of specific gate conformations of DAT translate into abnormal brain DA function and atypical complex animal behaviors in flies, such as social interactions and fear response.

Materials And Methods

Subjects and clinical assessment

Subjects from this ASD family were recruited by the Autism Simon Simplex Collection as described previously (Fischbach and Lord, 2010). The proband was evaluated for ASD with the

Autism Diagnostic Interview-Revised (ADI- R) and the Autism Diagnostic Observation Schedule (ADOS), and a battery of behavioral and cognitive tests to characterize phenotype. Additional measures captured sub-clinical ASD-related traits in parents and unaffected siblings, and a comprehensive family medical history was obtained.

hDAT ΔN336 identification

Exome capture, sequencing, data processing, and variant calling were conducted as described previously (O'Roak et al., 2012). The ΔN336 variant was validated and inheritance patterns determined by PCR and Sanger sequencing of all family members. Amplifying primers were designed using Primer3 and subjected to a BLAST-like alignment tool search to ensure specificity. PCR was carried out using 7.1 nmol of amplifying primers and 12 ng genomic DNA in a final volume of 20 µl. Sequence analysis was performed using Sequencher v5.0.1 (Gene Codes).

Electron Paramagnetic Resonance (EPR) protocol

Cysteine residues were introduced using site directed mutagenesis into LeuT, LeuT ΔV269, and LeuT V269N constructs. Experiments were conducted as in Claxton *et al*. (Claxton et al., 2010). In figures 17 and 24, apo refers to Na^+ and leucine-free transporter, while the +Na/Leu state was obtained by addition of 200 mM NaCl and 4-fold molar excess of Leu relative to LeuT. Double Electron Electron Resonance (DEER) (Jeschke & Polyhach, 2007) was performed at 83K on a Bruker 580 pulsed EPR spectrometer operating at Q-band frequency using a standard 4-pulse sequence (Zou & McHaourab, 2010). DEER echo decays were analyzed to obtain distance distributions.

Purification, crystallization, and structure determination

The purification and crystallization of LeuT ΔV269 was performed as previously reported (Singh, Yamashita, & Gouaux, 2007; Yamashita et al., 2005). Briefly, the plasmid encoding *A. aeolicus* LeuT ΔV269 was transformed into E. coli C41 electrocompetent cells. The transformed cells expressing LeuT ΔV269 were grown in large quantities in Terrific Broth to an absorbance at 600 nm of 0.8. The culture was then induced using 0.1 mM isopropyl-β-D- thiogalactopyranoside and was incubated on a shaker for 20 h at 20°C. The cell membranes were harvested from the bacterial culture by sonication followed by centrifugation. The harvested membranes were solubilized using a buffer containing 20 mM Tris-HCl, pH 8.0, 200 mM NaCl, 40 mM DDM, and 5 mM leucine. LeuT ΔV269 was purified from this solubilized material using metal affinity chromatozgraphy. The partially purified protein was subjected to thrombin digestion overnight to remove the affinity tag. The protein sample was further purified and exchanged into the crystallization buffer (50 mM Tris-HCl, pH 8.0, 150 mM NaCl, 40 mM β-OG, and 5 mM leucine) by size exclusion chromatography. The purified protein was concentrated up to 4 mg/mL in presence of 10% glycerol and 10 μM phospholipids.

Crystallization attempts were performed with the purified protein using the 96 well hanging drop vapor diffusion method at 20°C. The diffraction data was collected at the Advanced Light Source (Lawrence Berkeley National Laboratory, beamline 5.0.2) using a crystal that was grown in the condition containing 10% PEG 3000, 100 mM sodium cacodylate trihydrate, pH 6.5, and 200 mM magnesium chloride hexahydrate. The diffraction data was indexed, integrated, and scaled using the microdiffraction assembly method in the XDS program (Kabsch, 2010). The structure was determined at 2.6 Å in the C2 space group by the molecular replacement method using the program Phaser from the Phenix software suite. The LeuT structures available in several different conformations were used individually as a search model in the molecular replacement method (Krishnamurthy & Gouaux, 2012; Malinauskaite et al., 2016; H. Wang, Elferich, & Gouaux, 2012). The best solution was obtained using LeuT in the outward facing-occluded conformation (PDB ID 2Q72) (Supplemental Table 1). The region comprising the V269

deletion in the model was manually built using Coot (Emsley, Lohkamp, Scott, & Cowtan, 2010). The structure was refined to reasonable R-factors using Phenix Refine. The data collection, model building, and refinement statistics are tabulated in Supplemental Table 2.

Rosetta molecular modeling

Structural models for hDAT and hDAT ΔN336 were created in parallel using the Rosetta molecular modeling suite (revision 57712, Rosetta Commons). Models were generated based on the hDAT sequence and the *Drosophila melanogaster* DAT (PDB ID 4XP9) as a structural template. The sequence identity was 55% percent. The sequence was threaded onto the template based on a sequence alignment generated by ClustalW2. Backbone coordinated in gap regions were reconstructed using the cyclic coordinate decent (CCD) algorithm and refined with the kinematic loop closure (KIC) algorithm and Rosetta Membrane. 1,000 models were generated. The model for analysis is the best scoring model by the Rosetta Membrane energy function that had a root mean-squared deviation (RMSD) to the template of less than 1 Å. The Rosetta energies for hDAT and hDAT ΔN336 were normalized, and the per- residue differences between hDAT and hDAT ΔN336 were calculated. These energy differences were mapped onto the structural models, and PyMOL visualization revealed sites where the energy difference was the greatest.

Homology modeling and fine-grained simulations

We created 250 homology models of the transmembrane domain of hDAT (residues 60 to 603) based upon the outward- open crystal structure of the *Drosophila melanogaster* dopamine transporter (dDAT) (PDB ID 4XP1) (K. H. Wang, Penmatsa, & Gouaux, 2015b) using MODELLER v.9.16 following the procedure described in Buchmayer *et al*. (Buchmayer et al., 2013). The models contained 2 Na+ and 1 Cl- ions in their respective putative binding sites, and a single DA molecule in the central binding site, as observed in the dDAT crystal structure. A previously modeled extracellular loop 2 (EL2) (Baumann et al., 2014) was introduced as a replacement for

the crystal structure EL2, due to extensive crystallographic contacts between the EL2 and the co-crystallized antibody, as well as the truncation introduced in the dDAT EL2 sequence for crystallization. The deletion at residue 336 in the hDAT sequence was introduced either as a single deletion of N336 or a deletion of N336 followed by moving K337 to the previous 336 position. The resulting ΔN336 hDAT sequence is the same in each model, but TM6 is shorter by one residue in the former models, while IL2 is shorter by one residue in the latter. The 250 models were scored and sorted by their discrete optimized protein energy (DOPE) score. The best 20 being ranked by their root mean-squared deviation (RMSD) of the Cα atoms from the template, secondary ranking of side chain RMSD to the template. The three models with the lowest Cα atoms RMSD to template were inserted into a pre- equilibrated 1-palmitoyl-2-oleoyl-sn-glycero-3-phosphocholine (POPC) membrane bilayer using the membed procedure (Wolf, Hoefling, Aponte-Santamaría, Grubmüller, & Groenhof, 2010). The lipids are described by the Berger parameters (Berger, Edholm, & Jähnig, 1997), the protein described by the AMBER99sb-ildn forcefield (Lindorff-Larsen et al., 2010), dopamine described by the GAFF (J. Wang, Wolf, Caldwell, Kollman, & Case, 2004) parameters and RESP charges. Simulation was performed with GROMACS version 5.1.2. The inserted systems were equilibrated by restraining the protein with 1000, 100, 10 and 1 kJ mol-1 nm-2 restraints, each for 2.5 ns. The equilibrated systems were then put into production and run for 150 ns per model. The temperature was maintained at 310 K using a v-rescale thermostat, and the pressure was maintained semiisotropically with Parrinello-Rahman pressure coupling at 1 bar. The pressure coupling time constant was set to 20 ps and the compressibility to 4.5x10-5 bar-1. Long- range electrostatic interactions were represented with a particle mesh Ewald method (1 nm cutoff) and Van der Waals interactions were imposed utilizing a Lennard Jones potential with a 1 nm cutoff.

Cell culture

The hDAT-pCIHygro and hDAT-pEGFP expression vectors were engineered to contain hDAT, hDAT ΔN336, or hDAT N336V sequence. Vector sequences were confirmed via Sanger sequence to ensure no off-target mutations were generated. Vector DNA was transiently transfected into cells. hDAT expression vectors contained green fluorescence protein (GFP) for cell selection. Fugene-6 (Promega) in serum free media was used to transfect chinese hamster ovary (CHO) cells approximately 24 h after plating using a 1:3 DNA:lipid ratio. Cells were maintained in a 5% CO2 incubator at 37°C in Ham's F-12 medium supplemented with 10% fetal bovine serum (FBS), 1 mM L- glutamine, 100 U/mL penicillin, and 100 µg/mL streptomycin. Assays were conducted 24-48 h after transfection.

[^{3}H]DA uptake

Saturation kinetics of [^{3}H]DA uptake was performed as described previously (P. J. Hamilton, Campbell, Sharma, Erreger, Herborg Hansen, et al., 2013). DAT-dependent DA uptake was determined using a range of concentrations (10 nM-10 µM) of a mixture of [^{3}H]DA and unlabeled DA. Forty-eight hours prior to each uptake assay, hDAT, hDAT ΔN336, or hDAT V336N cells were seeded (50,000 cells per well) into 24-well plates. Preceding each uptake experiments, cells were washed in KRH buffer (25 mM HEPES, 120 mM NaCl, 5 mM KCl, 1.2 mM CaCl2 and 1.2 mM MgSO4 supplemented with 5 mM d-glucose, 100 µM ascorbic acid, 1 mM tropolone, and 100 µM pargyline, pH 7.4). DA uptake was terminated after 10 min by washing twice in ice-cold KRH buffer. Scintillation fluid was added and concentrations were quantified in a microplate liquid scintillation counter. Non-specific binding was calculated in the presence of 10 µM cocaine.

For each data point in the uptake assays in whole *Drosophila* brain, four brains were dissected and placed in 1 mL Schneider's *Drosophila* Medium with 1.5% BSA. Brains were placed in a 12 µm pore standing well containing 1.4 mL HL3 with 1.5% BSA per well. Brains were removed and treated with 50 µM cocaine or vehicle, and incubated for 10 min. Brains were again removed, allowed for excess solution to drain, and incubated for 15 min in 0.7 mL HL3 with 1.5% BSA

containing 200 nM [^{3}H]DA. Brains were washed with KRH and placed in 100 µL of 0.1% SDS solution in a top count plate. Scintillation fluid was added and [^{3}H]DA measured. Km and Vmax values were determined in all experiments by nonlinear regression using GraphPad Prism 4.0 (GraphPad Software).

Cell surface biotinylation and immunoblotting

Cell surface biotinylation and immunoblotting experiments were performed as described previously (P. J. Hamilton, Campbell, Sharma, Erreger, Herborg Hansen, et al., 2013). Cells were seeded in 6-well plates (10^6 cells/well) and transfected for 24-48 h prior to assaying. For each experiment, cells were incubated with sulfo-NHS-S-S-biotin (Pierce Chemical Company; Rockford, IL) to label surface-localized transporter. Biotinylated protein was pulled down using streptavidin-coupled beads. Protein was separated via SDS-PAGE and immunoblotting performed using an anti-DAT monoclonal antibody at 1:1000 (#MAB369, Millipore; Billerica, MA), β-actin antibody used at 1:5000 (#A5441, Sigma-Aldrich; St. Louis, MO), and goat-anti-rat-HRP-conjugated secondary antibody used at 1:5000 (#sc-2006, Santa Cruz Biotechnology). ECL substrate (#170-5061, Bio- Rad) was used for chemiluminescence detection. Protein quantification was performed on an ImageQuant LAS4000 imager (GE Healthcare Life Sciences), and analyzed using image J.

Amperometry and patch-clamp electrophysiology

Cells were plated at a density of ~20,000 per 35-mm culture dish. To intracellularly load DA, a programmable puller (model P-2000 Sutter Instruments) was used to fabricate quartz recording pipettes with a resistance of 3-5 mΩ. Pipettes were filled with 2 mM DA in an internal solution containing 120 mM KCl, 10 mM HEPES, 0.1 mM CaCl2, 2 mM MgCl2, 1.1 mM EGTA, 30 mM dextrose adjusted to pH 7.35 and 275 mOsm. Upon gaining access to the cells, the internal solution was allowed to diffuse into the cell for 10 min. To record DA efflux, a carbon fiber

electrode was juxtaposed to the plasma membrane and held at +700 mV (a potential greater than the oxidation potential of DA). Amperometric current was calculated in response to the 10 μM AMPH addition using an Axopatch 200B amplifier and pCLAMP software (Molecular Devices). DA efflux was quantified as the peak value of the amperometric current.

Male flies of the appropriate genotype (5 males, 1-3 day old) were selected and treated with standard food supplemented with vehicle (5 mM ascorbic acid and 10 mM sucrose) or L-3,4-dihydroxyphenylalanine (L-DOPA) (5 mM). After 24 h, whole brains were manually removed and placed in a mesh holder in Lub's external solution (130 mM NaCl, 10 mM HEPES, 1.5 mM CaCl2, 0.5 mM MgSO4, 1.3 mM KH2PO4, 34 mM dextrose, adjusted to pH 7.35 and 300 mOsm). A carbon fiber electrode was held at +700 mV and positioned in the TH-positive PPL1 DA neuronal region. Amperometric current was calculated in response to 20 μM AMPH addition using an Axopatch 200B amplifier and pCLAMP software (Molecular Devices). DA efflux was quantified as the peak value of the amperometric current.

Steady state currents and current-voltage relationships

Cells were cultured on 12 mm round glass coverslips (CS-12R, Warner) for 24-48 h prior to recording. Patch-clamp recordings were performed using an Axopatch 200B amplifier and currents were acquired using pCLAMP software. Rapid application of 10 μM AMPH was achieved by a piezoelectric translator (PZ-150M, Burleigh) moving a theta glass (#1407201, Hilgenberg) with vehicle solution flowing continuously through one barrel and AMPH solution through the other barrel. The piezoelectric translator was driven through the pCLAMP software with a voltage step (5-10 ms) filtered at 25-250 Hz. Current traces plotted in all figures represent the mean current for at least 10 sweeps.

Drosophila genetics

Drosophila homozygotes for the DAT null allele DATfmn (dDAT KO) (Kume et al., 2005) and flies harboring TH-Gal4 (Friggi-Grelin et al., 2003) were outcrossed to a control line (Bloomington Indiana (BI) 6326) and selected by PCR or eye color. TH-GAL4 (BI 8848) and M{vas-int.Dm}ZH-2A, M{3xP3-RFP.attP'} ZH-22A (BI 24481) were obtained from the BI stock center and outcrossed to dDAT KO flies carrying the white (w1118) mutation (BI stock number 6236) for 5 - 10 generations. Transgenes (hDAT or hDAT ΔN336) were cloned into pBI-UASC (J.-W. Wang, Beck, & McCabe, 2012) and constructs were injected into embryos from M{vas-int.Dm}ZH-2A, M{3xP3-RFP.attP'}ZH-22A (BI 24481). Initial potential transformants were isolated and selected.

Drosophila locomotion behavioral analysis

Three days post eclosion, male *Drosophila* were collected and placed into tubes with food for 72 h. Locomotion was recorded by beam breaks and analyzed using equipment/software from TriKinetics. For the AMPH- induced locomotion, males were starved for 6 h and then fed sucrose (5 mM) containing either AMPH (10 mM) or vehicle.

Drosophila escape-response behavioral analysis

Drosophila were reared on a 12 h day/night cycle at 25°C with behavioral experiments performed during the day cycle. Adult male flies (2-5 day old) were selected, manually transferred, and allowed to acclimate to the recording chamber, 2.65 x 1.35 Sylgard silicone testing encapsulant (Dow Corning). The testing chamber was illuminated and basal locomotion was recorded for 2 s prior to the auditory stimulus (sound of a predatory wasp) and for 3 s following the auditory stimulus. Each auditory stimulus was presented for 1000 ms. *Drosophila* behavior was recorded at 1,000 frames per second using a Phantom v310 (Vision Research). Behaviors were analyzed using custom code written in MATLAB (v. R2016a, Mathworks).

Results

Exome sequencing of ASD subjects reveal a rare inherited in-frame deletion of residue N336 in the hDAT gene

Exome capture and sequence analysis identified a rare in-frame deletion at the conserved residue N336 (hg19 Chr5:1416233 (CTTG/C)) in the hDAT gene (*SLC6A3*) in a single autism spectrum disorder (ASD) family. The family harboring ΔN336 belongs to the Simons Simplex Collection, a well-characterized ASD collection (Fischbach & Lord, 2010). Sanger sequencing evaluation of inheritance and carrier status in available family members confirmed paternal transmission to the proband and absence of this allele in the unaffected sibling (Figure 16, left). ΔN336 was absent in all other analyzed Simons Simplex Collection families (n = 825) and absent in an independent cohort of non-autistic controls (n = 869) from the ARRA Autism Sequencing Consortium (Neale et al., 2012). High cross-species conservation at position 336 (Figure 16, right) suggests a damaging effect of the deletion on transporter function. Relevant family medical history and multiple assessment scores are provided in Supplemental Information. The affected ASD male subject displayed normal IQ (Full scale IQ: 94) and no history of related medical comorbidities. The father of the subject transmitted the variant and tested broader autism phenotype.

Deletion of V269 in LeuT (which corresponds to N336 in hDAT) traps the intracellular gate in an intermediate open conformation

The leucine transporter (LeuT), a bacterial homolog of hDAT, has been extensively used as a model system for understanding the structural and dynamic bases of Na^+- coupled transport in the neurotransmitter:sodium symporter (NSS) superfamily (Beuming, Shi, Javitch, & Weinstein, 2006; Yamashita et al., 2005). Models of the conformational changes underlying Na^+ and

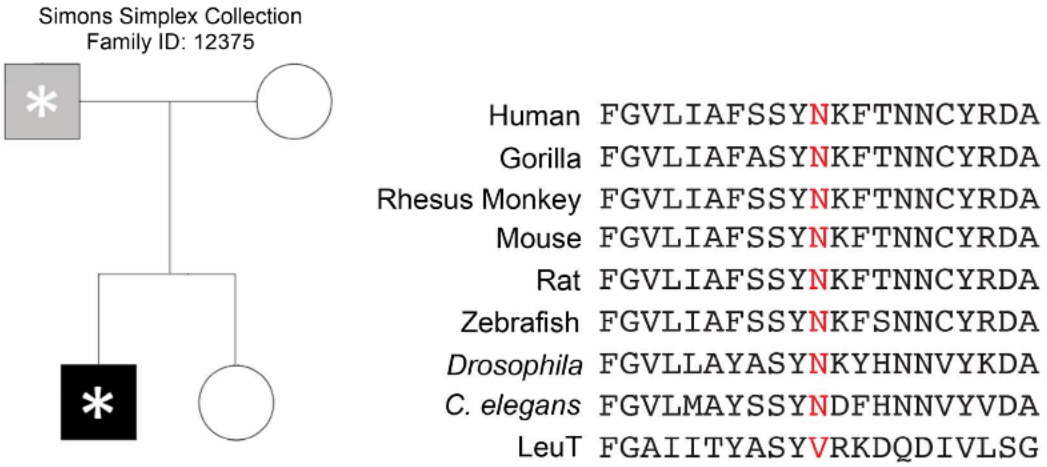

Figure 16: Identification of an in-frame deletion of N336 in hDAT in an ASD family.

Left: An inherited in-frame deletion was identified in an ASD family within the Simons Simplex Collection. Black filled boxes indicate affected individuals (diagnosed with ASD), and grey filled boxes indicate individuals testing broad autism phenotype on the BAPQ. Asterisks indicate individuals heterozygous for the variant. Right: High residue conservation across species at and surrounding the residue N336 (in red), predicts a functional effect of the variant.

substrate-coupled alternating access have been inferred from crystal structures and investigated spectroscopic analyses using electron paramagnetic resonance (EPR). A common feature of these models is the opening and closing of the intracellular and extracellular gates through the coordination of the N-terminus and the extracellular loop (EL4) respectively, although there are substantial differences between the models regarding other structural elements involved in alternating access (Claxton et al., 2010; Kazmier et al., 2014).

To determine the effects of the ΔN336, we introduced the corresponding deletion in LeuT (LeuT ΔV269) and monitored the ligand-dependent conformational dynamics of the extracellular and intracellular gates using spin label pairs 309/480 and 7/86 respectively. These pairs have been used previously to monitor the isomerization of the transporter between outward-facing, inward-facing and doubly occluded conformation. In LeuT ΔV269 the distance measurements between the spin labels using DEER reveals profound changes in the distance distributions relative to the wild type (Figure 17). In the absence of Na^+ and substrate (apo form), the dominant distance component for the extracellular pair is substantially shorter in the ΔV269 than the wild type. This suggests collapse of the extracellular gate, as previously observed for the same spin label pairs in the Y268A mutation, which traps the transporter in an inward-open conformation (Figure 17B-C) (Kazmier et al., 2014). Consistent with this interpretation, the pair monitoring the intracellular gate shows a predominantly long-distance component (inward-open conformation), with the short-distance component, assigned to the occluded state in the wild type background, greatly suppressed (Figure 17E-F). Remarkably, Na^+/Leu has no effect on the probability distribution on the extracellular side of LeuT ΔV269 (Figure 17B-C). However, it resets the intracellular gate to a distinct shorter-distance component here defined as “half open and inward-facing” (HOIF) (Figure 17F). While this component is observed in the wild type background (Figure 1E), its population is minimal compared to the more stable HOIF conformation in LeuT ΔV269.

The DEER distance distributions demonstrate that apo LeuT ΔV269 is predominantly in an outward-closed/inward-open conformation (compare Figure 17B to Figure 17C and Figure 17E to Figure 17F, black line), which would be predicted to slow down transport, as isomerization to an outward-facing conformation is a central step in symport. Moreover, binding of Na^+ alone (red) does not stabilize the outward-facing conformation, which is presumed to enable binding of substrate. Finally, binding of substrate and Na^+ (blue) to LeuT ΔV269 reduces the distance of the intracellular spin label pairs, stabilizing the intracellular gate in a HOIF conformation. This novel HOIF conformation promoted by a single amino acid deletion has a low probability in the wild type LeuT, where, in the presence of Na^+ and substrate, the intracellular gate is closed for the majority of transporters (compare Figure 17E to Figure 17F). Therefore, the native valine at position 269 shapes the dynamics of the intracellular gate by impairing the formation of a more open conformation when Na^+ and substrate are bound as well as the efflux of substrate.

Crystal structure of LeuT ΔV269 reveals structural rearrangements near the intracellular gate.

To identify the structural consequences of ΔV269, we determined the crystal structure of LeuT ΔV269 to 2.6 Å resolution. The structure of LeuT ΔV269 was solved in an L- leucine and sodium bound outward facing occluded conformation. The asymmetric unit contained a single protomer, and the structure determined was similar to previously solved structures in an occluded conformation (Cα RMSD ~ 0.5 Å with PDB ID 2Q72). L-leucine could be modeled into the substrate binding site, where F253, a key residue implicated in the extracellular gate, occludes access from the extracellular vestibule, a characteristic of LeuT in the outward-facing occluded conformation. Sodium ions at the Na1 and Na2 sodium binding sites could be modeled unambiguously.

Differences in the ΔV269 and wild type (PDB ID 2A65) structures were observed at the intracellular regions that interact with the loop harboring V269 (Figure 18). The N- terminus and

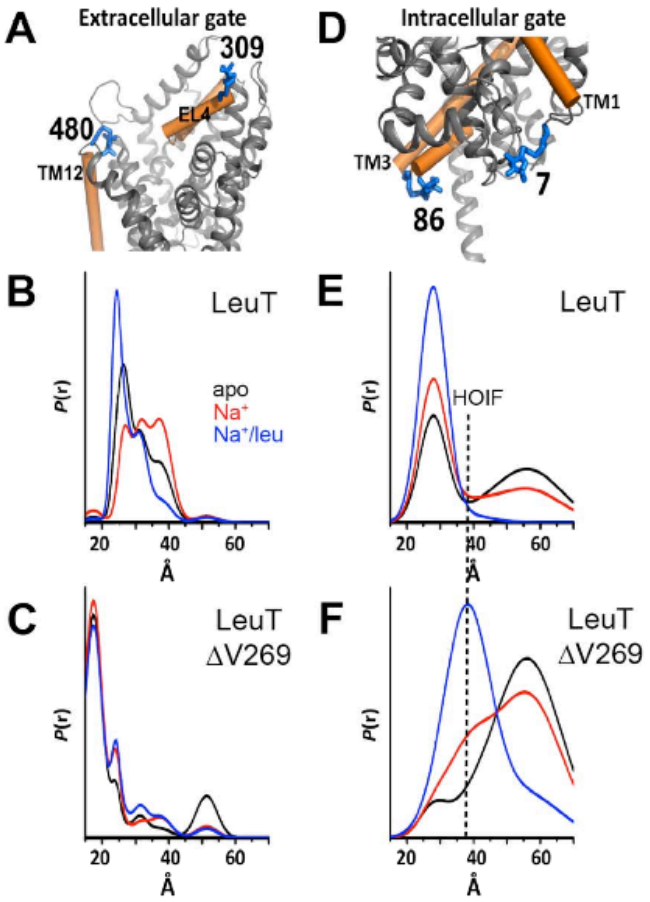

Figure 17: In LeuT, deletion of V269 supports a half-open inward-facing conformation of the intracellular gate.

Distance distributions of extracellular and intracellular spin labeled Cys pairs reveal changes in the conformational equilibrium induced by ΔV269 in LeuT. A: Extracellular reporter pairs (309-480) tagged on a three-dimensional structure of LeuT. D: Intracellular reporter pairs (7-86) tagged on a three-dimensional structure of LeuT. B,E: Distance distributions of the extracellular and intracellular reporter pair respectively for LeuT, in the apo conformation (black), in the presence of Na+ (red), or in the presence of Na+ plus Leu (blue). C,F: Distance distributions of the extracellular and intracellular reporter pair for LeuT ΔV269, in the apo conformation (black), in the presence of Na+ (red), or in the presence of Na+ and Leu (blue).

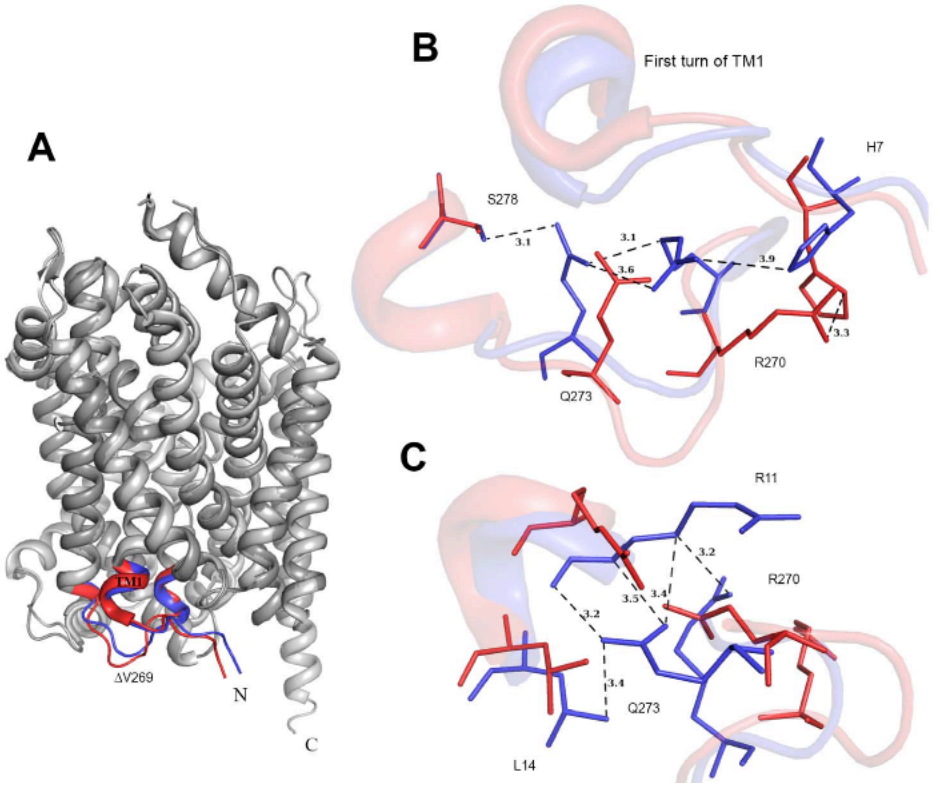

Figure 18: Structure of LeuT ΔV269.

A Superposition of LeuT ΔV269 with PDB ID 2A65. The primary differences in the intracellular region are highlighted in red (2A65) and blue (ΔV269). B Reorientation of the residues immediately following the ΔV269 is displayed. The movement of the first helical turn of the TM1 region is displayed in cartoon representation in the background. C The residues responsible for movements in first turn of TM1 are highlighted. See also Figure 19.

the first helical turn of TM1 showed significant side chain reorientations in the ΔV269 structure. The distance between the side chains of residues H7 and R270, which are within hydrogen bonding distance in 2A65, is greater in the ΔV269 structure. Furthermore, the deletion of V269 resulted in the translocation of the subsequent five residues (270-274) in the structure, such that the R270 side chain has shifted toward the first helical turn of TM1 and Q273 and away from H7. The deletion also results in a change in the side chain position of Q273, which moves closer to the first turn of TM1 and now exists within hydrogen bonding distance of S278 (Figure 18B) which corresponds to D345 in hDAT (see below). The movement of the first helical turn of TM1 nearer to the V269 deletion region is facilitated by a series of interactions between the L14 and R11 of TM1, and Q273 (Figure 18C).

The differences in the regions other than the N-termini are highlighted in red (2A65) and blue (ΔV269) (Figure 19A). On the extracellular side, the differences in the structures are minimal. The loop region (153-162) present at the entrance of the extracellular vestibule moves towards the central transmembrane axis in the ΔV269 structure when compared to 2A65, and occupies the position similar to the loop in the Y268A mutant structure, 3TT3, which is inward-facing (Figure 19B). The deletion of V269 also resulted in a side chain flip of residue W63. The superposition of the ΔV269 structure with 2A65, and 3TT3 (inward-open LeuT, represented in green), shows the progression of the indole ring flip of W63. A water molecule now resides in the space that was occupied by the side chain of V269 in 2A65. This water molecule is coordinated by the indole ring of W63 (Figure 19C). The region 438-444 in the ΔV269 structure has also moved away from the deletion region when compared to 2A65. The side chain of N274 has shifted ‘outwards’ and Ile441 has moved away from the V269 deletion region, while also displacing the 438- 444 loop. A similar reorientation is also observed in the 3TT3, but the loop region slides ‘up’ towards the membrane instead of moving out away from the transmembrane core (Figure 19D).

These differences and similarities between the ΔV269 structure, 2A65, and 3TT3 suggest that the deletion of V269 in LeuT could favor a conformation that is neither completely outward-

facing nor inward-facing, as observed in EPR experiments. However, usage of β-OG, L-leucine, and sodium in the purification and crystallization conditions favored crystallization of ΔV269 in an outward facing occluded-conformation, which accounts for diminished changes in the EL4 region as compared to the DEER data.

Modeling predicts hDAT ΔN336 disrupts coordination between the N-terminus, IL3, and TM7 through the formation of a new K337-D345 interaction.

To extend our understanding of the consequences of the mutation to hDAT, we carried out *homology* modeling of hDAT ΔN336 using the Rosetta algorithm. We found that the deletion of N336 leads to a change in orientation of K337. ΔN336 positions K337 in an orientation that enables an interaction linking IL3 to TM7 through D345 (Figure 20A, red) while in the wild type (Figure 20A, blue), IL3 does not interact with TM7 through D345 since K337 faces the intracellular side. Of note, in the ΔV269 structure the R270 side chain (K337 in hDAT) has shifted towards the first helical turn of TM1 and Q273. The deletion also results in a change in the side chain position of Q273, which now exists within hydrogen bonding distance of S278 (D345 in hDAT). Our finding of a potential hydrogen bond interaction Q273-S278 in LeuT and K337-D345 hydrogen bond interaction in hDAT ΔN336 (Q273-S278 in LeuT ΔV269) is mechanistically significant in light of recent molecular dynamic simulations suggesting that the Na2 is regulated by the K66-D345 interaction (Razavi, Khelashvili, & Weinstein, 2017). According to these simulations, impairments of the K66-D345 interaction affects the kinetics of inward-open to inward-close transition of the intracellular gate (Cheng & Bahar, 2015; Razavi et al., 2017).

Next, we probed the stability of the K337-D345 interaction in hDAT ΔN336 by molecular dynamics (MD) simulations. In our simulations, the K66-D345 salt bridge in wild type hDAT strengthens the interactions between transmembrane 1a (TM1a) and TM7 (Figure 20B), and stabilizes the bundle domain (TMs 1, 2, 6, 7) at the intracellular side (Figure 20C). Simulations of hDAT showed a stable salt bridge between the side chains of K66 and D345 over the 150 ns time

course (Figure 21A). Rare occasional short breaking of the salt bridge was observed in all three replicas, but it reformed after a few nanoseconds. No direct interaction between the side chain of K337 and D345 was seen (Figure 21B). In contrast, the simulations suggest a very different scenario for hDAT ΔN336 (Figure 21D), representations of the hDAT ΔN336 bundle at two different times in the simulation). The K66-D345 salt bridge is much less stable, with the distance increasing substantially for long time periods, indicative for a much weaker interaction (Figure 21C). The reorientation of the side chain of K337 promoted by ΔN336 shortens the IL3 loop, as observed in the crystal structure of the LeuT Δ269, and consequently weakens the interaction of K66 with D345. The new orientation of K337 favors an increased interaction with D345 (Figure 21D) effectively promoting a competition between the side chains of K337 and K66 and, as a consequence, weakening the interaction between TM7 and TM1a. The new K337-D345 interactions, as noted in Figure 20A, may promote a less dynamic intracellular gate thereby establishing the conserved N336 as a pivotal residue to the dynamics of the intracellular gate of hDAT and possibly to transport function.

ΔN336 impairs hDAT function

EPR analysis, X-ray crystallography, and hDAT modeling predict that ΔN336 disrupts intracellular gating dynamics, and potentially compromise function. Therefore, we asked whether hDAT ΔN336 is capable of DA transport. We found that hDAT ΔN336 cells display a significant reduction in DA uptake. hDAT ΔN336 expressing cells, as compared to hDAT, were below measurable DA uptake levels to calculate the maximal velocity of DA transport (V_{max}) and apparent DA affinity (K_m). Figure 22A show representative plots of DA uptake kinetics for hDAT (V_{max} = 4.33 ± 0.44 pmol/min/10^8 cell; K_m = 2.10 ± 0.59 μM) and hDAT ΔN336 cells. The reduced DA transport was not associated with a reduction in either total or surface expression of

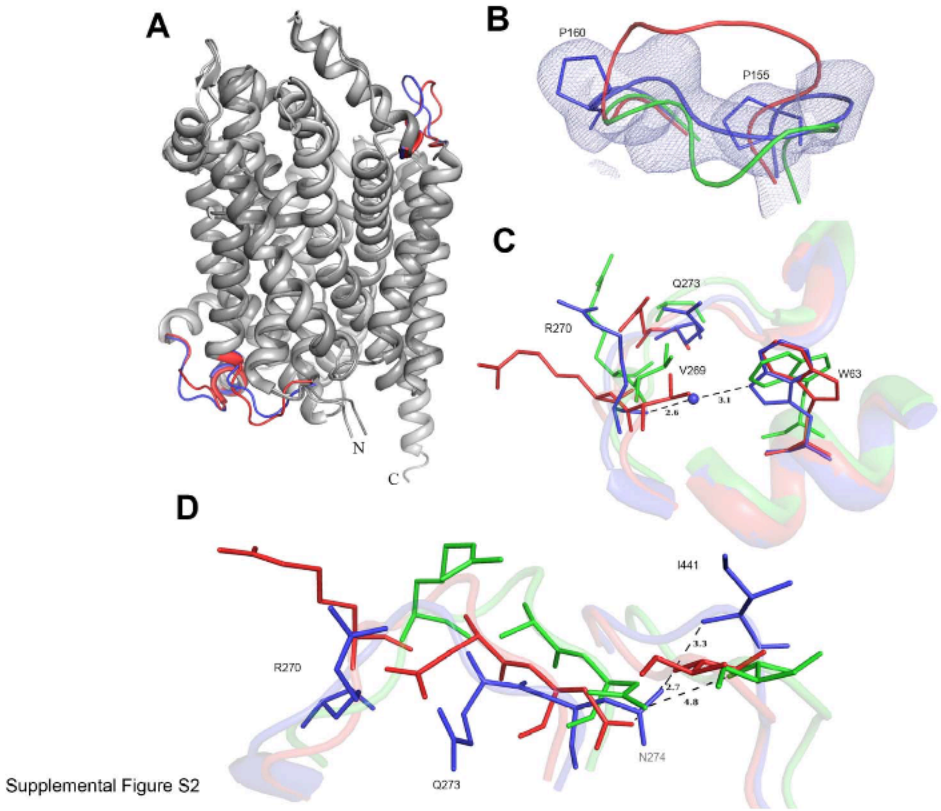

Figure 19: Related to Figure 18. Structure of LeuT ΔV269.

A: Differences in the regions other than the N-termini are highlighted in red (2A65) and blue (ΔV269). B: Movement of loop 153-162. The residues in ΔV269 are highlighted by a 2Fo-Fc density map. The same regions in 2A65 and 3TT3 (green) are displayed in cartoon representation in the background. C: Side chain flip of W63. The water molecule coordinating the indole ring is displayed as a blue sphere. D: Movement of loop 438-444. Residue I441 and N274 are highlighted.

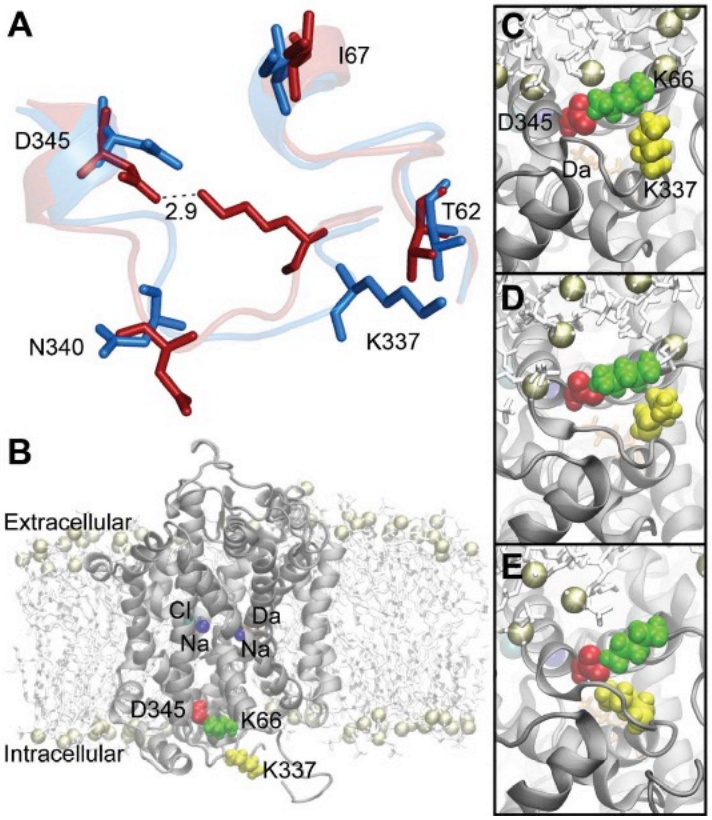

Figure 20: Modeling of hDAT ΔN336 predicts the formation of a new K337-D345 hydrogen bond.

A: Modeling using Rosetta shows that hDAT (blue) positions a free residue K337 towards the intracellular space. Modeling hDAT ΔN336 (red) reveals a repositioning of K337 that in turn forms a new K337-D345 hydrogen bond that is absent in hDAT. This K337-D345 bond may stabilize IL3 by linking it to TM7. B: Cartoon representation of a homology model of hDAT embedded in a POPC lipid bilayer. The chloride (cyan) and Na+ (blue) ions, dopamine (orange), and the side chains of K66 (green), K337 (yellow), and D345 (red) are highlighted. C: hDAT at 50 ns: salt bridge between K66 and D345. D: hDAT ΔN336 at 50 ns: salt bridge between K66 and D345 (Replica 2). E: hDAT ΔN336 at 100 ns: residue D345 forms two salt bridges, one to K66, a second to K337 (Replica 2). See also Figure S3.

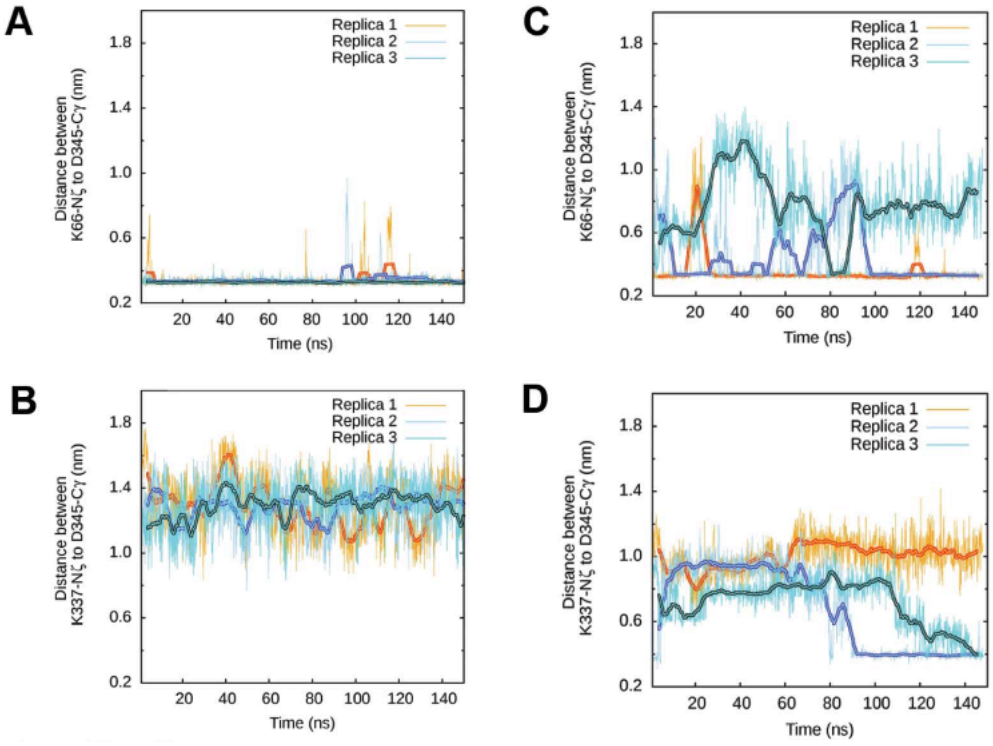

Figure 21: Related to Figure 20. In hDAT, the ΔN336 promotes repositioning of K337 that weakens the K66-D345 interaction by competing for D345.

A: Time evolution of distances in hDAT. Distances are measured between K66 atom Nζ, and D345 atom Cɣ. B: Time evolution of distances in hDAT. Distances are measured between K337 atom Nζ, and D345, atom Cɣ. C: Time evolution of distances in hDAT ΔN336. Distances are measured between K66 atom Nζ, and D345 atom Cɣ. D: Time evolution of distances in hDAT ΔN336. Distances are measured between K337 atom Nζ, and D345, atom Cɣ. All simulations were conducted in triplicate from independent starting structures.

hDAT ΔN336 (Figure 23; top). Surface fractions were quantitated, normalized to total hDAT, and expressed as a percent of hDAT (Figure 23; bottom) ($p = 0.781$ by *t*-test; $n = 4$, in duplicate).

ΔN336 support reverse transport of DA

AMPH is a psychostimulant that promotes DAT-mediated DA efflux (reverse transport of DA). To measure DA efflux, we adopted the patch clamp technique in whole-cell patch configuration to allow intracellular perfusion of an internal solution containing 2 mM DA. An amperometric probe was juxtaposed to the plasma membrane of the cell and used to measure reverse transport of DA via oxidation/reduction reactions. The whole cell electrode, in current clamp configuration, allows the cell to control its membrane voltage and ensures that cells were equally loaded with intracellular DA (hDAT ΔN336 cells are incapable of DA uptake). Figure 22B show representative traces of DA efflux in hDAT and hDAT ΔN336 cells. Quantitation of the peak amperometric currents show reduced DA efflux in hDAT ΔN336 compared to hDAT cells ($p \leq 0.01$ by *t*-test; $n = 5$) (Figure 22C). Considering that hDAT ΔN336 has impaired DA uptake while retaining DA efflux, these data support a model where the N336 as well as the intracellular gate of hDAT differentially regulate inward versus outward transport of DA.

ΔN336 exhibits impaired conformational changes defining the transport cycle

Rapid (msec) application of AMPH induces an hDAT-mediated fast activating transient current that represents the synchronized inward reorientation of hDAT with the substrate bound (Erreger et al., 2008). This transient current is followed by a cocaine-sensitive inward steady state current that represents substrate (i.e. AMPH) uptake (Erreger, Grewer, Javitch, & Galli, 2008). Therefore, these two currents define, at least in part, the hDAT transport cycle. We voltage clamped hDAT or hDAT ΔN336 cells using the whole-cell patch configuration at - 60 mV while applying 10 μM AMPH. As expected, hDAT cells displayed a fast activating transient current followed by a steady state current (Figure 22D). Upon washout of AMPH, the steady-state current decayed to baseline

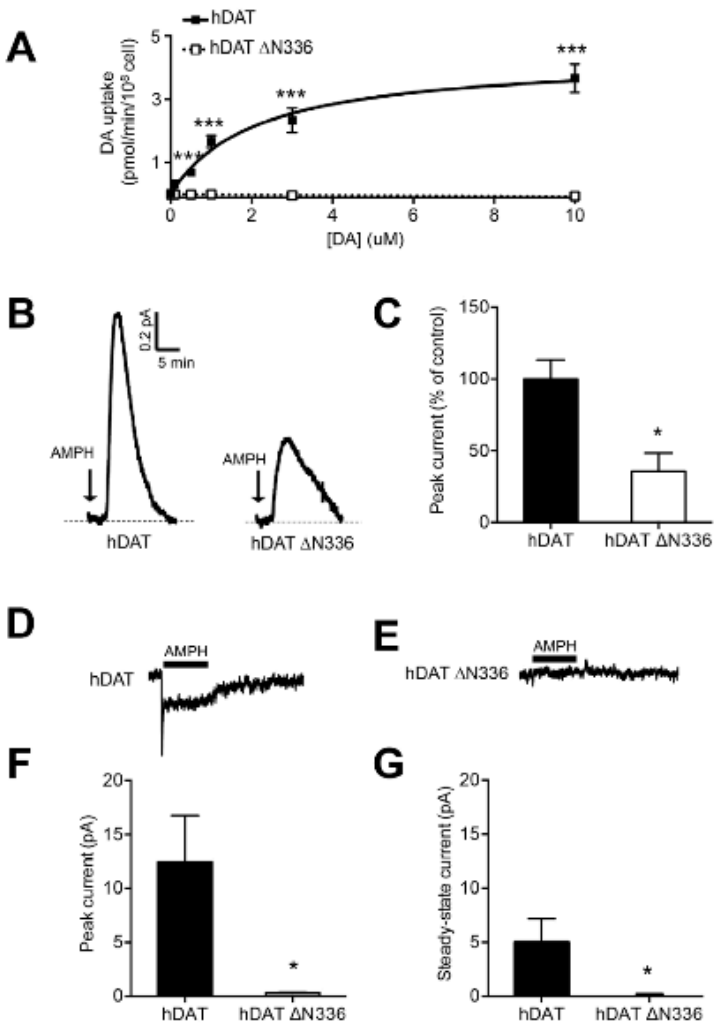

Figure 22: hDAT ΔN336 displays impaired DA transport, reduced AMPH-induced DA efflux, and diminished AMPH-induced currents.

A: Representative plot of [^{3}H]DA uptake kinetics in hDAT (filled squares) or hDAT ΔN336 (empty squares) cells (*** = $p \leq 0.0001$ by two- way ANOVA followed by Bonferroni post test; n = 6, performed in triplicate). B: Representative AMPH-induced amperometric currents recorded from hDAT and hDAT ΔN336 cells. Cells were patch loaded with DA. Arrows indicated application of 10 μM AMPH. C: Quantification of AMPH-induced DA efflux. Data are represented as the peak amperometric current ± SEM (* = $p \leq 0.01$ by t-test; n = 5). D,E: The mean AMPH (10 μM)- induced whole cell current of 10 consecutive sweeps obtained from hDAT and hDAT ΔN336 cells is plotted. hDAT and hDAT ΔN336 cells were kept under voltage clamp (-60 mV) and AMPH was rapidly applied to the cells for 1 sec by a piezoelectric translator (see Methods). In contrast to hDAT ΔN336 cells, hDAT cells display a peak and a steady-state current. F,G: Quantification of AMPH-induced peak current and steady-state current for hDAT and hDAT ΔN336 expressing cells. Data are represented as amperometric current ± SEM (* = $p \leq 0.05$ by t-test; n = 9). See also Figure 23.

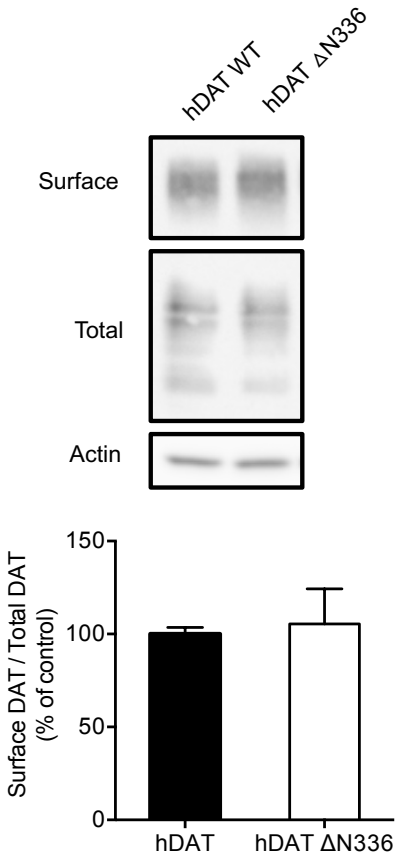

Figure 23: Related to Figure 22. hDAT ΔN336 displays equivalent expression of total and surface protein.

Representative immunoblots for biotinylated (surface) and total protein fractions from hDAT and hDAT ΔN336 cells. Surface fractions were quantitated, normalized to total DAT, and expressed a percent of control ($p \geq 0.05$ by Students t-test; $n = 4$). Actin serves as a loading control.

levels (Figure 22D). These characteristic fast activating transient currents and steady state currents were notably absent in hDAT ΔN336 cells (Figure 22E). Quantitation of the peak current (Figure 22F) and steady state currents (Figure 22G) show ΔN336 significantly impairs synchronized inward reorientation of hDAT with the substrate bound, as well as substrate-induced transporter function ($p \leq 0.05$ by unpaired *t*-test; n = 9). These data further suggest that in hDAT ΔN336 substrate uptake and efflux are uncoordinated and independent processes.

A half-open inward-facing conformation is critical for transport

Our results point to a significant role for N336 in hDAT as well as V269 in LeuT for the dynamics of the intracellular gate. However, the question remains of whether the HOIF conformation stems exclusively from a deletion of V269 in LeuT or is a conformation that is regulated by that specific amino acid residue. In other words, what role does the N336 in hDAT have in the HOIF conformation? Furthermore, is the HOIF conformation important for the dynamics of substrate uptake and efflux? To begin to address these questions, we substituted the native LeuT amino acid V269 with the equivalent hDAT residue, N336. For this purpose, we analyzed the distance distributions of reporter pairs on the intracellular and extracellular gates. In the presence of Na^+ and substrate, the distance distributions of spin label pairs 309/480 monitoring the extracellular side (Figure 24A) was comparable for LeuT and LeuT V269N (compare Figure 24B to Figure 24C, blue lines), despite an observed increase of a short distance component in the apo state and in the presence of Na^+ in LeuT V269N (compare Figure 24B to Figure 24C, black and red lines, respectively).

LeuT V269N has considerable effects on the distribution of spin-label pairs 7/86 monitoring the intracellular gate (Figure 24D). In the apo state, LeuT V269N shows a dramatic shift in the transporter distributions favoring an inward-facing conformation (compare Figure 24E to Figure 24F, black line). Binding of Na^+ alone (Figure 24F, red lines) reduces the population of

inward-facing transporters and exposes a population of transporters wherein the intracellular gate in a HOIF. Binding of substrate and Na^+ (blue line) also promotes a conformation wherein the intracellular gate may reside in a HOIF conformation (compare Figure 24E to Figure 24F, blue lines). However, the population of the HOIF conformation in LeuT V269N is greatly reduced as compared to LeuT ΔV269, while it remains increased with respect to the wild type LeuT. This data strongly suggests that the residue at position 269 in LeuT and, possibly at position 336 in hDAT, regulates the mobility of the intracellular gate and its ability to occupy an inward-closed conformation. They also suggest that an asparagine at position 269 promotes a HOIF conformation that allows an occluded conformation in the presence of substrate and Na^+ and similar to the low probability conformation noticed in LeuT. These data imply that the probability distribution of the HOIF conformation and the mobility of the intracellular gate are regulated (from bacteria to higher organisms) by amino acid conservation in this loop including position 269 (i.e. V vs N). Our data suggest that valine at position 269 inhibits the HOIF conformation while an asparagine partially permits also allowing for an occluded conformation in the presence of substrate and Na+. In addition, the presence of either a valine or an asparagine is required for proper functioning of the extracellular gate.

To further explore the importance of the HOIF conformation and the role of N336 in transporter function and substrate uptake, we substituted N336 in hDAT with the corresponding valine residue in LeuT (hDAT N336V). We expected the hDAT N336V cells to display reduced maximum velocity of DA uptake (V_{max}). Figure 24G shows that hDAT N336V cells do exhibit a significant reduction (~85%) in V_{max}, and a significant decrease in DA affinity (K_m) as compared with hDAT cells (Fig. 24G; top). A representative plot of DA uptake kinetics for hDAT and hDAT N336V is shown (Figure 24G; bottom). These data suggest that N336 is pivotal for proper DA transport in addition to the dynamics of the intracellular gate.

Isolated brains from hDAT ΔN336 flies display decrease DA uptake and AMPH-induced DA efflux

We utilized *Drosophila melanogaster* as an animal model to determine, functionally and behaviorally DA dysfunction caused by ΔN336. We expressed hDAT or hDAT ΔN336 in flies homozygous for the dDAT null allele, DAT^{fmn} (dDAT KO), adopting the Gal4/UAS system to express a single copy of hDAT or hDAT ΔN336 in a $dDAT^{fmn}$ mutant background, selectively in DA neurons. The transgenic flies were generated by using phiC31 based integration, which should lead to the expression of comparable levels of mRNA for the relevant transgenes (hDAT or hDAT ΔN336).

We isolated the brains of flies expressing either hDAT or hDAT ΔN336 to determine possible changes in brain DA uptake (200 nM [^{3}H]DA). We detected a significant reduction in DA uptake in the flies expressing hDAT ΔN336 (93.7 ± 33.22 fmol/4brains) compared to the flies expressing hDAT (324.1 ± 49.14 fmol/4brains) ($p \leq 0.01$ by *t*-test, $n = 4$) (Figure 25A). To determine the ability of hDAT ΔN336 to support reverse transport of DA in brain we measured DA efflux from isolated *Drosophila* brains. We inserted a carbon fiber electrode into isolated *Drosophila* brains in close proximity to the mCherry tagged DA-specific neurons. Figure 25B shows representative traces of DA efflux in brains of flies expressing either hDAT or hDAT ΔN336.

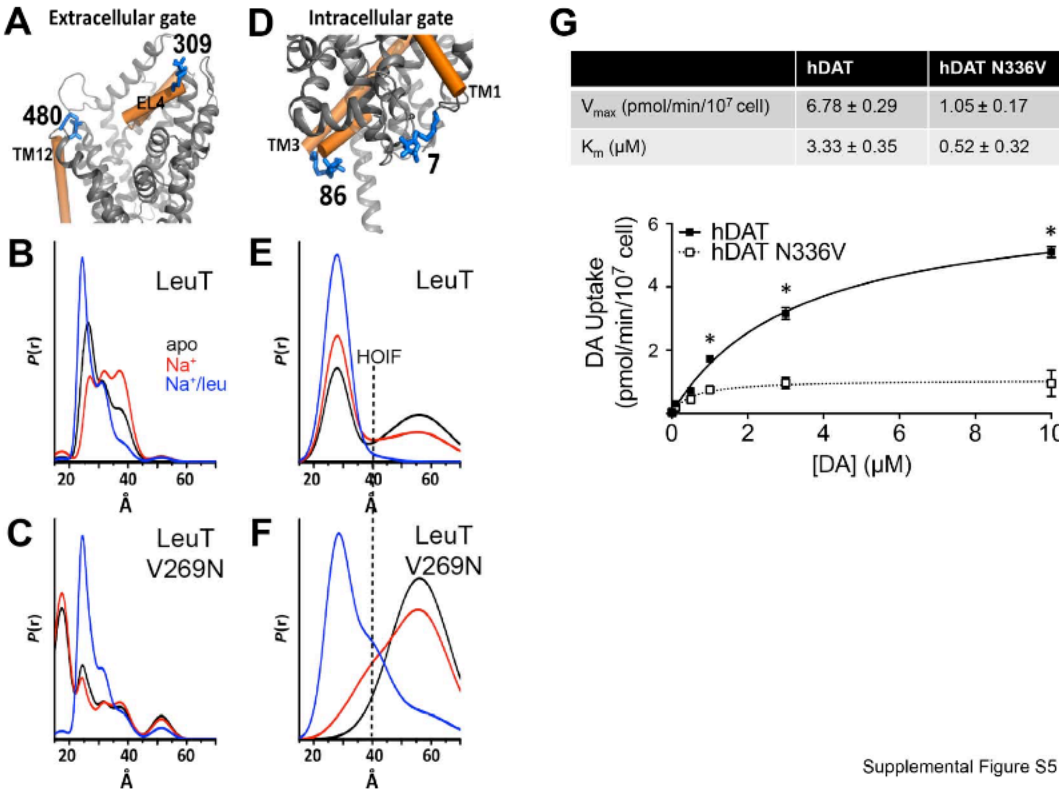

	hDAT	hDAT N336V
V_{max} (pmol/min/10^7 cell)	6.78 ± 0.29	1.05 ± 0.17
K_m (μM)	3.33 ± 0.35	0.52 ± 0.32

Figure 24: V269N increases the intracellular gate dynamics in LeuT.

A: Extracellular reporter pairs (309-480) tagged on a three-dimensional structure of LeuT. D: Intracellular reporter pairs (7-86) tagged on a three-dimensional structure of LeuT. B,E: Distance of the extracellular and intracellular reporter pair respectively for LeuT, in the apo conformation (black), in the presence of Na+ (red), or in the presence of Na+ plus Leu (blue). C,F: Distance of the extracellular and intracellular reporter pair for LeuT V269N, in the apo conformation (black), in the presence of Na+ (red), or in the presence of Na+ and Leu (blue). G: Top: Kinetic parameters (Vmax and Km) for hDAT and hDAT N336V (n = 3, in triplicate). Bottom: Representative plot of [^{3}H]DA uptake kinetics in hDAT (filled squares) or hDAT V336N (empty squares) cells (* = $p<0.05$ by two-way ANOVA followed by Bonferroni post-test; n = 3, in triplicate).

AMPH-induced DA efflux recorded in the brain of hDAT ΔN336 flies is significantly lower than that seen in hDAT flies (Figure 25C) ($p \leq 0.01$ by *t*- test; $n = 6$).

DA synthesis enhances reverse transport of DA in flies expressing hDAT ΔN336

Deficient DA uptake causes a decrease in neuronal DA content (Giros and Caron, 1993). Therefore, it is possible that the reduced ability of AMPH to induce reverse transport of DA in hDAT ΔN336 flies is due to low levels of intracellular DA. Thus, we used L-3,4-dihydroxyphenylalanine (L-DOPA), the direct precursor to DA, as a tool for increasing DA content in dopaminergic neurons of hDAT ΔN336 flies. We treated hDAT ΔN336 flies with L-DOPA or vehicle for 24 h and then recorded AMPH-induced amperometric signals from isolated brains. Representative amperometric traces of L-DOPA and vehicle treated hDAT ΔN336 files are shown in Figure 25D. Quantitation of peak amperometric currents show that DA efflux in L-DOPA fed hDAT ΔN336 flies is elevated (182 ± 6.3% increase) as compared to vehicle treated flies ($p \leq 0.05$ by *t*-test; $n = 4$ L-DOPA, $n = 5$ Vehicle) (Figure 25E). These data demonstrate that hDAT ΔN336 can support reverse transport of DA in intact brains.

hDAT ΔN336 supports hyperlocomotion

Across many species, locomotion is a fundamental behavior regulated by DA. In *Drosophila*, we and others have established that locomotion is a DA-associated and DAT-dependent behavior (P. J. Hamilton, Campbell, Sharma, Erreger, Herborg Hansen, et al., 2013; Kume et al., 2005). Therefore, measuring changes in locomotion offers a powerful behavioral indicator for probing DA dysfunction *in vivo*. To this end, we measured locomotion in flies expressing either hDAT or hDAT ΔN336. Figure 26A shows locomotor activity of these flies by beam crosses over a 36 h period during both the light (horizontal white bar) and dark (horizontal black bar) cycle. Although the hDAT ΔN336 flies are clearly hyperactive, we observed no changes in the locomotive circadian rhythms. Quantitation of total beam crossings in hDAT ΔN336 flies

over 24 h is significantly elevated compared with hDAT flies (Figure 26B) (* = $p \leq 0.0001$ by Mann-Whitney test; *n* = 30-31). This data supports the notion that hDAT ΔN336 results in impaired DA neurotransmission and increased locomotion.

hDAT ΔN336 flies exhibit increased grooming behavior

Repetitive behaviors, including self-grooming have been observed in animal models of neuropsychiatric disorders (Silverman, Tolu, Barkan, & Crawley, 2010). Grooming behavior in *Drosophila* is a stereotyped sequence of leg and body movements. In *Drosophila*, grooming requires functional DA neurotransmission (Chang et al., 2006). Therefore, it is possible that ΔN336 flies display altered grooming because of impaired DA clearance. We quantified the percent of time grooming in *Drosophila* expressing ΔN336 compared with wild type. ΔN336 displayed enhanced time grooming (22.9 ± 3.4% time grooming) compared to wild type (6.3 ± 4.2% time grooming) ($p \leq 0.05$ by *t*-test, *n* = 3-5).

hDAT ΔN336 flies exhibit increased freezing following an audible fear stimulus

A fear stimulus assay offers an opportunity to probe an evolutionarily conserved construct. A complex pattern of animal behaviors is involved in the detection and analysis of threat stimuli, and in the situations in which the threat is encountered. Risk assessment is therefore pivotal for establishing an appropriate response to threatening situations, such as the presence of a predator. Risk assessment evokes an evolutionarily conserved brain state, fear, which triggers defensive behaviors. Risk assessment is also important for determining one specific behavioral defense over another; for example flight over hiding or freezing. The appropriate behavioral choice in threating situations is controlled by specific neurocircuits and determines the ability to survive (Steimer, 2002). In humans, dysregulation of these evolutionary conserved circuits is implicated in anxiety-related disorders (LeDoux, 2003; Steimer, 2002) including ASD.

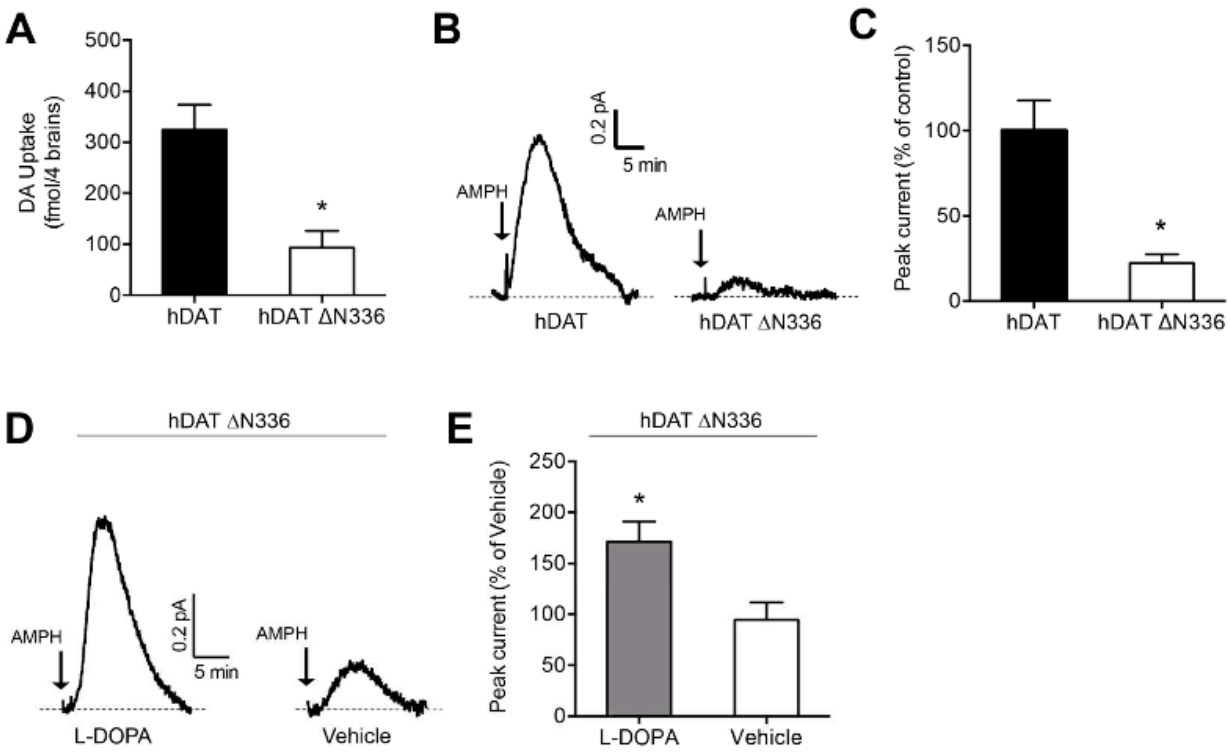

Figure 25: In *Drosophila* brain, hDAT ΔN336 display reduced DA uptake and AMPH-induced efflux.

A: Flies expressing hDAT ΔN336 display reduced DA uptake compared with hDAT expressing brains. Data are represented as DA uptake (200 nM DA) using 4 Drosophila brains per well ± SEM (* = $p \leq 0.01$ by t-test, n = 4). B: Representative AMPH- induced (20 µM) amperometric currents recorded from fly brains expressing hDAT or hDAT ΔN336. Arrows indicated application of AMPH. C: Quantitation of DA efflux. Data are presented as the peak amperometric current ± SEM (* = $p \leq 0.01$ by t-test, n = 4). D: Drosophila expressing hDAT ΔN336, when fed an L-DOPA (5 mM) diet for 24 h, display increased DA efflux compared to vehicle fed flies. Representative AMPH-induced (20 µM) amperometric currents recorded from hDAT ΔN336 fly brains. Arrows indicate application of AMPH. E: Quantitation of DA efflux. Data are presented as the peak amperometric current±SEM (* = $p \leq 0.05$ by t-test; n=4).

To evaluate if impairments in DA clearance from the variant ΔN336 alters defensive response (i.e. freezing or flight) we exposed either hDAT or hDAT ΔN336 flies to an auditory fear stimulus, the sound of a predatory wasp. In freely moving hDAT flies, the sound of a predatory wasp (Figure 26C arrow, predatory sound) elicits a short freezing period, followed by a distinctive and rapid increase in average velocity, fleeing (Figure 26C, Video 1 (hDAT WT, Supplemental information)). In contrast, when exposed to the sound of the predatory wasp, hDAT ΔN336 flies display prolonged freezing and delayed fleeing (Figure 26C, Video 2 (hDAT ΔN336, Supplemental information)).

The deficient fleeing-response of hDAT ΔN336 flies was quantified by calculating the area under the curve of the average velocity (total distance traveled, μm), from the onset of the predatory sound until flies returned to pre-stimulus velocity levels (~600 ms). Quantitation of the AUC reveals *Drosophila* expressing hDAT ΔN336 have a markedly reduced escape-response (3574 ± 1147 μm) compared to hDAT flies (7302 ± 1176 μm) (Figure 26D; $p \leq 0.05$ by *t*-test; $n = 8$). One possible explanation for this deficit in fleeing- response in hDAT ΔN336 flies is an increase in the freezing period.

hDAT ΔN336 flies show impairments in social interactions

Grouping is a widespread behavior observed across many animal populations that is often advantageous for survival and is defined as a temporary or permanent aggregation of animals (S.-H. Lee, Pak, & Chon, 2006). Grouping defines a wide variety of interactions that range from coincidental encountering to social gathering, and can lead to complex behaviors such as fleeing in response to a threat. In this context, fleeing is an escaping behavior of a prey population. During fleeing, the compression and expansion of the flock size is regulated by complex social interactions among the animals in the flock, and by prey- predator interactions (S.-H. Lee et al., 2006).

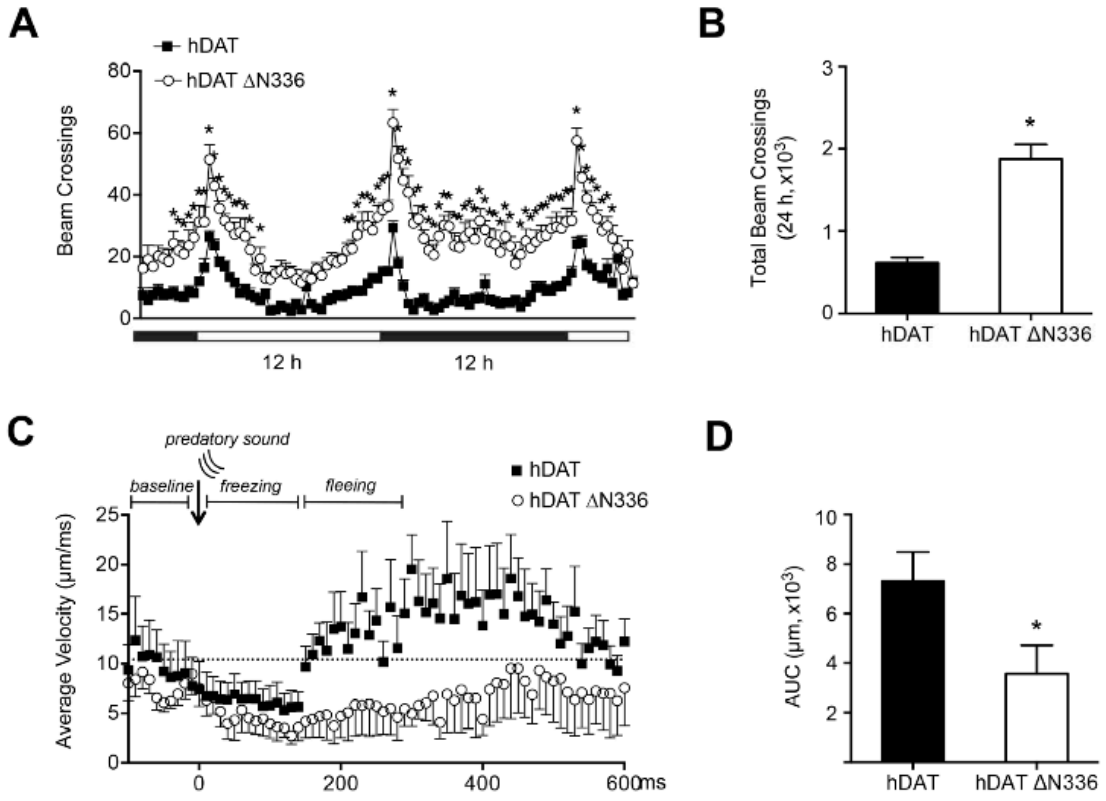

Figure 26: hDAT ΔN336 flies are hyperactive and show prolonged freezing and reduced fleeing.

A: Locomotor activity was assayed over 32 h during the light (horizontal white bars) or dark (horizontal dark bars) cycle. Flies expressing hDAT ΔN336 (open circle) were hyperactive as compared to flies expressing hDAT (black square). Beams crossings were binned into 20-minute intervals. B: Quantitation of total beam crossings over 24 h. Data are presented as the total beam crossing ± SEM (* = $p \leq 0.0001$ by Mann-Whitney test; n = 30-31). C: Average velocity (µm/ms) was assayed over 600 ms following an auditory stimulus for flies expressing hDAT (black square) or hDAT ΔN336 (open circle). The hashed line indicates pre-audible baseline velocity. D: Area under the curve (AUC) is calculated as the cumulative velocity from the onset to the end of the predatory sound. Quantitation of AUC over 600 ms for hDAT and hDAT ΔN336 flies. Data are presented as the total AUC ± SEM (* = $p \leq 0.05$ by t-test; n = 8).

Here, we explored whether hDAT dysfunction induced by ΔN336 influences flock size during an escape response induced by a fear stimulus. We measured the inter-fly distance across four flies before and after an escape-response and calculated their change in social space (sum of distances between a fly and his three neighbors) over time. A positive social space value indicates an expansion in flock size (a normal response under predatory pressure (S.-H. Lee et al., 2006) over time, while a negative social space value indicates a compression of flock size. Figure 27 illustrates that flies expressing hDAT have a preference for increasing the flock size following an auditory fear response, while *Drosophila* expressing hDAT ΔN336 have a propensity for a time-dependent aggregation. This significant inverse social space relationship ($p < 0.001$) was calculated using the slope of the sum of inter-fly distances in hDAT (2.30 ± 0.05 μm/ms) and hDAT ΔN336 flies (-9.36 ± 0.08 μm/ms) over time (Figure 27). These slopes were calculated over 1000 ms of recordings (data binned in 20 ms intervals) and normalized to the respective sum of inter- fly distances calculated at 700 ms after the start of the predatory stimulus. This time point (time zero) was chosen as it occurs immediately after the freezing behavior.

Discussion

ASD is phenotypically and etiologically complex disease, yet significant evidence for disease risk resides in the individual's genetics (De Rubeis et al., 2014; Geschwind & State, 2015). Rare variations represent an important class of this genetic risk, and sequencing efforts identified new risk variants associated with specific signaling pathways/molecules, including DA (E. Bowton et al., 2014; Cartier et al., 2015; P. J. Hamilton, Campbell, Sharma, Erreger, Herborg Hansen, et al., 2013). However, a limitation of these efforts is the difficulty of achieving genetic power to detect rare variant enrichment. Clearly, we are limited on the exact nature of the genetic risk for ASD conferred by ΔN336. However, this occurring variant provided a blueprint to gain valuable insights in the mechanisms of transporter function and gating, and how dysfunction of these processes translates in specific abnormal animal behaviors and DA neurotransmission.

We demonstrated that hDAT ΔN336 cells have impaired DA transport and DAT- mediated electrical currents, while partially supporting DA efflux. Using *Drosophila* as an animal model, we discovered that expression of hDAT ΔN336 reduces DA uptake in whole brain. These data combined with previous published data Bowton *et al*., 2014 (E. Bowton et al., 2014) support the idea that hDAT dysfunction in ASD stems from specific and yet distinct mechanisms.

The question remains as to whether a specific impairment in DAT function causes disruptions of defined behaviors and whether these disruptions reveal new mechanisms/behaviors underlying aberrant DA neurotransmission. We found that hDAT ΔN336 flies are hyperlocomotive, associating ΔN336 to an increase in extracellular DA levels. DA dysfunction in hDAT ΔN336 flies is also reflected in increased grooming. This is important since repetitive behaviors have been associated to dysregulated DA homeostasis.

To uncover whether ΔN336 as well as impaired DAT function disrupts complex behaviors, we developed new paradigms to explore "fear" and social interactions in flies. Neuron specific expression of ΔN336 disrupted flies' defensive behaviors. Our data demonstrate that hDAT ΔN336 flies display prolonged freezing and delayed fleeing upon an auditory fear stimulus, further supporting the role of DA in specific fear responses. Our results link DAT dysfunction associated with ΔN336 to impaired defensive behaviors and to increased fear.

ASD is also characterized by impairments in social-interactions and communications. Therefore, we measured the compression/expansion of a fly flock size under predatory pressure. As expected, flies expressing hDAT have a preference for increasing the flock size following an audible fear response. Instead, *Drosophila* expressing hDAT ΔN336 have a propensity for a time-dependent aggregation. These data define how specific impairments in hDAT function translate in disrupted social interactions.

The functional and behavioral characterization of variants is essential to provide insights into their impact on neurocircuits and signaling pathways. However, their structural characterization may shed light on the underpinnings of hDAT function. Using LeuT as a template,

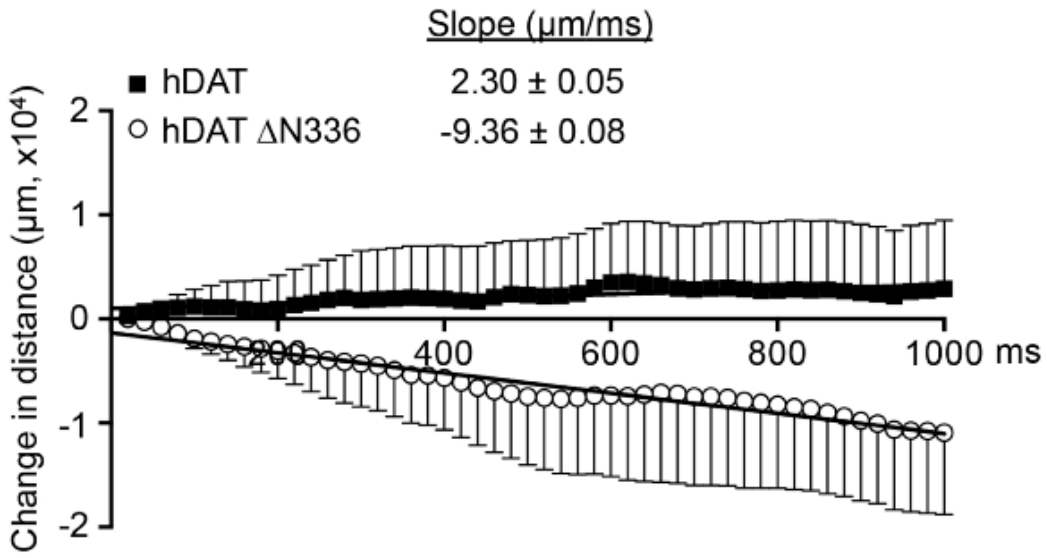

Figure 27: hDAT ΔN336 flies show social impairments as measured by proximity to their neighbors during escape-response.

The sum of distances (µm) across four flies (social space) was calculated and assayed over 1000 ms and normalized to the respective social space calculated at time 0. Over time hDAT flies (black squares) display increased flock size, as determined by the slope of the fitting of the sum of distances over time (black dotted line: 2.30 ± 0.05 µm/ms). In contrast, the hDAT ΔN336 flies (open circle) reveal decreased flock size over time (grey dotted line: -9.36 ± 0.08 µm/ms).

we show that ΔV269 stabilizes a previously unappreciated conformation of the intracellular gate where it resides in a “half-open and inward-facing” conformation. The loss of uptake function is a possible consequence of a locked conformation of the extracellular gate. In contrast, the unique conformation of the intracellular gate, favored by binding of ions and substrate, allows for reverse transport of DA. Therefore, the intracellular gate differentially regulates inward versus outward transport of DA. These results also suggest that defined coordination of the extracellular and intracellular gates is a requirement for DA uptake, but not DA efflux which is permitted under the HOIF conformation.

The LeuT ΔV269 crystal structure reveals, in atomic details, the structural rearrangements induced by the mutation. Substantial repacking is observed for IL3 which changes the side chain orientation of the highly conserved R270 (K377 in hDAT). The consequences of this repacking are a profound shift in the structure and ligand-dependent dynamics of the N-terminal loop, which acts as an intracellular gate, and the EL4 lid that blocks the permeation pathway on the extracellular side. While the crystal structure hints at movement of the intracellular gate that extends to the first turn of TM1, the extracellular vestibule adopts an outward-occluded conformation. Previous reports indicated the tendency of solutes, including detergent molecules, to bind in this vestibule and ‘wedge it’ in a more open configuration (H. Wang et al., 2012). The stabilization of this conformation may have limited the extent of the repacking on the intracellular side in the crystal structure.

De novo modeling and MD simulations extend these conclusions to hDAT by demonstrating a repacking of the side chain of K377 in hDAT ΔN336, which disrupts the interaction between K66 and D345. In light of recent MD simulations invoking a role for this hydrogen bond in intracellular gating, it is plausible that the weakening of this interaction leads to a more dynamic N-terminal domain supporting specific functions of hDAT (i.e. DA efflux).

Our results uncover how specific hDAT molecular impairments promoted by genetic variants are linked to altered social behaviors. We translated the consequences of the relative

changes in the conformational stability of transporter intermediates, both at the brain level as well as behaviorally. This entailed the development of new behavioral assays supported by recent technological advances including high speed video recording of predatory and social behaviors in flies. The experimental paradigms we describe here provide a framework for molecular and behavioral analysis of novel DAT variants that are discovered by genetic analyses of individuals with ASD or related neuropsychiatric illness as well as other disease-linked mutants that are emerging from precision medicine initiatives.

Supplemental Information

Diagnosis: The autism-affected male in this family of European ancestry was ascertained as part of the Simons Simplex Collection, which recruits families comprising of a proband, unaffected parents and an unaffected sibling. The proband received a consensus diagnosis of “autism” on the Autism Diagnostic Interview-Revised (ADI-R) and the Autism Diagnostic Observation Schedule (ADOS) classifications (Supplemental Figure 16). Cognitive testing indicated the proband had an IQ in the normal range (Full scale IQ: 94).

Scoring: Parsing ADI-R domains revealed deficits across all four categories: (1) Reciprocal Social Interaction (score=30; cutoff=10); (2) Abnormalities in Communication (score=22; cutoff=8); (3) Restricted, Repetitive and Stereotyped Patterns of Behavior (score=8; cutoff=3); (4) Development Evident at or Before 36 Months (score=1; cutoff=1).

ADOS testing was performed at 191 months using module 3, which is intended for verbally fluent children. The proband received a raw ADOS score of 27, and a calibrated severity score (CSS), a metric to approximate autism severity (Gotham, Pickles, & Lord, 2009), of 8. The average autism CSS score is 7.09 ± 2.45.

The Social Responsiveness Scale (SRS) is an instrument used to quantify social impairment across entire range of the autism spectrum and can be completed by parents and/or teachers. The proband received T-scores of 89 and 77 from the parents and teacher respectively, scores

indicating “severe” deficits in everyday social interactions. Female sibling assessment using the SRS indicated normal development.

The broad autism phenotype (BAP) describes a set of behavioral and language features/deficits which occur in individuals resulting from a milder expression of the underlying genetic liability for autism. One instrument to measure BAP in adults is the Broad Autism Phenotype Questionnaire (BAPQ). The BAPQ was designed to measure aloof personality, rigid personality, and pragmatic language deficits. In this family, the father received an overall BAPQ score of 3.58 (cutoff=3.15) indicating a broad autism phenotype (Supplemental Figure 16), with BAPQ subscale scores of Aloof=3.33 (cutoff 3.25), Rigid=3.25 (cutoff 3.50), and Pragmatic Language=3.25 (cutoff 2.75). The mother of the proband received an overall score of 2.22 (cutoff=3.15) indicating no broad autism phenotype, with BAPQ subscale scores of Aloof=2.25 (cutoff 3.25), Rigid=2.25 (cutoff 3.50), and Pragmatic Language=2.17 (cutoff 2.75).

Video 1: Movie of a hDAT WT fly showing the short freezing period, followed by a distinctive and rapid increase in average velocity (fleeing) upon a predatory sound (red highlighting shade). The video frame/rate was reduced 4X.

Video 2: Movie of a hDAT ΔN336 fly showing a prolonged freezing period, followed by a reduced increase in average velocity (fleeing) upon a predatory sound (red highlighting shade). The video frame/rate was reduced by 4X.

Chapter V

PHOSPHORYLATION STATES OF THE SNARE PROTEIN SYNTAXIN 1 REGULATE DOPAMINE TRANSPORTER EFFLUX PROPERTIES

The work described in this chapter is part of and adapted from the manuscript under preparation titled “Shekar A, Mabry SJ *et al*. Phosphorylation States of the SNARE Protein Syntaxin 1 Regulate Dopamine Transporter Efflux Properties”.

Preface

DAT reuptake properties have been widely studied in different cell-based and *in vivo* systems and substrate transport has been well-characterized structurally and functionally. Another widely-studied but lesser understood transporter phenomenon is reverse transport or efflux, wherein the transporter releases substrate (DA) into the synaptic cleft, the opposite of its “regular” function. Via its dual roles in forward and reverse transport, the hDAT helps maintain DA homeostasis in the extracellular space. Alterations in DA homeostasis, brought about by (but not limited to) changes in normal hDAT function, can lead to disruptions in DA-associated behaviors. Several groups have now shown that loss of hDAT uptake function in an organism can lead to accumulation of DA in the extracellular space, resulting in hyperactivity, increased impulsivity, heightened sexual impetus and cognitive behaviors. On the other hand, DA increased reverse transport via hDAT can also result in the same biochemical and behavioral effects. It is key to recognize that a balance between DA uptake and DA release (both transporter-mediated and transporter-independent) is essential to maintain normal DAergic tone and associated phenotypes.

In this study, we employ a gamut of biochemical, electrophysiological and behavioral assays that demonstrate the signaling mechanisms that determine when and how DA release occurs. Our hypotheses stemmed from a pivotal study in 2004 by Khoshbouei *et al.,*

demonstrating that hDAT N-terminal phosphorylation at the five distal serine residues (Ser2, Ser4, Ser7, Ser12 and Ser13) is imperative to promote reverse transport of DA via DAT. AMPH actions result in phosphorylation of DAT at these very serine residues, through which it modulates DA efflux. Interestingly, the disease-associated variant, hDAT A559V, which undergoes constitutive efflux, features a basally hyper-phosphorylated N-terminus. Fog *et al*. in 2004 and Foster *et al*. in 2002 identified the calcium-calmodulin dependent protein kinase II (CamKII) and Protein Kinase C-β (PKCβ) and key kinases activated by AMPH that phosphorylate hDAT, respectively (Fog et al., 2006; Foster, Pananusorn, & Vaughan, 2002). More recently, the Ser/Thr kinase casein kinase 2 (CK2) was recognized to be an important modulator of hDAT reverse transport, through its actions on the N-ethylmaleimide-sensitive factor attachment protein receptor (SNARE) protein, Syntaxin 1 (Stx1) (Cartier et al., 2015; Gil et al., 2011). This transmembrane SNARE protein was of specific interest to us because it has been seen to interact directly with the N-terminus of hDAT, and co-expression of Stx1 in hDAT cells results in significant amplification of AMPH-induced efflux magnitude. Moreover, AMPH actions result in CK2-dependent phosphorylation at a conserved Ser14 residue on Stx1's N-terminus, mutation of which to an Ala diminishes AMPH-induced efflux via hDAT. It is important to note that in each of these studies, researchers have detected the presence of basal levels of hDAT N-terminal phosphorylation, Stx1 Ser14 phosphorylation and CK2 activity. We predicted that the signaling pathway involving these proteins is activated when the transporter undergoes physiological efflux. In this study, we aimed at understanding the role and context of hDAT N-terminal phosphorylation, and its interaction dynamics with Stx1, in an effort to elucidate the molecular context and behavioral consequences of physiological DA efflux. We conducted biochemical, electrophysiological and behavioral analyses in vitro systems (cell lines) and *in vivo* systems (*Drosophila melanogaster*) on the wildtype hDAT (as a regularly functioning transporter) and a specially designed mutant transporter, the hDAT S/D (pseudo-phosphorylated hDAT with five N-terminal Ser mutated to Asp), as a "snapshot" of the transporter in its efflux-mode. Furthermore, we studied the interaction dynamics of hDAT and Stx1 in basal

or phosphorylated states, to understand the role of Stx1 and its phosphorylation by CK2 in hDAT reverse transport. Because AMPH has the ability to "switch" the wildtype transporter from the uptake to efflux mode, while seemingly having the opposite effect on transporters that exist in the efflux mode, we consistently use AMPH as a pharmacological tool to alter transporter states.

Introduction

Dopamine (DA) signaling plays an important role in the CNS by regulating a variety of functions, including attention, motivation, reward, movement and courtship (Kume et al., 2005; Kurian et al., 2009; Lammel, Ion, Roeper, & Malenka, 2011; Waddell, 2013). Disrupted DA function has been implicated in a number of neuropsychiatric disorders, including bipolar disorder (Horschitz et al., 2005), schizophrenia, attention-deficit hyperactivity disorder (ADHD) (Mazei-Robison et al., 2008; Mergy, Gowrishankar, Davis, et al., 2014; Mergy, Gowrishankar, Gresch, et al., 2014) and, more recently, autism spectrum disorder (ASD) (Anderson et al., 2008; Gadow et al., 2008; P. J. Hamilton, Campbell, Sharma, Erreger, Herborg Hansen, et al., 2013; Nguyen et al., 2016).

Several synaptic membrane proteins fine tune central DA homeostasis. The dopamine transporter (DAT), a presynaptic transmembrane Na^+/Cl^- symporter, acts by regulating the duration of the dopaminergic response by reuptake of released DA. The human DAT (hDAT) belongs to the neurotransmitter-sodium-symporter or the solute carrier 6 (*SLC6*) gene family predominantly expressed in the presynaptic neurons of the ventral tegmental area (VTA), dorsal and ventral striatum, and substantia nigra pars compacta (SNc) (Jaber, Jones, Giros, & Caron, 1997; Sotnikova, Beaulieu, Gainetdinov, & Caron, 2006). In terms of substrate reuptake, the DAT functional properties have been widely studied in several cell-based and *in vivo* systems. However, the DAT is a complex membrane protein capable of numerous functional modalities that are subject to differential regulations (Bermingham & Blakely, 2016; Cheng & Bahar, 2015; Cragg, Rice, & Greenfield, 1997; Gowrishankar et al., 2014; Mortensen & Amara, 2003; Vaughan

& Foster, 2013). One of these is the ability of DAT to sustain reverse transport of DA, here referred as DA efflux. DAT-mediated reverse transport of DA allows for the movement of cytosolic DA to the intersynaptic space, leading to accumulation of extracellular DA (Adell & Artigas, 2004; Gil et al., 2011; Saha, Swant, & Khoshbouei, 2012). This accumulation is known to support specific behaviors such as hyperactivity, increased impulsivity and heightened sexual impetus (Davis et al., 2018; Paredes & Agmo, 2004; Weiland et al., 2014). In recent years, we and others determined how reverse transport of DA is regulated by specific DAT structural domains by analyzing how DAT rare variants associated either with attention deficit hyperactivity disorder (A559V) (Mazei-Robison, Couch, Shelton, Stein, & Blakely, 2005; Mazei-Robison et al., 2008), autism (T356M) (P. J. Hamilton, Campbell, Sharma, Erreger, Herborg Hansen, et al., 2013) or Parkinson's disease (D421N) (Hansen et al., 2014) can support constitutive DA efflux. We found that these mutants promote constitutive DA efflux by mechanisms involving either DAT N-terminus phosphorylation (A559V) (E. Bowton et al., 2014; Mergy, Gowrishankar, Gresch, et al., 2014), a disrupted coordination of the extracellular gate (T356M mutant) or compromised Na^+ binding (D421N mutant). The definition of the signaling pathways involved in DA efflux, however, stems from studies determining how amphetamine (AMPH), which causes the reversal of DAT function, acts (Butcher, Fairbrother, Kelly, & Arbuthnott, 1988; Seiden, Sabol, & Ricaurte, 1993; D. Sulzer et al., 1995; David Sulzer et al., 2005). It is known that AMPH stimulates the activity of conventional kinases (Fog et al., 2006; Foster et al., 2012; Steinkellner et al., 2012), resulting in phosphorylation of multiple serine residues in the N-terminus of DAT. We demonstrated that AMPH-induced, DAT-mediated DA efflux is supported, at least in part, by the ability of AMPH to cause activation of Ca^{2+}/calmodulin-dependent protein kinases II (CaMKII), with subsequent phosphorylation of DAT N-Terminal serines (Foster et al., 2002; Sucic et al., 2010). Prevention of phosphorylation of DAT N-Terminus, by truncation or targeted mutations, dramatically inhibits the ability of AMPH to induce both DA efflux (Khoshbouei et al., 2004) and, in *Drosophila*, hyperlocomotion (Pizzo et al., 2013). More recently, we have demonstrated that

phosphatidylinositol-4,5-bisphosphate (PIP_2) is a regulator of AMPH-induced DA efflux and associated behaviors (Peter J. Hamilton et al., 2014). PIP_2 is a phospholipid mainly concentrated at the inner leaflet of the plasma membrane (van den Bogaart et al., 2011). It is enriched in lipid raft domains (Edidin, 2003), and is an essential cofactor regulating protein recruitment and function (Khelashvili, Doktorova, et al., 2015; Khelashvili, Galli, & Weinstein, 2012; Khelashvili, Stanley, et al., 2015; Khelashvili & Weinstein, 2015). Among those proteins is the DAT-associated protein N-ethylmaleimide-sensitive factor attachment protein receptor (SNARE) protein, syntaxin 1 (Stx1) (Khelashvili et al., 2012; Khuong et al., 2013), for which serine phosphorylation has been show to regulate reverse transport of DA (Binda et al., 2008; Cartier et al., 2015; Carvelli, Blakely, & DeFelice, 2008; Cervinski et al., 2010).

To date, there is not a clear understanding of how reverse transport of DA is regulated, the involvement of DAT associated proteins, and its impact on behaviors. In this study, we aimed to understand the role and context of DAT N-terminal phosphorylation for its dynamic interaction with Stx1, in an effort to elucidate the molecular context and behavioral consequences of DAT-mediated DA efflux under physiological conditions. We conducted biochemical and electrophysiological analyses *in vitro* (cell lines) and *ex vivo* (isolated brains of *Drosophila melanogaster*), as well as behavioral studies *in vivo* (adult *Drosophila melanogaster*) to determine whether reverse transport of DA participates in the regulation of complex behaviors (Cartier et al., 2015; P. J. Hamilton, Campbell, Sharma, Erreger, Hansen, et al., 2013b; Sanders et al., 2011; Ueno & Kume, 2014), and whether we can manipulate DAT N-terminus and/or Stx1 phosphorylation to rescue normal behaviors.

Materials and Methods

Vectors and cell lines

pEGFP-hDAT expression vectors harboring the hDAT, hDAT S/D, or hDAT S/A and pCDNA3-Stx1 expression vectors harboring the Stx1, Stx1 S14A (Ser14 mutated to alanine) or Stx1 S14D (Ser14 mutated to aspartate) sequences were generated, confirmed and transiently transfected into Human Embryonic Kidney (HEK293T) cells. Cells were maintained in a 5% CO2 incubator at 37°C in Dulbecco's Modified Eagle Medium (DMEM) supplemented with 10% fetal bovine serum (FBS), 1 mM L-glutamine, 100 U/mL penicillin, and 100 µg/mL streptomycin. Fugene-6 (Roche Molecular Biochemicals) in serum-free media was used to transiently transfect cells using a 6:1 transfection reagent:DNA ratio. Biochemical and electrophysiological assays were conducted 24-48 hours post transfection.

^{3}[H]DA Uptake assays

Cells were plated, transiently transfected on poly-D-lysine coated 24-well plates and grown to ~90% confluence. *Drosophila* brains were dissected in ice-cold Schneider's *Drosophila* Medium containing 5% BSA with surgical forceps. On the day of the experiment, cells (brains) were washed once with 37°C KRH buffer containing 10 mM dextrose, 100 µM pargyline, 1 mM tropolone, and 100 µM ascorbic acid, and equilibrated for 5 minutes at 37°C. Saturation kinetics of DA uptake (or single point DA uptake) was determined using a mixture of ^{3}[H]DA (PerkinElmer Life Sciences, Waltham, MA) and unlabeled DA diluting to final DA concentrations of 0.01 µM - 10 µM. Uptake was initiated by bath addition of the each DA dilution to a single column of wells (brains). Uptake was terminated after 10 minutes by washing twice in ice-cold KRH buffer. MicroScint Scintillation fluid (PerkinElmer Life Sciences) was added to the wells and the plates were counted in a TopCount Scintillation Counter (Perkin Elmer Life Sciences). Nonspecific binding was determined in the presence of 10 µM cocaine. Km and Vmax values were derived by fitting Michaelis-Menten kinetics to the background corrected uptake data, using GraphPad Prism 7.04 (GraphPad Software, San Diego, CA). Values reported from transport studies are derived from 3 to 5 replicate experiments.

For each data point in the uptake assays in whole *Drosophila* brain, four brains were dissected and placed in 1 mL Schneider's *Drosophila* Medium with 1.5% BSA. Brains were placed in a 12 μm pore standing well containing 1.4 mL HL3 with 1.5% BSA per well. Brains were removed and treated with 50 μM cocaine or vehicle, and incubated for 10 min. Brains were again removed, allowed for excess solution to drain, and incubated for 15 min in 0.7 mL HL3 with 1.5% BSA containing 200 nM [^{3}H]DA. Brains were washed with KRH and placed in 100 μL of 0.1% SDS solution in a top count plate. Scintillation fluid was added and [^{3}H]DA measured. Km and Vmax values were determined in all experiments by nonlinear regression using GraphPad Prism 4.0 (GraphPad Software).

Patch clamp electrophysiology assays

Cells were plated at 10^5 per 35-mm culture dish 24-48 hours prior to recording. Attached cells were washed three times at room temperature with Lub's External Solution containing 130 mM NaCl, 10 mM HEPES, 34 mM dextrose, 1.5 mM CaCl2, 0.5 mM MgSO4, and 1.3 mM KH2PO4 adjusted to pH 7.35. The pipette solution for the whole-cell recording contained 120 mM KCl, 10mM NaCl 0.1 mM CaCl2, 2 mM MgCl2, 1.1 mM EGTA, 10 mM Hepes, and 30 mM dextrose adjusted to pH 7.35. Free Ca2 was 0.1 mM. Patch electrodes were pulled from quartz pipettes on a P-2000 puller (Sutter Instruments, Novato, CA) and filled with the pipette solution. Whole cell currents were recorded using an Axopatch 200B with a low-pass Bessel filter set at 1,000 Hz. Current-voltage relationships were generated using a voltage step (500 ms) protocol ranging from -120 mV to 120 mV separated by 20 mV steps from a given holding potential. Data were recorded and analyzed offline using the software pCLAMP 9 from Axon Instruments.

Amperometry assays

Cells were prepared and washed as stated above. A carbon fiber electrode connected to an amplifier (Axopatch 200B) was attached to the plasma membrane of the cell and held at 700

mV for all experiments unless noted otherwise. The carbon fiber electrodes (ProCFE; fiber diameter is 5 m) were obtained from Axon Instruments. 10 μM AMPH or COC (unless otherwise specified) was added to the dish and amperometric currents were low pass filtered at 100 Hz, recorded and analyzed off-line using the software pCLAMP 9 from Axon Instruments (Figure 28). *Drosophila* brains were dissected with surgical forceps in ice-cold Schneider's *Drosophila* Medium containing 5% BSA. For drug conditions, flies were fed 100 nM CX-4945 or vehicle 24 hours prior to the assay. Whole brains were manually removed and placed in a mesh holder in Lub's external solution (130 mM NaCl, 10 mM HEPES, 1.5 mM CaCl2, 0.5 mM MgSO4, 1.3 mM KH2PO4, 34 mM dextrose, adjusted to pH 7.35 and 300 mOsm) containing 100 nM CX-4945. A carbon fiber electrode was held at +700 mV and positioned in the TH-positive PPL1 DA neuronal region. Amperometric current was calculated in response to 20 μM AMPH addition using an Axopatch 200B amplifier and pCLAMP software (Molecular Devices; Union City, CA). DA efflux was quantified as the peak value of the amperometric current.

Biochemical assays (Phospho-western blots and Co-immunoprecipitation assays)

Cells were transiently transfected and grown to 100% confluence in 6-well plates. On the day of the assay, following drug or vehicle treatment in with 37°C KRH buffer, cells were washed three times with 4°C phosphate-buffered saline (Gibco) containing 1 mM EGTA and 1 mM EDTA and lysed in RIPA buffer (100 mM NaCl, 1.0% IGEPAL CA-630 (NP-40), 0.5% sodium deoxycholate, 0.1% SDS, 50 mM Tris, pH = 8.0, supplemented with a protease inhibitor cocktail (Sigma Aldrich)). In ion replacement experiments, the extracellular Na concentration was adjusted by iso-osmotically changing the concentration of KCl in the KRH solution. Lysates were passed twice through a 27.5 gauge needle and centrifuged at 15,000 x g for 30 minutes. For phospho-western blots, total cell lysate was analyzed by SDS-PAGE and with a portion of the total cell lysate collected to run as the totals. For coimmunoprecipitation assays, 1 mL of the remaining supernatant was incubated at 4°C for 4 hours with Sepharose-G beads (Fisher Scientific),

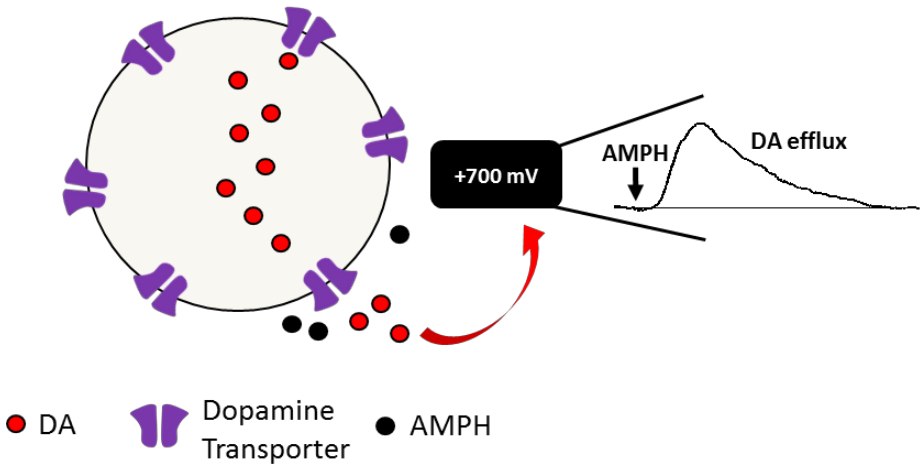

Figure 28: A schematic representation of dopamine signal measured via single-cell amperometry.

Dopamine, represented by red circles, is loaded into cells expressing hDAT. A carbon fiber electrode (middle) is charged to 700 mV and positioned next to a single cell. AMPH (black circles) reverses DA uptake (efflux), causing release of DA, which is oxidized by the carbon fiber electrode. Oxidation of DA is interpreted as a current and DA efflux is represented by an upwards deflection in current (top, during measurement of AMPH-induced efflux.

previously washed with 1% BSA in RIPA buffer and preincubated with 2.5 µg anti-GFP antibody ab290 (rabbit polyclonal from Abcam). For the negative control, supernatant was incubated with BSA-blocked Sepharose-G beads alone (no antibody control). As an additional control, lysate from mock transfected cells was incubated at 4°C for 4 hours with Sepharose-G beads (Fisher Scientific), previously washed with 1% BSA in RIPA buffer and preincubated with 2.5 µg anti-GFP antibody ab290. Beads were spun down, washed with cold RIPA buffer, and samples eluted with Laemmli sample buffer at 95°C for 5 minutes. Total lysates and eluates were analyzed by SDS-PAGE and immunoblotting (see below for antibody details). Band intensity was quantified using ImageJ software (National Institutes of Health). The association between Stx1 mutantts and hDAT mutants was represented as the ratio of eluate:total lysate band intensity, normalized to the eluate:total lysate ratio observed in control conditions and expressed as a fraction

Biotinylation assays

Cells were transiently transfected and grown to 100% confluence in 6-well plates. On the day of the assay, cells were washed three times with 4°C phosphate-buffered saline (Gibco) and sulfosuccinimidyl-2-(biotinamido)ethyl-1,3-dithiopropionate-biotin (sulfo-NHS-SS-biotin) (1.0 mg/ml, Pierce, Rockford, IL) was added to each well and allowed to incubate for 30 min at 4°C. Cells were quenched with 100 mM glycine and then solubilized in radioimmunoprecipitation assay buffer (RIPA) (10 mM Tris, pH 7.4, 150 mM NaCl, 1 mM EDTA, 0.1% SDS, 1% Triton X-100, 1% sodium deoxycholate, 250 µM PMSF, 1 µg/µl aprotinin, 1 µg/ml leupeptin, 1 µM pepstatin) for 30 min at 4 °C. Extracts were collected from wells and centrifuged for 30 min at 16,000 × g at 4 °C. The supernatant was added to immunopure immobilized streptavidin beads (Pierce). Beads were allowed to incubate for 45 min at room temperature, extensively washed, and Laemmli buffer with 2-mercaptoethanol was added. The eluate from the beads, as well as the biotinylated input (5 µg) was run on an SDS-PAGE gel, transferred to polyvinylidene fluoride membrane (PVDF) (Millipore, Bedford, MA) and immunoblotted for hDAT using a rat monoclonal primary antibody to the N-

terminus of hDAT (1:1000) (MAB369 from Millipore) and a goat-anti-rat-HRP-conjugated secondary antibody (1:5000, Jackson ImmunoResearch, West Grove, PA). Syntaxin 1 was probed using a rat monoclonal primary antibody (S0664 SIGMA). Band densities were quantified using NIH image software and data from 4 separate experiments were combined and analyzed using Prism software.

GST pulldown assays

Gluthathione transferase (GST) fusion proteins with the first 64 N-terminal amino acids of hDAT, hDAT S/D or hDAT S7D.S12D were generated by PCR-mediated amplification of the relevant DNA sequences using the Pfu polymerase (Stratagene, La Jolla, CA) and the full-length synDAT gene (Saunders et al., 2000). The resulting PCR products were cloned into pET41a (Novagen, Madison, WI). The GST and the GST fusion proteins were produced in Escherichia coli BL21 DE3 LysS. The culture was grown at 30°C, expression was induced by the addition of 0.02 mM isopropylβ-d-1-thiogalactopyranoside, and harvested following incubation at 22°C O/N. The pelleted bacteria were frozen, thawed in PBS, pH 7.4 containing 0.1% TX-100, 20μg/mL DNAse I, 1mM DTT and Bacterial Protease inhibitor Cocktail (Roche Diagnostics), refrozen, and thawed. The lysate was cleared by centrifugation and incubated for 1.5h at 4°C after the addition of glutathione Sepharose 4B beads (GE Healthcare, Chalfont St. Giles, Buckinghamshire, UK). The beads were pelleted and washed several times in PBS with 0.1% Triton X-100, 1mM DTT. The quality, size, and amount of GST fusions were determined by SDS-polyacrylamide gel electrophoresis and GelCode Blue stain (Pierce, Rockford, IL). The fusion protein was produced and isolated as the DAT N-terminal fusions. Stx1A was released by cleavage overnight at 4°C with thrombin (0.2 U; Novagen). Phenylmethylsulfonyl fluoride was added, and beads were removed by centrifugation. Equal amounts of GST fusion proteins were incubated with 2 μg of purified Stx1 in PBS containing 0.1% TX-100, 0.1% BSA in a total volume of 500μl for 1 hour at 4°C. The beads were washed 3 times in wash buffer (PBS with 0.1% TX-100, 1mM DTT). Bound

protein was eluted by addition of thrombin (0.2 U) incubated for 1 hour at RT following addition of loading buffer. The Stx1 bound was evaluated by immunoblotting using mouse anti-Syntaxin (Sigma, St. Louis, MO), horseradish peroxidase anti-mouse antibody, and visualization with ECL+ (GE Healthcare).

FRET assays

Flp-In HEK293 cells were maintained at 37°C in 5% CO2 in DMEM supplemented with 10% fetal bovine serum and 1% penicillin-streptomycin. Stable cell lines were generated according to the manufacturers protocol and selected for pCIN4 by addition of Geneticin 0.4mg/ml (Invitrogen, Carlsbad, CA) and cells expressing pCDNA 5 FRT/TO were selected by the addition of Hygromycin 0.125mg/ml as well as Blasticidin 15µl/ml (1mg/ml) (Invitrogen, Carlsbad, CA). Flp-In HEK293 cells stably expressing CFP-DAT, CFP-DAT S7D-S12D or CFP-DAT S7A- S12A from the pCIN4 vector (Promega, USA) with concomitant tetracycline-inducible expression of YFP-Tac, YFP-Stx1 or YFP-Stx1 TM ONLY in the pCDNA5 FRT/TO vector (Invitrogen, USA) were seeded two days prior to the experiments in poly-L-ornithine coated Lab-Tek 8-chamber plates (Thermo Scientific, USA). The following day the cells were induced by the addition of tetracycline in a 1:1000 ratio. The day of the experiment the cells were washed three times with imaging buffer (25 mM HEPES, 120 mM NaCl, 5 mM KCl, 1.2 mM CaCl2, 1.2 mM MgSO4, 5 mM D-glucose, pH 7.4). The third wash was left to equilibrate at RT for 10 minutes before measurements. The FRET measurements were done on an epifluorescence microscope (Carl Zeiss, TM210, Germany) using a 40x oil objective and a LUDL filter-wheel (LUDL electronic products Ltd., NY, USA) for rapid filter exchange. CFP, YFP and FRET images were combined to a stack, and the image stack was converted to a NFRET image using the PixFRET plugin in ImageJ. The spectral bleed through values (SBTs) of CFP and YFP were determined for each construct, using uninduced cell lines to quantity CFP SBT and induced cell lines not expressing CFP to quantify YFP SBT. The NFRET value was calculated as N_FRET=(I_FRET-〖BT〗_DONOR×I_DONOR-〖BT〗

_ACCEPTOR×I_ACCEPTOR)/√(I_DONOR×I_ACCEPTOR)×100 where 〖BT〗_DONOR=I_FRET/I_DONOR and 〖BT〗_ACCEPTOR=I_FRET/I_ACCEPTOR. A Gaussian blur was applied to all the images to smoothen the NFRET image. This improves the rendering of the computed image and prevents aberrant NFRET values. A value of 1.5 was chosen as this value provided the best image quality for the quantification of NFRET in the membrane. A threshold correction factor was used to determine the lowest NFRET value computed in the picture. This correction factor is a multiplication factor of the background signal, and values below this factor were set to zero. The threshold correction factor was set to 0.5. All image acquisitions were performed using MetaMorph software v. 4.6 (Molecular Devices, USA). Additional image treatment was performed with ImageJ software using the PixFRET plugin.

Drosophila genetics

Drosophila homozygotes for the DAT null allele DATfmn (dDAT KO) (Kume et al., 2005) and flies harboring TH-Gal4 (Friggi-Grelin et al., 2003) were outcrossed to a control line (Bloomington Indiana (BI) 6326) and selected by PCR or eye color. TH-GAL4 (BI 8848) and M{vas-int.Dm}ZH-2A, M{3xP3-RFP.attP'} ZH-22A (BI 24481) were obtained from the BI stock center and outcrossed to dDAT KO flies carrying the white (w1118) mutation (BI stock number 6236) for 5 - 10 generations. Transgenes (hDAT or hDAT S/D) were cloned into pBI-UASC (J.-W. Wang et al., 2012) and constructs were injected into embryos from M{vas-int.Dm}ZH-2A, M{3xP3-RFP.attP'}ZH-22A (BI 24481). Initial potential transformants were isolated and selected.

Drosophila behavior

Locomotion assays: Male flies were collected immediately post-eclosion and housed with other male flies until 3-5 days of age. Locomotion was analyzed after transfer to chambers in which activity was monitored by beam breaks. Data was analyzed using software from Trikinetics.

For AMPH-induced locomotion, flies were starved for 6 hours prior to drug exposure. Flies were administered CX-4945 or vehicle 24 hours prior to AMPH administration. Courtship assays: Male and female virgins were collected post-eclosion and housed with other flies of the same sex until 3-5 days of age to achieve sexual maturity. Single male flies were manually transferred to 3D printed chambers. The chamber was illuminated, and the male fly was allowed to acclimate for 10 minutes, following which a single female fly was introduced into the chamber. Courtship behavior of the male was recorded for ten minutes, following which videos were scored to quantify courtship index, latency to court and % that achieved copulation.

Results

N-terminal phosphorylation predisposes hDAT to undergo DA reverse transport

Prior studies from our group have demonstrated that hDAT phosphorylation at the five distal N-terminal Ser residues is necessary for reverse transport to occur (Khoshbouei et al., 2004). In our present study, we studied the impact of N-terminal phosphorylation on transporter biophysics and interaction dynamics with partner proteins, to understand the occurrence and context of DA reverse transport. To delineate the steps that occur upon N-terminal phosphorylation of the hDAT, we adopted a model of the transporter in its efflux-mode, the hDAT S/D (with the five N-terminal Ser mutated to Asp to mimic phosphorylation). This genetic mutant of hDAT presets the transporter in the conformational and interactive state that it would typically acquire while undergoing reverse transport. The first step of our study was to probe whether the hDAT S/D undergoes constitutive, drug-independent efflux. Adopting single-cell amperometry techniques, and a potent hDAT blocker (cocaine), we examined the differences in baseline efflux from cells expressing the wildtype hDAT (hDAT cells) and those expressing the hDAT S/D pseudophosphorylated mutant (hDAT S/D cells). As predicted, the application of 10 uM cocaine resulted in a steep drop in baseline in the hDAT S/D cells to achieve a newer and lower baseline,

indicating the presence of constitutive efflux. In contrast, cocaine had no effect on hDAT cells, indicated by the flat amperometry trace (Figure 29a). The constitutive efflux in hDAT S/D cells may decrease the ability of the transporter (and in turn, the ability of the cell) to accumulate DA over time. To test this potential consequence of constitutive efflux, we measured radioactive DA uptake in the hDAT S/D cells. hDAT S/D cells exhibit deficits in its kinetic uptake properties, namely apparent Vmax, compared to hDAT cells (Figure 29b).

Analyzing these findings, we hypothesized that the hDAT S/D cells would have similar physiology to the disease-associated variant hDAT A559V. This is based on the findings that the A559V variant transporter harbors a basally hyper-phosphorylated N-terminus and undergoes constitutive efflux as it prefers to exist in its efflux mode. A key finding with this variant was that it exhibited blockade of constitutive reverse transport in response to not only cocaine, but also to AMPH (E. Bowton et al., 2014). Indeed, in contrast to its efflux-inducing properties on hDAT cells, AMPH acts as a potent blocker of constitutive efflux in the hDAT S/D cells (Figure 29c). Therefore, the hDAT S/D preferentially exists in the efflux mode, and does not require AMPH actions to undergo reverse transport. Furthermore, expression of this pseudophosphorylated transporter might have the same consequences on the cell as that of AMPH. Khoshbouei *et al.* 2014 showed that AMPH causes depolarization in hDAT cells, which initiates the cascade of signaling events that result in reverse transport. We hypothesized that the N-terminal phosphorylation effects of AMPH cause membrane depolarization via changes in transporter physiology. We examined the electrophysiological properties of the hDAT S/D cells and noted that they exhibit basal membrane depolarization – i.e. in drug-naïve conditions, we were able to see similar effects as that of AMPH (Figure 29d). When we further examined the changes in inherent transporter properties upon pseudophosphorylation of the N-terminus by plotting an I-V relationship for the hDAT S/D cells, we noted large inward currents that were absent in the hDAT cells, and a more positive reversal potential (Figure 29e). The presence of significantly amplified inward currents at negative voltage steps points to the mechanism underlying basal membrane depolarization of the hDAT S/D cells.

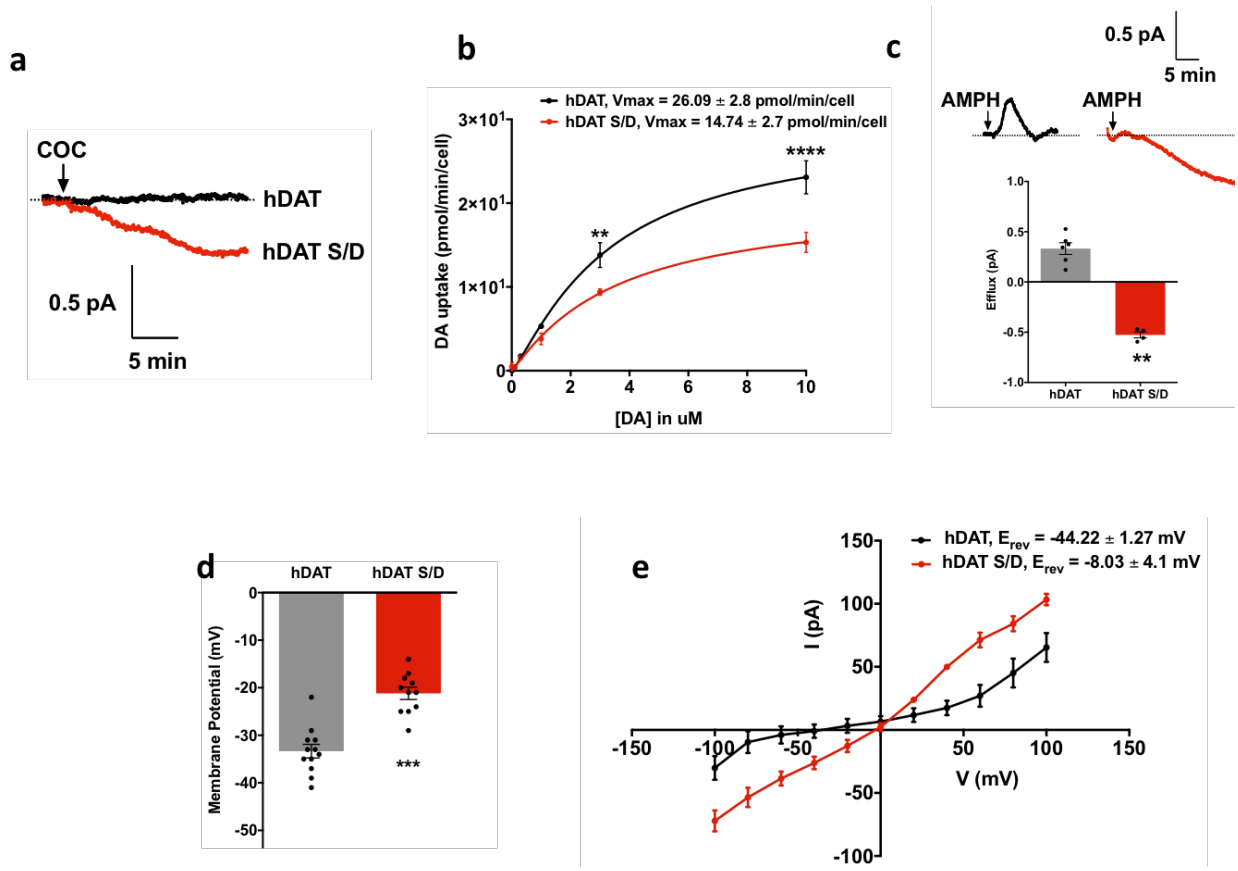

Figure 29: hDAT S/D exhibits constitutive dopamine efflux and altered intrinsic transporter properties.

(a) Cocaine blocks constitutive efflux in hDAT S/D cells. Representative amperometry traces recorded from cells transfected with hDAT or hDAT S/D. Arrow indicates application of 10 uM cocaine. Cocaine has no effect on hDAT cells. (b) Reduced ^{3}[H]DA uptake in hDAT S/D cells. Representative plot of ^{3}[H]DA uptake kinetics in cells expressing hDAT (in black) or hDAT S/D (in red) (** = $p < 0.01$, **** = $p < 0.0001$ by two-way ANOVA followed by Bonferroni post-test, in triplicate). Inset: kinetic parameters (Vmax) in cells expressing hDAT (in black) or hDAT S/D (in red) (Vmax: $p < 0.05$ by Student's t-test; n = 4, mean ± s.e.m, in triplicate); there were no significant differences in Km (data not shown). (c) Analysis of AMPH-induced efflux in hDAT or hDAT S/D cells. Top: Representative AMPH-induced DA efflux recorded from transiently transfected hDAT cells expressing hDAT or hDAT S/D. Arrows indicate application of 10 uM AMPH. Bottom: Quantitation of AMPH-induced DA efflux. Data are represented as peak oxidative current. (** = $p < 0.01$ by two-tailed Student's t-test; n = 4-6, mean ± s.e.m). (d) Quantitation of basal membrane potential difference measured in cells expressing hDAT (in black) or hDAT S/D (in red). hDAT S/D cells exhibited significantly more positive basal membrane potential (-33.33 ±1.427 mV) compared to hDAT cells (-21.18 ± 1.292 mV) (*** =$p< 0.001$ by two-tailed Student's t-test, n = 11-12, mean ± s.e.m). (e) Current-Voltage relationships measured in cells expressing hDAT (in black) or hDAT S/D (in red). hDAT S/D cells exhibit significantly amplified outward currents at voltage steps above +40 mV and inward currents at voltage steps below -40 mV. The reversal potential for hDAT S/D cells measured -8.03 ± 4.1 mV was significantly different from that of hDAT cells measured at -44.22 ± 1.27 mV (**** = $p < 0.0001$ by two-tailed Student's t-test, n = 5-7, 95% confidence intervals).

From these findings, we were able to infer that hDAT S/D cells behaved similarly to hDAT cells that have been treated with AMPH. Phosphorylation of the hDAT N-terminus might play a significant role as the transporter undergoing efflux under physiological conditions.

hDAT N-terminal phosphorylation promotes Stx1 phosphorylation, potentiation of AMPH-induced, DAT-mediated efflux and reduced hDAT-Stx1 interactions

Following our preliminary analyses, we wished to examine the consequences of the hDAT N-terminus phosphorylation and resulting membrane depolarization, specifically to understand if the transporter was now "primed" to engage reverse transport machinery. We were keenly interested in understanding the role of the SNARE protein Syntaxin 1, previously shown to be an important modulator of reverse transport via hDAT (Binda et al., 2008; Cervinski et al., 2010). Studies from our group and other groups in the past have shown that not only does co-expression of Stx1 with hDAT significantly potentiate AMPH-induced DA efflux, but also that phosphorylation of a key N-terminal residue on Stx1, Ser14, was an important step in the intracellular signaling pathway leading to reverse transport (Cartier et al., 2015). In our present study, we conducted biochemical analyses on the phosphorylation levels of Stx1 as well as interaction properties with the hDAT S/D, to study whether the hDAT S/D mimicked the state of the transporter that undergoes physiological reverse transport. Interestingly, we saw that Stx1 co-expressed with the hDAT S/D was basally hyper-phosphorylated at Ser14, in contrast to Stx1 that is co-expressed with hDAT, suggesting that hDAT phosphorylation is followed by Stx1 phosphorylation during reverse transport. Furthermore, it appeared to have achieved a ceiling effect, as there was no further elevation in phosphorylation by AMPH application, indicating that the hDAT S/D does not require AMPH to engage the reverse transport machinery (Figure 30a). We wished to delve deeper into understanding the role of Stx1 phosphorylation on hDAT reverse transport. We conducted single-cell amperometry assays on hDAT cells co-transfected with a pseudophosphorylated mutant of Stx1 (Stx1 S14D) or a phospho-deficient Stx1 (Stx1 S14A).

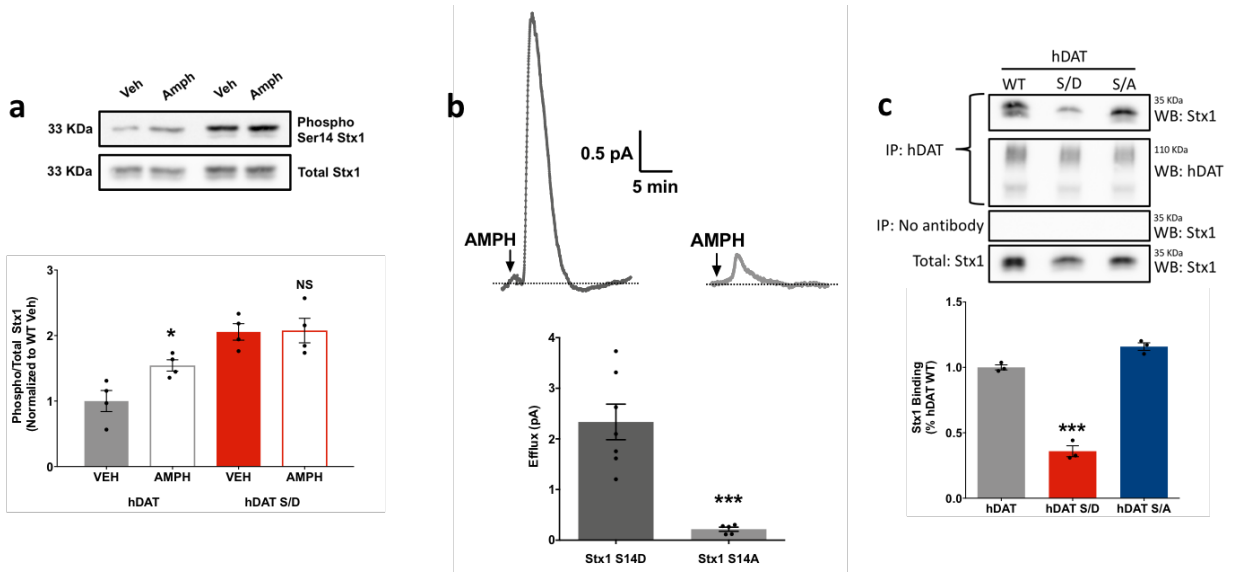

Figure 30: hDAT N-terminal phosphorylation causes cell depolarization, leading to Stx1 phosphorylation and efflux.

(a) Stx1 co-expressed with hDAT S/D is hyper-phosphorylated. hDAT or hDAT S/D cells were cotransfected with Stx1, followed by treatment with VEH or 10 uM AMPH for 10 minutes. Top: Representative western blot of whole-cell lysates immunoblotted with antibodies directed at phospho-Ser14 Stx1 or total Stx1. Bottom: Immunoblot band densities were quantified, normalized to the corresponding density of total Stx1, and expressed as a fraction of hDAT vehicle control (* = $p < 0.05$ compared to hDAT - VEH, NS = $p > 0.9999$ compared to hDAT S/D – VEH, by one-way ANOVA followed by Bonferroni post-test, n = 4, mean ± s.e.m). (b) Stx1 phosphorylation promotes AMPH-induced DA efflux. Top: Representative AMPH-induced DA efflux recorded from stably transfected hDAT cells expressing hDAT with Stx1 S14D or S14A. Arrows indicate application of 10 uM AMPH. Bottom: Quantitation of AMPH-induced DA efflux. Data are represented as peak oxidative current. (*** = $p < 0.001$ by one-way ANOVA followed by Bonferroni post-test; n = 5-7, mean ± s.e.m). (c) hDAT S/D exhibits diminished interaction with Stx1 WT. hDAT, S/D or S/A was co-transfected with Stx1. hDAT was immunoprecipitated with protein-G agarose beads and bead conjugates were analyzed for Stx1. Top: Representative western blot of hDAT immunoprecipitates immunoblotted with antibodies directed against either Stx1 or hDAT. Input or total Stx1 serves as a transfection and loading control. Bottom: Immunoblot band densities were quantified, normalized to corresponding density of hDAT pulldown, and expressed as a fraction of hDAT control (*** = $p < 0.001$ compared to hDAT, NS = $p > 0.1$ compared to hDAT, by one-way ANOVA followed by Bonferroni post-test, n = 3, mean ± s.e.m).

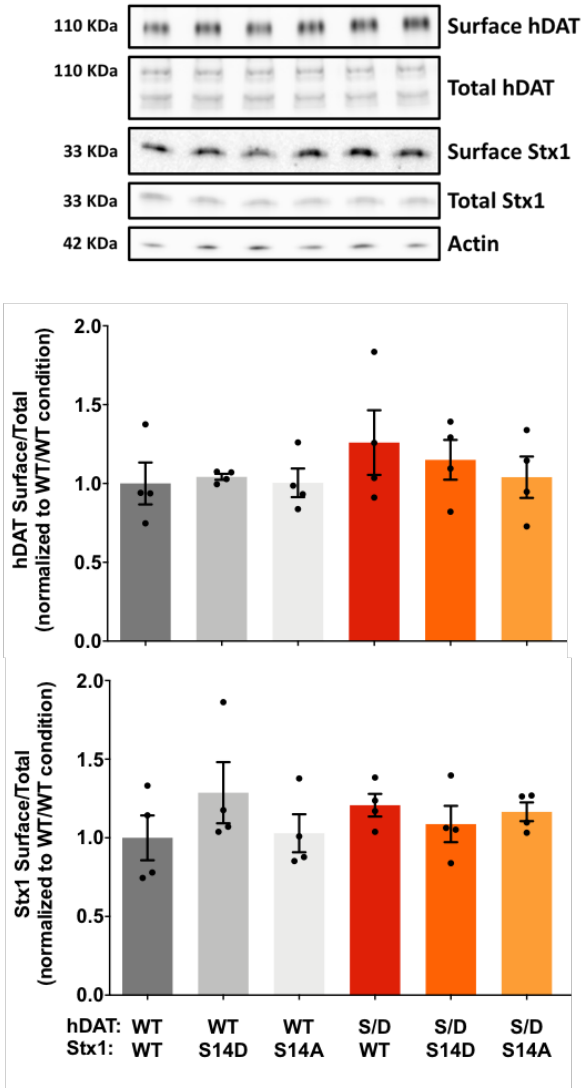

Figure 31: hDAT and hDAT S/D cotransfected with the Stx1 have comparable surface and total expression levels.

Representative immunoblots for biotinylated (surface) and total hDAT and Stx1 protein fractions from transiently transfected hDAT or hDAT S/D cells, co-expressing the 3 isoforms of Stx1 – WT, S14D and S14A. Surface fractions were quantitated, normalized to total protein, and normalized to WT/WT control condition ($p \geq 0.7$ by Student's t-test; n = 4 in duplicate; mean ± s.e.m).

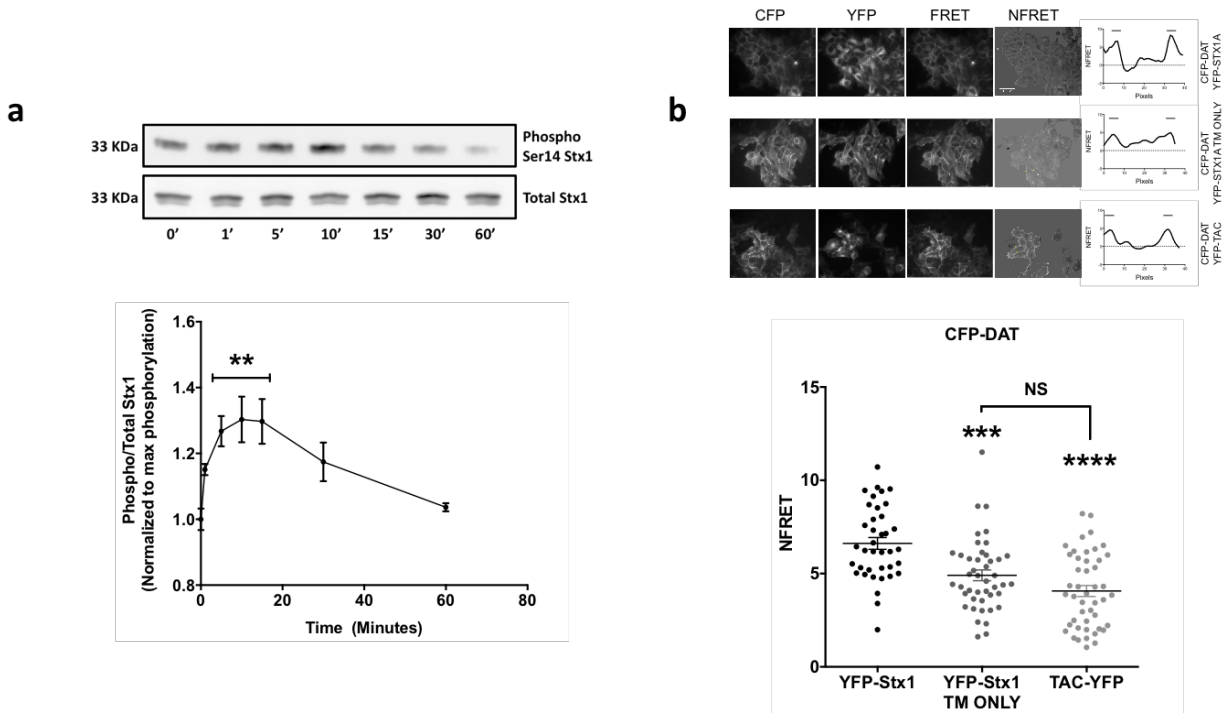

Figure 32: AMPH phosphorylates Stx1 at the N-terminus, the region of interaction with hDAT.

(a) Stx1 undergoes maximum phosphorylation at 10 minutes post AMPH treatment. hDAT cells were co-transfected with Stx1, followed by 10 uM AMPH treatment for 0', 1', 5', 10', 15' 30' and 1 hour. Top: Representative western blot of whole-cell lysates immunoblotted with antibodies directed at phospho-Ser14 Stx1 or total Stx1. Bottom: Immunoblot band densities were quantified, normalized to the corresponding density of total Stx1, and expressed as a fraction of hDAT vehicle control (** = $p < 0.005$ compared to 0' condition, by one-way ANOVA followed by Bonferroni post-test, n = 4, mean ± s.e.m). (b) hDAT interacts with the N-terminus of Stx1. Flp-In cells stably expressing CFP-DAT were cotransfected with tet-inducible expression of YFP-Stx1, YFP-Stx1 TM only or TAC-YFP. YFP, CFP, and FRET images were acquired from living cells at room temperature. NFRET was calculated as described under "Experimental Procedures". Top: Representative images and live NFRET signals in each experimental condition. Bottom: Quantification of NFRET values for each experimental condition. (*** = $p < 0.0005$, **** = $p < 0.0001$ compared to YFP-Stx1, by one-way ANOVA followed by Bonferroni post-test, n = 38-44, mean ± s.e.m)

hDAT cells cotransfected with Stx1 S14D showed significantly enhanced AMPH-induced efflux compared to cells cotransfected with Stx1 S14A, again pointing to the reverse transport machinery being “primed” for transporter-mediated efflux upon the actions of AMPH (Figure 30b). But, importantly, hDAT does not undergo constitutive efflux without N-terminal phosphorylation. Because it appeared that reverse transport occurs upon hDAT and Stx1 phosphorylation, we hypothesized that when both hDAT and Stx1 are phosphorylated (keeping in mind that Stx1 cotransfected with hDAT S/D is basally hyper-phosphorylated), the physical interaction between them falls apart and DA efflux occurs. To understand the interaction dynamics of hDAT upon phosphorylation with Stx1, we used coimmunoprecipitation assays and studied the interaction between Stx1 and hDAT, hDAT S/D or hDAT S/A (as a negative control). Interestingly, hDAT S/D has a significantly diminished interaction with Stx1, showing that indeed, phosphorylation mediates loss of interaction between hDAT and Stx1, leading to reverse transport of DA (Fig. 30c). It appeared that AMPH actions on the transporter hijacks the process of physiological transport by inducing N-terminal phosphorylation at the DAT, via membrane depolarization and kinase activation mechanisms. To confirm a strong correlation between Stx1 phosphorylation and reverse transport via hDAT, we demonstrated the temporal dynamics of AMPH’s effects on Stx1 phosphorylation. We show that Stx1 achieves maximal phosphorylation above baseline 10 minutes following AMPH treatment, providing a key insight that the Stx1 phosphorylation timeline is tightly coupled to that of AMPH-induced efflux via hDAT (Figure 32a). As a control experiment, we conducted FRET assays in live cells to confirm that Stx1’s N-terminus is the key region that interacts with hDAT, using the transmembrane region of Stx1 (Stx1 TM only) only with N-terminus cleaved off as a negative control (Figure 32b). Next, we looked to understand the mechanism underlying basal Stx1 phosphorylation in hDAT S/D cells, to see if it occurs in the same manner as that during AMPH actions.

Membrane depolarization and CK2 activation leads to Stx1 phosphorylation at Ser14

Previous studies by Cartier *et al*. have shown that for reverse transport to occur, Stx1 phosphorylation at the N-terminal Ser14 residue by CK2 is necessary (Cartier et al., 2015). CK2 has been widely studied to have numerous substrates and plays an important role in the activation of several intracellular signaling pathways, but the mechanism of activation of CK2 is not yet clear (Meggio & Pinna, 2003). We were interested to know if, specifically, depolarization of the membrane leads to CK2 activation and in turn, Stx1 phosphorylation. We treated hDAT cells with an extracellular solution containing high K^+ to induce membrane depolarization and saw an elevation of Stx1 phosphorylation at the Ser14 residue, which was reversible by CX-4945, a potent and highly bioavailable pharmacological inhibitor of CK2 activity (Figure 33a) (Siddiqui-Jain et al., 2010). To corroborate with our earlier findings that N-terminal phosphorylation during physiological conditions mimics the actions of AMPH, we demonstrate that phosphorylation of Stx1 at Ser14 by AMPH actions can be reversed by CX-4945 as well, pointing to CK2 as a key kinase in mediating reverse transport (Figure 33b). We went one step further to confirm that it is specifically the depolarizing actions of AMPH that result in Stx1 phosphorylation. Indeed, pre-treatment of hDAT cells with 1 uM or 10 uM Valinomycin (a potassium ionophore that maintains a hyperpolarized cell membrane) (Freyberg et al., 2016; Ruchala et al., 2014) prior to AMPH treatment prevents Stx1 phosphorylation in a dose-dependent manner (Figure 33c). These findings helped us conclude that in the hDAT S/D cells, the presence of large, transporter-mediated inward currents leads to membrane depolarization, CK2 activation, Stx1 phosphorylation and DA reverse transport. Moreover, hDAT S/D cells can mimic the actions of AMPH. Placing in a physiological context, when a cell or neuron expressing DAT undergoes depolarization, it may result in hDAT and Stx1 phosphorylation, and reverse transport of DA.

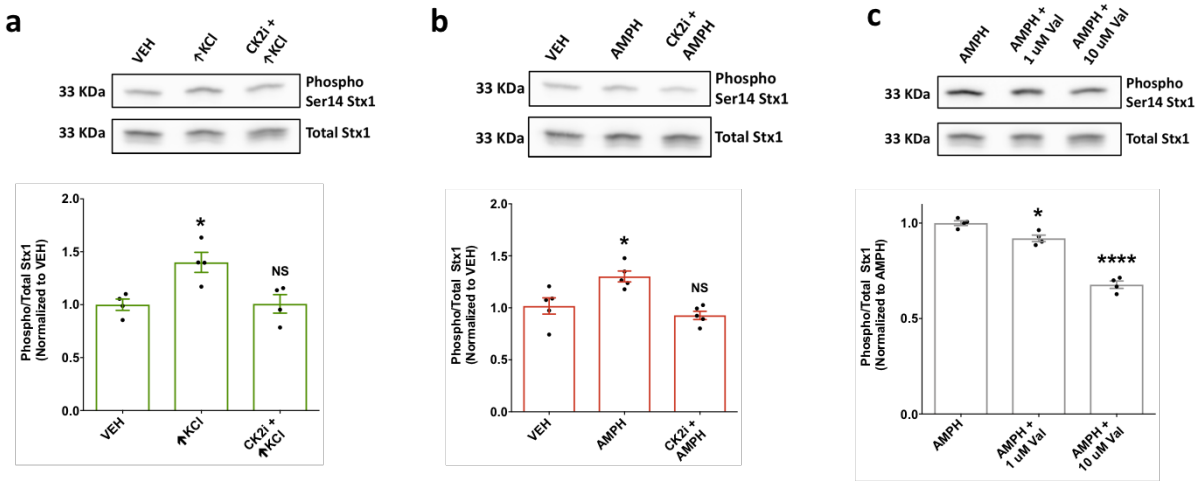

Figure 33: AMPH phosphorylates Stx1 via depolarization of the cell and activation of CK2.

(a) High potassium-induced cell depolarization elevates Stx1 phosphorylation at Ser14, reversible by CK2 inhibition. hDAT cells were cotransfected with Stx1, pre-treated with VEH or 100 nM CX-4945 for 30 minutes, followed by treatment with VEH or 40mM KCl for 10 minutes. Top: Representative western blot of whole-cell lysates immunoblotted with antibodies directed at phospho-Ser14 Stx1 or total Stx1. Bottom: Immunoblot band densities were quantified, normalized to the corresponding density of total Stx1, and expressed as a fraction of vehicle control (* = $p < 0.05$ compared to VEH only, NS = $p > 0.5$ compared to VEH only, by one-way ANOVA followed by Bonferroni post-test, n = 4, mean ± s.e.m). (b) AMPH treatment elevates Stx1 phosphorylation at Ser14, reversible by CK2 inhibition. hDAT cells were cotransfected with Stx1 and pre-treated with VEH or 100 nM CX-4945 for 30 minutes, followed by treatment with VEH or 10 uM AMPH for 10 minutes. Top: Representative western blot of whole-cell lysates immunoblotted with antibodies directed at phospho-Ser14 Stx1 or total Stx1. Bottom: Immunoblot band densities were quantified, normalized to the corresponding density of total Stx1, and expressed as a fraction of vehicle control (* = $p < 0.05$ compared to VEH only, NS = $p > 0.5$ compared to VEH only, by one-way ANOVA followed by Bonferroni post-test, n = 4, mean ± s.e.m). (c) Valinomycin-mediated cell hyperpolarization diminishes AMPH-induced Stx1 phosphorylation. hDAT cells were cotransfected with Stx1, pretreated with 10 uM AMPH for 10 minutes, followed by treatment with 1 uM or 10 uM Valinomycin for 10 minutes. Top: Representative western blot of whole-cell lysates immunoblotted with antibodies directed at phospho-Ser14 Stx1 or total Stx1. Bottom: Immunoblot band densities were quantified, normalized to the corresponding density of total Stx1, and expressed as a fraction of AMPH control (* = $p < 0.05$ compared to AMPH control, **** < 0.001, by one-way ANOVA followed by Bonferroni post-test, n = 4, mean ± s.e.m).

Stx1 phosphorylation is necessary for constitutive DA efflux

Next, we tried to understand the context and consequences of elevated Stx1 phosphorylation and decreased hDAT-Stx1 interactions in the hDAT S/D cells. We were interested in finding potential "brakes" in the reverse transport machinery, in an effort to delineate key mechanisms that regulate physiological DAT-mediated reverse transport. First, we probed the importance of Stx1 phosphorylation on the constitutive efflux phenotype of hDAT S/D cells. We speculated that prevention of Stx1 phosphorylation might hinder constitutive efflux. To this end, we conducted single-cell amperometry in hDAT S/D cells that were co-transfected with a phospho-deficient Stx1 (Stx1 S14A) or with a pseudophosphorylated Stx1 (Stx1 S14D). Remarkably, co-transfection with Stx1 S14A abolished constitutive DA efflux in hDAT S/D cells, pointing to Stx1 phosphorylation at Ser14 as a key mechanism that regulates constitutive efflux (Figure 34a). As a logical next step, we considered that in the absence of constitutive efflux, the cells must regain their ability to accumulate DA. In our radioactive uptake assays, DA uptake was restored to wildtype levels (showed as a dotted black line) in hDAT S/D cells that were co-transfected with Stx1 S14A (Figure 34b). In our control cells (hDAT S/D cells co-transfected with Stx1 S14D), there was a significant deficiency in DA uptake.

Earlier, we hypothesized that when hDAT and Stx1 interact in a tight complex, DA efflux cannot occur. When this complex falls apart (due to N-terminal phosphorylation, mutations, or AMPH actions), the transporter can efflux DA. To confirm this hypothesis, we looked to demonstrate that when we prevent Stx1 phosphorylation, hDAT and Stx1 are retained in a tight complex that prevents constitutive efflux. To do so, we conducted a coimmunoprecipitation assay in hDAT S/D cells co-transfected with Stx1 S14A, and showed that hDAT S/D has significantly higher interaction levels with Stx1 S14A (Figure 34c). To understand whether hDAT S/D and Stx1 undergo a direct interaction or exist as parts of a multiple protein-protein interaction complex, we conducted *in vitro* GST pulldown assays using Stx1 and hDAT peptide mutants consisting of the first 64 amino acids in the N-terminus (N64). Results from our GST pulldown assay mirrored the

findings from our CoIP, wherein N64-hDAT S7D.S12D (N64 hDAT peptide with Ser7 and Ser12 mutated to Ala) and N64-hDAT S/D displayed reduced interaction levels with Stx1 in a dose-dependent manner (Figure 36a). We found similar results in our live FRET assays, in which the hDAT S7D.S12D showed reduced interactions with Stx1 whereas the negative control hDAT S7A.S12A was not significantly different from hDAT (Figure 36b).

Due to the availability of a potent pharmacological inhibitor of Stx1's kinase, CK2, that we have already shown to possess the ability to preclude Stx1 phosphorylation, we were able to recapitulate the above findings without genetic manipulation of Stx1. In our single-cell amperometry assays on hDAT and hDAT S/D cells, pretreatment of hDAT cells with CX-4945 resulted in a significantly diminished AMPH-induced efflux, indicating the importance of Stx1 phosphorylation in reverse transport. On the other hand, pretreatment of hDAT S/D cells with CX-4945 completely abolished constitutive efflux and quite interestingly, resulted in the same magnitude of AMPH-induced efflux as its CX-4945-treated wildtype counterpart (Figure 34d). These findings show that CK2-mediated Stx1 phosphorylation at Ser14 is a pivotal step before reverse transport takes place. Moreover, prevention of Stx1 phosphorylation, either via genetic or pharmacological manipulation, can act as a "brake" on hDAT's ability to undergo constitutive DA efflux. This mechanism may help control the on-off dynamics of physiological efflux via DAT.

hDAT S/D transgenic *Drosophila melanogaster* brains exhibit constitutive efflux that can be blocked by CX-4945

Drosophila has now widely been used for many decades as a reliable model organism to study alterations in the DAergic system (S. Yamamoto & Seto, 2014). More specifically, previous members of our group have clearly defined the ability to isolate and study the effects of altering DAT function in the fly (P. J. Hamilton, Campbell, Sharma, Erreger, Hansen, et al., 2013b). Therefore, we wished to translate our cell-based discoveries on the hDAT S/D to *Drosophila*

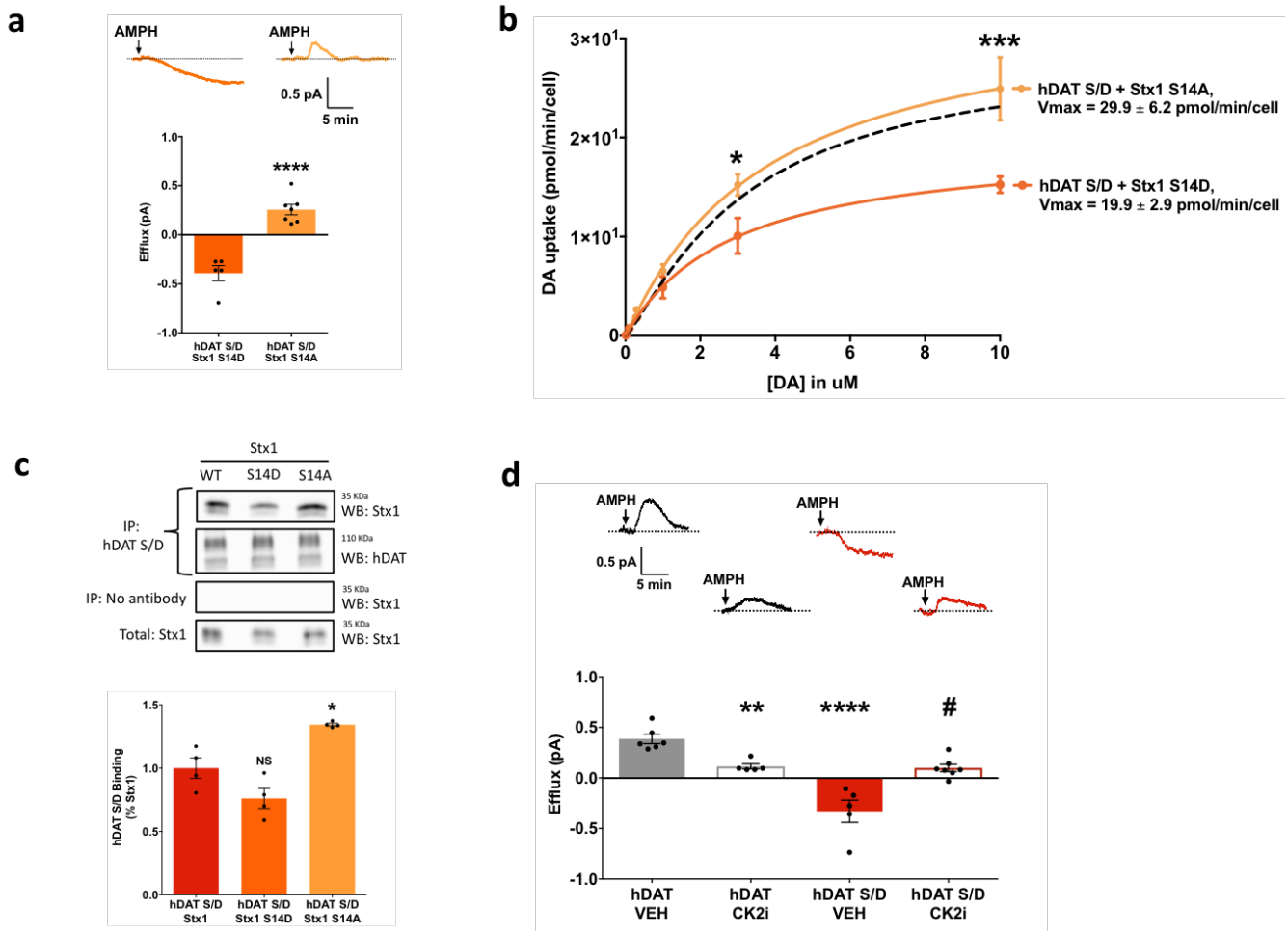

Figure 34: Genetic and pharmacological prevention of Stx1 phosphorylation abolishes constitutive efflux in hDAT S/D.

(a) Co-transfection with Stx1 S14A abolishes constitutive efflux in hDAT S/D cells. Top: Representative AMPH-induced DA efflux recorded from cells expressing hDAT S/D with Stx1 S14D or S14A. Arrows indicate application of 10 uM AMPH. Bottom: Quantitation of AMPH-induced DA efflux. Data are represented as peak oxidative current. (**** = $p < 0.0001$ by two-tailed student's t-test; n = 4-7, mean ± s.e.m). (b) Impaired uptake in hDAT S/D is rescued when cotransfected with Stx1 S14A. Representative plot of [^{3}H]DA uptake kinetics in cells expressing Stx1 S14D (in tangerine) or Stx1 S14A (in yellow). Inset: kinetic parameters (Vmax) in the same cells. Vmax in hDAT S/D cells when cotransfected with Stx1 S14A is rescued back to hDAT levels (* = $p < 0.05$, *** = $p < 0.001$ by one-way ANOVA followed by Bonferroni's post-test, n = 4, mean ± s.e.m, in triplicate); there were no significant differences in Km (data not shown). Dotted black line denotes uptake kinetics in control hDAT cells. (c) hDAT S/D exhibits enhanced interaction interaction with Stx1 S14A. hDAT was co-transfected with Stx1 WT, S14D or S14A. hDAT was immunoprecipitated with protein-G agarose beads and bead conjugates were analyzed for Stx1. Top: Representative western blot of hDAT immunoprecipitates immunoblotted with antibodies directed against either Stx1 or hDAT. Input or total Stx1 serves as a transfection and loading control. Bottom: Immunoblot band densities were quantified, normalized to corresponding density

of hDAT pulldown, and expressed as a fraction of hDAT control (* = $p < 0.05$ compared to Stx1 WT, NS = $p > 0.05$ compared to hDAT, by one-way ANOVA followed by Bonferroni post-test, n = 4, mean ± s.e.m). (d) CX-4945 treatment abolishes constitutive efflux in hDAT S/D cells. Top: Representative AMPH-induced DA efflux recorded from cells expressing hDAT or hDAT S/D co-transfected with Stx1, pre-treated with VEH or 100 nM CX-4945 for 1 hour. Arrows indicate application of 10 uM AMPH. Bottom: Quantitation of AMPH-induced DA efflux. Data are represented as peak oxidative current. (**** = $p < 0.0001$, ** = $p< 0.005$ compared to hDAT VEH and # = $p < 0.0001$ compared to hDAT S/D VEH by two-way ANOVA followed by Fisher's LSD post-test; n = 4-7, mean ± s.e.m).

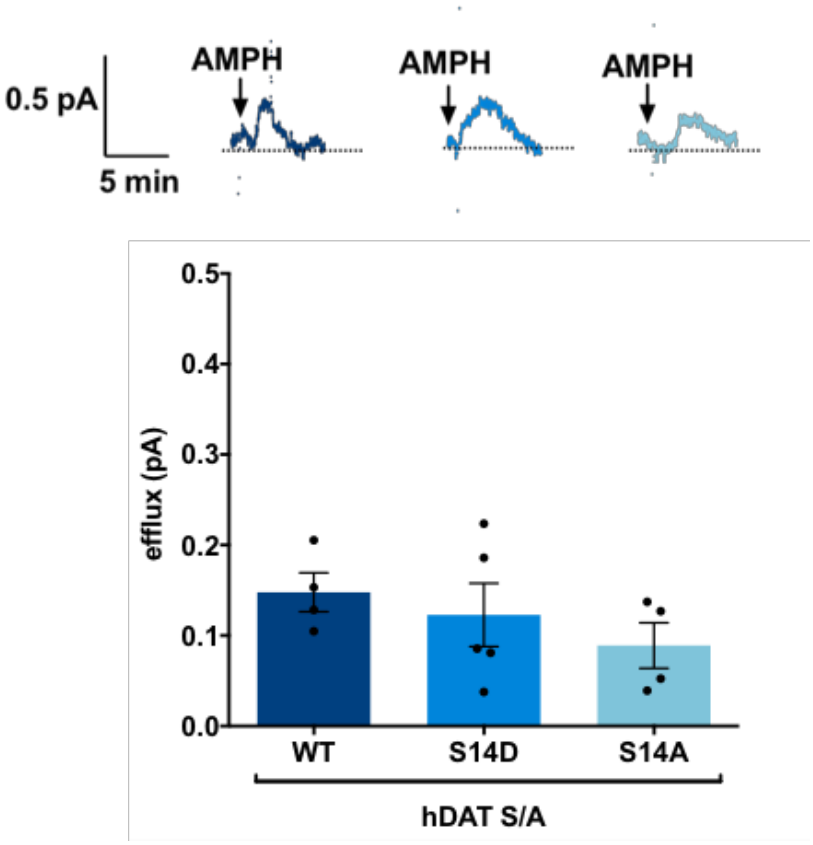

Figure 35: hDAT S/A cells do not exhibit constitutive efflux.

Co-transfection with Stx1 WT, S14D or S14A does not induce constitutive efflux in hDAT S/A cells. Top: Representative AMPH-induced DA efflux recorded from cells expressing hDAT S/A with Stx1 WT, S14D or S14A. Arrows indicate application of 10 uM AMPH. Bottom: Quantitation of AMPH-induced DA efflux. Data are represented as peak oxidative current. ($p > 0.05$ by one-way ANOVA followed by Bonferroni post-test; n = 4-7, mean ± s.e.m).

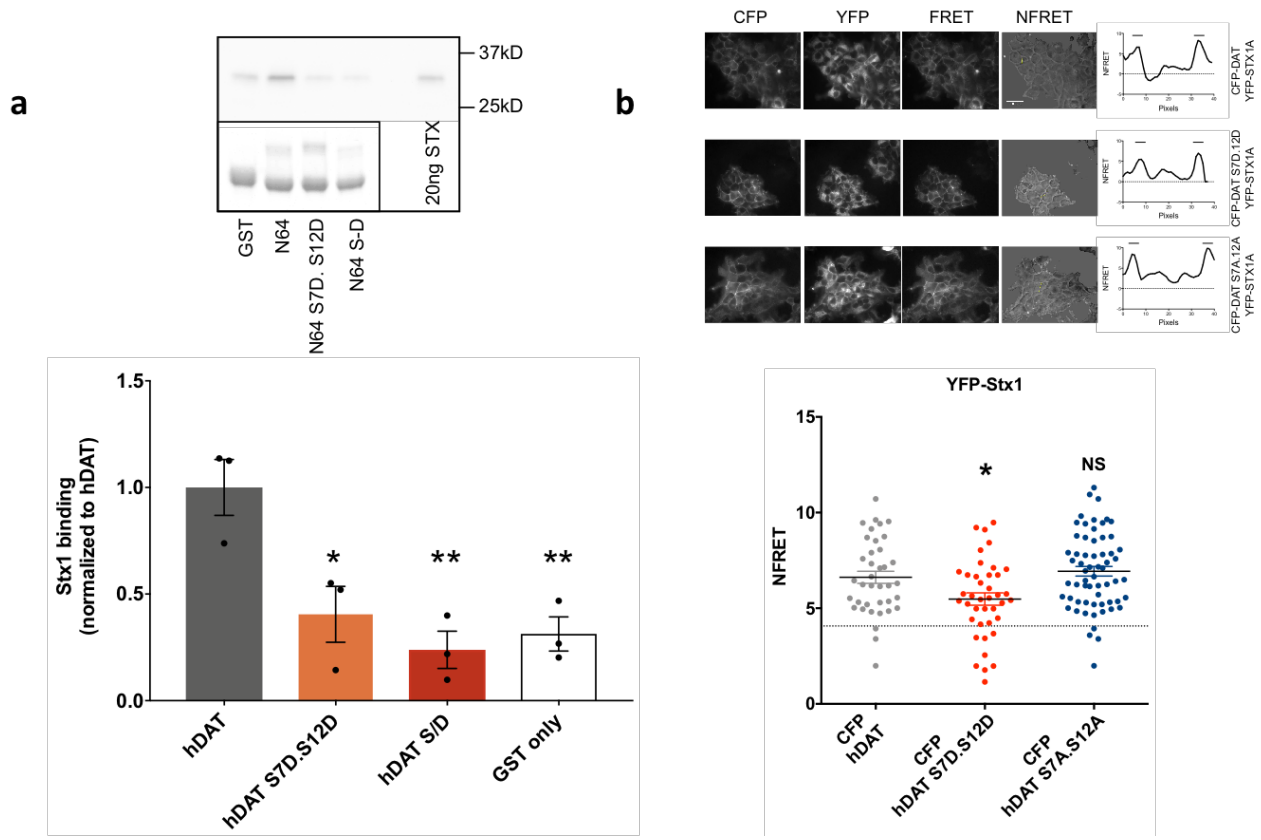

Figure 36: Stx1 has reduced interactions with pseudophosphorylated DAT N-terminus.

(a) GST pull-down experiments confirm that Stx1 interacts directly with the first 64 N-terminal residues of hDAT, and this interaction is reduced upon pseudophosphorylation of hDAT. Top: Representative SDS-PAGE blot stained with GelCode Blue stain. Total Stx1 serves as the loading control. Bottom: Immunoblot band densities were quantified, normalized to corresponding density and expressed as a fraction of hDAT control condition (* = $p < 0.05$, ** = $p < 0.01$ compared to hDAT, by one-way ANOVA followed by Bonferroni post-test, n = 3, mean ± s.e.m).(b) Live-cell FRET experiments further confirm reduced interactions between Stx1 and pseudophosphorylated hDAT. Flp-In cells stably expressing CFP-hDAT, CFP-hDAT S7D.S12D or CFP-hDAT S7A.S12A were cotransfected with tet-inducible expression of YFP-Stx1 and FRET images were acquired from living cells at room temperature. NFRET was calculated as described under “Experimental Procedures”. Top: Representative images and live NFRET signals in each experimental condition. Bottom: Quantification of NFRET values for each experimental condition. (* = $p < 0.05$, NS = $p > 0.9999$ compared to CFP-hDAT, by one-way ANOVA followed by Bonferroni post-test, n = 38-44, mean ± s.e.m)

melanogaster, to achieve the goal of studying the molecular and behavioral consequences associated with physiological efflux in an intact animal. Using novel *ex vivo* and *in vivo* assays, we attempted to understand the effects of disrupting hDAT's ability to undertake both forward and reverse transport functions to modulate DA homeostasis. Specifically, in our transgenic S/D flies, we hoped to see the effects of expressing an hDAT that has lost the ability to shut off DA reverse transport. We designed transgenic flies that expressed hDAT or hDAT S/D specifically in DAergic neurons, in a global dDAT knockout fly, to delineate the effects of constitutive efflux. Our initial steps involved the molecular characterization of the constitutive efflux in the flies. We pioneered the application of carbon fiber electrode amperometry to target measurement of DA release from whole, intact, excised fly brains. Consistent with our cell-based assays, our *ex vivo* fly brain amperometry experiments demonstrated that oral administration of CX-4945 to the flies attenuates AMPH-induced efflux in hDAT transgenic fly brains. Furthermore, CX-4945 administration abolished constitutive efflux in hDAT S/D brains, similar to our cell-based findings (Figure 37). It is especially remarkable that the translation of our *in vitro* experiments was achieved in this organism through oral administration of CX-4945 via regular food intake. These results helped us infer that CX-4945 is functional *in vivo* in a similar manner to that *in vitro*, and that the mechanism underlying reverse transport in flies is conserved with that of mammalian cell lines.

Transgenic flies expressing hDAT S/D exhibit hyperactivity and enhanced courtship behaviors, reversible by CX-4945

Previous studies from our laboratory have established that in *Drosophila*, basal and AMPH-induced locomotion is a DA-associated and DAT-dependent behavior (Pizzo et al., 2013; Ueno & Kume, 2014). In our hDAT S/D flies, we hoped to understand the behavioral outcome of constitutive reverse transport that would result in elevated DA levels in the extracellular space, potentially enhancing activation of DA receptors on the post-synaptic neuron and D2ARs on the

presynaptic neuron. Analysis of fly circadian rhythm demonstrated that as predicted, the hDAT S/D transgenic flies exhibit basal hyperactivity in comparison to hDAT flies over a period of 24 hours (Figure 38a). Cumulative beam breaks over a period of 24 hours showed significant increases in basal activity in the hDAT S/D flies compared to hDAT flies (Figure 38b). This behavioral paradigm further allowed us to determine the altered effects of AMPH and resulting DA-associated behaviors in the two genotypes. In hDAT flies, AMPH treatment induces hyperactivity, mirroring several previous studies from our group, due to initiating the DA reverse process in the brain (Figure 38c). Remarkably, AMPH treatment in the hDAT S/D flies rescued basal hyperactivity back to hDAT levels, suggesting that AMPH is able to block constitutive efflux in an intact organism (Figure 38d). Our next step was to determine whether impeding Stx1 phosphorylation decreases the ability of AMPH to augment extracellular DA levels and as a consequence, locomotion. Analysis of drug-induced locomotion demonstrates that oral administration of CX-4945 24 hours prior to AMPH treatment attenuates AMPH-induced locomotion in the hDAT flies, further implicating Stx1 phosphorylation as a key step for AMPH to cause hDAT-mediated reverse transport of DA (Figure 38c). In the hDAT S/D flies, CX-4945 administration significantly reduces basal hyperactivity, presumably by reversal of Stx1 phosphorylation (Figure 38d).

DA plays an important role in modulating courtship-stimulating cues, olfaction, contact chemoreception and pheromone response in male and female *Drosophil*a (Chang et al., 2006; Gailey, Lacaillade, & Hall, 1986). Dopamine-depleted female flies have a significantly reduced propensity to accept male courtship advances, compared to untreated females (Neckameyer, 1998). Males with increased dopamine levels tend to court other males, arising from altered sensory perception (Liu et al., 2008). Moreover, the dopamine receptors Dop1R and DopR2 play pivotal roles in signal transmission and learning during courtship behavior – wherein a male fly learns over time to adjust its mating behavior based on responses from the female (Chen et al., 2017). Based on these findings, we conducted courtship assays on the hDAT and hDAT S/D flies,

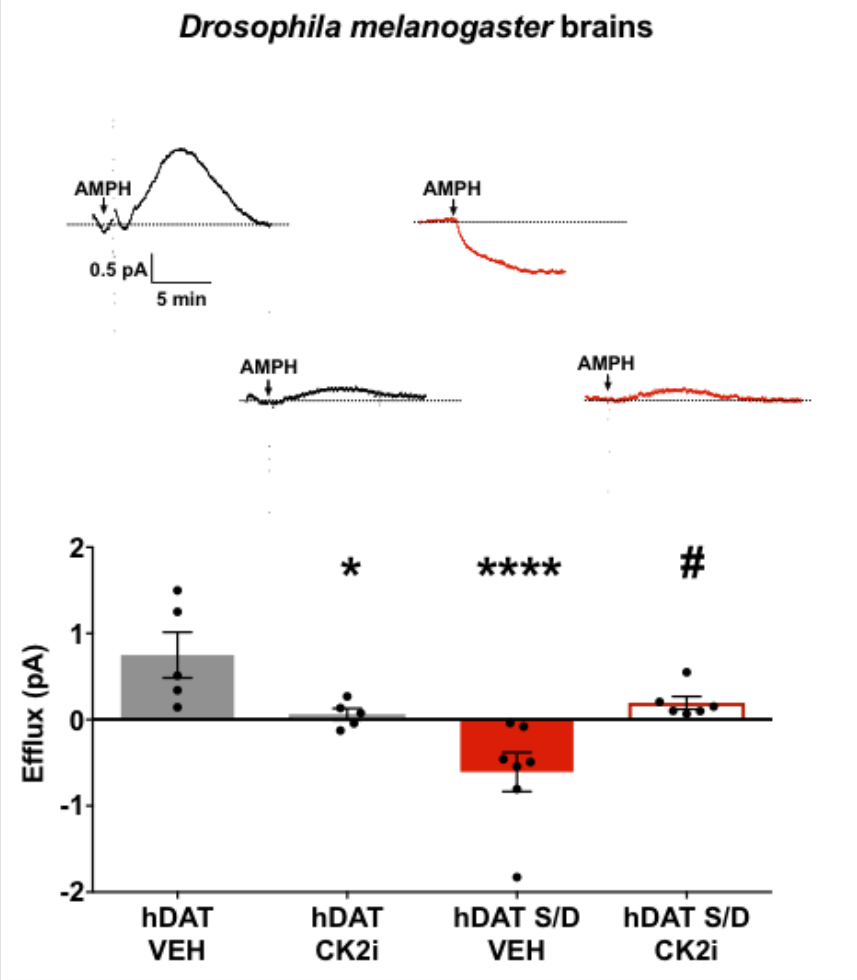

Figure 37: hDAT S/D transgenic flies have elevated extracellular DA arising from constitutive efflux, reversible by CX-4945.

CX-4945 treatment abolishes ADE in hDAT S/D fly brains. Top: Representative AMPH-induced DA efflux recorded from cells expressing hDAT or hDAT S/D dissected, intact brains, pre-treated with VEH or 100 nM CX-4945 for 1 hour. Arrows indicate application of 10 uM AMPH. Bottom: Quantitation of AMPH-induced DA efflux. Data are represented as peak oxidative current. (* = $p < 0.05$, **** = $p < 0.0001$ compared to hDAT VEH and # = $p < 0.005$ compared to hDAT S/D VEH by two-way ANOVA followed by Fisher's LSD post-test; n = 4-7, mean ± s.e.m).

to determine the behavioral effects of constitutive DA efflux in the fly brain. Strikingly, the hDAT S/D flies show over a five-fold increase in their courtship index compared to the hDAT flies, measured as a ratio of amount of time spent exhibiting courtship behavior compared to total time in the behavior chamber (Figure 39aa). Administration of CX-4945 significantly reduces the courtship index in the hDAT S/D flies, resonating our findings with the locomotion behavior. Additionally, percentage of male flies that achieved copulation was 16.67% in the WT flies as opposed to 50% in the S/D flies, and administration of CX-4945 completely abolishes the hDAT S/D fly's ability to achieve copulation (Figure 39b). These results signify that constitutive DA efflux from the dopaminergic neurons of the S/D fly leads to higher extracellular DA levels and enhanced DA-associated behaviors. These findings are consistent with our hypothesis that Stx1 phosphorylation is a key step in mediating reverse transport, and that preventing Stx1 phosphorylation can act as a "brake" on a transporter that is undergoing reverse transport in a physiological context. Through this novel courtship assay to understand the consequences of constitutive efflux, we hope to pave the way to discovering more complex behaviors that will help in the understanding of physiological uptake and efflux states of the transporter and its role in promoting key behaviors in the fly.

Discussion

The DAT is critical for maintaining DA homeostasis in the brain, and alterations in DAT function can lead to disruptions in important DA-associated behaviors. These behaviors are not only physiologically relevant, but also phenotypically associated with neuropsychiatric disorders like ADHD, autism, bipolar disorder and schizophrenia. One of the DAT's key functional modalities, reverse transport, is significant in understanding how the transporter contributes to maintaining DA homeostasis. But, the series of intracellular signaling mechanisms that take place in the cell resulting in reverse transport of DA is unclear. In this study, we illustrate the mechanisms that are involved in the reverse transport of DA via the DAT.

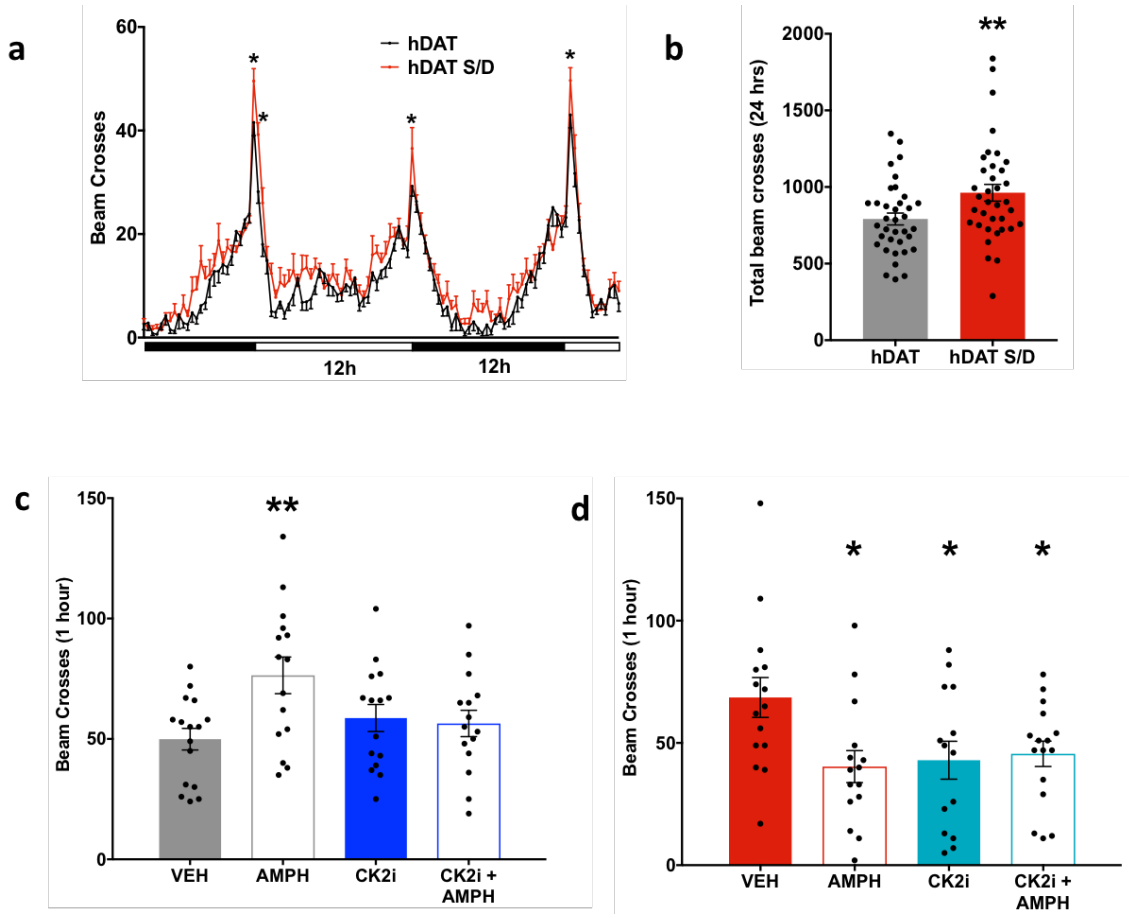

Figure 38: hDAT S/D transgenic flies exhibit hyperactive phenotype, reversible by CX-4945.

(a) hDAT S/D flies exhibit hyperactivity in their circadian cycle. hDAT or hDAT S/D was expressed in DA neurons of dDAT KO flies. Locomotor activity was assayed over 36 hours during the light (horizontal white bars) or dark (horizontal black bars) cycle. Flies expressing hDAT S/D (red symbols) were hyperactive at peak activity points tin the 36 hour period with respect to flies expressing hDAT WT (black symbols) (* = $p < 0.05$ by two-way ANOVA followed by Fisher's LSD post-test, n = 36, mean ± s.e.m, beam breaks binned in 15 minute intervals). (b) hDAT S/D flies exhibit hyperactivity over a period of 24 hours. Quantitation of total beam crosses over 24 hours for hDAT and hDAT S/D. hDAT S/D transgenic flies exhibit significantly higher locomotive behavior compared to hDAT flies. (** = $p \leq 0.005$ by Student's t-test, n = 36, mean ± s.e.m). (c) CX-4945 reverses AMPH-induced locomotion in hDAT flies. hDAT flies were orally administration of VEH or 100 nM CX-4945 for 24 hours, followed by oral administration of VEH or 10 uM AMPH for 1 hour. The flies administered with only 10 uM AMPH exhibited significant hyperactivity. (** = $p < 0.01$ by one-way ANOVA followed by Bonferroni post-test, n = 14-16, mean ± s.e.m). (d) AMPH and CX-4945 reduce basal hyperactivity in hDAT S/D flies. hDAT S/D flies were orally administration of VEH or 100 nM CX-4945 for 24 hours, followed by oral administration of VEH or 10 uM AMPH for 1 hour. Basal hyperactivity exhibited by the hDAT S/D flies is significantly reduced in the AMPH, CK2i and AMPH+CK2i conditions (* = $p < 0.05$ by one-way ANOVA followed by Bonferroni post-test, n = 14-16, mean ± s.e.m).

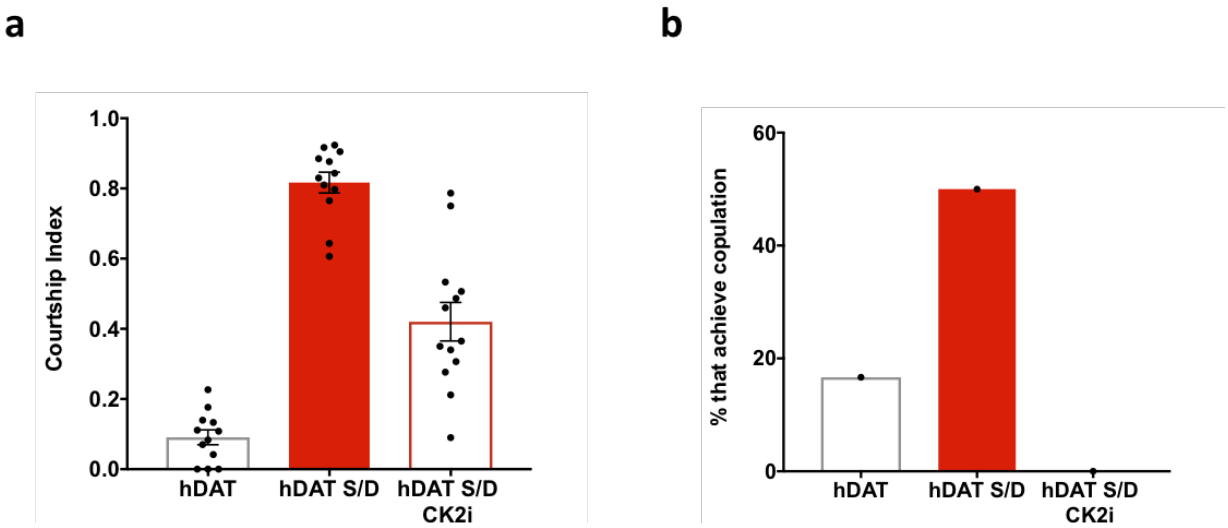

Figure 39: hDAT S/D transgenic flies exhibit heighted courtship behaviors, partially rescuable by CX-4945.

(a) Behaviors associated with courtship, including orientation, tapping, wing vibration, licking and attempting copulation were scored as a percentage of the 10-minute observation period. Flies expressing hDAT S/D exhibited significantly enhanced courtship behaviors. Administration of CX-4945 to flies expressing hDAT S/D displayed a trend for reduced courtship behaviors in these flies, but further analyses are warranted to optimize the effects of this drug on these behaviors. (b) Similarly, hDAT S/D flies had a high success rate of achieving copulation compared to hDAT WT flies. Interestingly, CX-4945 administration completely abolished copulation in the hDAT S/D flies.

Many groups in the past, including ours, have harnessed the ability of the widely abused psychostimulant, AMPH, as a pharmacological tool in studying DAT reverse transport (David Sulzer et al., 2005). AMPH causes reverse transport or efflux of DA from dopaminergic neurons, resulting in elevated DA levels in the synaptic cleft, altered neurotransmission and resultant behaviors. To understand the molecular mechanisms that underlie DAT reverse transport, we sought to identify key players (associated or modulatory proteins, signaling molecules and effectors) that may mediate the effects of AMPH on the transporter.

In 2004, Khoshbouei *et al*., established that AMPH actions at the DAT require phosphorylation five distal N-terminus serine residues as part of the signaling cascade resulting in transporter reversal (Khoshbouei et al., 2004). Mutation of these Ser residues to Ala prevents the ability of DAT to undergo reverse transport. Subsequent studies by Hamilton et al. showed additional roles of the DAT N-terminus in reverse transport. The residues Lys3 and Lys5 at the distal region of the N-terminus are significant in mediating DAT's interaction with the membrane phospholipid PIP2 (Peter J. Hamilton et al., 2014). Neutralizing mutations of these Lys residues reduces the interaction with PIP2, and also decreases AMPH-induced reverse transport of DA. Computational analyses demonstrated that DAT's interaction with PIP2 was important in sequestering the transporter with the SNARE protein Stx1 (Khelashvili, Doktorova, et al., 2015; Khelashvili et al., 2012). Interestingly, over-expression of Stx1 significantly enhances DAT reverse transport. Concurrent studies by Lee et al. 2004, Binda et al. 2008 and Khelashvili et al. 2012 provided key insights on DAT-Stx1 interactions at the N-terminus and Stx1 phosphorylation at the Ser14 residue by CK2 as necessary to mediate DAT reverse transport (Binda et al., 2008; Khelashvili et al., 2012; K.-H. Lee et al., 2004). These findings helped us hypothesize a model of DAT reverse transport, in which the dynamics of DAT-Stx1 interactions were key to the different modalities of DAT's function, and that phosphorylation states of these two proteins were important signaling components of reverse transport.

In this study, we delineated the signaling events that precede DAT reverse transport, focusing on the roles of DAT N-terminus and Stx1 phosphorylation, as well as DAT-Stx1 interaction dynamics. Additionally, we determined the physiological relevance of DAT reverse transport in *Drosophila melanogaster* through the study of various integral behaviors. We studied hDAT S/D (hDAT with a pseudo-phosphorylated N-terminus) as a "snapshot" of the transporter in its efflux mode. We found that cells expressing hDAT S/D exhibit constitutive DA efflux, in the absence of AMPH. As a result, hDAT S/D cells cannot accumulate DA, shown through our radioactive DA uptake assays. Surprisingly, constitutive efflux of hDAT S/D cells can be blocked by the application of AMPH, which is counter-intuitive to our understanding of the actions of AMPH on hDAT cells (that exhibit efflux upon AMPH application). Interestingly, the disease-associated variant, hDAT A559V, has earlier been shown to exhibit constitutive efflux and a hyper-phosphorylated N-terminus (Erica Bowton et al., 2010). Additionally, AMPH acts to block the constitutive efflux in the hDAT A559V cells. We hypothesized that constitutive efflux via the transporter was a result of N-terminus phosphorylation. These preliminary findings may explain one possible mechanism by AMPH-based treatments ameliorate ADHD- and Autism-associated phenotypes. In patients that are diagnosed with these disorders, AMPH may act to block DAT undergoing constitutive efflux, thus, decreasing overall extracellular DA and reestablishing DA homeostasis in the CNS.

We wished to further understand the role of Stx1 in the signaling mechanisms underlying DAT reverse transport. Using a multi-faceted approach including biochemical, electrophysiological and behavioral assays, we studied the impact of N-terminal phosphorylation on transporter biophysics and interaction dynamics with its key partner protein, Stx1, to understand the occurrence and context of physiological DA reverse transport. We harnessed the power of genetic mutations in hDAT and Stx1 to mimic phosphorylation as well as pharmacological tools to alter phosphorylation states of the two proteins. We initiated our studies by characterizing the hDAT S/D's biophysical and biochemical properties. Pseudo-

phosphorylating the hDAT N-terminus results in the significant elevation of basal Stx1 phosphorylation at Ser14. hDAT S/D also have a reduced affinity for Stx1, suggesting that phosphorylation of these two proteins leads to a decrease in binding affinity. In our model of DAT reverse transport, we hypothesized that decrease in binding affinity of DAT and Stx1 leads to enhanced reverse transport. In other words, Stx1 binding to DAT acts as a "brake" on reverse transport. Once the brake is released (by DAT N-terminus phosphorylation, followed by Stx1 phosphorylation at Ser14), DAT can undergo reverse transport. Indeed, when we co-transfected Stx1 S14D (pseudo-phosphorylated Stx1) with hDAT, AMPH-induced efflux increased five-fold (compared to hDAT co-transfected with Stx1 S14A).

But the key question still remained, which was - why did the hDAT S/D cells undergo constitutive efflux even in the absence of AMPH? During our preliminary analyses on the hDAT S/D, we found that under physiological conditions, hDAT S/D cells exhibit basal membrane depolarization, arising from large inward currents when the cells were clamped at negative potentials. We sought to understand if this cellular depolarization contributes to mediating constitutive DA efflux. Specifically, we thought that this depolarization may be initiating a signaling cascade that promotes DA reverse transport. To understand if cell depolarization mediates reverse transport, we depolarized hDAT cells using 40mM KCl, and found that it resulted in significantly increased Stx1 phosphorylation. Earlier work has identified CK2 as the key kinase that phosphorylates Stx1 at Ser14. To determine, whether Stx1 was undergoing phosphorylation through this kinase, we pre-treated cells with a pharmacological inhibitor of CK2, CX-4945. Pre-treatment of cells with CX-4945 inhibited high K^+-induced Stx1 phosphorylation at Ser14. These findings helped contribute to our model and established that cellular depolarization (that can be artificially induced but is also known to occur physiologically during neurotransmission) mediates DAT and Stx1 phosphorylation, resulting in a decreased interaction between the two proteins and reverse transport via the DAT.

To corroborate our findings with the signaling mechanisms that occur upon AMPH actions, we analyzed Stx1 phosphorylation and the importance of cellular depolarization on AMPH-induced reverse transport. Indeed, AMPH application elevated Stx1 phosphorylation in hDAT cells, which was reversible by pre-treatment with CX-4945. Moreover, AMPH-induced phosphorylation was absent in cells pre-treated with Valinomycin, a potassium ionophore that prevents membrane depolarization. These findings provided us with a mechanistic framework that membrane depolarization is one of the first steps that leads to DAT reverse transport by promoting CK2-mediated Stx1 phosphorylation at Ser14. These findings are supported by previous studies which demonstrated that inhibiting Stx1 phosphorylation at Ser14 severely attenuates AMPH-induced DA efflux via DAT.

Considering these findings, we probed the importance of Stx1 in constitutive efflux in the hDAT S/D. If Stx1 phosphorylation at Ser14 is a prerequisite for removing the “brake” on DAT, inhibition of Stx1 phosphorylation would serve as an impediment to DAT reverse transport. In the next series of experiments, we show via single-cell amperometry assays that Stx1 phosphorylation at Ser14 is necessary for constitutive efflux in the hDAT S/D, and that substitution of the Ser14 to an Ala abolishes constitutive efflux. Moreover, hDAT S/D regains the ability to accumulate DA in the cells similar to wildtype DAT levels, when co-transfected with Stx1 S14A. To corroborate with our earlier hypothesis that phosphorylation of hDAT and Stx1 leads to a decreased binding affinity between the two, resulting in hDAT being able to acquire an efflux mode, we conducted coimmunoprecipitation assays between the hDAT S/D and Stx1 WT, S14D or S14A. Indeed, Stx1 S14A has a higher affinity of interaction with hDAT S/D compared to that of Stx1 S14D and hDAT S/D, reaffirming our theory that Stx1 acts as a “brake” on DAT reverse transport. Furthermore, pharmacological inhibition of Stx1 phosphorylation using the CK2 inhibitor, CX-4945, mirrors findings from the genetic manipulation of Stx1: pre-treatment of cells with CX-4945 abolishes constitutive efflux in hDAT S/D.

Ultimately, we hoped to demonstrate that our findings on the reverse transport mechanism of DAT maintains relevance in an intact animal. We translated our in vitro findings to an *in vivo* model system, *Drosophila melanogaster*, and recapitulated that CK2 actions are necessary for constitutive efflux in hDAT S/D *ex vivo* transgenic fly brains. Oral administration of CX-4945 to hDAT S/D flies prior to ex vivo amperometry assays abolished constitutive efflux recorded from the drug-naïve animals. Behaviorally, hDAT S/D transgenic flies predictably exhibited basal hyperactivity and enhanced courtship-associated behavior (two well-established DA-associated behaviors), possibly arising from the heightened extracellular DA in the synaptic cleft. Remarkably, CX-4945 oral administration rescued the elevated activity and courtship behaviors in the hDAT S/D transgenic flies. These findings did not only help us bridge our in vitro discoveries to behavioral outcomes of constitutive efflux, but also begin to establish the possibility of using CX-4945 as a therapeutic agent to reverse this phenomenon in disease conditions and in patients suffering from AMPH abuse. Moreover, we are only beginning to understand the occurrence of DAT reverse transport in physiological conditions. Our findings in this study pave the way to understanding the mechanisms that underlie the reverse transport mode of DAT, and when and how it takes place. The design of a study that can identify and monitor physiological DAT N-terminus phosphorylation, Stx1 phosphorylation and DAT-Stx1 interactions in an intact animal, and the dynamic changes in these phenomena over time during different behaviors is warranted. Additionally, our findings also open a new window of opportunity into understanding the mechanism of action by which Adderall, which is an AMPH salt, treats symptoms in patients that are diagnosed with ADHD and autism spectrum disorders.

Chapter VI

FUTURE DIRECTIONS

The role of DAT in maintaining DA homeostasis has been well-established, and currently, many studies are focused on understanding the finer nuances of DAT function, including symporter uptake properties, structural dynamics, regulatory mechanisms and most intriguing of all, DAT reverse transport. Delineating the molecular mechanisms underlying this neurotransmitter transporter's regulation and function is instrumental to reversing the abnormal or atypical phenotypes associated with several neuropsychiatric and neurodevelopmental disorders. Additionally, DAT being a pharmacological target of psychostimulants like AMPH, cocaine and synthetic cathinones makes it an intriguing protein to study for developing therapies to counteract substance abuse disorders.

The studies outlined in this Ph.D. thesis concentrate on understanding DAT-mediated DA efflux in the several contexts that are mentioned above: in disease-associated variants and mechanisms for restoration of normal transporter properties, under the action of synthetic cathinones (a class of drugs separate from amphetamines), and the occurrence of efflux in a physiological setting. While the potential and scope for the directions that this research paves way to is enormous, this chapter focuses on harnessing the regulatory mechanisms that control DA efflux, in an effort to rescue aberrant transporter function and behaviors in disease-associated variants of the transporter, or under the influence of pharmacological agents like AMPH and MDPV. In the introduction in chapter I, as well as published and unpublished research described in chapters II, III and IV, our group's findings on the disease-associated hDAT variants identified in patients diagnosed with neuropsychiatric and neurodevelopmental disorders such as ADHD, autism, BPD and schizophrenia are discussed. Highlighted are the variants hDAT A559V and T356M that exhibit an anomalous DA "leak" or constitutive efflux in the absence of AMPH actions,

which may underlie the aberrant behaviors associated with these disorders. On the other hand, the autism-associated variant, hDAT ΔN336, exhibits a proclivity for the HOIF conformation that ablates DA uptake and essentially confers the same phenotype to *Drosophila* expressing the variant as does the *fumin* mutation in DAT. While the ΔN336 has provided the neurotransmitter transporter field with an accessible tool to be able to crystallize the hDAT in the future, this discussion will mainly focus on the ADE mutations in this discussion due to our path-breaking findings on the association between hDAT and Stx1, described in detail in chapter V that consists mostly of unpublished data.

Chapter V describes the regulation of the hDAT by the SNARE protein Stx1. In a bid to understand the context of physiological DAT-mediated DA efflux, our group attempted to determine the consequences of hDAT pseudophosphorylation at the five distal N-terminal serine residues: Ser2, Ser4, Ser7, Ser12 and Ser13, as Khoshbouei *et al.* in 2004 demonstrated that phosphorylation of these residues is a requirement of AMPH-induced DA efflux via the DAT. We wished to study the regulatory elements that interact with hDAT when phosphorylated, while it undergoes efflux. Interestingly, we found that in basal conditions, hDAT and Stx1 interact in a complex and upon phosphorylation (of both proteins) there is a reduction in the affinity of the interaction between the two proteins. Moreover, DA efflux via DAT can be abolished upon inhibition of CKII-mediated Stx1 phosphorylation, either *via* genetic or pharmacological manipulation. These findings helped us conclude that Stx1 phosphorylation is necessary for DAT-mediated DA efflux. But further studies are required to elevate the importance of this finding, in the context of constitutive efflux via the DAT in disease-associated variants, or in constitutive efflux that may contribute to neuronal excitability.

In disease-associated variants such as the hDAT A559V, T356M and D421, it would especially be interesting to conduct future studies on the effects of inhibiting Stx1 phosphorylation using the well-characterized CK2 inhibitor, CX-4945, on ADE. The hDAT A559V has been shown

to be hyper-phosphorylated at residues Ser3, Ser7 and Ser12 compared to wildtype hDAT, even in the absence of AMPH. We anticipate that in cells co-expressing the hDAT A559V and Stx1, the affinity of interaction between the two proteins will be reduced, which gives the hDAT A559V variant the ability to undergo ADE. Moreover, inhibition of CK2 by CK-4945 in cells expressing the hDAT A559V would (by harnessing a similar mechanism as that in hDAT S/D cells), will reduce ADE, and reestablish the interaction affinity between hDAT and Stx1. Reflecting our behavioral findings from the hDAT S/D transgenic flies, future studies on flies expressing the hDAT A559V variant are warranted. We predict that these flies will exhibit a basally hyperlocomotive phenotype, with increased courtship index (compared to WT), that can be rescued upon AMPH and CX-4945 actions, respectively. In the other hDAT variants that exhibit ADE, further studies are required to quantify the presence of hyperphosphorylated Ser residues on the N-terminus. Following confirmation of this, the above-described rescue experiments can be conducted. Our findings on the inhibition of Stx1 phosphorylation to prevent constitutive efflux via hDAT have paved the way for rescuing defective molecular phenotypes across the board in all disease-associated variants of the transporter that exhibit ADE. Furthermore, variants in the SERT and NET can also be assessed for similar findings, as Stx1 has been shown to regulate SERT and NET functions as well, particularly reverse transport.

A tangential, but significant aspect of studying the hDAT S/D as a representation of the hDAT A559V variant having a hyper-phosphorylated N-terminus and exhibiting ADE is the counter-intuitive effect of AMPH on the hDAT S/D compared to its WT counterpart. In multiple chapters, we noted that while AMPH caused DAT-mediated DA efflux in the WT transporter, it blocks ADE or constitutive efflux in the hDAT S/D (similar to its actions in the hDAT A559V). It is well-known that Adderall, an AMPH salt is now widely used in the treatment of symptoms associated with ADHD and autism spectrum disorders. As though drawing analogies to its molecular phenotype, in a WT fly, AMPH salts can produce hyperactivity, but conversely, decreases basally elevated hyperactivity in flies expressing the hDAT S/D. Further probing the

mechanism of action by which AMPH produces the opposite effects in typically functioning organisms vs. organisms harboring a disease-associated variant can help us understand the mechanisms by which Adderall has proven to be an effective treatment in patients suffering from ADHD.

In silico analysis have shown the relevance of the membrane lipid, PIP2, in the regulation of DAT efflux. PIP2 has been identified to be important in the sequestration of the Stx1 N-terminus and also interacts with the hDAT N-terminus. Moreover, Hamilton and colleagues have showed that PIP2 interactions with the N-terminus is important in mediating DA efflux, both *in vivo* and *in vitro*. Following the in-depth study on Stx1 interactions with hDAT in its "efflux mode", we further hypothesize that PIP2-Stx1 interactions also play a major role in the efflux mechanism. The hypothesis can be broken down into several segments: (1) that PIP2 is important in mediating or sequestering the interaction between hDAT and Stx1. To delve into this further, coimmunoprecipitation assays and FRET assays to analyze changes in the interaction between hDAT and Stx1 can be conducted in PIP2 depleted cells (methodology shown in Cartier and Hamilton 2015). (2) Stx1 and hDAT phosphorylation affect changes in the interaction with PIP2. Using genetic or pharmacological methods similar to those in Chapter V, analysis of PIP2 interactions with pseudophosphorylated or phospho-deficient mutants of hDAT and Stx1 using coimmunoprecipitation assays can elucidate the validity of this hypothesis. Further studies on the dynamics between hDAT, PIP2 and Stx1 is warranted given the multiple studies that have shown their individual involvement in DA reverse transport.

For many decades, our group has been deeply committed to understanding the mechanism of AMPH actions, but another psychostimulant, the heavily abused bath salt MDPV, caught our attention. Our studies showed that MDPV has actions similar to that of AMPH at low concentrations (DAT-mediated DA efflux) and of cocaine at high concentrations (DAT antagonism). Although these preliminary studies are extremely interesting, much is unknown yet about the actions of MDPV. Future studies on this drug can help unfold (similar to the hundreds

discovered about AMPH and cocaine in the past several decades) molecular targets, regulatory mechanisms, metabolites, resultant behaviors of MDPV abuse in vertebrates and invertebrates. Identifying key players that mediate MDPV actions can prove to be useful as pharmacological targets to reverse the effects of this very potent, dangerous drug.

Lastly, our laboratory has pioneered the use of *Drosophila melanogaster* as a powerful and useful genetic model for studying the DA system, with respect to disease-associated DAT variants as well as psychostimulant drugs that target the DAT. In the future, we hope for the development of more novel, robust and translational *Drosophila* behaviors to study DA associated behaviors, including impulsivity, reinforcement, memory and cognition. These behaviors can also be extrapolated to a wider scope of molecular and systems level changes that can affect DA-associated behaviors, for example, the up-and downregulation of DA signaling during development, as well as in identifying pharmacological agents that can potentially target the DAergic system.

REFERENCES

Adell, A., & Artigas, F. (2004). The somatodendritic release of dopamine in the ventral tegmental area and its regulation by afferent transmitter systems. *Neuroscience and Biobehavioral Reviews*, *28*(4), 415–431. https://doi.org/10.1016/j.neubiorev.2004.05.001

Adkins, E. M., Samuvel, D. J., Fog, J. U., Eriksen, J., Jayanthi, L. D., Vaegter, C. B., … Gether, U. (2007). Membrane mobility and microdomain association of the dopamine transporter studied with fluorescence correlation spectroscopy and fluorescence recovery after photobleaching. *Biochemistry*, *46*(37), 10484–10497. https://doi.org/10.1021/bi700429z

Aghajanian, G. K., & Bunney, B. S. (1977). Dopamine"autoreceptors": pharmacological characterization by microiontophoretic single cell recording studies. *Naunyn-Schmiedeberg's Archives of Pharmacology*, *297*(1), 1–7.

Anden, N. E., Carlsson, A., Dahlstroem, A., Fuxe, K., Hillarp, N. A., & Larsson, K. (1964). DEMONSTRATION AND MAPPING OUT OF NIGRO-NEOSTRIATAL DOPAMINE NEURONS. *Life Sciences (1962)*, *3*, 523–530.

Andersen, P. H., Gingrich, J. A., Bates, M. D., Dearry, A., Falardeau, P., Senogles, S. E., & Caron, M. G. (1990). Dopamine receptor subtypes: beyond the D1/D2 classification. *Trends in Pharmacological Sciences*, *11*(6), 231–236.

Anderson, B. M., Schnetz-Boutaud, N., Bartlett, J., Wright, H. H., Abramson, R. K., Cuccaro, M. L., … Haines, J. L. (2008). Examination of association to autism of common genetic variationin genes related to dopamine. *Autism Research: Official Journal of the*

International Society for Autism Research, *1*(6), 364–369. https://doi.org/10.1002/aur.55

Andretic, R., van Swinderen, B., & Greenspan, R. J. (2005). Dopaminergic modulation of arousal in Drosophila. *Current Biology: CB*, *15*(13), 1165–1175. https://doi.org/10.1016/j.cub.2005.05.025

Arias-Carrión, O., & Pöppel, E. (2007). Dopamine, learning, and reward-seeking behavior. *Acta Neurobiologiae Experimentalis*, *67*(4), 481–488.

Ashok, A. H., Mizuno, Y., Volkow, N. D., & Howes, O. D. (2017). Association of Stimulant Use With Dopaminergic Alterations in Users of Cocaine, Amphetamine, or Methamphetamine: A Systematic Review and Meta-analysis. *JAMA Psychiatry*, *74*(5), 511–519. https://doi.org/10.1001/jamapsychiatry.2017.0135

Bainton, R. J., Tsai, L. T., Singh, C. M., Moore, M. S., Neckameyer, W. S., & Heberlein, U. (2000). Dopamine modulates acute responses to cocaine, nicotine and ethanol in Drosophila. *Current Biology: CB*, *10*(4), 187–194.

Bass, C. E., Grinevich, V. P., Vance, Z. B., Sullivan, R. P., Bonin, K. D., & Budygin, E. A. (2010). Optogenetic control of striatal dopamine release in rats. *Journal of Neurochemistry*, *114*(5), 1344–1352. https://doi.org/10.1111/j.1471-4159.2010.06850.x

Baumann, M. H., Bulling, S., Benaderet, T. S., Saha, K., Ayestas, M. A., Partilla, J. S., … Sitte, H. H. (2014). Evidence for a role of transporter-mediated currents in the depletion of brain serotonin induced by serotonin transporter substrates. *Neuropsychopharmacology: Official Publication of the American College of Neuropsychopharmacology*, *39*(6), 1355–1365. https://doi.org/10.1038/npp.2013.331

Baumann, M. H., Partilla, J. S., Lehner, K. R., Thorndike, E. B., Hoffman, A. F., Holy, M., … Schindler, C. W. (2013). Powerful cocaine-like actions of 3,4-methylenedioxypyrovalerone (MDPV), a principal constituent of psychoactive "bath salts" products. *Neuropsychopharmacology: Official Publication of the American College of Neuropsychopharmacology*, *38*(4), 552–562. https://doi.org/10.1038/npp.2012.204

Beckstead, M. J., Grandy, D. K., Wickman, K., & Williams, J. T. (2004). Vesicular dopamine release elicits an inhibitory postsynaptic current in midbrain dopamine neurons. *Neuron*, *42*(6), 939–946. https://doi.org/10.1016/j.neuron.2004.05.019

Benoit-Marand, M., Jaber, M., & Gonon, F. (2000). Release and elimination of dopamine in vivo in mice lacking the dopamine transporter: functional consequences. *The European Journal of Neuroscience*, *12*(8), 2985–2992.

Berger, O., Edholm, O., & Jähnig, F. (1997). Molecular dynamics simulations of a fluid bilayer of dipalmitoylphosphatidylcholine at full hydration, constant pressure, and constant temperature. *Biophysical Journal*, *72*(5), 2002–2013. https://doi.org/10.1016/S0006-3495(97)78845-3

Berglund, E. C., Makos, M. A., Keighron, J. D., Phan, N., Heien, M. L., & Ewing, A. G. (2013). Oral administration of methylphenidate blocks the effect of cocaine on uptake at the Drosophila dopamine transporter. *ACS Chemical Neuroscience*, *4*(4), 566–574. https://doi.org/10.1021/cn3002009

Bermingham, D. P., & Blakely, R. D. (2016). Kinase-dependent Regulation of Monoamine Neurotransmitter Transporters. *Pharmacological Reviews*, *68*(4), 888–953. https://doi.org/10.1124/pr.115.012260

Berry, J. A., Cervantes-Sandoval, I., Nicholas, E. P., & Davis, R. L. (2012). Dopamine is required for learning and forgetting in Drosophila. *Neuron*, *74*(3), 530–542. https://doi.org/10.1016/j.neuron.2012.04.007

Bertler, A., & Rosengren, E. (1959a). Occurrence and distribution of catechol amines in brain. *Acta Physiologica Scandinavica*, *47*, 350–361.

Bertler, A., & Rosengren, E. (1959b). Occurrence and distribution of dopamine in brain and other tissues. *Experientia*, *15*(1), 10–11.

Bertler, A., & Rosengren, E. (1959c). On the distribution in brain of monoamines and of enzymes responsible for their formation. *Experientia*, *15*, 382–384.

Besson, M. J., Cheramy, A., Feltz, P., & Glowinski, J. (1969). Release of newly synthesized dopamine from dopamine-containing terminals in the striatum of the rat. *Proceedings of the National Academy of Sciences of the United States of America*, *62*(3), 741–748.

Beuming, T., Shi, L., Javitch, J. A., & Weinstein, H. (2006). A comprehensive structure-based alignment of prokaryotic and eukaryotic neurotransmitter/Na+ symporters (NSS) aids in the use of the LeuT structure to probe NSS structure and function. *Molecular Pharmacology*, *70*(5), 1630–1642. https://doi.org/10.1124/mol.106.026120

Binda, F., Dipace, C., Bowton, E., Robertson, S. D., Lute, B. J., Fog, J. U., … Galli, A. (2008). Syntaxin 1A interaction with the dopamine transporter promotes amphetamine-induced dopamine efflux. *Molecular Pharmacology*, *74*(4), 1101–1108. https://doi.org/10.1124/mol.108.048447

Björklund, A., & Dunnett, S. B. (2007a). Dopamine neuron systems in the brain: an update. *Trends in Neurosciences*, *30*(5), 194–202. https://doi.org/10.1016/j.tins.2007.03.006

Björklund, A., & Dunnett, S. B. (2007b). Fifty years of dopamine research. *Trends in Neurosciences*, *30*(5), 185–187. https://doi.org/10.1016/j.tins.2007.03.004

Blaschko, H. (1957a). Formation of catechol amines in the animal body. *British Medical Bulletin*, *13*(3), 162–165.

Blaschko, H. (1957b). Metabolism and storage of biogenic amines. *Experientia*, *13*(1), 9–13.

Blaschko, H. (1957c). Metabolism and storage of biogenic amines. *Experientia*, *13*(1), 9–12. https://doi.org/10.1007/BF02156938

Blaschko, H. (1958). [Amine oxidase in mammalian blood]. *Il Farmaco; Edizione Scientifica*, *13*(7), 521–533.

Blaskovic, S., Blanc, M., & van der Goot, F. G. (2013). What does S-palmitoylation do to membrane proteins? *The FEBS Journal*, *280*(12), 2766–2774. https://doi.org/10.1111/febs.12263

Blum, K., Braverman, E. R., Wu, S., Cull, J. G., Chen, T. J., Gill, J., … Comings, D. E. (1997). Association of polymorphisms of dopamine D2 receptor (DRD2), and dopamine transporter (DAT1) genes with schizoid/avoidant behaviors (SAB). *Molecular Psychiatry*, *2*(3), 239–246.

Bonano, J. S., Glennon, R. A., De Felice, L. J., Banks, M. L., & Negus, S. S. (2014). Abuse-related and abuse-limiting effects of methcathinone and the synthetic “bath salts” cathinone analogs methylenedioxypyrovalerone (MDPV), methylone and mephedrone on intracranial self-stimulation in rats. *Psychopharmacology*, *231*(1), 199–207. https://doi.org/10.1007/s00213-013-3223-5

Borek, H. A., & Holstege, C. P. (2012). Hyperthermia and multiorgan failure after abuse of “bath salts” containing 3,4-methylenedioxypyrovalerone. *Annals of Emergency Medicine*, *60*(1), 103–105. https://doi.org/10.1016/j.annemergmed.2012.01.005

Bowton, E., Saunders, C., Reddy, I. A., Campbell, N. G., Hamilton, P. J., Henry, L. K., … Galli, A. (2014). SLC6A3 coding variant Ala559Val found in two autism probands alters dopamine transporter function and trafficking. *Translational Psychiatry*, *4*, e464. https://doi.org/10.1038/tp.2014.90

Bowton, Erica, Saunders, C., Erreger, K., Sakrikar, D., Matthies, H. J., Sen, N., … Galli, A. (2010). Dysregulation of dopamine transporters via dopamine D2 autoreceptors triggers anomalous dopamine efflux associated with attention-deficit hyperactivity disorder. *The Journal of Neuroscience: The Official Journal of the Society for Neuroscience*, *30*(17), 6048–6057. https://doi.org/10.1523/JNEUROSCI.5094-09.2010

Breese, G. R., Kopin, I. J., & Weise, V. K. (1970). Effects of amphetamine derivatives on brain dopamine and noradrenaline. *British Journal of Pharmacology*, *38*(3), 537–545.

Brenneisen, R., Fisch, H. U., Koelbing, U., Geisshüsler, S., & Kalix, P. (1990). Amphetamine-like effects in humans of the khat alkaloid cathinone. *British Journal of Clinical Pharmacology*, *30*(6), 825–828.

Bromberg-Martin, E. S., Matsumoto, M., & Hikosaka, O. (2010). Dopamine in motivational control: rewarding, aversive, and alerting. *Neuron*, *68*(5), 815–834. https://doi.org/10.1016/j.neuron.2010.11.022

Buchmayer, F., Schicker, K., Steinkellner, T., Geier, P., Stübiger, G., Hamilton, P. J., … Sitte, H. H. (2013). Amphetamine actions at the serotonin transporter rely on the availability of

phosphatidylinositol-4,5-bisphosphate. *Proceedings of the National Academy of Sciences of the United States of America*, *110*(28), 11642–11647. https://doi.org/10.1073/pnas.1220552110

Budnik, V., & White, K. (1988). Catecholamine-containing neurons in Drosophila melanogaster: distribution and development. *The Journal of Comparative Neurology*, *268*(3), 400–413. https://doi.org/10.1002/cne.902680309

Bull, D. R., & Sheehan, M. J. (1991). Presynaptic regulation of electrically evoked dopamine overflow in nucleus accumbens: a pharmacological study using fast cyclic voltammetry in vitro. *Naunyn-Schmiedeberg's Archives of Pharmacology*, *343*(3), 260–265.

Bunzow, J. R., Van Tol, H. H., Grandy, D. K., Albert, P., Salon, J., Christie, M., … Civelli, O. (1988). Cloning and expression of a rat D2 dopamine receptor cDNA. *Nature*, *336*(6201), 783–787. https://doi.org/10.1038/336783a0

Butcher, S. P., Fairbrother, I. S., Kelly, J. S., & Arbuthnott, G. W. (1988). Amphetamine-induced dopamine release in the rat striatum: an in vivo microdialysis study. *Journal of Neurochemistry*, *50*(2), 346–355.

Caldwell, J., & Sever, P. S. (1974). The biochemical pharmacology of abused drugs. I. Amphetamines, cocaine, and LSD. *Clinical Pharmacology and Therapeutics*, *16*(4), 625–638.

Cameron, K. N., Kolanos, R., Solis, E., Glennon, R. A., & De Felice, L. J. (2013). Bath salts components mephedrone and methylenedioxypyrovalerone (MDPV) act synergistically at the human dopamine transporter. *British Journal of Pharmacology*, *168*(7), 1750–1757. https://doi.org/10.1111/bph.12061

Carlsson, A., Falck, B., Hillarp, N. A., Thieme, G., & Torp, A. (1961). A new histochemical method for visualization of tissue catechol amines. *Medicina Experimentalis: International Journal of Experimental Medicine*, *4*, 123–125.

Carlsson, A., Lindqvist, M., & Magnusson, T. (1957). 3,4-Dihydroxyphenylalanine and 5-hydroxytryptophan as reserpine antagonists. *Nature*, *180*(4596), 1200.

Carlsson, A., Lindqvist, M., Magnusson, T., & Waldeck, B. (1958). On the presence of 3-hydroxytyramine in brain. *Science (New York, N.Y.)*, *127*(3296), 471.

Cartier, E., Hamilton, P. J., Belovich, A. N., Shekar, A., Campbell, N. G., Saunders, C., … Galli, A. (2015). Rare autism-associated variants implicate syntaxin 1 (STX1 R26Q) phosphorylation and the dopamine transporter (hDAT R51W) in dopamine neurotransmission and behaviors. *EBioMedicine*, *2*(2), 135–146. https://doi.org/10.1016/j.ebiom.2015.01.007

Carvelli, L., Blakely, R. D., & DeFelice, L. J. (2008). Dopamine transporter/syntaxin 1A interactions regulate transporter channel activity and dopaminergic synaptic transmission. *Proceedings of the National Academy of Sciences of the United States of America*, *105*(37), 14192–14197. https://doi.org/10.1073/pnas.0802214105

Caudle, W. M., Colebrooke, R. E., Emson, P. C., & Miller, G. W. (2008). Altered vesicular dopamine storage in Parkinson's disease: a premature demise. *Trends in Neurosciences*, *31*(6), 303–308. https://doi.org/10.1016/j.tins.2008.02.010

Cervinski, M. A., Foster, J. D., & Vaughan, R. A. (2010). Syntaxin 1A regulates dopamine transporter activity, phosphorylation and surface expression. *Neuroscience*, *170*(2), 408–416. https://doi.org/10.1016/j.neuroscience.2010.07.025

Challasivakanaka, S., Zhen, J., Smith, M. E., Reith, M. E. A., Foster, J. D., & Vaughan, R. A. (2017). Dopamine transporter phosphorylation site threonine 53 is stimulated by amphetamines and regulates dopamine transport, efflux, and cocaine analog binding. *The Journal of Biological Chemistry*, *292*(46), 19066–19075. https://doi.org/10.1074/jbc.M117.787002

Chang, H.-Y., Grygoruk, A., Brooks, E. S., Ackerson, L. C., Maidment, N. T., Bainton, R. J., & Krantz, D. E. (2006). Overexpression of the Drosophila vesicular monoamine transporter increases motor activity and courtship but decreases the behavioral response to cocaine. *Molecular Psychiatry*, *11*(1), 99–113. https://doi.org/10.1038/sj.mp.4001742

Chen, S.-L., Chen, Y.-H., Wang, C.-C., Yu, Y.-W., Tsai, Y.-C., Hsu, H.-W., … Fu, T.-F. (2017). Active and passive sexual roles that arise in Drosophila male-male courtship are modulated by dopamine levels in PPL2ab neurons. *Scientific Reports*, *7*(1). https://doi.org/10.1038/srep44595

Cheng, M. H., & Bahar, I. (2015). Molecular Mechanism of Dopamine Transport by Human Dopamine Transporter. *Structure (London, England: 1993)*, *23*(11), 2171–2181. https://doi.org/10.1016/j.str.2015.09.001

Claxton, D. P., Quick, M., Shi, L., de Carvalho, F. D., Weinstein, H., Javitch, J. A., & McHaourab, H. S. (2010). Ion/substrate-dependent conformational dynamics of a bacterial homolog of neurotransmitter:sodium symporters. *Nature Structural & Molecular Biology*, *17*(7), 822–829. https://doi.org/10.1038/nsmb.1854

Cook, E. H., Stein, M. A., Krasowski, M. D., Cox, N. J., Olkon, D. M., Kieffer, J. E., & Leventhal, B. L. (1995). Association of attention-deficit disorder and the dopamine transporter gene. *American Journal of Human Genetics*, *56*(4), 993–998.

Coppola, M., & Mondola, R. (2012a). 3,4-methylenedioxypyrovalerone (MDPV): chemistry, pharmacology and toxicology of a new designer drug of abuse marketed online. *Toxicology Letters*, *208*(1), 12–15. https://doi.org/10.1016/j.toxlet.2011.10.002

Coppola, M., & Mondola, R. (2012b). Synthetic cathinones: chemistry, pharmacology and toxicology of a new class of designer drugs of abuse marketed as “bath salts” or “plant food.” *Toxicology Letters*, *211*(2), 144–149. https://doi.org/10.1016/j.toxlet.2012.03.009

Cousins, D. A., Butts, K., & Young, A. H. (2009). The role of dopamine in bipolar disorder. *Bipolar Disorders*, *11*(8), 787–806. https://doi.org/10.1111/j.1399-5618.2009.00760.x

Cowell, R. M., Kantor, L., Hewlett, G. H., Frey, K. A., & Gnegy, M. E. (2000). Dopamine transporter antagonists block phorbol ester-induced dopamine release and dopamine transporter phosphorylation in striatal synaptosomes. *European Journal of Pharmacology*, *389*(1), 59–65.

Cragg, S., Rice, M. E., & Greenfield, S. A. (1997). Heterogeneity of electrically evoked dopamine release and reuptake in substantia nigra, ventral tegmental area, and striatum. *Journal of Neurophysiology*, *77*(2), 863–873. https://doi.org/10.1152/jn.1997.77.2.863

Cremona, M. L., Matthies, H. J. G., Pau, K., Bowton, E., Speed, N., Lute, B. J., … Yamamoto, A. (2011). Flotillin-1 is essential for PKC-triggered endocytosis and membrane microdomain localization of DAT. *Nature Neuroscience*, *14*(4), 469–477. https://doi.org/10.1038/nn.2781

Davis, G. L., Stewart, A., Stanwood, G. D., Gowrishankar, R., Hahn, M. K., & Blakely, R. D. (2018). Functional coding variation in the presynaptic dopamine transporter associated with neuropsychiatric disorders drives enhanced motivation and context-dependent impulsivity in mice. *Behavioural Brain Research*, *337*, 61–69. https://doi.org/10.1016/j.bbr.2017.09.043

De bruyn, A., Souery, D., Mendelbaum, K., Mendlewicz, J., & Van Broeckhoven, C. (1996). A linkage study between bipolar disorder and genes involved in dopaminergic and GABAergic neurotransmission. *Psychiatric Genetics*, *6*(2), 67–73.

de Jong, J. W., Roelofs, T. J. M., Mol, F. M. U., Hillen, A. E. J., Meijboom, K. E., Luijendijk, M. C. M., … Adan, R. A. H. (2015). Reducing Ventral Tegmental Dopamine D2 Receptor Expression Selectively Boosts Incentive Motivation. *Neuropsychopharmacology: Official Publication of the American College of Neuropsychopharmacology*, *40*(9), 2085–2095. https://doi.org/10.1038/npp.2015.60

De Rubeis, S., He, X., Goldberg, A. P., Poultney, C. S., Samocha, K., Cicek, A. E., … Buxbaum, J. D. (2014). Synaptic, transcriptional and chromatin genes disrupted in autism. *Nature*, *515*(7526), 209–215. https://doi.org/10.1038/nature13772

dela Peña, I., Gevorkiana, R., & Shi, W.-X. (2015). Psychostimulants affect dopamine transmission through both dopamine transporter-dependent and independent mechanisms. *European Journal of Pharmacology*, *764*, 562–570. https://doi.org/10.1016/j.ejphar.2015.07.044

Diallinas, G. (2014). Understanding transporter specificity and the discrete appearance of channel-like gating domains in transporters. *Frontiers in Pharmacology*, *5*, 207. https://doi.org/10.3389/fphar.2014.00207

Dipace, C., Sung, U., Binda, F., Blakely, R. D., & Galli, A. (2007). Amphetamine induces a calcium/calmodulin-dependent protein kinase II-dependent reduction in norepinephrine transporter surface expression linked to changes in syntaxin 1A/transporter complexes. *Molecular Pharmacology*, *71*(1), 230–239. https://doi.org/10.1124/mol.106.026690

Drew, D., & Boudker, O. (2016). Shared Molecular Mechanisms of Membrane Transporters. *Annual Review of Biochemistry*, *85*, 543–572. https://doi.org/10.1146/annurev-biochem-060815-014520

Edidin, M. (2003). The state of lipid rafts: from model membranes to cells. *Annual Review of Biophysics and Biomolecular Structure*, *32*, 257–283. https://doi.org/10.1146/annurev.biophys.32.110601.142439

Emsley, P., Lohkamp, B., Scott, W. G., & Cowtan, K. (2010). Features and development of Coot. *Acta Crystallographica. Section D, Biological Crystallography*, *66*(Pt 4), 486–501. https://doi.org/10.1107/S0907444910007493

Erreger, K., Grewer, C., Javitch, J. A., & Galli, A. (2008). Currents in response to rapid concentration jumps of amphetamine uncover novel aspects of human dopamine transporter function. *The Journal of Neuroscience: The Official Journal of the Society for Neuroscience*, *28*(4), 976–989. https://doi.org/10.1523/JNEUROSCI.2796-07.2008

Eshleman, A. J., Wolfrum, K. M., Hatfield, M. G., Johnson, R. A., Murphy, K. V., & Janowsky, A. (2013). Substituted methcathinones differ in transporter and receptor interactions.

Biochemical Pharmacology, *85*(12), 1803–1815. https://doi.org/10.1016/j.bcp.2013.04.004

Faber, S., Zinn, G. M., Kern, J. C., & Kingston, H. M. S. (2009). The plasma zinc/serum copper ratio as a biomarker in children with autism spectrum disorders. *Biomarkers: Biochemical Indicators of Exposure, Response, and Susceptibility to Chemicals*, *14*(3), 171–180. https://doi.org/10.1080/13547500902783747

Fahn, S. (2018). The 200-year journey of Parkinson disease: Reflecting on the past and looking towards the future. *Parkinsonism & Related Disorders*, *46 Suppl 1*, S1–S5. https://doi.org/10.1016/j.parkreldis.2017.07.020

Falkenburger, B. H., Barstow, K. L., & Mintz, I. M. (2001). Dendrodendritic inhibition through reversal of dopamine transport. *Science (New York, N.Y.)*, *293*(5539), 2465–2470. https://doi.org/10.1126/science.1060645

Fallon, J. H., & Moore, R. Y. (1978). Catecholamine innervation of the basal forebrain. IV. Topography of the dopamine projection to the basal forebrain and neostriatum. *The Journal of Comparative Neurology*, *180*(3), 545–580. https://doi.org/10.1002/cne.901800310

Feany, M. B., & Bender, W. W. (2000). A Drosophila model of Parkinson's disease. *Nature*, *404*(6776), 394–398. https://doi.org/10.1038/35006074

Fernstrom, J. D., & Fernstrom, M. H. (2007). Tyrosine, phenylalanine, and catecholamine synthesis and function in the brain. *The Journal of Nutrition*, *137*(6 Suppl 1), 1539S-1547S; discussion 1548S. https://doi.org/10.1093/jn/137.6.1539S

Feuerstein, T. J. (2008). Presynaptic receptors for dopamine, histamine, and serotonin. *Handbook of Experimental Pharmacology*, (184), 289–338. https://doi.org/10.1007/978-3-540-74805-2_10

Filloux, F. M., Wamsley, J. K., & Dawson, T. M. (1987). Dopamine D-2 auto- and postsynaptic receptors in the nigrostriatal system of the rat brain: localization by quantitative autoradiography with [3H]sulpiride. *European Journal of Pharmacology*, *138*(1), 61–68.

Fischbach, G. D., & Lord, C. (2010). The Simons Simplex Collection: a resource for identification of autism genetic risk factors. *Neuron*, *68*(2), 192–195. https://doi.org/10.1016/j.neuron.2010.10.006

Fog, J. U., Khoshbouei, H., Holy, M., Owens, W. A., Vaegter, C. B., Sen, N., … Gether, U. (2006). Calmodulin kinase II interacts with the dopamine transporter C terminus to regulate amphetamine-induced reverse transport. *Neuron*, *51*(4), 417–429. https://doi.org/10.1016/j.neuron.2006.06.028

Ford, C. P. (2014). The role of D2-autoreceptors in regulating dopamine neuron activity and transmission. *Neuroscience*, *282*, 13–22. https://doi.org/10.1016/j.neuroscience.2014.01.025

Forrest, L. R., Zhang, Y.-W., Jacobs, M. T., Gesmonde, J., Xie, L., Honig, B. H., & Rudnick, G. (2008). Mechanism for alternating access in neurotransmitter transporters. *Proceedings of the National Academy of Sciences of the United States of America*, *105*(30), 10338–10343. https://doi.org/10.1073/pnas.0804659105

Foster, J. D., Adkins, S. D., Lever, J. R., & Vaughan, R. A. (2008). Phorbol ester induced trafficking-independent regulation and enhanced phosphorylation of the dopamine

transporter associated with membrane rafts and cholesterol. *Journal of Neurochemistry*, *105*(5), 1683–1699. https://doi.org/10.1111/j.1471-4159.2008.05262.x

Foster, J. D., Pananusorn, B., Cervinski, M. A., Holden, H. E., & Vaughan, R. A. (2003). Dopamine transporters are dephosphorylated in striatal homogenates and in vitro by protein phosphatase 1. *Brain Research. Molecular Brain Research*, *110*(1), 100–108.

Foster, J. D., Pananusorn, B., & Vaughan, R. A. (2002). Dopamine transporters are phosphorylated on N-terminal serines in rat striatum. *The Journal of Biological Chemistry*, *277*(28), 25178–25186. https://doi.org/10.1074/jbc.M200294200

Foster, J. D., & Vaughan, R. A. (2011). Palmitoylation Controls Dopamine Transporter Kinetics, Degradation, and Protein Kinase C-dependent Regulation. *Journal of Biological Chemistry*, *286*(7), 5175–5186. https://doi.org/10.1074/jbc.M110.187872

Foster, J. D., & Vaughan, R. A. (2017). Phosphorylation mechanisms in dopamine transporter regulation. *Journal of Chemical Neuroanatomy*, *83–84*, 10–18. https://doi.org/10.1016/j.jchemneu.2016.10.004

Foster, J. D., Yang, J.-W., Moritz, A. E., Challasivakanaka, S., Smith, M. A., Holy, M., … Vaughan, R. A. (2012). Dopamine transporter phosphorylation site threonine 53 regulates substrate reuptake and amphetamine-stimulated efflux. *The Journal of Biological Chemistry*, *287*(35), 29702–29712. https://doi.org/10.1074/jbc.M112.367706

Fraser, R., Chen, Y., Guptaroy, B., Luderman, K. D., Stokes, S. L., Beg, A., … Gnegy, M. E. (2014). An N-terminal threonine mutation produces an efflux-favorable, sodium-primed conformation of the human dopamine transporter. *Molecular Pharmacology*, *86*(1), 76–85. https://doi.org/10.1124/mol.114.091926

Freyberg, Z., Sonders, M. S., Aguilar, J. I., Hiranita, T., Karam, C. S., Flores, J., … Javitch, J. A. (2016). Mechanisms of amphetamine action illuminated through optical monitoring of dopamine synaptic vesicles in Drosophila brain. *Nature Communications*, *7*, 10652. https://doi.org/10.1038/ncomms10652

Friggi-Grelin, F., Coulom, H., Meller, M., Gomez, D., Hirsh, J., & Birman, S. (2003). Targeted gene expression in Drosophila dopaminergic cells using regulatory sequences from tyrosine hydroxylase. *Journal of Neurobiology*, *54*(4), 618–627. https://doi.org/10.1002/neu.10185

Gadow, K. D., Roohi, J., DeVincent, C. J., & Hatchwell, E. (2008). Association of ADHD, tics, and anxiety with dopamine transporter (DAT1) genotype in autism spectrum disorder. *Journal of Child Psychology and Psychiatry, and Allied Disciplines*, *49*(12), 1331–1338. https://doi.org/10.1111/j.1469-7610.2008.01952.x

Gailey, D. A., Lacaillade, R. C., & Hall, J. C. (1986). Chemosensory elements of courtship in normal and mutant, olfaction-deficientDrosophila melanogaster. *Behavior Genetics*, *16*(3), 375–405. https://doi.org/10.1007/BF01071319

Gainetdinov, R. R., Jones, S. R., Fumagalli, F., Wightman, R. M., & Caron, M. G. (1998). Re-evaluation of the role of the dopamine transporter in dopamine system homeostasis. *Brain Research. Brain Research Reviews*, *26*(2–3), 148–153.

Garabal, M. V., Arévalo, R. M., Díaz-Palarea, M. D., Castro, R., & Rodríguez, M. (1988). Tyrosine availability and brain noradrenaline synthesis in the fetus: control by maternal tyrosine ingestion. *Brain Research*, *457*(2), 330–337.

Garcia-Olivares, J., Baust, T., Harris, S., Hamilton, P., Galli, A., Amara, S. G., & Torres, G. E. (2017). Gβγ subunit activation promotes dopamine efflux through the dopamine transporter. *Molecular Psychiatry*, *22*(12), 1673–1679. https://doi.org/10.1038/mp.2017.176

Garcia-Olivares, Jennie, Torres-Salazar, D., Owens, W. A., Baust, T., Siderovski, D. P., Amara, S. G., … Torres, G. E. (2013). Inhibition of dopamine transporter activity by G protein βγ subunits. *PloS One*, *8*(3), e59788. https://doi.org/10.1371/journal.pone.0059788

German, C. L., Fleckenstein, A. E., & Hanson, G. R. (2014). Bath salts and synthetic cathinones: an emerging designer drug phenomenon. *Life Sciences*, *97*(1), 2–8. https://doi.org/10.1016/j.lfs.2013.07.023

Geschwind, D. H., & State, M. W. (2015). Gene hunting in autism spectrum disorder: on the path to precision medicine. *The Lancet. Neurology*, *14*(11), 1109–1120. https://doi.org/10.1016/S1474-4422(15)00044-7

Gether, U., Andersen, P. H., Larsson, O. M., & Schousboe, A. (2006). Neurotransmitter transporters: molecular function of important drug targets. *Trends in Pharmacological Sciences*, *27*(7), 375–383. https://doi.org/10.1016/j.tips.2006.05.003

Giambalvo, C. T. (1992). Protein kinase C and dopamine transport--1. Effects of amphetamine in vivo. *Neuropharmacology*, *31*(12), 1201–1210.

Gil, C., Falqués, A., Sarró, E., Cubi, R., Blasi, J., Aguilera, J., & Itarte, E. (2011). Protein kinase CK2 associates to lipid rafts and its pharmacological inhibition enhances neurotransmitter release. *FEBS Letters*, *585*(2), 414–420. https://doi.org/10.1016/j.febslet.2010.12.029

Gill, M., Daly, G., Heron, S., Hawi, Z., & Fitzgerald, M. (1997). Confirmation of association between attention deficit hyperactivity disorder and a dopamine transporter polymorphism. *Molecular Psychiatry*, *2*(4), 311–313.

Giros, B., & Caron, M. G. (1993). Molecular characterization of the dopamine transporter. *Trends in Pharmacological Sciences*, *14*(2), 43–49.

Giros, B., Jaber, M., Jones, S. R., Wightman, R. M., & Caron, M. G. (1996). Hyperlocomotion and indifference to cocaine and amphetamine in mice lacking the dopamine transporter. *Nature*, *379*(6566), 606–612. https://doi.org/10.1038/379606a0

Glennon, R. A., Yousif, M., Naiman, N., & Kalix, P. (1987). Methcathinone: a new and potent amphetamine-like agent. *Pharmacology, Biochemistry, and Behavior*, *26*(3), 547–551.

Gnegy, M. E., Khoshbouei, H., Berg, K. A., Javitch, J. A., Clarke, W. P., Zhang, M., & Galli, A. (2004). Intracellular Ca2+ regulates amphetamine-induced dopamine efflux and currents mediated by the human dopamine transporter. *Molecular Pharmacology*, *66*(1), 137–143. https://doi.org/10.1124/mol.66.1.137

Goldberg, L. I. (1972). Cardiovascular and renal actions of dopamine: potential clinical applications. *Pharmacological Reviews*, *24*(1), 1–29.

Goldberg, L. I. (1984). Dopamine receptors and hypertension. Physiologic and pharmacologic implications. *The American Journal of Medicine*, *77*(4A), 37–44.

Goldstein, M., Friedhoff, A. J., & Simmons, C. (1959). Metabolic pathways of 3-hydroxytyramine. *Biochimica Et Biophysica Acta*, *33*(2), 572–574.

Gotham, K., Pickles, A., & Lord, C. (2009). Standardizing ADOS scores for a measure of severity in autism spectrum disorders. *Journal of Autism and Developmental Disorders*, *39*(5), 693–705. https://doi.org/10.1007/s10803-008-0674-3

Gowrishankar, R., Gresch, P. J., Davis, G. L., Katamish, R. M., Riele, J. R., Stewart, A. M., … Blakely, R. D. (2018). Region-Specific Regulation of Presynaptic Dopamine Homeostasis by D2 Autoreceptors Shapes the In Vivo Impact of the Neuropsychiatric Disease-Associated DAT Variant Val559. *The Journal of Neuroscience: The Official Journal of the Society for Neuroscience*, *38*(23), 5302–5312. https://doi.org/10.1523/JNEUROSCI.0055-18.2018

Gowrishankar, R., Hahn, M. K., & Blakely, R. D. (2014). Good riddance to dopamine: roles for the dopamine transporter in synaptic function and dopamine-associated brain disorders. *Neurochemistry International*, *73*, 42–48. https://doi.org/10.1016/j.neuint.2013.10.016

Hamilton, P. J., Campbell, N. G., Sharma, S., Erreger, K., Hansen, F. H., Saunders, C., … Galli, A. (2013a). Drosophila melanogaster: a novel animal model for the behavioral characterization of autism-associated mutations in the dopamine transporter gene. *Molecular Psychiatry*, *18*(12), 1235. https://doi.org/10.1038/mp.2013.157

Hamilton, P. J., Campbell, N. G., Sharma, S., Erreger, K., Hansen, F. H., Saunders, C., … Galli, A. (2013b). Drosophila melanogaster: a novel animal model for the behavioral characterization of autism-associated mutations in the dopamine transporter gene. *Molecular Psychiatry*, *18*(12), 1235. https://doi.org/10.1038/mp.2013.157

Hamilton, P. J., Campbell, N. G., Sharma, S., Erreger, K., Herborg Hansen, F., Saunders, C., … Galli, A. (2013). De novo mutation in the dopamine transporter gene associates dopamine dysfunction with autism spectrum disorder. *Molecular Psychiatry*, *18*(12), 1315–1323. https://doi.org/10.1038/mp.2013.102

Hamilton, Peter J., Belovich, A. N., Khelashvili, G., Saunders, C., Erreger, K., Javitch, J. A., … Galli, A. (2014). PIP2 regulates psychostimulant behaviors through its interaction with a membrane protein. *Nature Chemical Biology*, *10*(7), 582–589. https://doi.org/10.1038/nchembio.1545

Hansen, F. H., Skjørringe, T., Yasmeen, S., Arends, N. V., Sahai, M. A., Erreger, K., … Gether, U. (2014). Missense dopamine transporter mutations associate with adult parkinsonism and ADHD. *The Journal of Clinical Investigation*, *124*(7), 3107–3120. https://doi.org/10.1172/JCI73778

Harsing, L. G., & Zigmond, M. J. (1998). Postsynaptic integration of cholinergic and dopaminergic signals on medium-sized GABAergic projection neurons in the neostriatum. *Brain Research Bulletin*, *45*(6), 607–613.

Hawkins, R. A., O'Kane, R. L., Simpson, I. A., & Viña, J. R. (2006). Structure of the blood-brain barrier and its role in the transport of amino acids. *The Journal of Nutrition*, *136*(1 Suppl), 218S-26S. https://doi.org/10.1093/jn/136.1.218S

Hendricks, J. C., Kirk, D., Panckeri, K., Miller, M. S., & Pack, A. I. (2003). Modafinil maintains waking in the fruit fly drosophila melanogaster. *Sleep*, *26*(2), 139–146.

Herborg, F., Andreassen, T. F., Berlin, F., Loland, C. J., & Gether, U. (2018). Neuropsychiatric disease-associated genetic variants of the dopamine transporter display heterogeneous

molecular phenotypes. *The Journal of Biological Chemistry*, *293*(19), 7250–7262. https://doi.org/10.1074/jbc.RA118.001753

Horschitz, S., Hummerich, R., Lau, T., Rietschel, M., & Schloss, P. (2005). A dopamine transporter mutation associated with bipolar affective disorder causes inhibition of transporter cell surface expression. *Molecular Psychiatry*, *10*(12), 1104–1109. https://doi.org/10.1038/sj.mp.4001730

Howell, M., Shirvan, A., Stern-Bach, Y., Steiner-Mordoch, S., Strasser, J. E., Dean, G. E., & Schuldiner, S. (1994). Cloning and functional expression of a tetrabenazine sensitive vesicular monoamine transporter from bovine chromaffin granules. *FEBS Letters*, *338*(1), 16–22.

Huang, C. L., Chen, H. C., Huang, N. K., Yang, D. M., Kao, L. S., Chen, J. C., … Chern, Y. (1999). Modulation of dopamine transporter activity by nicotinic acetylcholine receptors and membrane depolarization in rat pheochromocytoma PC12 cells. *Journal of Neurochemistry*, *72*(6), 2437–2444.

Huber, R., Panksepp, J. B., Nathaniel, T., Alcaro, A., & Panksepp, J. (2011). Drug-sensitive reward in crayfish: an invertebrate model system for the study of SEEKING, reward, addiction, and withdrawal. *Neuroscience and Biobehavioral Reviews*, *35*(9), 1847–1853. https://doi.org/10.1016/j.neubiorev.2010.12.008

Imperato, A., Honoré, T., & Jensen, L. H. (1990). Dopamine release in the nucleus caudatus and in the nucleus accumbens is under glutamatergic control through non-NMDA receptors: a study in freely-moving rats. *Brain Research*, *530*(2), 223–228.

Imperato, A., Scrocco, M. G., Bacchi, S., & Angelucci, L. (1990). NMDA receptors and in vivo dopamine release in the nucleus accumbens and caudatus. *European Journal of Pharmacology*, *187*(3), 555–556.

Inagaki, H. K., Ben-Tabou de-Leon, S., Wong, A. M., Jagadish, S., Ishimoto, H., Barnea, G., … Anderson, D. J. (2012). Visualizing neuromodulation in vivo: TANGO-mapping of dopamine signaling reveals appetite control of sugar sensing. *Cell*, *148*(3), 583–595. https://doi.org/10.1016/j.cell.2011.12.022

Ingram, S. L., Prasad, B. M., & Amara, S. G. (2002). Dopamine transporter-mediated conductances increase excitability of midbrain dopamine neurons. *Nature Neuroscience*, *5*(10), 971–978. https://doi.org/10.1038/nn920

Iversen, S. D., & Iversen, L. L. (2007). Dopamine: 50 years in perspective. *Trends in Neurosciences*, *30*(5), 188–193. https://doi.org/10.1016/j.tins.2007.03.002

Iwata, S., Hewlett, G. H., & Gnegy, M. E. (1997). Amphetamine increases the phosphorylation of neuromodulin and synapsin I in rat striatal synaptosomes. *Synapse (New York, N.Y.)*, *26*(3), 281–291. https://doi.org/10.1002/(SICI)1098-2396(199707)26:3<281::AID-SYN9>3.0.CO;2-3

Jaber, M., Jones, S., Giros, B., & Caron, M. G. (1997). The dopamine transporter: a crucial component regulating dopamine transmission. *Movement Disorders: Official Journal of the Movement Disorder Society*, *12*(5), 629–633. https://doi.org/10.1002/mds.870120502

Jackson, M. J., & Garrod, P. J. (1978). Plasma zinc, copper, and amino acid levels in the blood of autistic children. *Journal of Autism and Childhood Schizophrenia*, *8*(2), 203–208.

Jeschke, G., & Polyhach, Y. (2007). Distance measurements on spin-labelled biomacromolecules by pulsed electron paramagnetic resonance. *Physical Chemistry Chemical Physics: PCCP*, *9*(16), 1895–1910. https://doi.org/10.1039/b614920k

Johnson, L. A., Guptaroy, B., Lund, D., Shamban, S., & Gnegy, M. E. (2005). Regulation of amphetamine-stimulated dopamine efflux by protein kinase C beta. *The Journal of Biological Chemistry*, *280*(12), 10914–10919. https://doi.org/10.1074/jbc.M413887200

Jones, K. T., Zhen, J., & Reith, M. E. A. (2012). Importance of cholesterol in dopamine transporter function. *Journal of Neurochemistry*, *123*(5), 700–715. https://doi.org/10.1111/jnc.12007

Jonsson, G., & Sachs, C. (1970). Synthesis of noradrenaline from 3,4-dihydroxyphenylalanine (DOPA) and dopamine in adrenergic nerves of mouse atrium--effect of reserpine, monoamine oxidase and tyrosine hydroxylase inhibition. *Acta Physiologica Scandinavica*, *80*(3), 307–322. https://doi.org/10.1111/j.1748-1716.1970.tb04795.x

Joseph, M. H., Frith, C. D., & Waddington, J. L. (1979). Dopaminergic mechanisms and cognitive deficit in schizophrenia. A neurobiological model. *Psychopharmacology*, *63*(3), 273–280.

Kabsch, W. (2010). XDS. *Acta Crystallographica. Section D, Biological Crystallography*, *66*(Pt 2), 125–132. https://doi.org/10.1107/S0907444909047337

Kahlig, K. M., & Galli, A. (2003). Regulation of dopamine transporter function and plasma membrane expression by dopamine, amphetamine, and cocaine. *European Journal of Pharmacology*, *479*(1–3), 153–158.

Kahlig, K. M., Lute, B. J., Wei, Y., Loland, C. J., Gether, U., Javitch, J. A., & Galli, A. (2006). Regulation of dopamine transporter trafficking by intracellular amphetamine. *Molecular Pharmacology*, *70*(2), 542–548. https://doi.org/10.1124/mol.106.023952

Kantor, L., & Gnegy, M. E. (1998). Protein kinase C inhibitors block amphetamine-mediated dopamine release in rat striatal slices. *The Journal of Pharmacology and Experimental Therapeutics*, *284*(2), 592–598.

Kantor, L., Zhang, M., Guptaroy, B., Park, Y. H., & Gnegy, M. E. (2004). Repeated amphetamine couples norepinephrine transporter and calcium channel activities in PC12 cells. *The Journal of Pharmacology and Experimental Therapeutics*, *311*(3), 1044–1051. https://doi.org/10.1124/jpet.104.071068

Kaun, K. R., Devineni, A. V., & Heberlein, U. (2012). Drosophila melanogaster as a model to study drug addiction. *Human Genetics*, *131*(6), 959–975. https://doi.org/10.1007/s00439-012-1146-6

Kazmier, K., Sharma, S., Quick, M., Islam, S. M., Roux, B., Weinstein, H., … McHaourab, H. S. (2014). Conformational dynamics of ligand-dependent alternating access in LeuT. *Nature Structural & Molecular Biology*, *21*(5), 472–479. https://doi.org/10.1038/nsmb.2816

Kehr, J., Ichinose, F., Yoshitake, S., Goiny, M., Sievertsson, T., Nyberg, F., & Yoshitake, T. (2011). Mephedrone, compared with MDMA (ecstasy) and amphetamine, rapidly increases both dopamine and 5-HT levels in nucleus accumbens of awake rats. *British Journal of Pharmacology*, *164*(8), 1949–1958. https://doi.org/10.1111/j.1476-5381.2011.01499.x

Khelashvili, G., Doktorova, M., Sahai, M. A., Johner, N., Shi, L., & Weinstein, H. (2015). Computational modeling of the N-terminus of the human dopamine transporter and its

interaction with PIP2 -containing membranes. *Proteins*, *83*(5), 952–969. https://doi.org/10.1002/prot.24792

Khelashvili, G., Galli, A., & Weinstein, H. (2012). Phosphatidylinositol 4,5-biphosphate (PIP(2)) lipids regulate the phosphorylation of syntaxin N-terminus by modulating both its position and local structure. *Biochemistry*, *51*(39), 7685–7698. https://doi.org/10.1021/bi300833z

Khelashvili, G., Stanley, N., Sahai, M. A., Medina, J., LeVine, M. V., Shi, L., … Weinstein, H. (2015). Spontaneous inward opening of the dopamine transporter is triggered by PIP2-regulated dynamics of the N-terminus. *ACS Chemical Neuroscience*, *6*(11), 1825–1837. https://doi.org/10.1021/acschemneuro.5b00179

Khelashvili, G., & Weinstein, H. (2015). Functional mechanisms of neurotransmitter transporters regulated by lipid-protein interactions of their terminal loops. *Biochimica Et Biophysica Acta*, *1848*(9), 1765–1774. https://doi.org/10.1016/j.bbamem.2015.03.025

Khoshbouei, H., Sen, N., Guptaroy, B., Johnson, L. ’Aurelle, Lund, D., Gnegy, M. E., … Javitch, J. A. (2004). N-terminal phosphorylation of the dopamine transporter is required for amphetamine-induced efflux. *PLoS Biology*, *2*(3), E78. https://doi.org/10.1371/journal.pbio.0020078

Khoshbouei, H., Wang, H., Lechleiter, J. D., Javitch, J. A., & Galli, A. (2003). Amphetamine-induced dopamine efflux. A voltage-sensitive and intracellular Na+-dependent mechanism. *The Journal of Biological Chemistry*, *278*(14), 12070–12077. https://doi.org/10.1074/jbc.M212815200

Khuong, T. M., Habets, R. L. P., Kuenen, S., Witkowska, A., Kasprowicz, J., Swerts, J., … Verstreken, P. (2013). Synaptic PI(3,4,5)P3 is required for Syntaxin1A clustering and neurotransmitter release. *Neuron*, *77*(6), 1097–1108. https://doi.org/10.1016/j.neuron.2013.01.025

King, H. E., Wetzell, B., Rice, K. C., & Riley, A. L. (2015). An assessment of MDPV-induced place preference in adult Sprague-Dawley rats. *Drug and Alcohol Dependence*, *146*, 116–119. https://doi.org/10.1016/j.drugalcdep.2014.11.002

Kolanos, R., Solis, E., Sakloth, F., De Felice, L. J., & Glennon, R. A. (2013). "Deconstruction" of the abused synthetic cathinone methylenedioxypyrovalerone (MDPV) and an examination of effects at the human dopamine transporter. *ACS Chemical Neuroscience*, *4*(12), 1524–1529. https://doi.org/10.1021/cn4001236

Koob, G. F., & Bloom, F. E. (1988). Cellular and molecular mechanisms of drug dependence. *Science (New York, N.Y.)*, *242*(4879), 715–723.

Kopin, I. J. (1994). Monoamine oxidase and catecholamine metabolism. *Journal of Neural Transmission. Supplementum*, *41*, 57–67.

Kramer, J. M., & Staveley, B. E. (2003). GAL4 causes developmental defects and apoptosis when expressed in the developing eye of Drosophila melanogaster. *Genetics and Molecular Research: GMR*, *2*(1), 43–47.

Kriikku, P., Wilhelm, L., Schwarz, O., & Rintatalo, J. (2011). New designer drug of abuse: 3,4-Methylenedioxypyrovalerone (MDPV). Findings from apprehended drivers in Finland. *Forensic Science International*, *210*(1–3), 195–200. https://doi.org/10.1016/j.forsciint.2011.03.015

Krishnamurthy, H., & Gouaux, E. (2012). X-ray structures of LeuT in substrate-free outward-open and apo inward-open states. *Nature*, *481*(7382), 469–474. https://doi.org/10.1038/nature10737

Kristensen, A. S., Andersen, J., Jørgensen, T. N., Sørensen, L., Eriksen, J., Loland, C. J., … Gether, U. (2011). SLC6 neurotransmitter transporters: structure, function, and regulation. *Pharmacological Reviews*, *63*(3), 585–640. https://doi.org/10.1124/pr.108.000869

Kume, K., Kume, S., Park, S. K., Hirsh, J., & Jackson, F. R. (2005). Dopamine is a regulator of arousal in the fruit fly. *The Journal of Neuroscience: The Official Journal of the Society for Neuroscience*, *25*(32), 7377–7384. https://doi.org/10.1523/JNEUROSCI.2048-05.2005

Kurian, M. A., Zhen, J., Cheng, S.-Y., Li, Y., Mordekar, S. R., Jardine, P., … Maher, E. R. (2009). Homozygous loss-of-function mutations in the gene encoding the dopamine transporter are associated with infantile parkinsonism-dystonia. *The Journal of Clinical Investigation*, *119*(6), 1595–1603. https://doi.org/10.1172/JCI39060

Lammel, S., Ion, D. I., Roeper, J., & Malenka, R. C. (2011). Projection-specific modulation of dopamine neuron synapses by aversive and rewarding stimuli. *Neuron*, *70*(5), 855–862. https://doi.org/10.1016/j.neuron.2011.03.025

LeDoux, J. (2003). The emotional brain, fear, and the amygdala. *Cellular and Molecular Neurobiology*, *23*(4–5), 727–738.

Lee, K.-H., Kim, M.-Y., Kim, D.-H., & Lee, Y.-S. (2004). Syntaxin 1A and receptor for activated C kinase interact with the N-terminal region of human dopamine transporter. *Neurochemical Research*, *29*(7), 1405–1409.

Lee, M. R. (1982). Dopamine and the kidney. *Clinical Science (London, England: 1979)*, *62*(5), 439–448.

Lee, S.-H., Pak, H. K., & Chon, T.-S. (2006). Dynamics of prey-flock escaping behavior in response to predator's attack. *Journal of Theoretical Biology*, *240*(2), 250–259. https://doi.org/10.1016/j.jtbi.2005.09.009

Li, S., Wang, J., Bjørklund, G., Zhao, W., & Yin, C. (2014). Serum copper and zinc levels in individuals with autism spectrum disorders. *Neuroreport*, *25*(15), 1216–1220. https://doi.org/10.1097/WNR.0000000000000251

Lindorff-Larsen, K., Piana, S., Palmo, K., Maragakis, P., Klepeis, J. L., Dror, R. O., & Shaw, D. E. (2010). Improved side-chain torsion potentials for the Amber ff99SB protein force field. *Proteins*, *78*(8), 1950–1958. https://doi.org/10.1002/prot.22711

Lisek, R., Xu, W., Yuvasheva, E., Chiu, Y.-T., Reitz, A. B., Liu-Chen, L.-Y., & Rawls, S. M. (2012). Mephedrone ('bath salt') elicits conditioned place preference and dopamine-sensitive motor activation. *Drug and Alcohol Dependence*, *126*(1–2), 257–262. https://doi.org/10.1016/j.drugalcdep.2012.04.021

Liu, T., Dartevelle, L., Yuan, C., Wei, H., Wang, Y., Ferveur, J.-F., & Guo, A. (2008). Increased Dopamine Level Enhances Male-Male Courtship in Drosophila. *Journal of Neuroscience*, *28*(21), 5539–5546. https://doi.org/10.1523/JNEUROSCI.5290-07.2008

Loder, M. K., & Melikian, H. E. (2003). The dopamine transporter constitutively internalizes and recycles in a protein kinase C-regulated manner in stably transfected PC12 cell lines. *The Journal of Biological Chemistry*, *278*(24), 22168–22174. https://doi.org/10.1074/jbc.M301845200

Lohani, S., Martig, A. K., Underhill, S. M., DeFrancesco, A., Roberts, M. J., Rinaman, L., … Moghaddam, B. (2018). Burst activation of dopamine neurons produces prolonged post-burst availability of actively released dopamine. *Neuropsychopharmacology: Official Publication of the American College of Neuropsychopharmacology*, *43*(10), 2083–2092. https://doi.org/10.1038/s41386-018-0088-7

Loland, C. J., Norregaard, L., & Gether, U. (1999). Defining proximity relationships in the tertiary structure of the dopamine transporter. Identification of a conserved glutamic acid as a third coordinate in the endogenous Zn(2+)-binding site. *The Journal of Biological Chemistry*, *274*(52), 36928–36934.

Loland, Claus Juul, Norregaard, L., Litman, T., & Gether, U. (2002). Generation of an activating Zn(2+) switch in the dopamine transporter: mutation of an intracellular tyrosine constitutively alters the conformational equilibrium of the transport cycle. *Proceedings of the National Academy of Sciences of the United States of America*, *99*(3), 1683–1688. https://doi.org/10.1073/pnas.032386299

Lowe, S. A., Hodge, J. J. L., & Usowicz, M. M. (2018). A third copy of the Down syndrome cell adhesion molecule (Dscam) causes synaptic and locomotor dysfunction in Drosophila. *Neurobiology of Disease*, *110*, 93–101. https://doi.org/10.1016/j.nbd.2017.11.013

Malinauskaite, L., Said, S., Sahin, C., Grouleff, J., Shahsavar, A., Bjerregaard, H., … Nissen, P. (2016). A conserved leucine occupies the empty substrate site of LeuT in the Na(+)-free return state. *Nature Communications*, *7*, 11673. https://doi.org/10.1038/ncomms11673

Martín, F., & Alcorta, E. (2017). Novel genetic approaches to behavior in Drosophila. *Journal of Neurogenetics*, *31*(4), 288–299. https://doi.org/10.1080/01677063.2017.1395875

Marusich, J. A., Antonazzo, K. R., Wiley, J. L., Blough, B. E., Partilla, J. S., & Baumann, M. H. (2014). Pharmacology of novel synthetic stimulants structurally related to the "bath salts" constituent 3,4-methylenedioxypyrovalerone (MDPV). *Neuropharmacology*, *87*, 206–213. https://doi.org/10.1016/j.neuropharm.2014.02.016

Mayfield, R. D., & Zahniser, N. R. (2001). Dopamine D2 Receptor Regulation of the Dopamine Transporter Expressed in Xenopus laevis Oocytes Is Voltage-Independent. *Molecular Pharmacology*, *59*(1), 113–121. https://doi.org/10.1124/mol.59.1.113

Mazei-Robison, M. S., Bowton, E., Holy, M., Schmudermaier, M., Freissmuth, M., Sitte, H. H., … Blakely, R. D. (2008). Anomalous dopamine release associated with a human dopamine transporter coding variant. *The Journal of Neuroscience: The Official Journal of the Society for Neuroscience*, *28*(28), 7040–7046. https://doi.org/10.1523/JNEUROSCI.0473-08.2008

Mazei-Robison, M. S., Couch, R. S., Shelton, R. C., Stein, M. A., & Blakely, R. D. (2005). Sequence variation in the human dopamine transporter gene in children with attention deficit hyperactivity disorder. *Neuropharmacology*, *49*(6), 724–736. https://doi.org/10.1016/j.neuropharm.2005.08.003

Meggio, F., & Pinna, L. A. (2003). One-thousand-and-one substrates of protein kinase CK2? *The FASEB Journal*, *17*(3), 349–368. https://doi.org/10.1096/fj.02-0473rev

Melchior, J. R., Ferris, M. J., Stuber, G. D., Riddle, D. R., & Jones, S. R. (2015). Optogenetic versus electrical stimulation of dopamine terminals in the nucleus accumbens reveals local modulation of presynaptic release. *Journal of Neurochemistry*, *134*(5), 833–844. https://doi.org/10.1111/jnc.13177

Mergy, M. A., Gowrishankar, R., Davis, G. L., Jessen, T. N., Wright, J., Stanwood, G. D., … Blakely, R. D. (2014). Genetic targeting of the amphetamine and methylphenidate-sensitive dopamine transporter: on the path to an animal model of attention-deficit hyperactivity disorder. *Neurochemistry International*, *73*, 56–70. https://doi.org/10.1016/j.neuint.2013.11.009

Mergy, M. A., Gowrishankar, R., Gresch, P. J., Gantz, S. C., Williams, J., Davis, G. L., … Blakely, R. D. (2014). The rare DAT coding variant Val559 perturbs DA neuron function, changes behavior, and alters in vivo responses to psychostimulants. *Proceedings of the National Academy of Sciences of the United States of America*, *111*(44), E4779-4788. https://doi.org/10.1073/pnas.1417294111

Moritz, A. E., Rastedt, D. E., Stanislowski, D. J., Shetty, M., Smith, M. A., Vaughan, R. A., & Foster, J. D. (2015). Reciprocal Phosphorylation and Palmitoylation Control Dopamine Transporter Kinetics. *The Journal of Biological Chemistry*, *290*(48), 29095–29105. https://doi.org/10.1074/jbc.M115.667055

Mortensen, O. V., & Amara, S. G. (2003). Dynamic regulation of the dopamine transporter. *European Journal of Pharmacology*, *479*(1–3), 159–170.

Muqit, M. M. K., & Feany, M. B. (2002). Modelling neurodegenerative diseases in Drosophila: a fruitful approach? *Nature Reviews. Neuroscience*, *3*(3), 237–243. https://doi.org/10.1038/nrn751

Murray, B. L., Murphy, C. M., & Beuhler, M. C. (2012). Death following recreational use of designer drug “bath salts” containing 3,4-Methylenedioxypyrovalerone (MDPV). *Journal*

of Medical Toxicology: Official Journal of the American College of Medical Toxicology, *8*(1), 69–75. https://doi.org/10.1007/s13181-011-0196-9

Musso, N. R., Brenci, S., Setti, M., Indiveri, F., & Lotti, G. (1996). Catecholamine content and in vitro catecholamine synthesis in peripheral human lymphocytes. *The Journal of Clinical Endocrinology and Metabolism*, *81*(10), 3553–3557. https://doi.org/10.1210/jcem.81.10.8855800

Nakamura, K., Sekine, Y., Ouchi, Y., Tsujii, M., Yoshikawa, E., Futatsubashi, M., … Mori, N. (2010). Brain serotonin and dopamine transporter bindings in adults with high-functioning autism. *Archives of General Psychiatry*, *67*(1), 59–68. https://doi.org/10.1001/archgenpsychiatry.2009.137

Naoi, M., Riederer, P., & Maruyama, W. (2016). Modulation of monoamine oxidase (MAO) expression in neuropsychiatric disorders: genetic and environmental factors involved in type A MAO expression. *Journal of Neural Transmission*, *123*(2), 91–106. https://doi.org/10.1007/s00702-014-1362-4

Neale, B. M., Kou, Y., Liu, L., Ma'ayan, A., Samocha, K. E., Sabo, A., … Daly, M. J. (2012). Patterns and rates of exonic de novo mutations in autism spectrum disorders. *Nature*, *485*(7397), 242–245. https://doi.org/10.1038/nature11011

Neckameyer, W. S. (1998). Dopamine Modulates Female Sexual Receptivity in *Drosophila Melanogaster*. *Journal of Neurogenetics*, *12*(2), 101–114. https://doi.org/10.3109/01677069809167259

Ng, J., Zhen, J., Meyer, E., Erreger, K., Li, Y., Kakar, N., … Kurian, M. A. (2014). Dopamine transporter deficiency syndrome: phenotypic spectrum from infancy to adulthood.

Brain: A Journal of Neurology, *137*(Pt 4), 1107–1119. https://doi.org/10.1093/brain/awu022

Nguyen, J. D., Aarde, S. M., Cole, M., Vandewater, S. A., Grant, Y., & Taffe, M. A. (2016). Locomotor Stimulant and Rewarding Effects of Inhaling Methamphetamine, MDPV, and Mephedrone via Electronic Cigarette-Type Technology. *Neuropsychopharmacology: Official Publication of the American College of Neuropsychopharmacology*, *41*(11), 2759–2771. https://doi.org/10.1038/npp.2016.88

Nguyen-Legros, J., Krieger, M., & Simon, A. (1994). Immunohistochemical localization of L-dopa and aromatic L-amino acid-decarboxylase in the rat retina. *Investigative Ophthalmology & Visual Science*, *35*(7), 2906–2915.

Nirenberg, M. J., Chan, J., Liu, Y., Edwards, R. H., & Pickel, V. M. (1996). Ultrastructural localization of the vesicular monoamine transporter-2 in midbrain dopaminergic neurons: potential sites for somatodendritic storage and release of dopamine. *The Journal of Neuroscience: The Official Journal of the Society for Neuroscience*, *16*(13), 4135–4145.

Nirenberg, M. J., Vaughan, R. A., Uhl, G. R., Kuhar, M. J., & Pickel, V. M. (1996). The dopamine transporter is localized to dendritic and axonal plasma membranes of nigrostriatal dopaminergic neurons. *The Journal of Neuroscience: The Official Journal of the Society for Neuroscience*, *16*(2), 436–447.

Norregaard, L., Frederiksen, D., Nielsen, E. O., & Gether, U. (1998). Delineation of an endogenous zinc-binding site in the human dopamine transporter. *The EMBO Journal*, *17*(15), 4266–4273. https://doi.org/10.1093/emboj/17.15.4266

Novellas, J., López-Arnau, R., Carbó, M. L., Pubill, D., Camarasa, J., & Escubedo, E. (2015). Concentrations of MDPV in rat striatum correlate with the psychostimulant effect. *Journal of Psychopharmacology (Oxford, England)*, *29*(11), 1209–1218. https://doi.org/10.1177/0269881115598415

O'Connor, R. M., Stone, E. F., Wayne, C. R., Marcinkevicius, E. V., Ulgherait, M., Delventhal, R., … Shirasu-Hiza, M. M. (2017). A Drosophila model of Fragile X syndrome exhibits defects in phagocytosis by innate immune cells. *The Journal of Cell Biology*, *216*(3), 595–605. https://doi.org/10.1083/jcb.201607093

Olivier, V., Guibert, B., & Leviel, V. (1995). Direct in vivo comparison of two mechanisms releasing dopamine in the rat striatum. *Brain Research*, *695*(1), 1–9.

Opazo, F., Schulz, J. B., & Falkenburger, B. H. (2010). PKC links Gq-coupled receptors to DAT-mediated dopamine release. *Journal of Neurochemistry*, *114*(2), 587–596. https://doi.org/10.1111/j.1471-4159.2010.06788.x

O'Roak, B. J., Vives, L., Girirajan, S., Karakoc, E., Krumm, N., Coe, B. P., … Eichler, E. E. (2012). Sporadic autism exomes reveal a highly interconnected protein network of de novo mutations. *Nature*, *485*(7397), 246–250. https://doi.org/10.1038/nature10989

Paredes, R. G., & Agmo, A. (2004). Has dopamine a physiological role in the control of sexual behavior? A critical review of the evidence. *Progress in Neurobiology*, *73*(3), 179–226. https://doi.org/10.1016/j.pneurobio.2004.05.001

Penders, T. M., & Gestring, R. (2011). Hallucinatory delirium following use of MDPV: "Bath Salts." *General Hospital Psychiatry*, *33*(5), 525–526. https://doi.org/10.1016/j.genhosppsych.2011.05.014

Penmatsa, A., Wang, K. H., & Gouaux, E. (2015). X-ray structures of Drosophila dopamine transporter in complex with nisoxetine and reboxetine. *Nature Structural & Molecular Biology*, *22*(6), 506–508. https://doi.org/10.1038/nsmb.3029

Pizzo, A. B., Karam, C. S., Zhang, Y., Yano, H., Freyberg, R. J., Karam, D. S., … Javitch, J. A. (2013). The membrane raft protein Flotillin-1 is essential in dopamine neurons for amphetamine-induced behavior in Drosophila. *Molecular Psychiatry*, *18*(7), 824–833. https://doi.org/10.1038/mp.2012.82

Prüßing, K., Voigt, A., & Schulz, J. B. (2013). Drosophila melanogaster as a model organism for Alzheimer's disease. *Molecular Neurodegeneration*, *8*, 35. https://doi.org/10.1186/1750-1326-8-35

Ramsay, R. R., & Hunter, D. J. B. (2003). Interactions of D-amphetamine with the active site of monoamine oxidase-A. *Inflammopharmacology*, *11*(2), 127–133. https://doi.org/10.1163/156856003765764290

Rastedt, D. E., Vaughan, R. A., & Foster, J. D. (2017). Palmitoylation mechanisms in dopamine transporter regulation. *Journal of Chemical Neuroanatomy*, *83–84*, 3–9. https://doi.org/10.1016/j.jchemneu.2017.01.002

Razavi, A. M., Khelashvili, G., & Weinstein, H. (2017). A Markov State-based Quantitative Kinetic Model of Sodium Release from the Dopamine Transporter. *Scientific Reports*, *7*, 40076. https://doi.org/10.1038/srep40076

Reith, M. E., Xu, C., & Chen, N. H. (1997). Pharmacology and regulation of the neuronal dopamine transporter. *European Journal of Pharmacology*, *324*(1), 1–10.

Richardson, B. D., Saha, K., Krout, D., Cabrera, E., Felts, B., Henry, L. K., … Khoshbouei, H. (2016). Membrane potential shapes regulation of dopamine transporter trafficking at the plasma membrane. *Nature Communications*, *7*, 10423. https://doi.org/10.1038/ncomms10423

Richtand, N. M., Kelsoe, J. R., Segal, D. S., & Kuczenski, R. (1995). Regional quantification of D1, D2, and D3 dopamine receptor mRNA in rat brain using a ribonuclease protection assay. *Brain Research. Molecular Brain Research*, *33*(1), 97–103.

Riemensperger, T., Issa, A.-R., Pech, U., Coulom, H., Nguyễn, M.-V., Cassar, M., … Birman, S. (2013). A single dopamine pathway underlies progressive locomotor deficits in a Drosophila model of Parkinson disease. *Cell Reports*, *5*(4), 952–960. https://doi.org/10.1016/j.celrep.2013.10.032

Ritz, M. C., & Kuhar, M. J. (1989). Relationship between self-administration of amphetamine and monoamine receptors in brain: comparison with cocaine. *The Journal of Pharmacology and Experimental Therapeutics*, *248*(3), 1010–1017.

Ross, E. A., Reisfield, G. M., Watson, M. C., Chronister, C. W., & Goldberger, B. A. (2012). Psychoactive “bath salts” intoxication with methylenedioxypyrovalerone. *The American Journal of Medicine*, *125*(9), 854–858. https://doi.org/10.1016/j.amjmed.2012.02.019

Ruchala, I., Cabra, V., Solis, E., Glennon, R. A., De Felice, L. J., & Eltit, J. M. (2014). Electrical coupling between the human serotonin transporter and voltage-gated Ca2+ channels. *Cell Calcium*, *56*(1), 25–33. https://doi.org/10.1016/j.ceca.2014.04.003

Saha, K., Swant, J., & Khoshbouei, H. (2012). Single cell measurement of dopamine release with simultaneous voltage-clamp and amperometry. *Journal of Visualized Experiments: JoVE*, (69). https://doi.org/10.3791/3798

Sakrikar, D., Mazei-Robison, M. S., Mergy, M. A., Richtand, N. W., Han, Q., Hamilton, P. J., … Blakely, R. D. (2012). Attention deficit/hyperactivity disorder-derived coding variation in the dopamine transporter disrupts microdomain targeting and trafficking regulation. *The Journal of Neuroscience: The Official Journal of the Society for Neuroscience*, *32*(16), 5385–5397. https://doi.org/10.1523/JNEUROSCI.6033-11.2012

Salvaterra, P. M., & Kitamoto, T. (2001). Drosophila cholinergic neurons and processes visualized with Gal4 / UAS–GFPq. *Gene Expression Patterns*, 10.

Sanders, S. J., Ercan-Sencicek, A. G., Hus, V., Luo, R., Murtha, M. T., Moreno-De-Luca, D., … State, M. W. (2011). Multiple recurrent de novo CNVs, including duplications of the 7q11.23 Williams syndrome region, are strongly associated with autism. *Neuron*, *70*(5), 863–885. https://doi.org/10.1016/j.neuron.2011.05.002

Sano, I., Gamo, T., Kakimoto, Y., Taniguchi, K., Takesada, M., & Nishinuma, K. (1959). Distribution of catechol compounds in human brain. *Biochimica Et Biophysica Acta*, *32*, 586–587.

Saunders, C., Ferrer, J. V., Shi, L., Chen, J., Merrill, G., Lamb, M. E., … Galli, A. (2000). Amphetamine-induced loss of human dopamine transporter activity: an internalization-dependent and cocaine-sensitive mechanism. *Proceedings of the National Academy of Sciences of the United States of America*, *97*(12), 6850–6855. https://doi.org/10.1073/pnas.110035297

Savica, R., & Benarroch, E. E. (2014). Dopamine receptor signaling in the forebrain: recent insights and clinical implications. *Neurology*, *83*(8), 758–767. https://doi.org/10.1212/WNL.0000000000000719

Schmitt, K. C., & Reith, M. E. A. (2010). Regulation of the dopamine transporter: aspects relevant to psychostimulant drugs of abuse. *Annals of the New York Academy of Sciences*, *1187*, 316–340. https://doi.org/10.1111/j.1749-6632.2009.05148.x

Seeman, P., & Niznik, H. B. (1990). Dopamine receptors and transporters in Parkinson's disease and schizophrenia. *FASEB Journal: Official Publication of the Federation of American Societies for Experimental Biology*, *4*(10), 2737–2744.

Seidel, S., Singer, E. A., Just, H., Farhan, H., Scholze, P., Kudlacek, O., … Sitte, H. H. (2005). Amphetamines take two to tango: an oligomer-based counter-transport model of neurotransmitter transport explores the amphetamine action. *Molecular Pharmacology*, *67*(1), 140–151. https://doi.org/10.1124/mol.67.1.

Seiden, L. S., Sabol, K. E., & Ricaurte, G. A. (1993). Amphetamine: effects on catecholamine systems and behavior. *Annual Review of Pharmacology and Toxicology*, *33*, 639–677. https://doi.org/10.1146/annurev.pa.33.040193.003231

Sharma, A., & Couture, J. (2014). A review of the pathophysiology, etiology, and treatment of attention-deficit hyperactivity disorder (ADHD). *The Annals of Pharmacotherapy*, *48*(2), 209–225. https://doi.org/10.1177/1060028013510699

Sharma, R., Javaid, J. I., Janicak, P., Faull, K., Comaty, J., & Davis, J. M. (1989). Plasma and CSF HVA before and after pharmacological treatment. *Psychiatry Research*, *28*(1), 97–104.

Sharpe, A. L., Varela, E., Bettinger, L., & Beckstead, M. J. (2014). Methamphetamine self-administration in mice decreases GIRK channel-mediated currents in midbrain dopamine neurons. *The International Journal of Neuropsychopharmacology*, *18*(5). https://doi.org/10.1093/ijnp/pyu073

Siddiqui-Jain, A., Drygin, D., Streiner, N., Chua, P., Pierre, F., O'Brien, S. E., … Anderes, K. (2010). CX-4945, an Orally Bioavailable Selective Inhibitor of Protein Kinase CK2, Inhibits Prosurvival and Angiogenic Signaling and Exhibits Antitumor Efficacy. *Cancer Research*, *70*(24), 10288–10298. https://doi.org/10.1158/0008-5472.CAN-10-1893

Silverman, J. L., Tolu, S. S., Barkan, C. L., & Crawley, J. N. (2010). Repetitive self-grooming behavior in the BTBR mouse model of autism is blocked by the mGluR5 antagonist MPEP. *Neuropsychopharmacology: Official Publication of the American College of Neuropsychopharmacology*, *35*(4), 976–989. https://doi.org/10.1038/npp.2009.201

Singh, S. K., Yamashita, A., & Gouaux, E. (2007). Antidepressant binding site in a bacterial homologue of neurotransmitter transporters. *Nature*, *448*(7156), 952–956. https://doi.org/10.1038/nature06038

Sitte, H. H., Farhan, H., & Javitch, J. A. (2004). Sodium-dependent neurotransmitter transporters: oligomerization as a determinant of transporter function and trafficking. *Molecular Interventions*, *4*(1), 38–47. https://doi.org/10.1124/mi.4.1.38

Smythe, G. A. (1977). The role of serotonin and dopamine in hypothalamic-pituitary function. *Clinical Endocrinology*, *7*(4), 325–341.

Sonders, M. S., & Amara, S. G. (1996). Channels in transporters. *Current Opinion in Neurobiology*, *6*(3), 294–302.

Sonders, M. S., Zhu, S. J., Zahniser, N. R., Kavanaugh, M. P., & Amara, S. G. (1997). Multiple ionic conductances of the human dopamine transporter: the actions of dopamine and psychostimulants. *The Journal of Neuroscience: The Official Journal of the Society for Neuroscience*, *17*(3), 960–974.

Sossi, V., Fuente-Fernández, R. de la, Schulzer, M., Troiano, A. R., Ruth, T. J., & Stoessl, A. J. (2007). Dopamine transporter relation to dopamine turnover in Parkinson's disease: a positron emission tomography study. *Annals of Neurology*, *62*(5), 468–474. https://doi.org/10.1002/ana.21204

Sotnikova, T. D., Beaulieu, J.-M., Gainetdinov, R. R., & Caron, M. G. (2006). Molecular biology, pharmacology and functional role of the plasma membrane dopamine transporter. *CNS & Neurological Disorders Drug Targets*, *5*(1), 45–56.

Stefani, A., Pierantozzi, M., Olivola, E., Galati, S., Cerroni, R., D'Angelo, V., … Liguori, C. (2017). Homovanillic acid in CSF of mild stage Parkinson's disease patients correlates with motor impairment. *Neurochemistry International*, *105*, 58–63. https://doi.org/10.1016/j.neuint.2017.01.007

Steimer, T. (2002). The biology of fear- and anxiety-related behaviors. *Dialogues in Clinical Neuroscience*, *4*(3), 231–249.

Steinkellner, T., Montgomery, T. R., Hofmaier, T., Kudlacek, O., Yang, J.-W., Rickhag, M., … Sitte, H. H. (2015). Amphetamine action at the cocaine- and antidepressant-sensitive serotonin transporter is modulated by αCaMKII. *The Journal of Neuroscience: The Official Journal of the Society for Neuroscience*, *35*(21), 8258–8271. https://doi.org/10.1523/JNEUROSCI.4034-14.2015

Steinkellner, T., Yang, J.-W., Montgomery, T. R., Chen, W.-Q., Winkler, M.-T., Sucic, S., … Kudlacek, O. (2012). Ca(2+)/calmodulin-dependent protein kinase IIα (αCaMKII) controls the activity of the dopamine transporter: implications for Angelman syndrome. *The Journal of Biological Chemistry*, *287*(35), 29627–29635. https://doi.org/10.1074/jbc.M112.367219

Stephenson, R., & Metcalfe, N. H. (2013). Drosophila melanogaster: a fly through its history and current use. *The Journal of the Royal College of Physicians of Edinburgh*, *43*(1), 70–75. https://doi.org/10.4997/JRCPE.2013.116

Stockner, T., Montgomery, T. R., Kudlacek, O., Weissensteiner, R., Ecker, G. F., Freissmuth, M., & Sitte, H. H. (2013). Mutational analysis of the high-affinity zinc binding site validates a refined human dopamine transporter homology model. *PLoS Computational Biology*, *9*(2), e1002909. https://doi.org/10.1371/journal.pcbi.1002909

Stuber, G. D., Hnasko, T. S., Britt, J. P., Edwards, R. H., & Bonci, A. (2010). Dopaminergic terminals in the nucleus accumbens but not the dorsal striatum corelease glutamate. *The Journal of Neuroscience: The Official Journal of the Society for Neuroscience*, *30*(24), 8229–8233. https://doi.org/10.1523/JNEUROSCI.1754-10.2010

Sucic, S., Dallinger, S., Zdrazil, B., Weissensteiner, R., Jørgensen, T. N., Holy, M., … Sitte, H. H. (2010). The N terminus of monoamine transporters is a lever required for the action of amphetamines. *The Journal of Biological Chemistry*, *285*(14), 10924–10938. https://doi.org/10.1074/jbc.M109.083154

Sulzer, D., Chen, T. K., Lau, Y. Y., Kristensen, H., Rayport, S., & Ewing, A. (1995). Amphetamine redistributes dopamine from synaptic vesicles to the cytosol and promotes reverse

transport. *The Journal of Neuroscience: The Official Journal of the Society for Neuroscience*, *15*(5 Pt 2), 4102–4108.

Sulzer, David, Sonders, M. S., Poulsen, N. W., & Galli, A. (2005). Mechanisms of neurotransmitter release by amphetamines: a review. *Progress in Neurobiology*, *75*(6), 406–433. https://doi.org/10.1016/j.pneurobio.2005.04.003

Takahashi, N., Miner, L. L., Sora, I., Ujike, H., Revay, R. S., Kostic, V., … Uhl, G. R. (1997). VMAT2 knockout mice: heterozygotes display reduced amphetamine-conditioned reward, enhanced amphetamine locomotion, and enhanced MPTP toxicity. *Proceedings of the National Academy of Sciences of the United States of America*, *94*(18), 9938–9943.

Tamai, I., & Tsuji, A. (2000). Transporter-Mediated Permeation of Drugs Across the Blood–Brain Barrier. *Journal of Pharmaceutical Sciences*, *89*(11), 1371–1388. https://doi.org/10.1002/1520-6017(200011)89:11<1371::AID-JPS1>3.0.CO;2-D

Torres, G. E., Carneiro, A., Seamans, K., Fiorentini, C., Sweeney, A., Yao, W.-D., & Caron, M. G. (2003). Oligomerization and trafficking of the human dopamine transporter. Mutational analysis identifies critical domains important for the functional expression of the transporter. *The Journal of Biological Chemistry*, *278*(4), 2731–2739. https://doi.org/10.1074/jbc.M201926200

Ueno, T., & Kume, K. (2014). Functional characterization of dopamine transporter in vivo using Drosophila melanogaster behavioral assays. *Frontiers in Behavioral Neuroscience*, *8*, 303. https://doi.org/10.3389/fnbeh.2014.00303

Ugur, B., Chen, K., & Bellen, H. J. (2016). Drosophila tools and assays for the study of human diseases. *Disease Models & Mechanisms*, *9*(3), 235–244. https://doi.org/10.1242/dmm.023762

van Alphen, B., & van Swinderen, B. (2013). Drosophila strategies to study psychiatric disorders. *Brain Research Bulletin*, *92*, 1–11. https://doi.org/10.1016/j.brainresbull.2011.09.007

van den Bogaart, G., Meyenberg, K., Risselada, H. J., Amin, H., Willig, K. I., Hubrich, B. E., … Jahn, R. (2011). Membrane protein sequestering by ionic protein-lipid interactions. *Nature*, *479*(7374), 552–555. https://doi.org/10.1038/nature10545

Van Rossumj, null, & Hurkmans, A. T. (1964). MECHANISM OF ACTION OF PSYCHOMOTOR STIMULANT DRUGS. SIGNIFICANCE OF DOPAMINE IN LOCOMOTOR STIMULANT ACTION. *International Journal of Neuropharmacology*, *3*, 227–239.

Vaughan, R. A., & Foster, J. D. (2013). Mechanisms of dopamine transporter regulation in normal and disease states. *Trends in Pharmacological Sciences*, *34*(9). https://doi.org/10.1016/j.tips.2013.07.005

Venton, B. J., Zhang, H., Garris, P. A., Phillips, P. E. M., Sulzer, D., & Wightman, R. M. (2003). Real-time decoding of dopamine concentration changes in the caudate-putamen during tonic and phasic firing. *Journal of Neurochemistry*, *87*(5), 1284–1295.

Vickrey, T. L., Xiao, N., & Venton, B. J. (2013). Kinetics of the dopamine transporter in Drosophila larva. *ACS Chemical Neuroscience*, *4*(5), 832–837. https://doi.org/10.1021/cn400019q

Volkow, N. D., Ding, Y. S., Fowler, J. S., & Wang, G. J. (1996). Cocaine addiction: hypothesis derived from imaging studies with PET. *Journal of Addictive Diseases*, *15*(4), 55–71. https://doi.org/10.1300/J069v15n04_04

Volkow, N. D., Fowler, J. S., & Wang, G. J. (1999). Imaging studies on the role of dopamine in cocaine reinforcement and addiction in humans. *Journal of Psychopharmacology (Oxford, England)*, *13*(4), 337–345. https://doi.org/10.1177/026988119901300406

Volkow, Nora D., Wang, G.-J., Newcorn, J., Telang, F., Solanto, M. V., Fowler, J. S., … Swanson, J. M. (2007). Depressed dopamine activity in caudate and preliminary evidence of limbic involvement in adults with attention-deficit/hyperactivity disorder. *Archives of General Psychiatry*, *64*(8), 932–940. https://doi.org/10.1001/archpsyc.64.8.932

Waddell, S. (2013). Reinforcement signalling in Drosophila; dopamine does it all after all. *Current Opinion in Neurobiology*, *23*(3), 324–329. https://doi.org/10.1016/j.conb.2013.01.005

Wang, H., Elferich, J., & Gouaux, E. (2012). Structures of LeuT in bicelles define conformation and substrate binding in a membrane-like context. *Nature Structural & Molecular Biology*, *19*(2), 212–219. https://doi.org/10.1038/nsmb.2215

Wang, J., Wolf, R. M., Caldwell, J. W., Kollman, P. A., & Case, D. A. (2004). Development and testing of a general amber force field. *Journal of Computational Chemistry*, *25*(9), 1157–1174. https://doi.org/10.1002/jcc.20035

Wang, J.-W., Beck, E. S., & McCabe, B. D. (2012). A modular toolset for recombination transgenesis and neurogenetic analysis of Drosophila. *PloS One*, *7*(7), e42102. https://doi.org/10.1371/journal.pone.0042102

Wang, K. H., Penmatsa, A., & Gouaux, E. (2015a). Neurotransmitter and psychostimulant recognition by the dopamine transporter. *Nature*, *521*(7552), 322–327. https://doi.org/10.1038/nature14431

Wang, K. H., Penmatsa, A., & Gouaux, E. (2015b). Neurotransmitter and psychostimulant recognition by the dopamine transporter. *Nature*, *521*(7552), 322–327. https://doi.org/10.1038/nature14431

Watterson, L. R., Kufahl, P. R., Nemirovsky, N. E., Sewalia, K., Grabenauer, M., Thomas, B. F., … Olive, M. F. (2014). Potent rewarding and reinforcing effects of the synthetic cathinone 3,4-methylenedioxypyrovalerone (MDPV). *Addiction Biology*, *19*(2), 165–174. https://doi.org/10.1111/j.1369-1600.2012.00474.x

Watterson, L. R., Watterson, E., & Olive, M. F. (2013). Abuse liability of novel "legal high" designer stimulants: evidence from animal models. *Behavioural Pharmacology*, *24*(5–6), 341–355. https://doi.org/10.1097/FBP.0b013e3283641ec8

Weiland, B. J., Heitzeg, M. M., Zald, D., Cummiford, C., Love, T., Zucker, R. A., & Zubieta, J.-K. (2014). Relationship between impulsivity, prefrontal anticipatory activation, and striatal dopamine release during rewarded task performance. *Psychiatry Research*, *223*(3), 244–252. https://doi.org/10.1016/j.pscychresns.2014.05.015

Weil-Malherbe, H., Whitby, L. G., & Axelrod, J. (1961). The uptake of circulating [3H]norepinephrine by the pituitary gland and various areas of the brain. *Journal of Neurochemistry*, *8*, 55–64.

Wiesel, F. A., Blomqvist, G., Halldin, C., Sjögren, I., Bjerkenstedt, L., Venizelos, N., & Hagenfeldt, L. (1991). The transport of tyrosine into the human brain as determined with L-[1-

11C]tyrosine and PET. *Journal of Nuclear Medicine: Official Publication, Society of Nuclear Medicine*, *32*(11), 2043–2049.

Witkovsky, P., Patel, J. C., Lee, C. R., & Rice, M. E. (2009). Immunocytochemical identification of proteins involved in dopamine release from the somatodendritic compartment of nigral dopaminergic neurons. *Neuroscience*, *164*(2), 488–496. https://doi.org/10.1016/j.neuroscience.2009.08.017

Wolf, M. G., Hoefling, M., Aponte-Santamaría, C., Grubmüller, H., & Groenhof, G. (2010). g_membed: Efficient insertion of a membrane protein into an equilibrated lipid bilayer with minimal perturbation. *Journal of Computational Chemistry*, *31*(11), 2169–2174. https://doi.org/10.1002/jcc.21507

Wright, T. H., Cline-Parhamovich, K., Lajoie, D., Parsons, L., Dunn, M., & Ferslew, K. E. (2013). Deaths involving methylenedioxypyrovalerone (MDPV) in Upper East Tennessee. *Journal of Forensic Sciences*, *58*(6), 1558–1562. https://doi.org/10.1111/1556-4029.12260

Wu, X., & Gu, H. H. (1999). Molecular cloning of the mouse dopamine transporter and pharmacological comparison with the human homologue. *Gene*, *233*(1), 163–170. https://doi.org/10.1016/S0378-1119(99)00143-2

Wyman, J. F., Lavins, E. S., Engelhart, D., Armstrong, E. J., Snell, K. D., Boggs, P. D., … Miller, F. P. (2013). Postmortem tissue distribution of MDPV following lethal intoxication by “bath salts.” *Journal of Analytical Toxicology*, *37*(3), 182–185. https://doi.org/10.1093/jat/bkt001

Yamamoto, R., & Takasaki, K. (1983). Involvement of presynaptic alpha 2-adrenoreceptors in the depressor response produced by repeated administration of dextro-methamphetamine. *Journal of Autonomic Pharmacology*, *3*(2), 79–88.

Yamamoto, S., & Seto, E. S. (2014). Dopamine dynamics and signaling in Drosophila: an overview of genes, drugs and behavioral paradigms. *Experimental Animals*, *63*(2), 107–119.

Yamashita, A., Singh, S. K., Kawate, T., Jin, Y., & Gouaux, E. (2005). Crystal structure of a bacterial homologue of Na+/Cl--dependent neurotransmitter transporters. *Nature*, *437*(7056), 215–223. https://doi.org/10.1038/nature03978

Yasumoto, S., Tanaka, E., Hattori, G., Maeda, H., & Higashi, H. (2002). Direct and indirect actions of dopamine on the membrane potential in medium spiny neurons of the mouse neostriatum. *Journal of Neurophysiology*, *87*(3), 1234–1243. https://doi.org/10.1152/jn.00514.2001

Yavas, E., & Young, A. M. J. (2017). N-Methyl-d-aspartate Modulation of Nucleus Accumbens Dopamine Release by Metabotropic Glutamate Receptors: Fast Cyclic Voltammetry Studies in Rat Brain Slices in Vitro. *ACS Chemical Neuroscience*, *8*(2), 320–328. https://doi.org/10.1021/acschemneuro.6b00397

Ye, Y., Xi, W., Peng, Y., Wang, Y., & Guo, A. (2004). Long-term but not short-term blockade of dopamine release in Drosophila impairs orientation during flight in a visual attention paradigm. *The European Journal of Neuroscience*, *20*(4), 1001–1007. https://doi.org/10.1111/j.1460-9568.2004.03575.x

Yorgason, J. T., Zeppenfeld, D. M., & Williams, J. T. (2017). Cholinergic Interneurons Underlie Spontaneous Dopamine Release in Nucleus Accumbens. *The Journal of Neuroscience: The Official Journal of the Society for Neuroscience*, *37*(8), 2086–2096. https://doi.org/10.1523/JNEUROSCI.3064-16.2017

Zawilska, J. B., & Wojcieszak, J. (2013). Designer cathinones--an emerging class of novel recreational drugs. *Forensic Science International*, *231*(1–3), 42–53. https://doi.org/10.1016/j.forsciint.2013.04.015

Zhang, H., & Sulzer, D. (2012). Regulation of striatal dopamine release by presynaptic auto- and heteroreceptors. *Basal Ganglia*, *2*(1), 5–13. https://doi.org/10.1016/j.baga.2011.11.004

Zhang, K., Guo, J. Z., Peng, Y., Xi, W., & Guo, A. (2007). Dopamine-mushroom body circuit regulates saliency-based decision-making in Drosophila. *Science (New York, N.Y.)*, *316*(5833), 1901–1904. https://doi.org/10.1126/science.1137357

Zhang, S. X., Rogulja, D., & Crickmore, M. A. (2016). Dopaminergic Circuitry Underlying Mating Drive. *Neuron*, *91*(1), 168–181. https://doi.org/10.1016/j.neuron.2016.05.020

Zou, P., & McHaourab, H. S. (2010). Increased sensitivity and extended range of distance measurements in spin-labeled membrane proteins: Q-band double electron-electron resonance and nanoscale bilayers. *Biophysical Journal*, *98*(6), L18-20. https://doi.org/10.1016/j.bpj.2009.12.4193